Phenomenological Tests of Modified Gravity

Ana Aurelia Avilez-López

Thesis submitted to the University of Nottingham for the degree of
Doctor of Philosophy

July 2015

For Ana Lucía and Jorge .

DECLARATION

I hereby declare that except where specific reference is made to the work of others, the contents of this dissertation are original and have not been submitted in whole or in part for consideration for any other degree or qualification in this, or any other university. This dissertation is my own work and contains nothing which is the outcome of work done in collaboration with others, except as specified in the text and Acknowledgements. This dissertation contains fewer than 100,000 words including appendices, bibliography, footnotes, tables and equations.

The thesis is based in the following research

- Avilez, A. and Skordis, C., *Cosmological Constraints on Brans-Dicke Theory*, Phys.Rev.Lett.113(2014)011101, arXiv:1303.4330 [astro-ph.CO].
- Ana Avilez-Lopez, Antonio Padilla, Paul M. Saffin, Constantinos Skordis, *The Parametrized Post-Newtonian-Vainshteinian Formalism*, (Submitted to JCAP) arXiv:1501.01985 [gr-qc].

Paper 1 is described in chapters 3 and 4. The motivation and part of the calculations of chapter 6 are based paper 2.

Ana Aurelia Avilez-López
July 2015

ACKNOWLEDGEMENTS

I would like to thank my supervisor Costas Skordis for his dedicated, patient and fruitful guidence and support during my doctoral course. I am deeply grateful to him for giving me his trust and support even in hard moments. Also, thank you Costas for the freedom you gave me to explore new ideas and your flexibility about times and forms that made possible to carry on with this research work. Also, I am grateful to the people in the department for supported me and encourage me to give my best effort. I am grateful to my collaborators Tony Padilla and Paul Saffin for their guidence, discussions and support. I would also like to thank my external collaborator Yong-Seon Song for his interesting questions and discussions. I am grateful with the national council of science and technology of Mexico CONACYT for the financial and institutional support. Many thanks to my husband Jorge for all his patience, love and support. Thanks to Ana Lucia for the time she donated to this research I promisse it will be worth. Thank you to my mother Margarita Elena López and Bertha Fernandez-Quiroz, without their support this work would have not been possible at all. Thank you: Cristina, Victoria, Gerardo, Janette, Fernando, Giovanna, Bruno, Paul Tognarelli, Mou Zong Gang and Ana Chies for your friendship and support during this period.

ABSTRACT

The main goal of this thesis is to test the viability of some modified theories of gravity suitable to describe gravitational phenomena at cosmological and astronomical scales. In the first part of the Thesis we study the viability of the Brans-Dicke theory (BDT) and the effective scalar-tensor theory according (gBDT) to cosmological observations. We assume that either BDT as gBDT are limiting cases on very large scales of more general scalar-tensor theories involving derivative self-interactions which have running Newton's constant. In order to implement this assumption in a simple way we consider two types of models. The *restricted* models that correspond to the standard BDT with Newton constant today equal to measured Newton constant in solar-system experiments. The *unrestricted* models, correspond to the case where the Newton's constant today is a free parameter, and the cosmological G_N is allowed to be different than in the solar system as in more general theories. We first explore the relevant theoretical aspects of these models. Afterwards, by using different analysis techniques we fitted cosmological observations. Finally we forecast limits of BDT by considering estimated covariance matrices for measurements of the matter power spectrum in redshift space from Euclid. The effective scalar-tensor theory gBDT arises from a phenomenological setup of parametrization of the LSS growth equations, we found estimates of modifications of the growth by using the correspondance between the estimates for the gBDT parameters.

In the second part of the Thesis we present an extension of the Parameterized Post-Newtonian (PPN) formalism that is able to handle Vainsteinian corrections. We argue that theories with a Vainshtein mechanism must be expanded using two small parameters. In this Parameterized Post-Newtonian-Vainshteinian (PPNV) expansion, the primary expansion parameter which controls the PPN order is as usual the velocity v. The secondary expansion parameter, α, controls the strength of the Vainshteinian correction and is a theory-specific combination of the Schwarzschild radius and the Vainshtein radius of the source that is independent of its mass. We present the general framework and apply it to the Cubic galileon theory both inside and outside the Vainshtein radius. The PPNV framework can be used to determine the compatibility of such theories with solar system and other strong-field data.

TABLE OF CONTENTS

LIST OF FIGURES

CHAPTER 1

INTRODUCTION

1.1 Historical Review Of General Relativity

1.1.1 Solar System Precision Tests

1.1.1.a The Origins

The first seed that gave rise to the birth of general relativity(GR) was special relativity which at the same time was rooted in the accomplishment of two great experimental discoveries: the Michelson-Morley [211] and Eotvos [119] experiments. At this initial stage, the focus was placed on the theoretical realizations of the paradigm. The sophisticated mathematical bases on which GR is constructed revolutionized the way of formulating and understand physical theories in modern physics. For instance, GR became one of the pillars of gauge theories that nowadays is the leading paradigm to describe the fundamental interactions in nature and their unification. Besides its magnificent structure, the principles supporting GR are very deep and link the phenomenon of gravitation with the nature of matter and space-time itself. Since the very beginning when Einstein formulated general relativity [112–114], such elegance and consistency left its empirical aspects and implications in a secondary position. Nevertheless, Einstein did calculate observable effects of general relativity, such as the perihelion advance of Mercury and the deflection of light. These phenomena could not be understood before that date, so when his predictions were found to be in agreement with experiment a new revolutionary era started and General Relativity was set as the paradigmatic theory of gravitation and a cornerstone of theoretical physics of the XX century.

1.1.1.b The Golden Era of Experimental Gravitation

From 1920 onwards a period of hibernation of experimental gravitation started that lasted 40 years [326]. During this time theoretical work was intense while the experimental and technological achievements were on pause. At the beginning of the 1960's GR recovered attention thanks to the great astronomical discoveries as quasars, pulsars, cosmic background radiation among other experiments. This event was the starting point of a large period of activity in the field, the so called Golden Era of experimental gravitation [327]. During this stage great effort was invested to understand the observable predictions of GR. Also, important ideas and frameworks arise initially aimed to design tests for GR. Furthermore, given the scope of these achievements, during this period many people figured out possible extensions and alternatives to GR and large amount of work was devoted to compare and contrast the corresponding predictions with those from GR. During this period the validity of GR was challenged as never before. This stage began with the successful measurement of the gravitational redshift of light from the Venus radar echo in the Pound-Rebka experiment in 1960 [249] and finished with the reported decrease in the orbital period of the Hulse-Taylor binary pulsar at a rate consistent with the GR prediction of gravity wave energy loss in 1979 for which they won the 1993 Nobel Prize in Physics [300, 301].

During these years many astrophysicists turned their attention towards General Relativity and many theoreticians started to gain interest in observational aspects of gravitation. This feedback gave rise to a completely new arena of activity in the field. On one hand, GR became an essential tool for astrophysicists, the astonishing precision at which GR passed the three classical astrophysical tests (perihelion precession of Mercury, deflection of light and the gravitational redshift of light) invited astrophysicists to trust in its predictions. On the other hand, theoreticians started to address deep questions about the nature of gravitation inspired in the observations set on the table at that time. A torrent of theoretical and experimental discoveries characterized those two decades. For instance, since the 1950 Penrose initiated a new trend for relativity theorists, sophisticated pure mathematical techniques were applied to solve problems in general relativity. The gap between physics, mathematics and astrophysics was filled by works of Bondi, Dicke, Sciama, Pirani, Penrose, Sachs, Ehlers and Misner. In this direction, Carl H. Brans and Robert H. Dicke developed a peculiar alternative to GR by implementing the Mach's principle with a varying gravitational constant inspired in ideas of Dirac [94]. On the experimental front, this golden period brought cutting edge technological developments in the field in the subsequent decade. For example, the Pound-Rebka experiment displayed the use of

powerful quantum technology which spread in various experiments as tools as atomic clocks, laser ranging, superconducting gravimeters and gravitational waves detectors among others. Also, after the recording of the radar echos from Venus and the quick development of the interplanetary program, in the 1960's the radar ranging became an essential tool for testing gravitational effects, specially those of general relativity. Later on by 1964, the theoretical discovery of the time-delay effect [276] provided a new and accurate test of GR. These achievements eventually yield along the next decade, that the solar system became exclusively an ideal laboratory for high-precision tests of general relativity.

Until then, all gravitational effects involved in the tests were difficult and expensive to detect because they were originated by weak gravitational fields. However, the discovery of "quasars" (quasi-stellar radio source) by Thomas Matthews and Allan Sandage at Mount Palomar [205], pulsars and black holes presented a new theoretical challenge to General Relativity since it had to explain the huge outburst of energy from objects so compact that the luminosity could vary in timescales as small as days or hours. From this discovery many theorists started to look at the strong gravitational fields predicted by GR and tried to understand how these violent events occur. This was the first use of the strong aspect of general relativity in an attempt to understand these observations. Since 1980 the focus in the field shifted to experiments to probe the effects of strong gravitational fields. Within this set of strong field phenomena, there are two regimes associated with different features. On one hand, there are the strong fields associated with the quantum Planck scale physics and on the other hand the strong fields associated with compact objects. Yet at the present time Astrophysical observations and gravitational wave detectors are being planned to explore and test GR in the strong-field, highly-dynamical regime associated with the formation and dynamics of these objects.

Along all this process, the use of general relativity in astrophysical model building forced experimentalist and theoreticians to wonder : Is general relativity the correct relativistic theory of gravitation? This quest emerged from the need of a firm certainty about the physical principles behind the astrophysical models describing strong field phenomena. Given the success of GR, the activity in relativistic astrophysics increased at that time, then the need to strengthen the empirical evidence against or in favor to GR. In this attempt to figure out how to test general relativity, the formulation of the Brans-Dicke theory provided a important insight about the theoretical nature of gravitation which helped to move forth the subsequent experimental and theoretical achievements at that date. Since the predictions of this alternative theory to General Relativity were found to be compatible with observations the community realised that general relativity was not the only viable relativistic theory of gravitation. Further-

more, some preferred the Brans-Dicke theory over GR since its formulation relies on broader theoretical framework, this feature is convenient when one intends to confront theoretical predictions with experimental observations. It also was useful to recognize the need of higher precision experiments since the bare detection of relativistic effects was not sufficient. The required accuracy of the measurement of effects (such as the shift of the perhelion of mercury or the gravitational deflection of light) was less than 10%, in order to distinguish among contesting theories of gravitation.

Finally, it's worth stressing that other new and unexpected tests of gravity have arisen from new theoretical ideas and experimental techniques, often from unlikely sources [326]. Examples include the use of laser-cooled atom and ion traps to perform ultra-precise tests of special relativity; the proposal of a "fifth" force, which led to a host of new tests of the weak equivalence principle; and recent ideas of large extra dimensions, which have motivated new tests of the inverse square law of gravity at sub-millimeter scales.

1.1.2 Origins Of The Standard Cosmology

"One usually deals with the physical world as a hierarchy of structures, from elementary particles, to atoms, molecules, living organisms, the earth, the solar systems, our galaxies up to edge of the local group for galaxies. A discipline in physical science generally isolates a thin slice of this hierarchy and takes into account the interaction from other parts. In the case of cosmology one is able to study independently the physical world at very large scales as an isolated problem thanks to the fact that in average the universe is remarkably simple, matter in it distributes nearly homogeneously and isotropically. Modern cosmology is based on this simple characterization of the universe." Peebles

1.1.2.a Cosmological and Mach's Principles

" We now regard the principle of equivalence as the foundation, not of Newtonian gravity or of GR, but of the broader idea that spacetime is curved. Much of this viewpoint can be traced back to Robert Dicke, who contributed crucial ideas about the foundations of gravitation theory between 1960 and 1965. These ideas were summarized in his influential Les Houches lectures of 1964 , and resulted in what has come to be called the Einstein equivalence principle (EEP)" Clifford Will [326].

An important antecedent of the standard cosmological model is the problem of defining inertial frames of reference in special and general relativity. The reason why this puzzle is important is that the property of inertia traces the connection with the cosmological principle. Since Newton's original conception, inertial motion had been

conceived as an absolute property of space-time. Although Einstein in great extent breaks such Newtonian absolute character of space-time, the way of determining whether a reference frame is inertial or not within general relativity is still arbitrary. Indeed, the Mach's principle challenges the Einstein's definition of inertia:

Mach's Principle: "*the physical properties of space have their origin in the matter contained therein, and that the only meaningful motion of a particle is motion relative to other matter in the universe*.

This principle asserts that it is absurd to think that inertial frames reflect an absolute property. Instead it proposes, inertial frames are determined by the distribution and motion of the rest of the matter in the universe. In response to Mach, Einstein reinterpreted the Mach's principle by considering coordinates as arbitrary labels of points in space-time without absolute significance. Although, there are GR solutions which are consistent with the Mach's principle, there are other ones that violate Mach's ideas. For example, the metric tensor for flat spacetime with $g_{\mu\nu} = \eta_{\mu\nu}$ the Minkowski form is the unique nonsingular spherically symmetric solution to Einstein's field equations in the vacuum. On the other hand, it is reasonable that solution describes the spacetime surrounding us since in our neighborhood of galaxies the mass density is quite small. However, this solution allows one to postulate that a particle can move arbitrarily far from the rest of the matter in the universe. This metric tensor defines inertial frames for the particle. In conclusion, we have a solution to the Einstein's equations that defines inertial frames arbitrarily far from the rest of matter in the universe which is absolutely contrary to Mach's ideas.

By 1916 de Sitter and Einstein in an attempt to solve this problem [see [169] and [166] for a review] realised that the transition of the metric to Minkowski could not be caused by any of the observed objects such as stars or spiral nebulae since one would expect strong curvature which is contrary to the observations. Thus such transition would be due to the space curvature produced by unobserved masses. However these hypothetical masses were discarded straightaway. Einstein changed the hypothetical masses idea by the proposal: The mass distribution in the universe is homogeneous on the large-scale average and the spatial volume of the universe finite without boundary. Otherwise, it would be impossible for a particle to move apart from the rest of the matter in the universe. For astronomers at that time, the universe was the system of stars in the Milky Way thus this sentence was unlikely to realise. However, nowadays we know such mass distribution is referred to the mean distribution of galaxies averaged over the fluctuations in their clustering that traces the nearly homogeneous large-scale distribution of mass. Nevertheless, the Einstein's idea was rapidly accepted when Hubble's counts of galaxies to fainter limits revealed increasingly large numbers of galaxies as expected for an unbounded distribution [238].

However there appeared strong warnings about his assertion. Particularly, de Sitter [90] objected "all this talk about the universe involves a tremendous extrapolation, which is very dangerous in operation". Around 1933 Hubble research was in its most active moment and the resulting observations favored Einstein's position: "Hubble's research has, furthermore, shown that these objects are distributed in space in a statistically uniform fashion, by which the schematic assumption of the theory of an uniform mean density receives experimental confirmation" [116].

From the empirical point of view de Sitter's was the most sensible position for many people since it was well known that galaxies tend to appear in groups and clusters, for them it would have been reasonable that the hierarchy of clustering continues to indefinitely large scales. GR predicts that Hubble would continue to find galaxies as his surveys proved to increasing distances, but the mean number density would decrease as the limits of the surveys expanded through the levels of the hierarchy [62, 63]. Interestingly, Einstein in 1922 granted that this picture is consistent with general relativity however he rejected it as it is inconsistent with Mach's principle [115]. In the cosmological model we have today, the cosmological principle reduces to a consistency condition, that the large-scale departures from homogeneous and isotropic mass distribution and motion have to be consistent with observable consequences: the anisotropies of the radiation background, counts of objects as function of distance and direction and peculiar velocities derived from Doppler shifts.

1.1.2.b Birth and Evolution of the Big Bang Theory

Although since ancient Copernicus times the cosmological principle was an accepted statement about our universe, during modern times it arose as a posteriori outcome from a collective quest about the consistency conditions for GR initiated by Einstein and de Sitter and the subsequent observation of the uniform distribution of structures of matter in the universe. Since the time of Hubble, people were intrigued on whether galaxies were uniformly distributed since Einstein had postulated so for matter. Hubble in 1926 designed a test to figure out the answer by adapting a well-known method used to test the distribution of stars [157, 238]. In that work Hubble reported that galaxy counts at the date were consistent with the idea that the galaxy distribution is nearly homogeneous in the large-scale average. Hubble encountered no pronounced evidence of an edge to the galaxy distribution and such finding was an impressive first extensive and quantitative test of Einstein's homogeneity postulate.

Another finding that was a key piece to complete the picture of the Big Bang theory was the discovery by Hubble and Slipher in the 1920s of the recession of distant galaxies from which it was inferred that the universe is expanding [156, 157, 282–

285]. This discovery was arisen by an interplay between theory and observations. A crucial step in the theory appeared in the paper of de Sitter in 1917 were he explored possible astronomical implications of Einstein's static model of the universe. De Sitter pointed out that one can find another solution to Einstein's field equations for a static, homogeneous and isotropic universe. De Sitter solution has negligibly small values for the mass density and pressure of ordinary matter and its only source is assumed to be the cosmological constant.

At that time it was known that the distant galaxies were shifted toward the red many people started to pay attention to de Sitter solution since this phenomenon could be interpreted as the de Sitter scattering effect. However, a prediction of a cosmological red-shift in this context required certain initial conditions for position and velocities of galaxies. This problem was addressed by Weyl [325], Lemaître [179], Robertson [259, 260] and they figured out a prescription consistent with the cosmological principle: if initial conditions are fixed such that galaxies move on geodesics with fixed spatial positions then the pattern of relative velocities of galaxies is independent of the galaxy to which the distances and velocities are referred. In this prescription the redshift is proportional to its distance.

Robertson in [259] pointed out that this linear relation was consistent with observations of Hubble and Slipher and the constant of proportionality was close to what Hubble reported the following year. However this result is only valid following the prescription described above. The result is illustrated by figure (1.2), the distance of a supernovae which is normally proportional to its luminosity or apparent magnitude[1] is proportional to its redshift $z \equiv \lambda_d/\lambda_0$ [2] which is a measure of the change in the wavelength due to the recession velocity.

At that point however, the problem was not solved at all. On one hand, observational evidence of the distribution of galaxies favored the Einsten's matter-filled static solution rather than de Sitter's empty static solution . On the other hand the galaxy red-shifts don't fit with the static Einstein's matter filled solution but could be interpreted within de Sitter static solution. While in 1930 de Sitter and Eddington were puzzled about this problem [90, 105, 106, 182] they were informed by Lemaître that the expanding matter-filled solution did fit the data.

[1] Where the apparent magnitude is an integrated measure of the brightness of an extended object such as a nebula, cluster or galaxy [235].

[2] where λ_d corresponds to the detected wavelength of the source whilst λ_0 is the one measured from the source's frame.

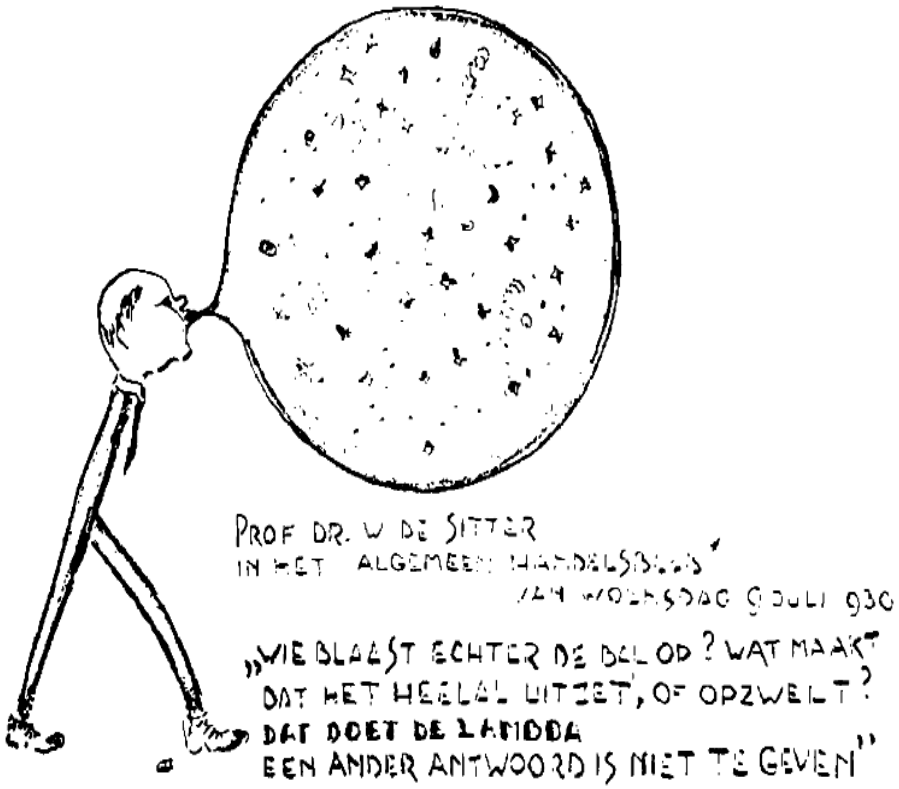

Fig. 1.1 This sketch appeared following an interview of DE Sitter published in a Dutch newspaper. The quote is translated by van der Laan as: "What however blows up the ball?What makes the universe expand or swell up? That is done by the Λ. another answer cannot be given". Figure taken from [238].

The solution was discovered by Friedmann in 1922 [130] and rediscovered by Lemaître in 1927 [181] who saw the possible connection to the galaxy red-shifts. By 1931 Eddington and Lemaître published a series of papers that were the base for the new paradigm of the expanding universe [180, 183]. Soon after Lemaître modified the picture and introduced the idea that the universe expanded from a dense state keeping the cosmological constant to increase the age of the universe over $\sim H_0^{-1}$ if the universe expanded from a dense initial state with $\Lambda = 0$, however this solution was only apparent. The matter of what causes the expansion was still unsolved.

By 1940 there were many gaps without filling that gave rise to doubts about the applicability of the Lemaître Big Bang theory. For instance, the age of the universe can be estimated from extrapolating the expansion of the universe from the big bang up to today using the equations of general relativity. However, the observed values of the present expansion rate were so large that the inferred age of the universe was

shorter than the age of the Earth [44, 150]. This problem was partially solved in the 1950s by reviewing that the extra-galactic distance scale was reduced by factor of 5 implying the reduction of Hubble constant and thus the resulting increasing age of the universe a value greater than the age of our galaxy. From the second half of the 1960's and the 1970s, the model faced a list of other serious issues that motivated people to formulate remarkable ideas aimed to solve them and at the end of the day all these pieces together gave rise to a more complete and consistent standard cosmological model we know today.

One of those issues was pointed out by Misner in 1968. He highlighted that the standard model (with pressure that is not negative) has a particle horizon such that we can see distant objects that were causally disconnected right after the beginning of expansion [212]. Another problem was that the Friedmann-Lemaître universe is gravitationally unstable. Another issue is the so called "horizon problem" that our observable patch of the universe nowadays would come from a non zero-sized patch in the early universe if it would grow according to the standard Friedmann models [339]. The most remarkable model that solve all the gaps in the model is inflation. However, this paradigm is yet to be discovered given the fact that the energy-scale associated to it is extremely high, however it gives us a viable and testable picture on what happened just after the big-bang [see [238] for further details] and current and future observations set strong constraints on it. Inflation was introduced by Guth in 1981 [141, 217], Linde in 1982 [190] and Albrecht and Steinhardt in 1982 [8] partly to solve why causally disconnected regions had the same temperature, however it was soon realised that the same mechanism was able to originate the perturbations in the universe.

Another crucial pillar of the standard cosmological model we use today, was the discovery of the 3K cosmic background microwave radiation by Penzias and Wilson around 1965 [244]. It implied that the universe was much hotter and denser than it is today and moreover it was a decisive confirmation of the cosmological principle. Furthermore, it also was sufficient evidence to decide the controversy during the 1960's in favor of the Big Bang over the Steady State universe. It is important to mention that it also served to resolved the discrepancy between the observed cosmic abundances of helium and the estimates of production of helium in stars [239, 316].

It wasn't until the 1980s that Harrison, Peebles, Yu and Zel'dovich realised that the early universe would have to have inhomogeneities of order 10^{-5} [143, 241, 342]. Rashid Sunyaev later calculated the observable imprint that these inhomogeneities would have on the cosmic microwave background. Increasingly stringent limits on the anisotropy of the cosmic microwave background were set by ground based experiments during the 1980s. $RELIKT-1$, a Soviet cosmic microwave background anisotropy

experiment gave upper limits on the large-scale anisotropy. The NASA COBE mission clearly confirmed the primary anisotropy with the Differential Microwave Radiometer instrument, publishing their findings in 1992 [33, 287] The team received the Nobel Prize in physics for 2006 for this discovery. During the next decade ground and balloon-based experiments, measured cosmic microwave background anisotropies on smaller angular scales. The primary goal of these experiments was to measure the scale of the first acoustic peak, which COBE did not detect due to its low resolution. These measurements demonstrated that the geometry of the Universe is approximately flat, rather than curved [87]. Besides they suggested cosmic inflation as the most viable theory to give rise to the initial perturbations to the uniform universe.

Finally, I would like to mention something important about the nowadays standard model of cosmology. The fact that it describes the evolution of the matter distribution at very large scales (that is from mega-parsec to larger scales), is rooted on two great pillars. Both enable GR to predict a dynamical universe that expands or contracts and also make it a theory capable of dealing with the structure and evolution of the universe as a whole in contrast to Newtonian theory where space-time is fixed a-priori and the problem of fixing and interpreting the boundary remains unsolved. These two pieces I'm talking about are: the Einstein equivalence principle and the cosmological principle. In principle both are shared with other metric theories of gravity which imply that space-time is equipped with a metric which is a dynamical entity determined by the matter contents of the universe.

1.2 Challenges for the Standard Cosmology

"*On one hand, we have a simple model that fits our observations extremely well, but on the other hand, we see some strange features which force us to rethink some of our basic assumptions. This is the beginning of a new journey, and we expect our continued analysis of Planck data will help shed light on this conundrum.*" Jan Tauber, the European Space Agency's Planck project.

1.2.1 Dark Matter-Energy Mysteries

The expansion history inferred according to the standard cosmological model by using measurements of the type Ia supernovae is not accomplished if only standard matter contents like baryonic matter and radiation are considered. In order to match predictions with observations it is needed to consider an exotic component in the Friedmann equation which effectively plays the role of a fluid with negative pressure usually named as "Dark Energy". Because we don't know what such thing could be so far, this quantity basically stands as a model fitting parameter of observations and it will remain so until we get consistent theoretical hints of its nature and direct observational evidence of its existence.

Another not yet well understood piece of the standard cosmological model is dark matter. The net mass of stars in galaxies in the cluster of galaxies is one order of magnitude less than that estimated from other sources like gravitational lensing, dynamics of the cluster plasma and galaxy motions or the spectrum of the CMB. This has been solved by the assumption that not all the contents of the cluster have been detected and the lacking part has been called "dark matter". In other words, by looking at the gravitational effects produced by the total mass in the galaxy there's no way that it might be formed only by baryonic matter, of course under the assumption that its galactic dynamics are governed by general relativity. Indeed, according to the standard picture the most part of the mass in the galaxy is made of cold dark matter (CDM). Although this type of matter has not been detected so far, an active area of research is devoted to investigate its nature. Today, a large part of the scientific community is optimistic about the detections of WIMPS (or weakly interacting massive particles) along the coming decades. Presumably, the heavy non-baryonic mass needed to reproduce the velocity curves, lies around the galaxy in form of halos made by WIMPS. However, as long as these WIMPS remain not detected, this discrepancy between the general relativity predictions and the observed velocity curves of galaxies stands as a mystery.

In conclusion, if we bet for general relativity as the best framework to describe the cosmological phenomena we must face these puzzles. Within the standard cosmological model these gaps are filled up by assuming the simplest possibilities: dark energy is given by the cosmological constant Λ and dark matter is *CDM* to eventually be detected. Under this prescription, the visible detected matter in the universe is just a small portion of the total mass. Most of the matter-energy producing the gravitational effects in our universe is made actually by these dark undetected and not yet understood components.

1.2.1.a What May be Causing the Accelerated Expansion of the Universe?

Right after the discovery of the accelerated expansion of the universe during the late 1990's, theorists came up with three possible of answers to this question. The first possibility was that the expansion arose from the abandoned version of Einstein's theory of gravity whit a "cosmological constant." The second answer might be that the space was filled of some strange kind of energy-fluid exerting large negative pressure. Some theorists have named this "quintessence," after the fifth element of the Greek philosophers. But, if quintessence is the answer, we still don't know what it is like, what it interacts with, or why it exists.

The last possibility is that Einstein's theory of gravity is wrong or incomplete and a new theory could include some kind of field or hold different geometrical properties that create this cosmic acceleration. In general, a modification of general relativity would not only affect the expansion of the Universe, but it would also lead to a different behavior of normal matter in galaxies and clusters of galaxies. Actually, this fact would provide a way to decide whether the solution to the dark energy problem is a new gravity theory or not. But if it does turn out that a new theory of gravity is needed, what kind of theory would it be? How could it correctly describe the motion of the bodies in the Solar System, as Einstein's theory is known to do, and still give us the different prediction for the Universe that we need?.

Neither theorists or observational cosmologists still have a correct answer, however they have given the unknown solution the generic name of "dark energy".

Cosmological Constant Problem Historically it has arisen a link between dark energy and the cosmological constant, as we saw above. Initially it helped to well fit the observation of the recession on distant galaxies, thus since early decades the cosmological constant has been set as the most viable candidate to play the role of this strange component. As we know, it was first introduced by Einstein as a theoretical artifact and finally abandoned and coined by him as a terrible blunder. However

along the period from the 1930 to the 1960, Eddington, de Sitter and Lemaître pick it up to build the theoretical basis to describe the Hubble's observations. However, in these studies the cosmological constant was nothing but a model fitting parameter and nothing about its nature was understood or even questioned. It was until 1968 when it was realised that the zero-point vacuum fluctuations must respect Lorentz invariance and therefore its momentum tensor in average should be related to the metric in the following way $\langle T_{ik} \rangle = g_{ik}\Lambda$ [265, 344]. On the other hand, by using the standard theory of elementary particles, the resulting energy of vacuum regularized using the Planck scale as the cut-off scale is $\sim 10^{76} GeV^4$. This value is 123 orders of magnitude larger than the inferred value of the cosmological constant from cosmological observations $\rho_\Lambda \sim 10^{-47} GeV^4$ [266]. A smaller cut-off scale does not improve the situation, for example the QCD cut-off scale $10^{-3} GeV^4$ still gives a 40 orders of magnitude larger value than the currently observed one. For further details on this problem the following reviews are available [60, 108, 232, 266, 322].

Additional to the smallness of the observed cosmological constant, there's another riddle related to the cosmological constant dubbed as "coincidence problem". As we'll see in the next section, measurements of the luminosity-redshift relation for type Ia supernovae combined with measurements of the cosmic microwave background lead to a small positive value of the cosmological constant. Even if this were confirmed or directly detected, since the vacuum energy density is constant in time, while the matter energy density decreases as the universe expands, it is more than surprising that the two are comparable just at the present time, while their ratio has to be infinitesimal in the early universe.

1.2.1.b Observational Evidence of Dark Energy

We already saw in the historical review, that the astonishing discovery of the recession of galaxies in the 1920's by Hubble was the key observation that allowed to infer that we live in an expanding universe. In those early decades of the standard model. However, people were not certain on how the expansion should evolve along the whole history of the universe. About the early 1990's, according to the mainstream picture, the universe might have enough energy density to stop its expansion and recollapse or it might have so little energy density that it would never stop expanding, but gravity was certain to slow the expansion as time went on. They granted, the slowing had not been observed, but, theoretically, the universe had to slow given that the universe was full of matter. In the late 1980s and early 1990s, however, a variety of indirect evidence began to accumulate in favor of a cosmological constant though. Studies of large scale galaxy clustering, interpreted in the framework of cold dark matter

models with inflationary initial conditions, implied a low matter density parameter $\Omega_m = 0.15 - 0.4$ [109], in agreement with direct dynamical estimates that assumed galaxies to be fair tracers of the mass distribution. However, it wasn't until 1998 when observations of very distant supernovae from the Hubble Space Telescope (HST) by Riess, Perlmutter and Schmidt [123, 247, 257, 336] verified that, a long time ago, the Universe was actually expanding more slowly than it is today [126]. So the expansion of the Universe has not been slowing due to gravity, as everyone thought, it has been accelerating and something had to cause such effect. Riess, Perlmutter and Schmidt won the nobel prize in 2011 for this discovery.

Basically, observations from the Hubble space telescope (HST) have revealed that type Ia supernovae, when treated as standard candles [3], at higher redshifts are consistently dimmer than similar SN Ia at lower redshifts relative to what might be expected in CDM cosmology.

Assuming that effects such as cosmological evolution and dimming by intergalactic dust are not very important, this systematic dimming of supernovae at high redshift can be interpreted as evidence for an accelerated expansion of the universe caused by a form of 'dark energy' having large negative pressure [265]. Specifically, this evidence was extracted from a large set of measurements of luminosity distances of high redshift supernovae carried out by several groups along the last two decades which are shown by figure (1.2).

According to these observations, dark energy should have an equation of state parameter $w = P/\rho < -1/3$ for the universe to undergo accelerated expansion. The simplest model within this set is the standard one where the cosmological constant plays the role of dark energy with $w = -1$ which has been fitted to agree with observations. However, in order to solve some of the theoretical issues that this choice brings up (we'll study them shortly) many other scenarios have been explored included quintessence [26, 77, 201, 254, 267, 308, 312, 323], k-essence [16, 17, 51, 67], tachyon fields [21, 131] and phantom fields [60, 224, 231]. In these models $w \neq -1$ and in general it varies with redshift. Many reviews are available where the details of specific models are studied [108, 232, 266]. The possibility of a varying w can be tested by observations. Supernova observations permit a large variation in w. However combined supernova observations with CMB data and abundance of rich clusters of galaxies provides tight constraints on variation of dark energy.

[3] The type Ia supernova (SN Ia) can be observed when white dwarf stars exceed the Chandrasekhar mass limit and explode. It is believed that SN Ia are formed in the same way independently of where they are in the universe, which means that they have a common absolute magnitude independent of the redshift. Thus they can be treated as an ideal standard candle (a source that has a known luminosity)

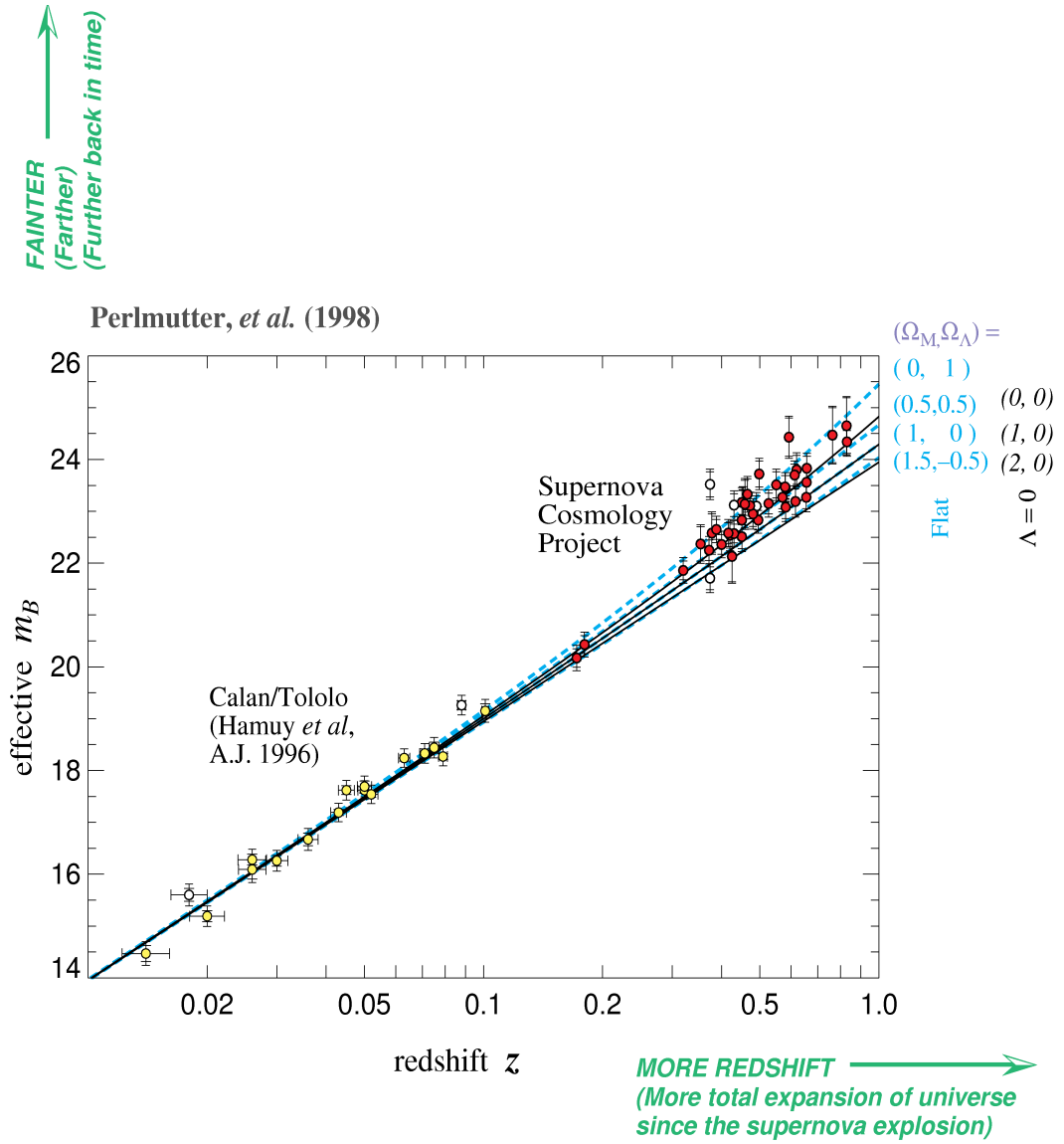

Fig. 1.2 Effective magnitude-redshift relation for the Hubble flow of a sample of IaSN from the Supernovae Cosmology Project. Different ΛCDM models are plotted, for the flat case (which is in agreement with observations of the CMB) the data is fitted by a model in which the cosmological constant dominates. Further details about this figure can be found in [247].

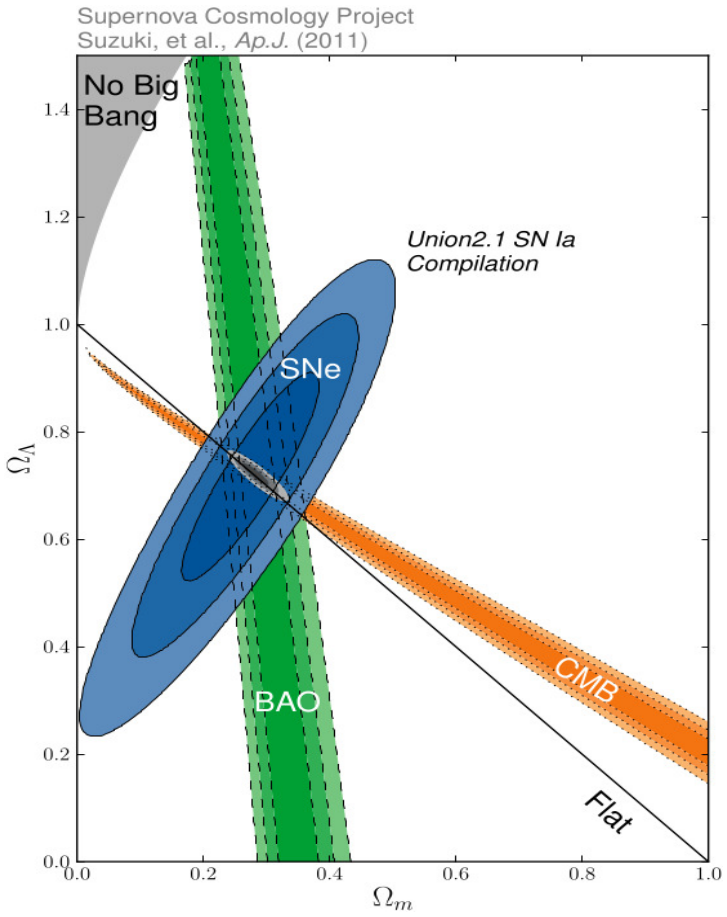

Fig. 1.3 Constraints on dark energy according to CMB measurements from WMAP5. Taken from [126].

Dark energy models are also tested by using measurements of the CMB temperature and polarization anisotropies. These observations constrain dark energy in two ways, through the distance to the last scattering surface and through the Integrated Sachs Wolfe (ISW) effect [311]. The CMB alone does not strongly constrain w, due to the two-dimensional geometric degeneracy with other cosmological parameters. Nevertheless, this might be broken down by combining lower redshift distance measures of BAO along with the CMB data. According to the latest measurements from Planck in companion with BAO the estimate for w inside the 95% confidence level region is given by

$$w = -1.13^{+0.24}_{-0.25}$$

Assuming constant equation of state and combining CMB data with measurements of luminosity distance of supernovae from Union2.1 and SNLS leads to the constraints [6]

$$\begin{aligned} w &= -1.09 \pm 0.17 \qquad Planck + WP + Union2.1 \\ w &= -1.13^{+0.14}_{-0.13} \qquad Planck + WP + SNLS \end{aligned}$$

Also, the constraint using Planck and the measurement of H_0 of Riess gives

$$w = -1.24^{+0.18}_{-0.19} \tag{1.1}$$

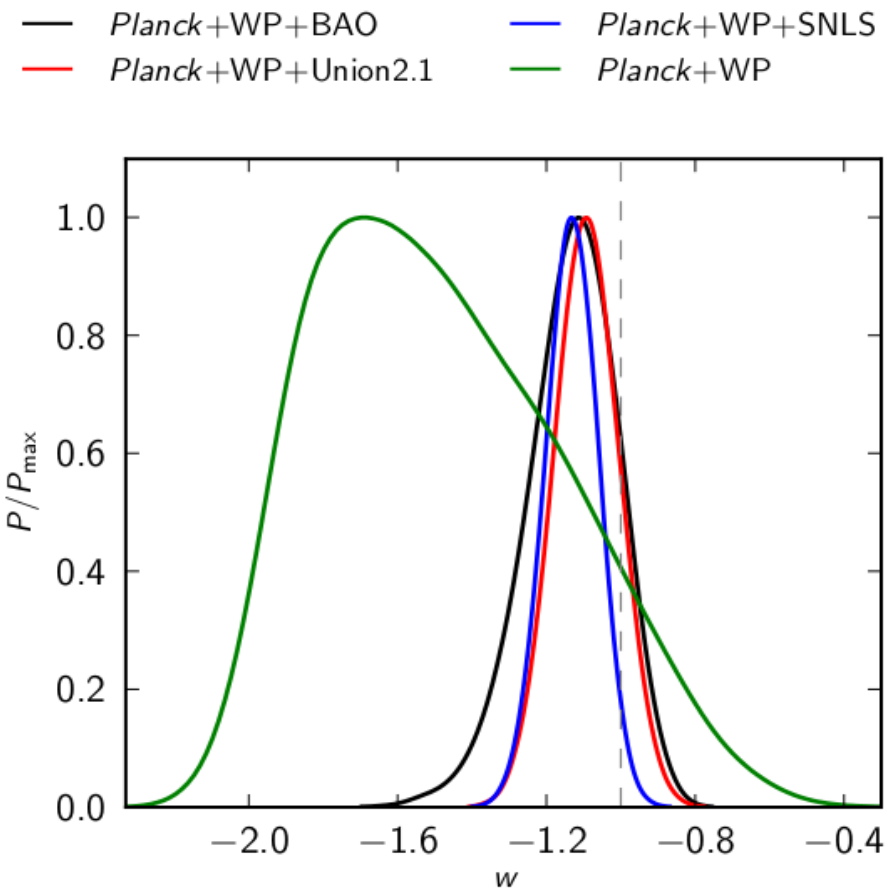

Fig. 1.4 Marginalized posterior distributions for the dark energy equation of state parameter w (assumed constant), for Planck+WP alone (green) and in combination with SNe data (SNLS in blue and the Union2.1 compilation in red) or BAO data (black). The dashed grey line indicates the cosmological constant solution $w = -1$. Figure taken from [6].

These results reveal some tensions between the supernovae data sets and the ΛCDM cosmology in agreement with Planck. The BAO data are in excellent agreement with the Planck standard model. In turn, the addition of the H_0 measurement, or SNLS SNe data, to the CMB data favors models with exotic physics in the dark energy sector. The SNLS data favors larger dark energy density than Planck within the ΛCDM model. The tension can be eased away by making the dark energy density to fall away faster in the past than for a cosmological constant [6]. As it is demonstrated in [142] the constraints on dark energy parameters for varying w models are the same as the constraints on constant w models if we consider w_{eff} for varying dark energy models.

Another important source of evidence are observations of the large scale structure of matter in the universe. They are useful to carry out tests of the expansion of the universe and hence to the dark energy phenomenon. For instance, large-scale galaxy redshift surveys, like the 2dF Galaxy Redshift Survey, SDSS, WiggleZ, etc [57, 58, 236] provide valuable information about the galaxy distribution in space and redshift which leads to shed light about the nature of dark energy. Because the process of formation of structures of matter in the universe and the history of expansion have occurred simultaneously as a whole, the pace and structure of the growth of matter over-densities depends very closely on the geometry and rate of expansion of the universe.

Therefore information about the physical nature of the mysterious dark energy can be extracted from features of the history of structure formation. For instance, there are two important methods of testing the physics of dark energy in these surveys. The first one are the measurement of the cosmic distance using the baryon acoustic oscillations [38, 86, 95, 117, 275]and the second one are measurements of the growth of structure using redshift-space distortions [69, 73]. In these surveys another host of tests of cosmological models are available, of our particular interest are those for probing the cosmic expansion history via the Alcock-Paczynski effect [68] and those to measure the galaxy bias by measurements of the topology of the cosmic density foam.

1.2.2 Other Observations in Tension with the Standard Model

Although the most concerning conundrums of the standard model are the nature of dark energy and dark matter, there are another features of the model which are worth to keep under sharp sight. For example, after the recently launched Planck's dataset, the analysis has indicated that different sets of data give rise to estimations of parameters potentially in tension within the standard model. Some of the most discussed in the literature lately, are the cases of the Hubble constant and counts of clusters of galaxies just to mention a couple of remarkable examples. However it is worth mentioning that because the field is passing through a decisive stage of testing and experiments are still running, all the discussion in this section might become obsolete very soon. The important thing that I would like to point out, is that even though the standard model were to remain as the best fit, we must test this model stoically.

Firstly, the Hubble constant H_0 has been the most popular testable quantity related to the accelerated expansion within the standard cosmology. This parameter quantifies the current rate of expansion of the universe and, within the ΛCDM scope, it also corresponds to the proportionality constant in the linear relation between redshifts and distances of neighbor galaxies.

In recent times, precise estimations of the Hubble parameter have been obtained from different observations like the CMB, BAO and SNe. Using the temperature angular spectrum from Planck and the polarization data from WMAP9 the estimated value of H_0 at 68% c.l. is given by $H_0 = 68 \pm 1.4$ km s^{-1}Mpc^{-1}. This value turns out to be low in comparison with previous measurements of the CMB and with the value obtained using supernovae data alone. For example, from estimates using only SNe $H_0 = 74.2 \pm 3.6$ km s^{-1}Mpc^{-1} measured by the SHOES team [258]. However, in more recent works, this story has been advancing towards a set of consistent estimates. In specific, a recalibration of the absolute distance of NGC 4258, one of the three distance anchors involved in this direct measurement, is given in [191]. They report a slightly smaller value determined from this anchor $H_0 = 72.0 \pm 3.0$ km s^{-1}Mpc^{-1}. In addition, Efstathiou in 2013 suggests that possible biases were introduced in the Cepheid period-luminosity relation by subluminous, low-metallicity Cepheids and shows some sensitivity of the results. He finds 70.60 ± 3.3 km s^{-1}Mpc^{-1} using only one recalibrated anchor and 72.5 ± 2.5 km s^{-1}Mpc^{-1} combining three anchors [110]. The next year, Betoule et. al use the combination of the CMB, BAO and SN Ia data to constrain the value of the Hubble parameter at better than 2% as $H_0 = 68.50 \pm 1.27$ km s^{-1}Mpc^{-1} [37] which is in (1.4σ) agreement with the first recalibrated value. It is important to mention that the value of the Hubble constant is currently being

updated frequently due to the speed at which the amount of data grows and the intense research currently underway.

Another source of tension arisen from Planck as well, is a possible discrepancy between constraints for cosmological parameters using CMB data and BAO, and those coming from the counts of galaxy clusters using the Sunyaev Zel'dovich effect [5]. These number counts as a function of redshift is usually quantified by the ratio of total matter density to the critical density $\Omega_m = \Omega_b + \Omega_{dm}$ and the amplitude of overdensities at $8h^{-1}\ Mpc$, σ_8 which are derived parameters. The Planck CMB constraints for Ω_b and σ_8 parameters, differ significantly from the ones arisen from SZ counts in the same survey [figure (1.5)].

This leads to a factor of 2 larger number of predicted clusters than is actually observed. There is therefore some tension between the results from the Planck CMB analysis and the current cluster analysis. It is claimed in [5] that this tension may arise from systematics and statistical residual errors. However the possibility this discrepancy is real should not be discarded. Nevertheless, this tension can be eased down by introducing massive neutrinos to the model [28] or well by considering a more complex bias dependence [7].

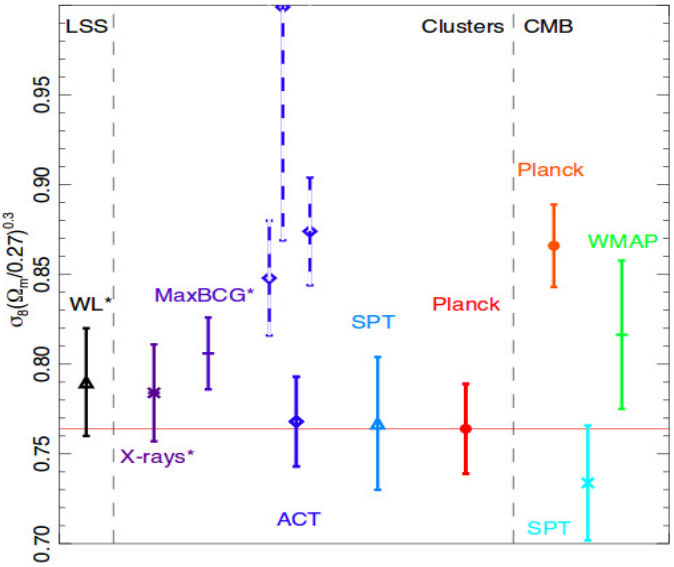

Fig. 1.5 Constraints at 1σ on $\sigma_8(\Omega_m/0.27)^{0.3}$ from different experiments of large scale structure, clusters and CMB. The solid line is the estimation for the parameter using CMB from Planck. Figure taken from [5], further details about this plot can be found there.

1.2.2.a A Comment on the Need of Testing Gravity at Cosmological Scales

Finally, as a conclusion of this section, I'd like to quote a very interesting comment made by Peebles in his acclaimed review about the cosmological constant [232]. "The observations of supernovae in distant galaxies offer evidence for the detection of dark energy, under the assumption that distant and nearby supernovae are drawn from the same statistical sample (that is, that they are statistically similar enough for the purpose of this test). There is no direct way to check this, and it is easy to imagine differences between distant and nearby supernovae of the same nominal type. Astronomers have checks for this and other issues of interpretation of the observations used in the cosmological tests. But it takes nothing away from this careful and elegant work to note that the checks seldom can be convincing, because the astronomy is complicated and what can be observed is sparse. What is more, we do not know ahead of time that the physics that is well tested on scales ranging from the laboratory to the Solar System survives the enormous extrapolation to cosmology." This assertion set on the table, two interesting points to keep in mind when one is trying to shed some light on the dark energy problem: first, as we are not certain of physics driving the dynamics of gravity at very large scales, we can't be sure if the assumptions involved in the discovery of the expansion hold within every cosmological model different than the standard one. Second, and the most important in my opinion, gravity is not fully tested at cosmological scales hence extrapolating GR as a model describing gravitational effects at these scales a priori may be a hazardous step. Even though it has been a successful tool to fit the data, the dark energy problem and other puzzles are enough reason to keep a sharp eye on it and to explore other feasible alternatives.

1.3 Alternatives to The Standard Cosmology

Since the effects of recession of distant galaxies and the observed rotation curves around the center of galaxies are merely due to gravity which, in the case of metric theories, are originated by geometric properties of space-time we do not have a hint on whether these phenomena are generated by exotic dark components or by a different law of gravity than GR. Thus, as long the cosmological constant problem remains unsolved and dark matter remains undetected, the possibility that the universe is described by a model different than the standard one stands as feasible.

The reason why GR has been granted as the standard model to describe the structure and dynamics of the universe at cosmological scales is merely historical. Furthermore, since cosmology is a rather young discipline, we live in a crucial moment of its history. It is worth mentioning that GR has not being fully tested observationally so far and we are placed indeed in the golden moment of precision cosmology at which highly accurate detections are about to define the fate of either the standard model and its alternatives.

Motivated by these circumstances, many people have devised various alternatives to the standard cosmology. A common feature of almost all alternative models is to introduce new degrees of freedom apart from the metric and the matter fields. We can distinguish the following two large categories of such theories: those which introduce new types of matter or extra matter degrees of freedom and those in which the law of gravity is modified, that is, gravity is mediated by more degrees of freedom than the metric or well that the dynamics of the metric is not governed by GR. In this work and this section we are concerned about the second category which is usually denominated as modified gravity. In the following subsection we'll make a brief review of the variety of modified theories of gravity. We'll mention in some relevant cases for this work, the theoretical basics on which they were constructed and some of the advances in the phenomenological aspects, that is the state of art of these theories in describing consistently observations.

In this work we turn our sight to alternative theories describing the dark energy phenomena rather than dark matter

1.3.1 Lovelock's Theorem

There is an important theorem on which the structure of General Relativity and its solutions rely and give us important hints on how the resulting phenomenology should work. In some alternative theories of gravity this theorem fail, however this allows new behaviors that would otherwise be impossible.

This theorem [80, 193] limits the theories that one can construct from the metric tensor alone. This theorem states that if we try to create any gravitational theory in a four-dimensional Riemannian space from an action principle involving the metric tensor and its derivatives only, then the only field equations that are second order or less are Einstein's equations and/or a cosmological constant. The Lovelock's theorem means that to construct metric theories of gravity with field equations that differ from those of General Relativity we must do one (or more) of the following:

- Consider other fields apart from the metric.
- Allow the introduction of higher order derivatives than second order.
- Consider different dimensionality of space-time.
- Give up on either rank $(2,0)$ tensor field equations or the symmetry of the field equations.
- Consider non-local actions.

1.3.2 Overlook to the Zoo of Modified Theories of Gravity

The most popular sort of modified theories of gravity are those in which new degrees of freedom apart from the metric are introduced. Scalars, vectors and tensors are introduced in order to produce specific features in different theories. In dynamical relativistic theories considered in here, new kinetic terms are added to the Einstein-Hilbert action involving these extra degrees of freedom and some of them introduce mass terms and/or interaction terms. In principle there's no way to figure out whether these alternative theories are models where gravity is being modified or if the model is general relativity with exotic matter contents in the universe. However, we adopt the most common convention to classify such models depending on how the new fields are coupled to matter. When the coupling to matter is more complex than the minimal one, that is, when not only the metric but also the extra fields couple to the matter fields we say that we are dealing with a model of modified dark energy. In turn, when the new fields only couple to the metric and matter couples minimally to the metric we say we deal with a modified theory of gravity. In these models test particles travel

along modified geodesics. Said in other words, matter fields are coupled only to the metric, for that reason the matter "feels" the modification only because the geometry is affected. There is a large collection of this last category, among the most important classes we can outline the following:

- **Scalar Tensor Theories** Scalar Tensor theories are one of the better understood modification of general relativity [35, 165]. Historically, its first version, the Brans-Dicke theory became one of the paradigmatic alternative theories that helped to conceive and design tests of general relativity. The simplicity of their formulation has allowed to solve exactly their equations in many interesting physical situations. Particularly, these models have been popular when trying to model a varying coupling constant, specially the gravitational strength. In this work, this class of theories is our main concern since they arise as a limit of more complicated and realistic theories.

- **Galileons and Horndenski Theories** Galileon theory was originally proposed by Nicolis et al. [222] to carry out an independent analysis of a large class of modified gravity models. The modification to General Relativity on perturbed Minkowski space is achieved by an additional scalar field, the galileon, with derivative self-interactions. The vacuum Lagrangian of this theory is invariant under translations in the galileon field $\pi \to b_\mu x^\mu + c$ which is the generalization of the galilean symmetry. This model was inspired in the D-brane DGP gravity, the boundary effective theory arisen in the brane is described by

$$S_{\text{eff}}^{\text{DGP}} = \int d^4x \left[\mathscr{L}_{\text{GR}} + \mathscr{L}_\pi^{\text{DGP}}\right], \tag{1.2}$$

where

$$\begin{aligned}
\mathscr{L}_{\text{GR}} &= \frac{1}{16\pi G_N}\left\{\frac{1}{4}h^{\mu\nu}\left[\partial^2\left(h_{\mu\nu} - \frac{1}{2}h^\alpha_\alpha\eta_{\mu\nu}\right) + ...\right]\right\} + \frac{1}{2}h_{\mu\nu}T^{\mu\nu}, \\
\mathscr{L}_\pi^{\text{DGP}} &= \frac{1}{16\pi G_N}\left\{\frac{1}{2}\left[3\pi\partial^2\pi - r_c^2(\partial\pi)^2\partial^2\pi\right]\right\} + \frac{1}{2}\pi T.
\end{aligned}$$

Where r_c is the crossover scale [75]. This action has basically two pieces: a GR action plus a modifying term due to the scalar bending mode in the brane. This effective theory is valid only in the decoupling limit where all interactions are neglected except the self-interactions of the scalar. Nicolis noticed that this term was made only of second derivatives of the bending mode. This feature

ensures that the resulting equations of motion are of second order exclusively so that the Cauchy problem is well defined. One might expect that almost any co-dimension one braneworld model with large distance deviations from GR will be described, in part, and in some appropriate limit, by a generalised π Lagrangian possessing the Galilean symmetry. Thus, motivated by these basic features, Nicolis generalized the boundary effective action to build up the galileon theory [50, 54, 222]. In these theories the self-interactions can help shut down the scalar at short distances through Vainshtein screening. In the decuopling limit, the action is given by

$$S[h_{\mu\nu},\pi] = \int d^4x \ \left[\mathscr{L}_{GR} + \mathscr{L}_{\pi}\right],$$

where

$$\mathscr{L}_{\pi} = \mathscr{L}_{gal}\left(\pi, \partial\pi, \partial\partial\pi\right) + \pi T$$

represents the generalisation of the π-lagrangian in DGP gravity. The vacuum part of the generalised lagrangian $\mathscr{L}_{gal}$ gives second order field equations and is assumed be invariant under galilean transformations up to a total derivative. The most general lagrangian with such property in four dimensions is [223]

$$\mathscr{L}_{gal}\left(\pi, \partial\pi, \partial\partial\pi\right) = \sum_{i=1}^{5} c_i \mathscr{L}_i\left(\pi, \partial\pi, \partial\partial\pi\right) \tag{1.3}$$

where the ci are constants, and

$$\begin{aligned}
\mathscr{L}_1 &= \pi \\
\mathscr{L}_2 &= -\frac{1}{2}(\partial\pi)^2 \\
\mathscr{L}_3 &= -\frac{1}{2}\partial^2\pi(\partial\pi)^2 \\
\mathscr{L}_4 &= -\frac{1}{2}\left[(\partial^2\pi)^2 - (\partial\partial\pi)^2\right](\partial\pi)^2 \\
\mathscr{L}_5 &= -\frac{1}{2}\left[(\partial^2\pi)^3 - 3(\partial^2\pi)(\partial\partial\pi)^2 + 2(\partial\partial\pi)^3\right](\partial\pi)^2.
\end{aligned}$$

An even more general class of scalar tensor theories yielding second order field equations has recently been presented in [53], and is now known to be equivalent to Horndeski's general theory [148] in four dimensions [296].

- **Dvali-Gabadadze-Porrati (DGP) Gravity**

  The DGP model, developed by Dvali, Gabadadze and Porrati [104] is the most praised braneworld model exhibiting quasi-localization and an infra-red modification of gravity. The model admits two regimes: The normal branch and the self-accelerating branch. The self-accelerated one has been phenomenologically appealing since it gives rise to cosmic acceleration without the need for dark energy [55, 56, 91]. However, perturbations upon the self-accelerating vacuum are ghosts [52, 81, 252], or in other words physically bad behaving solutions. Though the normal branch is not as interesting phenomenologically it is more healthy and brings the most consistent non-linear approach of massive gravity. In contrast to massive gravity, in the normal branch of DGP the Vainshtein mechanism works well, screening the longitudinal graviton without introducing any ghosts [56, 92]. The breakdown of classical perturbation theory at the Vainshtein scale can be linked to quantum fluctuations on the vacuum becoming strongly coupled at around 1000 km [103, 195].

- **Einstein-Aether Theories** These vector-tensor theories have been of great interest over the past decade [162, 328]. They have the particular property that they favor a preferred reference frame and have become a theoretical framework for studying violations of Lorentz symmetry in gravity theories. In the Einstein-aether theory [162] violations of Lorentz invariance arise within the framework of a diffeomorphism-invariant theory. The presence of a Lorentz-violating vector field is the so called aether and it dramatically affects cosmology since it can lead to a renormalization of the Newton constant [59], leave an imprint on perturbations in the early universe [189], and in more elaborate actions it can even affect the growth rate of structure in the Universe [161, 295].

- **Bimetric Theories**

  The first formulation of a bimetric theory was due to Rosen [261, 262]. It is about introducing an extra non-dynamical rank-2 tensor into the theory. However, it has been found that Rosen's theory leads to the existence of states that are unbounded from below in their energy. As a consequence, this property leads to serious violations to the constraints on pulsars that have been imposed by observations of millisecond pulsars [83]. In following years there appeared number of proposals of a viable bimetric theories of gravity. For instance,

Drummond's bimetric (or "bi-vierbein") theory, which is claimed to mimic the dark matter in spiral galaxies [99]. More recently, Bañados and collaborators have shown that a general form of bigravity, which includes specific forms previously proposed in [294] might allow one to account for some aspects of the dark sector [196, 197].

- **Higher Derivatives and Non-Local Theories**

  One way to extend GR is to allow the field equations to be higher than second order. Indeed, such a generalization might be considered desirable as it will cause the resulting theory to be renormalizable. However, such modifications of gravity hold instabilities such as ghost-like degrees of freedom [177].

  Among these modified theories the fourth-order theories of gravity have a long history and are quite popular nowadays because they hold potentially interesting cosmological phenomenology, also they ease in some extent the non-renormalizability of GR [225, 290, 324, 335]. These theories generalize the Einstein-Hilbert action by adding additional scalar curvature invariants to the action or by making the action a more general function of the Ricci scalar (usually called $F(R)$ theories) than the simple linear one that leads to Einstein's equations. Such theories, have been intensively studied [88, 225, 270, 297]. This interest started in the 1960s, 70s and 80s by the discovery that the quantization of matter fields in an unquantized space-time can lead to such theories [310] and that $F(R)$ theories can have improved renormalization properties [136, 293].

1.3.3 The Need of Screening Mechanisms in Modified Theories of Gravity

The astonishing success of general relativity to describe the observations at the solar system and laboratory scales places the theory in a leading place among all the possible theories of gravitation. This fact sets stringent requirements for any theory of gravity aiming to be a feasible description of gravitational phenomena at very large scales. Specifically, many modified theories of gravity aimed to shed light over unsolved pieces of GR at cosmological scales, however in order to stand as viable they are required to pass the solar-system tests as victoriously or better than GR. A way to overcome this tight constraint has been to screen the extra degrees of freedom responsible for the modification, the effect is that these theories mimic GR at the well tested regimes so they result triumphant as well.

Many of the most relevant modified theories today introduce a light scalar to modify gravity. Within these set of models one roughly can distinguish two large

classes of theories: the ones that add curvature invariants to the spacetime which are equivalent to the classic scalar-tensor theories [65, 66] and the ones that give "mass" to the graviton [4]. The second class of theories is more subtle than the first but also reduces to scalar-tensor theories on sub-Hubble scales as we'll see later on. Both sorts of theories have quite different screening mechanisms to hide the scalar mode at small scales. In the first type, the scalar is screened via the so-called chameleon mechanism, basically it consists in giving a effective mass to the scalar that depends on the environmental density [152, 170, 171]. Theories such as DGP, and its cousins the galileons, screen the scalar via the so called Vainshtein mechanism [20, 313], which is accomplished by dynamical strong coupling effects that suppress the scalar on small scales [195, 221].

1.4 Thesis Goals and Outline

In this Thesis I report the results of two main research works pointing to solve a main single goal: to facilitate a way to estimate the viability of a wide set of modified theories of gravity, in particular we study general non-linear scalar-tensor theories with kinetic self-interactions driving a screening mechanism of the scalar a la Vainshtein. Among this set, our treatment is restricted to a subset of theories which tend to behave as the Brans-Dicke theory at cosmological scales. This goal, rather than being a concise research problem to be solved thoroughly here, should be thought as a north-star-like goal. However keeping it in mind has helped to define and solve small specific problems that being joint together have brought insights on how to design possible solutions to the north-star-like objective and to give rise to further questions and specific problems in the same direction.

This current chapter is devoted to put into context the modified gravity subject and the problem of this thesis. We aim to introduce the reader to the history of gravitation and give to her/him a broad overview of the prototypical paradigms and state of art in the discipline as far as it's relevant for the further parts of this work. The remaining bit of the work is formed mainly by two parts at which the concise problems are addressed. Along the second chapter we explore the standard model of cosmology and explore briefly the history of the universe according to such framework, this will help us to understand how the modifications in alternative theories arise and also to contrast their phenomenological implications with those of ΛCDM.

Chapters in the first part are devoted to present theoretical and observational frameworks, tools and implications regarding to cosmological phenomena. In particular

[4] braneworld theories fall into this category since its has a resonance width playing the role of a mass.

we study two different theories, both very simple modifications of general relativity. Firstly we explore the Brans-Dicke theory and secondly a particular case of its generalized cousins: the effective scalar-tensor theory. In despite of the simplicity of these theories, they occupy a special place among the modified theories since they arise as limits of more complex and realistic theories at very large scales when self interactions can be neglected. The mentioned limits in both cases arise in very different prescriptions which are prototypical frameworks to study phenomenological aspects of modified theories of gravity. For the first BDT case, we actually provide a proof in the second part of this thesis. There we demonstrate that the BD theory arises as a limit of the galileon theory when the observer stands far away from the source well outside the Vainshtein region[5] of a bounded source. Because the Vainshtein threshold lies at scales smaller, the outer region is closer to the cosmological regime and hence the galileon behaves as a simple linear Brans-Dicke field. The second theory studied here, the effective scalar-tensor theory, is built up in a phenomenological way. Starting from a parametrization of the equations governing the growth of sub-horizon perturbations for a broad set of modified theories involving a scalar, one arrives to specific functional forms for some observables like the growth function and the lensing potential. On the other hand, neglecting mass and interaction terms and using a power law ansatz for the growth, a specific scalar-tensor theory emerges and we name it *effective scalar tensor-theory*.

Chapter 3 is devoted to study theoretical aspects of the Brans-Dicke theory (BDT). Here we adopt the standard interpretation of the scalar as a dynamical gravitational strength however, in order to carry out a more general analysis we consider two types of models: the classical BDT in which the initial conditions for the scalar are fixed to the value of the Newton constant today that would be measured in a Cavendish-like experiment, we call these models "restricted" (rBDT); and a more general class where the initial condition for the scalar is a free parameter so its cosmological values may differ from that at solar system. We call these models "unrestricted" (uBDT). We should mention that in the analysis carried out in this chapter we are not concerned on the origins of the expansion history. We skip this subject since it is well known that there's a degeneracy between ΛCDM and some self-accelerated alternative theories of gravity in that both lead to the same predictions [107]. Nevertheless this degeneracy can be broken down by testing perturbations of these modified models either by measurements of the CMB and the Large Scale Structure formation of the universe. Therefore, in this work we consider the standard ΛCDM prescription for matter and we limit to study the effects only due to the modification of the gravitational sector.

[5] as we'll see in chapter 6, at this region the self-interactions are dominant and drive the mechanism responsible of the screening of scalar allowing the theory to pass the tests at the solar system.

In chapter 4 we test the BDT with cosmological observations like the CMB and LSS. First we derive strong cosmological constraints on the BDT of gravity using Cosmic Microwave Background data from Planck. We argue that these constraints have greater validity than for the BD theory and they can tell us about the viability of some Horndeski theories which approximate BDT on cosmological scales. Let us recall that Horndenski theories are the most general second-order scalar-tensor theories with derivative self-interactions. In this sense, our constraints place strong limits on possible modifications of gravity that might explain cosmic acceleration. Additionally we derive complementary constraints by using LSS and the Alcock-Pazcynski test. Chapter 5 has the same structure as chapters 3 and 4, however we limit to derive constraints only using the CMB.

The second part is made only by chapter 6 where we present a generalization of the parametrized post-Newtonian (PPN) formalism to treat theories that present Vainshtein mechanism. This framework is useful on one hand to determine the solutions of the corresponding modified Einstein and field equations in the weak field and slow motion approximation at small scales like our solar system for any type of source. We named this extension of the PPN formalism as the Parametrized Post-Newtonian Post-Vainshteinian formalism (PPNV). One of the advantages of this PPNV formalism is that the different components of the solution of the metric are linked to testable observables so it turns out to be a powerful tool to perform observational tests suitable for theories presenting Vainshtein screening mechanism. We apply the formalism to a particular case in this part: the cubic galileon. As mentioned above, like any theory of its type, the cubic galileon theory has a characteristic classical strong scale additional to the gravitational strong scale corresponding to the Schwarzchild radius: the Vainshtein radius. The dynamics of the theory inside and outside this radius behave dramatically differently. In the outer region the standard theory is suitable to be treated with standard perturbation theory thanks to its linear nature, whilst in the inner one the dominant non-linearities in the standard theory makes its almost unsolvable. Happily, these issue can be turned around by using the dual formulation of the cubic galileon firstly proposed by [137] and improved by [233]. In this part of the thesis we find the relevant PPNV solutions for the cubic galileons in both regimes. For scales outside the Vainshtein region we use the standard theory and, in turn, for scales where the Vainshtein mechanism is carried out, we apply the formalism to the dual cubic galileon theory which is suitable to be treated perturbatively.

Finally, we knit the individual conclusions arisen in the various chapters of this thesis into the final summary and outcome of this thesis. This material will bring up an overall perspective that will allow us to draw up future research projects and achievements to be completed beyond this work.

CHAPTER 2

STANDARD COSMOLOGY BASED ON GENERAL RELATIVITY

2.1 Introduction

As we already realise in the introduction, during the first half of the XX century, after General Relativity was launched by Einstein, it was confronted with difficult questions and tests either theoretical and phenomenological. Once after GR passed them it staged as the most respected and solid paradigm to describe gravitation. The realisation that the gravitational interaction was not an interaction like electromagnetism but rather a manifestation of the geometry of spacetime itself, brought a completely revolutionary way of conceiving not only gravitation but many fundamental conceptions about spacetime and matter. As it is well known, the main building blocks of GR are two principles: the equivalence principle (all bodies fall the same way in a gravitational field) and the Mach's principle.

Technically, GR is grounded on the following notions: spacetime is a four-dimensional manifold on which is defined a metric, $g_{\mu\nu}$, of Lorentz signature. This metric is related to the matter distribution over space-time by Einstein's equations. These complex non-linear relations describe how the geometry of the spacetime is affected by the matter contained in it . The way in which physics operates in this context relies on the principle of general covariance which can be stated as: the metric and quantities derivable from it are the only spacetime quantities that can appear in the equations of physics. Equations describing the physics should reduce to the equations satisfied in special relativity where the metric is flat. Thus physical quantities must be the same type of tensorial objects as in special relativity [61, 318].

In order to build up an equation satisfied by the spacetime metric, we need a key ingredient: the Mach's principle. It implies that the geometry of the spacetime should not be determined a-priori, rather it is influenced by the matter distribution in the

universe [46, 318]. Thus the spacetime is not just a background on which the laws of physics lay but also a dynamical entity which responds to matter. A way to accomplish the previous is to compare the description of the tidal force in Newtonian gravity and GR and the Poisson equation. This should be done using the requirement that the Bianchi equation holds, as a result the analogy will lead us to the Einstein equations [318]:

$$G_{\mu\nu} \equiv R_{\mu\nu} - \frac{1}{2} g_{\mu\nu} R = 8\pi G_N T_{\mu\nu}. \tag{2.1}$$

Where G_N is the Newton's constant. These Einstein equations (EE) imply that $\nabla^\mu T_{\mu\nu} = 0$, so for a perfect fluid this equation contains the whole amount of information about the motion of matter. They also imply that for a test body whose self gravity is weak enough to be neglected must travel on a geodesic of the metric. Thus the EE are consistent with the basic principles of GR. Further details and a nice interpretation of this model can be found in [243].

2.2 The Standard Homogeneous and Isotropic Universe

Since long time ago it has been assumed that the universe is isotropic and homogeneous basically because we do no occupy a special position in the universe and also because there are not preferred directions in space on sufficiently large scales. It is well known that this hypothesis has been assumed since the ancient times of Coperncous and it is known as the cosmological principle. However, until modern times, observations of distribution of galaxies have confirmed these assumptions. Counts of radio sources and the isotropy of X-ray and γ-ray background radiation also support such hypothesis. Furthermore, the discovery of the cosmic background thermal radiation which seems to be uniform and isotropic at high precision all over the universe has strongly confirmed the cosmological principle. The mathematical formulation of this assumption raises from the following premises [318]

- Homogeneity means: at an instant of time every single point should look the same as any other. In other words there should exist a one parameter family of space-like hypersurfaces $\{\Sigma_t\}$foliating the space-time such that for each t and any x and y points in the hypersurface Σ_t exists an isometry of the metric which takes x into y.

- Isotropy means: A spacetime is isotropic if one can probe the existence of a set of congruent time-like curves with tangents denoted by u_a filling the spacetime. These hypersurace are such that for a given point x any two spatial tangent

vectors s_1 and s_2 orthogonal to u_a there is an isometry of the metric which rotates s_1 and s_2 and x and u_a remain unchanged. So there's no preferred u_a at all.

- u_a should be orthogonal to Σ_t, that is in a homogeneous and isotropic universe homogeneous surfaces should be orthogonal to the world lines of isotropic observers.

It has been shown that a requirement to preserve isotropy and homogeneity is that the curvature of the space-time must be constant [318]. This condition is satisfied for three types of geometries of the space-time: the flat structure held by the spacetime in special relativity, a 3-sphere spatial geometry finite with no-boundary usually called closed universe and a non-compact spacetime with hyperbolic geometry usually called open universes. At each case it is convenient to chose Cartesian, spherical or hyperbolic coordinates respectively to write down the spatial metric. Finally each surface is labeled by a parameter which is usually the "proper time" measured by isotropic observers. The most general form of the metric of spacetime with constant curvature is written in spherical coordinates

$$ds^2 = -dt^2 + a^2(t)\left\{\frac{dr^2}{1-Kr^2} + r^2(d\theta^2 + \sin\theta d\varphi^2)\right\} \tag{2.2}$$

I would like to stress here that in this work we are only concerned for the flat universe case where $K = 0$. In that case, the metric written in Cartesian coordinates reduces to

$$ds^2 = -dt^2 + a^2(t)(dx^2 + dy^2 + dz^2). \tag{2.3}$$

which is usually called the Friedmann-Robertson-Walker metric. In order to predict the evolution of the universe we need to insert this metric in the Einstein equations. Before that we need to specify the matter contents of the universe in terms of its energy momentum tensor $T_{\mu\nu}$. A fraction of the mass-energy of the universe is due to ordinary matter concentrated in galaxies. Due to the discrepancies in estimations of the total amount of baryonic mass by measurements of velocity curves of galaxies and the structure of the CMB it is quite probable that a non-visible exotic sort of matter (called dark matter) exists generating the required gravitational strength to reproduce the observations. Because on cosmic scales the mean velocity of galaxies is very small then pressure can be neglected and ordinary matter can be modeled as dust. There's also an energy contribution due to radiation which can be described as a fluid with

pressure $P = \rho/3$, at the present time this contribution is practically zero. However, along with neutrinos, it was the dominant contribution at early times of the history of the universe. Thus in general we might consider the matter contained in the universe as a perfect fluid with

$$T_{\mu\nu} = \rho u_\mu u_\nu + P(g_{\mu\nu} + u_\mu u_\nu) \tag{2.4}$$

Given the symmetries of the FRW spacetime, the 10 components of Einstein equations reduce to two independent ones.

$$G_{00} = 8\pi G_N T_{00} \tag{2.5}$$
$$G_{ss} = 8\pi G_N T_{ss} \tag{2.6}$$

where ss denotes any spatial-spatial component in Cartesian coordinates. In terms of the metric components the Einstein tensor above are given by

$$G_{00} = 3\frac{\dot{a}^2}{a^2} \tag{2.7}$$
$$G_{ss} = -2\frac{\ddot{a}}{a} - \frac{\dot{a}^2}{a^2} \tag{2.8}$$

where dotted quantities denote derivatives with respect to proper time. Equations (2.5) and (2.6) are equivalent to

$$H^2 = \frac{\dot{a}^2}{a^2} = \frac{8\pi G_N}{3} \tag{2.9}$$
$$3\frac{\ddot{a}}{a} = -4\pi G_N(\rho + 3P). \tag{2.10}$$

where $H(t) \equiv \frac{\dot{a}}{a}$ is defined as the Hubble rate, ρ is the energy density of the energy-matter contents of the universe, ρ_0 is its present value and

$$\rho_{cr} \equiv \frac{3H_0^2}{8\pi G_N} \tag{2.11}$$

is the critical density. H_0 is the Hubble rate today usually called Hubble's constant. Note that if the universe is flat, as we are considering in this work, $\rho_0 = \rho_{cr}$. The Friedmann equations above imply that the universe is not static, it is either expanding or contracting. The distance scale between isotropic observers is not constant in time

and there's no preferred center of expansion or contraction. The expansion of the universe produces that an isotropic observer sees that distant objects like galaxies have a recesion velocity which is proportional to their separation from the observer. The recession velocity of such objects is given by

$$v \equiv a\frac{dD}{dt} = HD \qquad H \equiv \frac{1}{a}\frac{da}{dt}. \tag{2.12}$$

The previous relation is called the Hubble's Law. It summarizes the observed relation between the distance of a galaxy (or any distant object) and its velocity inferred from the redshift of its spectral lines.

The redshift arisen in the spectral lines of distant galaxies is given by [318]

$$z+1 \equiv \frac{a_0}{a(t)} \tag{2.13}$$

where is conventionally $a_0 = 1$ and $a(t)$ is the scalar factor associated to the distant object. For nearby galaxies we can make the following approximation $z \sim HR$ where R is the proper distance to the galaxy.

Lets turn to study how the energy density of matter evolves in the universe according to this model. This can be achieved by using the FRW geometry and assuming that matter behaves as a perfect fluid described by (2.4) in the conservation equation $\nabla^{\mu} T_{\mu\nu} = 0$ resulting in the energy density and pressure of the cosmic fluid satisfying

$$\dot{\rho} + 3H(\rho + P) = 0 \tag{2.14}$$

which has different solutions depending on the sort of component being considered:

- For matter, $P = 0$ and its energy density behaves as $\rho_m a^3 =$ constant. This solution makes sense with our intuition since the number density of matter particles decreases at the rate in which the volume increases, that is a^3. In terms of the critical density we can write the matter density solution as $\frac{\rho_m}{\rho_{cr}} \equiv \Omega_m a^{-3}$. Observations show that the amount of visible baryonic matter is not sufficient to produce the velocity curves exterior components of galaxies, this has made people assume the existence of halos of "dark matter" in the surroundings of galaxies which would only interact gravitationally with the rest of matter. Thus, in the following we will distinguish baryonic matter from dark matter, though their density drops down obeying the same power law, we will denote them ρ_c and ρ_b respectively. Finally

$$\frac{\rho_{dm}}{\rho_{cr}} = \frac{\Omega_{dm}}{a^3} \qquad \frac{\rho_b}{\rho_{cr}} = \frac{\Omega_b}{a^3}. \tag{2.15}$$

- For radiation $P = \frac{\rho}{3}$ we find that the energy density of photons decrease as $\rho_r a^4 =$ constant. The energy density decreases even quicker than matter, because they lose energy due to the expansion. In terms of the critical density:

$$\frac{\rho_r}{\rho_{cr}} = \frac{\Omega_r}{a^4} \tag{2.16}$$

  here we consider as the radiation contribution due to photons and massless neutrinos then $\Omega_r = \Omega_\gamma + \Omega_\nu$, where the subindex γ and ν are associated to photons and neutrinos respectively.

- Cosmological Constant- Note that at early times right after inflation, the radiation term $\sim a^{-4}$ in the Friedmann equation dominates and term due to dark energy is negligible. At the matter dominated era sets on as scale factor a increases, the cosmological constant starts to be important until finally it dominates at late times. In terms of the critical density can be written as

$$\Omega_\Lambda = \frac{\rho_\Lambda}{\rho_{cr}} \tag{2.17}$$

With this behavior of the energy-matter components, the FRW equations can be re-cast as

$$\frac{H^2(t)}{H_0^2} = \frac{\rho}{\rho_{cr}} = \frac{\Omega_b}{a^3} + \frac{\Omega_{dm}}{a^3} + \frac{\Omega_r}{a^4} + \Omega_\Lambda \tag{2.18}$$

or

$$H^2 = \left(\frac{\omega_b}{a^3} + \frac{\omega_{dm}}{a^3} + \frac{\omega_r}{a^4} + \omega_\Lambda\right) \times (100 km/s/Mpc)^2 \tag{2.19}$$

where $\omega \equiv \Omega h^2$ and $h \equiv H_0/(100 km/s/Mpc)$.

2.3 The Birth of Baryonic Matter: Nucleosynthesis and Recombination

2.3.1 The Boltzmann Equation

Matter and radiation fluids in the early universe can be usually described in terms of a bath of particle excitations of the corresponding quantum fields. In particular, at high temperatures these interactions occur very quickly and this ensures thermodynamical equilibrium. The statistics of particles of each species is encoded in an equilibrium distribution function, which is homogeneous and isotropic, defined in the phase space [160]

$$f_i(p,T) = \frac{1}{e^{\frac{E_i(p)-\mu_i}{T}} \pm 1} \tag{2.20}$$

the coordinates of this homogeneous and isotropic phase space p and E_i are the modulus of the comoving spatial-momentum of the $i-th$ species and its energy respectively. The latter depends on the former as $E = \sqrt{p^2+m_i^2}$, which is energy-momentum relation corresponding to a classical relativistic massive particle . T is the temperature of the thermal bath where the reaction occurs. Finally $+/-$ corresponds to Fermi-Dirac/Bose-Einstein statistics for bosons and fermions respectively. μ_i is the chemical potential of the $i-th$ species. In the comoving frame, the number density, energy density and pressure can be expressed in terms of the distribution function as follows

$$\begin{aligned} n_i(T) &= g_i \int \frac{d^3p}{(2\pi)^3} f_i(p,T) \\ \rho_i(T) &= g_i \int \frac{d^3p}{(2\pi)^3} E_i(p) f_i(p,T) \\ P_i(T) &= g_i \int \frac{d^3p}{(2\pi)^3} \frac{p^2}{3E_i(p)} f_i(p,T) \end{aligned}$$

where g_i is the number of internal degrees of freedom. Let us consider a process like the following $1+2 \to 3+4$ in which incoming particles of types 1 and 2 produce outcome 3 and 4 types of particles. The Boltzmann equation governs how this reaction happens in an expanding universe as follows

$$\begin{aligned} a^{-3}\frac{d(n_1a^3)}{dt} &= \int \frac{d^3p_1d^3p_2d^3p_3d^3p_4}{16(2\pi)^2E_1E_2E_3E_4}(2\pi)^4 \\ &\times \delta^3(p_1+p_2-p_3-p_4)\delta(E_1+E_2-E_3-E_4) \\ &\times |\mathscr{M}|^2\{f_3f_4(1\pm f_1)(1\pm f_2)-f_1f_2(1\pm f_3)(1\pm f_4)\} \end{aligned} \quad (2.21)$$

As the universe expands the number of a given particle drops as the volume increases, that is $\sim a^{-3}$. So in absence of interactions the left hand side of the Boltzmann equation reflects that. Interactions between particles are described by the right hand side. p_i , E_i and f_i are the momentum, energy and occupation number of particles of the i-species and $\mathscr{M}$ is the amplitude of the interaction and it is determined by fundamental physics. The $(1\pm f_i)$ terms represent the Pauli blocking $(-)$ or the Bose enhancement $(+)$ depending whether the particles are bosons or fermions. The Dirac deltas involved, imply the energy-momentum conservation in the process. Energy is related to momentum in a relativistic way as $E=\sqrt{p^2+m^2}$. The total number of interactions is achieved by integrating over all 4-momenta space constrained to a sub-space satisfying $E=\sqrt{p^2+m^2}$. This is achieved by adding E_i in the denominator of the measure of the integral.

Despite the complexity of equation (2.21), it can be simplified thanks to the following facts:

- Scattering processes typically enforce thermal equilibrium. Scattering takes place so rapidly that distributions of many species end up into the Bose-Einstein and Fermi-Dirac distributions. Similarly for annihilations, if they occur at equilibrium , the total chemical potential has to be zero.

- For some processes out of chemical equilibrium, the equation to determine the chemical potential μ can be simplified by the feature of kinetic equilibrium turning it into an ordinary differential equation.

- In the limit when the energy is less than $E-\mu$ the quantum statistics can be ignored and the distributions become $f(E)\to e^{\frac{E-\mu}{T}}$. The Pauli blocking and Bose enhancement can be ignored.

In order to write the mentioned simplified version of the Boltzmann equation we first use that fact that at these limits

$$f_3f_4(1\pm f_1)(1\pm f_2)-f_1f_2(1\pm f_3)(1\pm f_4)\to e^{-\frac{(E_1+E_2)}{T}}\{e^{\frac{(\mu_4+\mu_3)}{T}}-e^{\frac{(\mu_1+\mu_2)}{T}}\}. \quad (2.22)$$

After defining the thermally averaged cross section as

$$\sigma_v \equiv \int \frac{d^3p_1 d^3p_2 d^3p_3 d^3p_4}{32(2\pi)^8 E_1 E_2 E_3 E_4} \delta^3(p_1+p_2-p_3-p_4)\delta(E_1+E_2-E_3-E_4)|\mathscr{M}|^2, \tag{2.23}$$

finally the Boltzmann equation is simplified to a simple ordinary differential equation for the number density:

$$a^{-3}\frac{d(n_1 a^3)}{dt} = n_1^{(0)} n_2^{(0)} \sigma_v \left\{ \frac{n_3 n_4}{n_3^{(0)} n_3^{(0)}} - \frac{n_1 n_2}{n_1^{(0)} n_2^{(0)}} \right\}. \tag{2.24}$$

The right hand side is order $n_1 n_2 \sigma_v$ while the left side is order $n_1 H$. Thus if the reaction rate is much larger than the expansion rate the only way to maintain equality is that the two terms on the right side cancel [97]:

$$\frac{n_3 n_4}{n_3^{(0)} n_3^{(0)}} = \frac{n_1 n_2}{n_1^{(0)} n_2^{(0)}} \tag{2.25}$$

which is typically called Saha equation.

2.3.2 The Epoch of Nucleosynthesis

Now we know, thanks to those efforts, that more than ninety percent of the baryonic matter in the universe is composed of hydrogen and helium. Both elements have been around since shortly after the beginning of the universe. Yet, hydrogen and helium together will not make anything as complex and as interesting as the earth, or a bacterium, or a refrigerator, or you and me. To do that we need carbon and oxygen and nitrogen and silicon and chlorine and every other naturally occurring element. Almost all the hydrogen and helium present in the universe today (and some of the lithium) were created in the first three minutes after the big bang. All of the other naturally occurring elements were created in stars [118].

The synthesis of elements during the early universe has been extensively studied since the 1950's by Gamow, Alpher and others [133, 251]. The initial detailed nucleosynthesis calculations were made by Peebles and Wagoner, Fowler and Hoyle (1967) [237, 239, 315, 316]. This study was motivated by a series of discoveries which made people realize that the primordial production of light elements was a pregalactic phenomenon. On one hand, the discovery of dwarf blue galaxies [272, 273] in which the abundance of Helium is normal while abundances of heavy elements are lower with respect to the solar neighborhood, has provided strong evidence for a universal pregalactic source of helium. Also, people found out that the expected amount of

deuterium existing in the intergalactic medium could not be produced by any galactic process [256] and neither by cosmic rays which usually produce rare light elements. On the other hand the increasing evidence that the CMB is of primordial origin, improvements in knowledge about nuclear physics and electroweak theory together with the development of better computational tools made people start to test the idea that light elements like hydrogen and helium could only be produced during the early universe [315].

In general using an arbitrary model, in order to predict the primordial abundances of D,^3He,^4He and ^7Li we need: the current temperature of the universe, the baryon density, the expansion rate and the neutron-to-proton ratio [230, 315]. Assuming that the standard electroweak theory is right [209, 322] at energy scales $\sim MeV$. In the context of GR, all that is needed to predict abundances of light elements is the baryon density. The single parameter that usually is used to tune the predictions of the standard BBN is $\eta_{10} \equiv 273\Omega_B h^2$ [230].

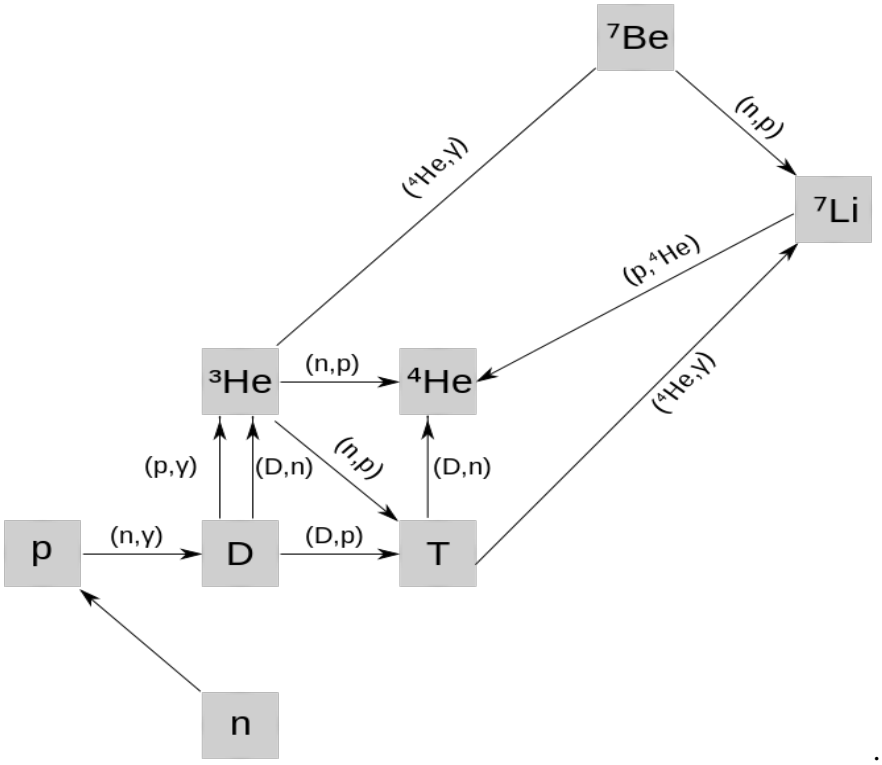

Fig. 2.1 Chain of nuclear reactions occurring during the nucleosynthesis epoch. Figure taken from [118]

At $T <\sim 100MeV$ the cosmic inventory was formed by photons, electrons, positrons and neutrinos which were all relativistic at that moment (see figure (2.1)).

The baryon number was conserved at those temperatures, the fraction of baryon-to-photon was $\eta_B = \frac{n_B}{n_\gamma} \sim 10^{-8}\Omega_B h^2 = constant$. The contribution from muon-antimuon pairs can be neglected since it decays exponentially via $\mu + \bar{\nu}_\mu \rightarrow e + \bar{\nu}_e$. If there had been no asymmetry in the initial number of baryons and anti-baryons both would be annihilated by $T \sim 1MeV$ and this story would not had been told , however there existed such a difference $n_B - \bar{n}_b \sim 10^{-10}$ and this ratio remains the same during the expansion. Antibaryons where annihilated away around $T \sim 1MeV$. At that temperature relativistic particles dominated in relation with baryons [102].

Thus, at that time the universe was dominated by relativistic matter and the Hubble rate at this stage is given by the following Friedmann equation [230]:

$$H^2 = \left(\frac{\dot{a}}{a}\right)^2 \sim \frac{8\pi G_N}{3}\rho \tag{2.26}$$

where $\rho = \rho_\gamma + \rho_e + \rho_\nu$ at the time of nucleosynthesis.

At temperatures above 30 MeV all the light nuclei existing in the universe were unstable. At this temperature baryons form a mixture of protons and neutrons in thermal equilibrium with each other and with electrons, protons and neutrinos. Masses of neutrinos are not very well constrained, however the oscillation experiments [127] imply their masses are below $1eV$ if there is no degeneracy. Therefore we can neglect the masses of the neutrinos [102].

A competition of the expansion rate, the electroweak rates of scattering processes of neutrons and protons and the nuclear reactions involved in the production of heavy nuclei, was responsible for the formation of the primordial light elements. At hight temperatures ($T > MeV$), the electroweak scattering processes are faster than the expansion rate then the neutron-to-proton ratio reached the equilibrium value. Once these scattering rates became less than the expansion rate, the ratio of neutron-to-proton "freezes-out" slowly increasing due to neutron decay [230].

The highest binding energy is the one of ^4He which is about $28MeV$. Nevertheless, ^4He cannot form at this temperature since the baryon density is not high enough for many-body interactions to occur in thermal equilibrium. Therefore, before any nucleosynthesis can occur, the temperature has to drop below the binding energy of deuterium which is about $2.2MeV$. But even at this temperature there are still far too many high-energy photons around for deuterium to be stable. This is due to the very low baryon to photon ratio [102].

As soon as deuterium becomes stable, nucleosynthesis happens around $T \sim 0.1MeV$. At this point, most of the existing neutrons are converted into ^4He, a small fraction turns into deuterium and some more is converted into ^3He and ^7Li. The

most abundant is ^4He, its mass fraction can be easily estimated by simple counting as [160, 230]

$$Y_P = \frac{2(n_n/n_p)}{1+n_n/n_p} = 0.25. \tag{2.27}$$

Where n_n and n_p are the number densities of neutrons and protons respectively. At this point, a whole nuclear process network sets in, leading to heavier nuclei production, until BBN eventually stops. It is worth to mention that the final density of ^4He is very weakly sensitive to the whole nuclear network, and a very good approximation is to assume that all neutrons which have not decayed at $T \sim 0.1MeV$ are eventually bound into helium nuclei.

The determination of all light nuclei produced during BBN, and a more accurate determination of ^4He , can be only achieved by solving a set of coupled Boltzmann equations. This is typically obtained numerically, although nice semi-analytical studies have been also recently performed [215] (see [160] for a more detailed review).

In principle, the direct way to determine how baryons end up at temperatures below $0.1MeV$ is governed by the Boltzmann equation. Strictly speaking we need to solve (2.24) for all nuclei. However two important simplifications give rise thanks to the facts: 1 . Helium is the heavier nucleus produced at appreciable levels and thus only hydrogen and helium (and their isotopes) need to be traced. 2. At $T > 0.1MeV$ the light nuclei production stops, and only free protons and neutrons exist. Then we need to find the neutron-to-proton ratio first and use its abundance as an input for the synthesis of helium and its isotopes [97]. Both simplifications rely on the fact that at high-energies close to the binding energies of nuclei, every time a nucleus is produced it is destroyed straightaway by a photon. To see in detail how this arises from the Boltzmann equation see the nice example for Deuterium in [97].

In order to draw how the Boltzmann equation works, we are going to consider a neutron-to-proton process. First we are going to study the process by which protons scatter into neutrons via weak interactions, for example by means of the reaction $p + e^- \rightarrow n + \nu_e$. This reactions keep neutrons and protons at equilibrium up to $T \sim MeV$. Thereafter one must solve the rate equation in order to track the neutron abundance. In the non-relativistic limit the proton-to-neutron equilibrium ratio is given by

$$\frac{n_p^{(0)}}{n_n^{(0)}} = e^{\frac{Q}{T}} \tag{2.28}$$

where $Q \equiv (m_n - m_p) \sim MeV$. As temperature drops beneath $1MeV$ the amount of neutrons decreases. If the weak interaction would be efficient enough to keep equilibrium then neutrons would simply disappear. However, in real world we have to solve equation (2.24) which in this case is

$$a^{-3}\frac{d(a^3 n_n)}{dt} = n_l^{(0)}\sigma_v \left\{ \frac{n_p n_n^{(0)}}{n_p^{(0)}} - n_n \right\} \tag{2.29}$$

where n_l is number of leptons (electrons, mouns, etc.). For convenience we can define $X_n \equiv \frac{n_n}{n_n+n_p}$ the fraction of neutrons to total nuclei and $\lambda_{np} \equiv n_l^{(0)}\sigma_v$. Using the previous definitions, equation (2.29) becomes

$$\frac{dX_n}{dt} = \lambda_{np}\left\{(1-X_n)e^{-\frac{Q}{T}} - X_n\right\}. \tag{2.30}$$

Taking into account that the contribution to energy from relativistic particles is given by

$$\rho = \frac{\pi^2}{30} g_{eff} T^4 \tag{2.31}$$

where g_{eff} is the effective number of relativistic degrees of freedom and it is dependent on the temperature. At $T \sim 1MeV$ $g_{eff} \sim 10.75$ [97, 102]. Originally, the full set of differential equations governing the whole net of reactions giving rise to the fractions of all nuclei at nucleosynthesis were solved by Wagoner and Peebles [97, 121, 122, 315].

2.3.2.a Observational Abundances of Light Elements

The abundances of primordial elements are inferred from measurements made in various astrophysical environments. Precision cosmology era has increased the number and precision of spectroscopic data over the past two decades. Currently, many efforts are being made due to the presence of relevant systematic errors which are comparable to the statistical uncertainties.

Helium - Deuterium and ^3He are converted into complex nuclei and thus their abundance decreases quickly as η increases [230]. The primordial abundance is inferred from measurements of the $^4He/H$ ratio in regions of hot, ionized gas in other galaxies [263]. The post-BBN evolution of ^4He can be simply understood in terms of nuclear stellar processes which, through successive generations of stars, have burned hydrogen into ^4He and heavier elements, hence increasing the ^4He abundance above

its primordial value [292]. Also Y_p can be obtained by indirect methods, for example from studies of Galactic Globular Clusters [268] and the CMB [6].

Deuterium- Deuterium (D) turns into complex nuclei and its abundance decreases as η_{10} increases [230] figure BNN. D and ^3He is converted into complex nuclei and thus it abundance decreases quickly as η increases [230]. It is the most fragile of the light elements and so its abundance has been declining since the big bang. The inferred deuterium ratio from various astrophysical observations lies around [160, 263]

$$\frac{D}{H} = (2.78 \pm 0.29) \times 10^{-5}. \tag{2.32}$$

It is worth to mention that D is an ideal baryometer since the BBN-predicted D/H ratio is a strong function of the baryon-to-photon ratio. A determination of the primordial abundance to 10%, leads to an η_b determination accurate to 6% [263]. Furthermore, since deuterium is faded away in stellar processes, and there are no astrophysical sites capable of producing deuterium in anywhere near its observed abundance [120], any observed D-abundance provides a lower bound to its primordial abundance.

Lithium- Lithium is produced in stellar processes, some stars destroy lithium and others produce it. The primeval value is inferred from the ^7Li abundance in the atmospheres of the oldest stars in the halo of our galaxy

$$(7Li/H) = (1.7 \pm 0.15)^{-10.} \tag{2.33}$$

The less massive halo stars have depleted some of their lithium, the "lithium plateau" for stars with higher surface temperatures suggests that these stars have not [263]. There is a long story with lithium and its determinations by many astrophysical means summarized in [160] . Lately some of them have been ruled out by the CMB which fits remarkably with deuterium abundance. A conservative bound of its abundance is an average and half-width of the available set of data as best estimate of the average and "systematic" error on $^7Li/H$, obtaining [160].

$$^7Li/H = (1.86^{+1.30}_{-1.10}) \times 10^{-10} \tag{2.34}$$

2.3.3 Recombination of Neutral Hydrogen

Decoupling of matter from the primeval plasma plays an important role in the origin of galaxies. The end of recombination of neutral hydrogen fixes the epoch at which non-relativistic bound systems started to form. It also fixes the time at which radiation decoupled from matter and started to travel freely forming the cosmic background radiation [240].

At temperatures around $1eV$, hydrogen and helium are both fully ionized [74] due to the fact that photons are still tightly coupled to their electrons via Compton scattering [97]. At these temperatures there are a very little fraction of neutral hydrogen. Since the binding energy of hydrogen is $\varepsilon_0 = 13.6eV$ one naively could think that the production of neutral hydrogen is natural. However due to the large baryon-to-photon ratio , any newly created hydrogen atom is enforced to be ionized [97]. Since helium has larger ionization potential than hydrogen, it recombines before while the former is fully ionized and the free electron is substantial.

At a temperature of about $T \sim 4000K \sim 0.4eV$, the amount of photons with energies above the hydrogen ionization energy drops below the baryon density of the Universe, and the protons begin to recombine to form neutral hydrogen. Photons and baryons were tightly coupled before recombination by Thompson scattering of electrons. During recombination the free electron density suddenly drops and photons scatter less frequently with electrons until finally the universe becomes transparent at the temperature $T_{dec} \sim 3000K$ when photons decouple from the electrons [102].

Lets analyze in more detail how the recombination of hydrogen is described by the Boltzmann equation. As long the reaction $e^- + p \rightarrow H + \gamma$ remains in equilibrium [97] the Saha equation is a good approximation

$$\frac{n_e n_p}{n_H} = \frac{n_e^{(0)} n_p^{(0)}}{n_H^{(0)}}. \tag{2.35}$$

When hydrogen recombines, the free electron density decreases and the ionization goes out from equilibrium and the Saha approximation breaks down. Since helium recombination is over at this point, it's acceptable to treat helium as fully neutral. Lets define $x_e = \frac{n_e}{n_H}$ were n_H is the total number density of hydrogen nuclei and n_e the number density of free electrons. The kinetic equation that describes the ionization rate is [240, 289]:

$$\frac{dx_e}{d\tau} = aC_r \left[\beta(T)(1-x_e) - n_H \alpha^{(2)}(T) x_e^2 \right]. \tag{2.36}$$

- The collisional ionization rate from the ground states is

$$\beta(T) = \left(\frac{m_e T}{2\pi}\right)^{\frac{3}{2}} e^{-\frac{B_1}{T}} \alpha^{(2)}(T) \tag{2.37}$$

  where $B_1 = 13.6eV$ is the ground state binding energy.

- The recombination rate to excited states is

$$\alpha^{(2)}(T) \sim \left(\frac{B_1}{T}\right)^{\frac{1}{2}} \ln\left(\frac{B_1}{T}\right). \tag{2.38}$$

- The reduction factor C_r is the ratio of the net dacay rate to the sum of the decay and ionization rates from the $n = 2$ level.

Decoupling occurs when the free electron fraction decreases so the ionization rate is slower than the expansion rate. This happens around $z^* = 1100$. (See [102] and [97] for further details). At this point recombination freezes and the ionization fraction tends to a constant value and photons become free to propagate without further scattering. As long as the temperature is larger than T_f, the reaction $p + e^- \to H + \gamma$ happens in equilibrium. The temperature at which H equates the rate γ_R is defined by the freeze-out temperature and it is defined by the following implicit relation

$$\left(\frac{T_f}{1eV}\right)^{\frac{1}{4}} e^{-\frac{B_1}{2T_f}} = 1.2 \times 10^{-13} \left(\frac{\Omega_m}{\Omega_b}\right)^{\frac{1}{2}}. \tag{2.39}$$

The final fraction is given by

$$x_R \equiv x_e(T_f) \sim 1 \times 10^{-5} \frac{\Omega_m^{1/2}}{\Omega_b h}. \tag{2.40}$$

A more accurate deduction of it, taking into account the exact Friedmann equation has been found by Peebles [238] and Mukhanov [213]. The optical depth to a certain z redshift is defined as the Thompson scattering probability of a photon integrated from z until today [102]

$$\kappa(z) \equiv \int_0^z \sigma_T n_e H^{-1} (1 + z')^{-3} dz'. \tag{2.41}$$

As we shall see later on, the universe is re-ionized at low redshift $z \sim 10$, which increases the optical depth by about an order of magnitude. This re-scattering of CMB photons affects in a considerable extent the evolution of the temperature and polarization fluctuations of photons in their way towards us. The temperature at which photons decouple from baryons can be estimated by equating the Thompson scattering

rate to the expansion rate $\Gamma_T(T_{dec}) = H(T_{dec})$, a rough estimate is $T_{dec} \sim 0.26eV$ and it happens at $z_{dec} \sim 1100$ [97, 102, 238].

2.3.4 Linear Cosmological Perturbations

In the introduction we already told the history on how it was discovered that the matter contained in the universe is uniformly distributed at very large scales. However, it is evident that matter is not evenly distributed at smaller scales, for example around our local surroundings. It is well known that on larger scales than our solar system, other similar systems clump together into galaxies, which at the same time form groups and clusters of galaxies. If we were to zoom out our sight and look at larger and larger scales, at some point we would observe a uniform heap of objects. when we lay close to that point (above 1 Mpc), fluctuations of the uniform homogeneous universe are perceptible and but quite small. At these scales the universe is not dense at all so it generates weak gravitational fields, and linearized theory of gravity provide reliable predictions. Said more precisely, these lumps can be modeled accurately by still assuming a FRW background geometry upon which small perturbations are set up by the inhomogeneities of matter. By assuming such an universe and applying linear perturbation theory to general relativity (or an alternative metric theory), a powerful predicting tool in cosmology arises.

Moreover, this powerful machinery has been useful to reproduce the observed structure of matter and the evolution of its fluctuations from the early stage to late times of our structured universe. Although the process of galaxy formation in recent epochs is well described by the Newtonian theory of gravity, a general relativistic treatment is required for perturbations with wavelength larger than the size of the horizon (super-horizon perturbations). Historically, the use of general relativity brought in the issue of gauge freedom. In order to fix consistently the coordinates, Lifshitz (1946) [194] introduced the "synchronous gauge", which has become the most popular gauge used to treat cosmological perturbation theory. However, this gauge has some drawbacks such as the appearance of coordinate singularities and some remaining gauge freedom. This was finally addressed by Bardeen (1980) [25] and others (e.g. Kodama and Sasaki, 1984) [174] by formulating an alternative approach in which only gauge-invariant variables for perturbations are used. Additionally, is important to mention that this wealthy paradigm of cosmological perturbation theory has been applied to successfully describe the observed anisotropies of the cosmic background radiation.

There exist a heuristic explanation on how these lumps in the universe are generated, a process usually called gravitational instability would be the responsible for the beginnings of the formation of the first inhomogeneities. This process is produced

basically by competing forces on one hand due to early gravitational potentials and pressure of photons on the other hand happening in a time close to the epoch of equality of matter and radiation. However, this answer is still inconclusive since still remains the question: How those first perturbations in space-time that we call gravitational potentials were generated? This question set up one of the most important problems in cosmology. A mechanism that explains consistently how this may happen, first proposed by Alan Guth in the 1980's [141], is the model of inflation. At first time, inflation was introduced to explain the uniformity of the temperature of the universe in the very early universe just before radiation domination era.

Soon after, it was realized that inflation provides also an explanation about the origins of perturbations [45, 139, 140, 146, 291]. Basically, the idea is that the initial conditions for perturbations in the universe are generated by quantum fluctuations of the scalar field, the inflaton, that generates the expansion of the universe during inflation. Thus, those small lumps in matter that perturb the homogeneous background (which were very well explained by Newtonian theory at sub-horizon scales) are the same lumps that leaded Lifshitz to propose the general relativistic cosmological perturbation theory that we use now. It is fascinating to realize that these cosmic fluctuations are connected to one of the most fundamental problems of physics and that this mechanism enjoys strong support from the CMB data.

2.3.4.a Setup of Linear Perturbations: Synchronous and Newtonian-Conformal Gauges

Thus the cosmological perturbations history summarizes as follows: small perturbations of the FRW space time are generated by quantum fluctuations of the inflaton, these grow all along the expansion history. During radiation era they oscillate due to gravitational instability producing the first structures of baryonic and dark matter, afterwards, matter tends to clump due to gravitational collapse produced by "gravitational potentials" which are nothing but the perturbations of the space-time. Now, Although this picture gives a reference to think about the evolution of perturbation, the exact physics behind changes depending on the gauge we chose.

Now, let us turn to formally study cosmological perturbation theory based on general relativity. We consider only spatially flat background space-times with isentropic scalar perturbations. The spacetime coordinates are denoted by $x_\mu, \mu = 0,1,2,3$ where x_0 is the time coordinate and x_i are the spatial coordinates. Here we adopt the Einstein's notation so repeated index means summation. Since we are perturbing the spacetime of an expanding universe, we use comoving coordinates $x_\mu = (\tau, \vec{x})$ with the

expansion factor $a(\tau)$. The comoving coordinates are related to the proper time and positions t and $\vec{r}$ by $dx^0 = d\tau = dt/a$ and $dx = dr/a$. The units are such that $c = 1$

We first are going to perturb the metric around the background $\bar{g}_{\mu\nu}$ up to linear order

$$g_{\mu\nu} = \bar{g}_{\mu\nu} + \delta g_{\mu\nu}, \tag{2.42}$$

It is convenient to decompose the metric in scalar, vector and tensor variables. A general symmetric metric describing a generic space-time has ten degrees of freedom in total. Once the perturbed metric variables are decomposed it turns out that it has 4 scalar degrees of freedom, 4 vector degrees of freedom and 2 tensor ones recovering the original number of modes in GR. In this work only scalar pertubations are relevant, a possible line element describing scalar pertubations of the metric is [214, 281]:

$$ds^2 = a^2 \left\{ -(1-2\Theta)d\tau^2 - 2\vec{\nabla}_i \beta d\tau dx^i + [(1+\frac{1}{3}\chi)q_{ij} + D_{ij}\nu]dx^i dx^j \right\}, \tag{2.43}$$

where $D_{ij} \equiv \vec{\nabla}_i \vec{\nabla}_j - \frac{1}{3} q_{ij} \nabla^2$ is the traceless spatial derivative operator and $\vec{\nabla}$ is the covariant derivative associated to the spatial metric q_{ij} and χ is usually known as the curvature perturbation. Here we assume a flat universe then $q_{ij} = \delta_{ij}$. These variables are not necessarily an observable quantity and may depend on the gauge. Along this thesis we are going to cast the equations in two gauges: the Newtonian-conformal gauge and the synchronous gauge.

Variables in the Newtonian-conformal gauge are equal to gauge invariant variables and then the perturbations can be linked with physical quantities straightaway [25, 74]. The physics are more directly read in the conformal-Newtonian gauge ($\nu = \beta = 0$) since the remaining metric perturbations give rise to the Newtonian potentials $\Phi = -\frac{1}{6}\chi$ and $\Psi = -\Theta$. The line-element reduces to

$$ds^2 = a^2[-(1+2\Psi)d\tau^2 + (1-2\Phi)\delta_{ij}dx^i dx^j]. \tag{2.44}$$

where we have introduced the conformal time τ related to the proper time as $d\tau = adt$. In our study of perturbations we will use τ instead of t and we will denote $f' = df/d\tau$.

Although the Newtonian-conformal gauge is restricted because the metric is applicable only for scalar metric perturbations it can be easily generalized to include the vector and the tensor modes [74]. Another advantage is that the metric in these coordinates is diagonal. The two scalar perturbations in this gauge are simply related

to the gauge-invariant Bardeen-variables Φ_A and Φ_H [25] and Ψ and Φ of Kodama and Sasaki [174][See [74] for further details].

For computational purposes in this work we use the synchronous gauge variables. Coordinates in this gauge are defined by spatial surfaces perpendicular to the trajectory of a freely falling observer, this surfaces foliate the whole spacetime. In this gauge g_{00} and g_{i0} are not perturbed by definition. So the line element is given by

$$ds^2 = a^2(\tau)\{-d\tau^2 + (\delta_{ij} + h_{ij})dx^i dx^j\} \tag{2.45}$$

the metric perturbation can be decomposed into traceless and trace parts as

$$h_{ij} = h\frac{\delta_{ij}}{32} + h^{||}_{ij} + h^{\perp}_{ij} + h^{T}_{ij} \tag{2.46}$$

where

$$\begin{aligned} h &\equiv h_{ii} \\ \varepsilon_{ijk}\partial_j\partial_n h^{||}_{nk} &= 0, \\ \partial_i\partial_j h^{\perp}_{ij} &= 0, \\ \partial_i h^{T}_{ij} &= 0. \end{aligned} \tag{2.47}$$

This assures that there exist some scalar field μ and a divergenceless vector $\vec{A}$ such that

$$\begin{aligned} h^{||}_{ij} &= \left(\partial_i\partial_j - \frac{1}{3}\delta_{ij}\partial^2\right)\mu \\ h^{\perp}_{ij} &= \partial_i A_j \ + \ \partial_j A_i \ \ \partial_i A_i = 0. \end{aligned} \tag{2.48}$$

Another useful scalar perturbation which is a mixture of the longitudinal and trace modes is η and is defined as

$$k^2\mu(\vec{k},\tau) = h(\vec{k},\tau) + 6\eta(\vec{k},\tau). \tag{2.49}$$

The scalar modes of the metric perturbations are characterized by h and μ while the vector and tensor ones are described by $\vec{A}$ and h^T_{ij} respectively. In the following we are going to work in Fourier space. An arbitrary variable in spacetime coordinates expressed as a Fourier decomposition is

$$F(\vec{x},\tau) = \int d^3k \ \ e^{i\vec{k}\cdot\vec{x}}\,\tilde{F}(\vec{k},\tau). \tag{2.50}$$

Where $\tilde{F}$ is the Fourier transform of an arbitrary function F. In the following we are going to omit the˜and work only with Fourier variables.

The conformal Newtonian potentials are related to the synchronous variables as follows

$$\Psi(\vec{k},\tau) = \frac{1}{2k^2}\left\{h''(\vec{k},\tau)+6\eta(\vec{k},\tau)+\frac{a'}{a}\left[h'(\vec{k},\tau)+6\eta'(\vec{k},\tau)\right]\right\} \quad (2.51)$$

$$\Phi(\vec{k},\tau) = \eta(\vec{k},\tau)-\frac{1}{2k^2}\frac{a'}{a}\left[h'(\vec{k},\tau)+6\eta'(\vec{k},\tau)\right]. \quad (2.52)$$

where the longitudinal part of the spatial tensor component of the metric is rewritten as

$$h_{ij}^{||} = \int d^3k e^{i\vec{k}\cdot\vec{x}}\left(\hat{k}_i\hat{k}_j-\frac{1}{3}\delta_{ij}\right)\left[h(\vec{k},\tau)+6\eta(\vec{k},\tau)\right], \quad (2.53)$$

where $\vec{k}=k\hat{k}$. Despite the synchronous gauge is widely used by the community, it has serious disadvantages. Since the choice of the initial hyper-surface and its coordinate assignments are arbitrary, the synchronous gauge conditions do not fix the gauge degrees of freedom completely. Such residual gauge freedom is manifested in the spurious gauge modes contained in the solutions to the equations for the density perturbations.Nevertheless, this gauge is still very useful for computational purposes. Usually, one computes the perturbations in synchronous gauge and the remaining gauge ambiguity is removed by making a gauge transformation to the conformal-Newtonian gauge or equivalently computing the Bardeen gauge invariant perturbations so the coordinates of spacetime are fully determined.

The perfect fluid describing matter in this space-time looked by an observer moving along test particles has an energy-momentum tensor given by

$$T_{\mu\nu} = (\rho+P)u_\mu u_\nu + Pg_{\mu\nu}+\Sigma_{\mu\nu}$$

where $u_\mu = \frac{dx_\mu}{\sqrt{-ds^2}}$ is the 4-velocity of the fluid, ρ is the energy density and P is the pressure at a given point and instant measured by a comoving observer at rest with the rest of the fluid. $\Sigma_{\mu\nu}$ is the anisotropic stress tensor which satisfies $u^\mu\Sigma_{\mu\nu}=0$. Due to isotropy, the fluid moves slowly and thus its velocity $V_i=\nabla_i\theta=q_{ij}\frac{dx^j}{d\tau}$ can be thought as a perturbation of the same order than $\delta\rho\equiv\rho-\bar{\rho}$ and $\delta P\equiv P-\bar{P}$. Inhomogeneities and anisotropies in the energy-momentum tensor of matter are given by

$$\delta T_0^0 = -\rho\delta\rho \tag{2.54}$$
$$\delta T_i^0 = -(\rho+P)\vec{\nabla}_i\theta \tag{2.55}$$
$$\delta T_j^i = \delta_j^i P + (\rho+P)D_j^i\Sigma \tag{2.56}$$

2.3.4.b Einstein and Conservation Equations

As pointed before we assume that the linear theory holds in the weak field regime so small perturbations in matter produce small perturbations in the metric $|\delta g_{\mu\nu}| = |\bar{g}_{\mu\nu} - g_{\mu\nu}| << 1$. From this metric we can calculate the Christoffel connection ,the Riemann tensor and the Ricci scalar up to linear order in order to finally obtain the Einstein tensor $G_\mu^\nu = \bar{G}_\mu^\nu + \delta G_\mu^\nu$.

The scalar perturbations characterized by $h(\vec{k},\tau)$ and $\eta(\vec{k},\tau)$ in the Fourier space are described by the time-time, longitudinal time-space, trace space-space and longitudinal traceless space-space components of Einstein equations to the linear order

$$k^2\eta - \frac{a'}{2a}h' = 4\pi G_N a^2\delta T_0^0(Syn), \tag{2.57}$$
$$k^2\eta' = 4\pi G_N a^2(\bar{\rho}+\bar{P})\theta(Syn), \tag{2.58}$$
$$h'' + 2\frac{a'}{a}h' - 2k^2\eta = -8\pi G_N a^2\delta T_i^i(Syn), \tag{2.59}$$
$$h'' + 6\eta'' + 2\frac{a'}{a}\left(h' + 6\eta'\right) - 2k^2\eta = -24\pi G_N a^2(\bar{\rho}+\bar{P})\sigma(Syn). \tag{2.60}$$

where we have used the definitions

$$(\bar{\rho}+\bar{P})\theta(Syn) \equiv ik^j\delta T_j^0, \tag{2.61}$$
$$(\bar{\rho}+\bar{P})\sigma \equiv -(\hat{k}_i\hat{k}_j - \frac{1}{3}\delta_{ij})\Sigma_i^j \tag{2.62}$$

where $\Sigma_i^j \equiv T_i^j - \frac{1}{3}\delta_i^j T_k^k$ denotes the traceless component of T_i^j.

The Bianchi relation and the Einstein equations lead to the conservation of energy:

$$T_{;\mu}^{\mu\nu} = \partial_\mu T^{\mu\nu} + \Gamma_{\alpha\beta}^\nu T^{\alpha\beta} + \Gamma_{\alpha\beta}^\alpha T^{\nu\beta} = 0 \tag{2.63}$$

which in the Fourier space for the synchronous gauge gives rise to the evolution equations for matter perturbations and their peculiar velocities [74]

$$\delta' = -(1+w)\left(\theta+\frac{1}{2}\dot{h}\right)-3\frac{\dot{a}}{a}\left(\frac{\delta P}{\delta\rho}-w\right)\delta, \tag{2.64}$$

$$\theta' = -\frac{a'}{a}(1-3w)\theta-\frac{w'}{1+w}\theta+\frac{\delta P}{1+w}\frac{k^2}{\rho}-k^2\sigma, \tag{2.65}$$

where w is the equation of state of dark energy. For isentropic primordial perturbations $\delta P = c_s^2\delta\rho$. For simplicity, all along our cosmological study in this work, we assume that a cosmological constant plays the role of dark energy with $w=-1$. In this case $c_s^2 \equiv w$. Photons and baryons form the only collisional fluid with pressure, the corresponding equation of state for photons is $w=1/3$ and $w\sim 0$ for baryons since they are non-relativistic particles at the relevant times.

2.3.4.c Perturbed Boltzmann Equation

Before recombination photons and baryons are tightly coupled via Thompson scattering [102] and the respective entropy generated by this collisions should be added to their respective equations. In the phase space the coordinates of positions and momenta of particles depend on the gauge. In the synchronous gauge the conjugate momenta to the comoving position is just the spatial part of the 4-momentum with lower indices given by

$$P_i = a(\delta_{ij}+\frac{1}{2}h_{ij})p^j \tag{2.66}$$

where p^j is defined as the proper momentum.

In absence of metric perturbations, the Hamilton's equations imply that the conjugate momenta are constant. The phase space distribution of particles gives the number of particles in a differential of volume

$$f(x^i,P_j,\tau)d^3x^jd^3P^j = N \tag{2.67}$$

as we already saw in previous sections, the unperturbed phase space distribution is just the Fermi-Dirac one for fermions and the Bose-Einstein distribution for bosons. When the spacetime is perturbed, the phase space distribution can be written as the unperturbed distribution plus a fluctuation Ω

$$f(x^i,P_j,\tau) = f_0[1+\Omega] \tag{2.68}$$

The evolution of this fluctuation of the Boltzmann equation is governed by

$$\frac{\partial \Omega}{\partial \tau} + i\frac{q}{\varepsilon}(\vec{k}\cdot\hat{n})\Omega\frac{d\ln f_0}{d\ln q}\left[\dot{\eta} - \frac{\dot{h}+6\dot{\eta}}{2}(\hat{k}\cdot\hat{n})^2\right] = \frac{1}{f_0}\left(\frac{\partial f}{\partial \tau}\right)_C, \tag{2.69}$$

$$\frac{\partial \Omega}{\partial \tau} + i\frac{q}{\varepsilon}(\vec{k}\cdot\hat{n})\Omega\frac{d\ln f_0}{d\ln q}\left[\dot{\phi} - i\frac{\varepsilon}{q}(\hat{k}\cdot\hat{n})^2\psi\right] = \frac{1}{f_0}\left(\frac{\partial f}{\partial \tau}\right)_C, \tag{2.70}$$

where $q_i = ap_i = qn_i$ is the comoving momentum (n_i are the components of an unitary vector $\hat{n}$ pointing in the direction of $\vec{q}$) and $\varepsilon = (q^2 + a^2m^2)^{1/2}$ is the scale factor times the proper energy measured by a comoving observer.

It is interesting to note that the Boltzmann equation depends on the direction of the momentum only through $\vec{k}\cdot\hat{n}$. If the momentum-dependence of the initial phase space perturbation is axially symmetric about $\vec{k}$, it will remain axially symmetric along its evolution. Thus, if axially-asymmetric perturbations in the neutrinos or other collisionless particles are produced, they would generate no scalar metric perturbations and thus would have no effect on other species [74].

Cold Dark Matter Cold Dark Matter (CDM) only interacts with other particles by means of gravity. It can be treated as a pressureless perfect fluid. The synchronous coordinates can be defined so that the peculiar velocities of CDM particles are zero. By setting $\theta = \sigma = 0$ and $\omega = 0$ equations (2.64,2.65) reduce to

$$\delta_c' = -\frac{1}{2}h' \tag{2.71}$$

Massless Neutrinos For massless neutrinos $\rho_\nu = 3P_\nu$. The Boltzmann equation simplifies significantly for massless particles resulting in

$$F_\nu(\vec{k},\hat{n},\tau) = \sum_{l=0}^{\infty}(-i)^l(2l+1)F_{\nu l}(\vec{k},\tau)P_l(\hat{k}\cdot\hat{n}). \tag{2.72}$$

where $\vec{x} = r\hat{n}$ and $F_{\nu l} = j_l(kr)$ given by the spherical Bessel functions. After integrating the perturbed Boltzmann equations in synchronous gauge it gives

$$\frac{\partial F_\nu}{\partial \tau} + ik\mu F_\nu = -\frac{2}{3}h' - \frac{4}{3}(h'+6\eta')P_2(\mu). \tag{2.73}$$

Where $\mu = \hat{k}\cdot\hat{n}$ and P_2 is the second Legendre polynomial. After inserting the explicit forms of the Legendre polynomials [320] and using their recursion relation one obtains

$$\begin{aligned}
\delta'_\nu &= -\frac{4}{3}\theta_\nu - \frac{2}{3}\phi', \\
\theta'_\nu &= k^2\left(\frac{1}{4}\delta_\nu - \sigma_\nu\right), \\
F'_{\nu 2} &= 2\sigma'_\nu = \frac{8}{15}\theta_\nu - \frac{3}{5}kF_{\nu 3} + \frac{4}{15}h' + \frac{8}{5}\eta', \\
F'_{\nu l} &= \frac{k}{2l+1}\left[lF_{\nu(l-1)} - (l+1)F_{\nu(l+1)}\right], \quad l > 1.
\end{aligned} \tag{2.74}$$

In this work we assume neutrinos are exactly massless.

Photons The evolution of photons can be treated in a similar way to massless neutrinos. However collisional terms on the right hand side of the Boltzmann equation are present and they depend on polarization [74]. Photons with $\vec{k}$ propagating along an axis $\hat{n}$ are linearly polarized in the plane perpendicular to that axis due to the Thompson scattering. In order to describe the polarization state of photons we need to track the sum $F_\gamma(\vec{k},\hat{n},\tau)$ and the difference $G_\gamma(\vec{k},\hat{n},\tau)$ of the phase space densities in the two linear polarization components. Using the linearized collision operators for Thompson scattering [41, 42, 176], expanding F_γ and G_γ in Legendre series and using the same left-hand-sides of Boltzmann equation for F_γ and G_γ as for massless neutrinos, one gets [41, 74, 274, 334]

$$\begin{aligned}
\delta'_\gamma &= -\frac{4}{3}\theta_\gamma - \frac{2}{3}h', \\
\theta'_\gamma &= k^2\left(\frac{1}{4}\delta_\gamma - \sigma_\gamma\right) + an_e\sigma_T(\theta_b - \theta_\gamma), \\
F'_{\gamma 2} &= 2\sigma'_\gamma = \frac{8}{15}\theta_\gamma - \frac{3}{5}kF_{\gamma 3} + \frac{4}{15}h' + \frac{8}{5}\eta' - \frac{9}{5}an_e\sigma_T\sigma_\gamma + \frac{1}{10}an_e\sigma_T(G_{\gamma 0} + G_{\gamma 2}), \\
F'_{\gamma l} &= \frac{k}{2l+1}\left[lF_{\gamma(l-1)} - (l+1)F_{\gamma(l+1)}\right] - an_e\sigma_T F_{\gamma l} \quad , \quad l > 2, \\
G'_{\gamma l} &= \frac{k}{2l+1}\left[lG_{\gamma(l-1)} - (l+1)G_{\gamma(l+1)}\right] \\
&+ an_e\sigma_T\left[-G_{\gamma l} + \frac{1}{2}(F_{\gamma 2} + G_{\gamma 0} + G_{\gamma 2})\left(\delta_{l0} + \frac{\delta_{l2}}{5}\right)\right]
\end{aligned} \tag{2.75}$$

Let us note that perturbations in the phase space distribution correspond to the photon anisotropy of the CMB. The photon brightness temperature perturbation $\Delta \equiv \frac{\Delta T}{T}$ is defined by

$$f(x^i, q, n_j, \tau) = f_0\left(\frac{q}{1+\Delta}\right), \tag{2.76}$$

where f_0 is the Bose-Einstein distribution and $q = \varepsilon$. At first order we have that the anisotropy is related to the perturbation of phase-space distribution of photons as follows

$$\Delta = -\left(\frac{d\ln f_0}{d\ln q}\right)^{-1}\Omega. \tag{2.77}$$

The anisotropy Δ is related to the total energy density perturbation of the photon as $F_{l\gamma} = 4\Delta_l$ [309] and the total scalar polarization mode $\Delta_P = 4G_\gamma$ as well.

In order to handle the angular dependence, it is convenient to make a multipole decomposition of the anisotropies

$$\Delta = \sum_l (2l+1)(-i)^l \Delta_l P_l(\mu), \tag{2.78}$$

$$\Delta_P = \sum_l (2l+1)(-i)^l \Delta_{Pl} P_l(\mu), \tag{2.79}$$

where $P_l(\mu)$ is the Legendre polynomial of order l , Δ_l is called the multipole moment of the temperature fluctuation Δ.

I would like to stress a curious fact about the equations governing the evolution of photon's temperature perturbations. Note that, on one hand, equation (2.75) describe the evolution of the multipoles of the anisotropy. On the other hand, by making a gauge transformation over equation (2.69) to the Newtonian gauge and using Δ as variable instead of Ω, the Boltzmann equation for photons in the conformal Newtonian gauge [1] turns out to coincide with the evolution equation of the scalar photon perturbation given by [41]

$$\Delta' + ik\mu\Delta = \Phi' - ik\mu\Psi + \kappa'\left\{-\Delta + \delta_0 + i\mu v_b + \frac{1}{2}P_2(\mu)(\Delta_2 + \Delta_{P2} + \Delta_{P0})\right\}, \tag{2.80}$$

$$\Delta'_P + ik\mu\Delta_P = \kappa'\left\{-\Delta + \frac{1}{2}[1 - P_2(\mu)](\Delta_2 + \Delta_{P2} + \Delta_{P0})\right\}, \tag{2.81}$$

[1] where the collisional part is determined by the Thompson scattering term

where Δ_0, Δ_2 and Δ_{P0}, Δ_{P2} are the monopole and quadrupole of the temperature and polarization anisotropies respectively and $P_2(\mu)$ is the Legendre polynomial of order 2. The derivative of the optical depth was introduced and it is defined as $\kappa' = an_e x_e \sigma_T$. Let us mention that the quadrupole of the anisotropy represents the angular dependence of Compton scattering.

These equations are equivalent to (2.75) when the multipoles are summed up. Thus, despite it may appear redundant, I consider useful to keep at hand both sets of expressions since different versions of them are used for different computational purposes. For instance, the multipole decomposed version is useful to solve directly the whole coupled system of equations whilst the (2.81) version is a basic expression to derive the line-sight integral to compute the anisotropies [309].

A useful variable is the visibility function defined as

$$g(\tau) \equiv \kappa' e^{-\kappa}. \tag{2.82}$$

It can be thought as the probability of a photon to be Thompson scattered for the last time since its integral $\int_0^{\tau_0} d\tau g(\tau) = 1$ [97]. It takes its maximum at the time of recombination of hydrogen when the dominant contribution to the CMB anisotropies arises.

Baryons After recombination baryons and electrons behave like a non-relativistic fluid by equations governing energy-momentum conservation with $c_s^2 = \omega$ and $\sigma = 0$. Baryons are non-relativistic specially after the neutrino decoupling then we can neglect ω in all terms except in the $c_s^2 k^2 \delta$ term which is important for sufficiently small scales. Before recombination, however, the history is different due to an important transfer of energy and momentum between baryons and photons. Since $\delta T_i^0 = (\bar{\rho} + \bar{P})\theta$ such transfer is represented by the $an_e \sigma_T (\theta_b - \theta_\gamma)$. Momentum conservation in Thompson scattering implies that a new term has to be added to the equations for θ_b' so

$$\delta_b' = -\theta_b - \frac{1}{2}h', \tag{2.83}$$

$$\theta_b' = -\frac{a'}{a}\theta_b + c_s^2 k^2 \delta_b + \frac{4\bar{\rho}_\gamma}{3\bar{\rho}_b} an_e \sigma_T (\theta_\gamma - \theta_b). \tag{2.84}$$

If $c_s^2 \neq 0$ the baryon density equation is a wave equation. It describes what we shall call 'acoustic oscillations' of the fluid where the fluid pressure counter-acts gravitational collapse [102].

This set of coupled equations for different species and metric perturbations have been numerically solved by many authors (e.g. Peebles and Yu 1970 [241], Wilson and

Silk 1981 [334], Bond and Efstathiou 1984 [42], Vittorio and Silk [314]. However, the most general analytic approach to solve these equations has been proposed by Hu and Sugiyama [151] in order to compute the CMB anisotropies. Many other analytic calculations of CMB anisotropies (less general than the former) have been performed in the past under less general, and often unrealistic, assumptions. Doroshkevich, Zel'dovich, and Sunyaev (1978) [98] presented an analytic expression for temperature anisotropies on the last scattering surface. Based on this work, Naselsky and Novikov (1992) [218], Atrio-Barandela and Doroshkevich (1994) [18] have recently calculated the anisotropies in the cold dark matter (CDM) scenario. We are going to study this equation in more detail during the next section.

2.3.4.d Initial Conditions

As we already roughly mentioned, the question on how the physics of the early universe should be tuned so the universe ends up with the structure we observe today is consistently solved by the theory of inflation [8, 141, 190]. As we know, this theory provides a possible explanation for the origin of perturbations in the universe. Although to the date we haven't verified with total certainty whether inflation did actually occur, so far there is no viable alternative and today it is the most plausible explanation. However, we are in the middle of an exciting era in which very accurate measurements of the CMB may reveal the fate of inflation.

In the scenario of inflation, the inhomogeneities observed today arose from quantum fluctuations of the inflaton about its vacuum state. These perturbations turn out to be gaussian, adiabatic and close to scale invariant. More precisely, classical physics predicts that the inflaton becomes homogeneous and isotropic on scales well inside the horizon. However at the quantum level there are remnent vacuum fluctuations which right after horizon exit become classical quantities with almost constant value. Thus the cosmological perturbation theory studied previously starts before the epoch when scales of cosmological interest start to re-enter the horizon, that is well after nucleosynthesis so that the initial conditions are observable [97].

Is important to say that in this work we do not study inflation at all, we only refer to it in order to set our initial conditions and highlight its importance within the standard cosmological model. In this sense also we'd like to point that in the next chapters, when we consider alternatives to the standard model, we'll maintain this building block unaltered. Further details on inflation can be found at [13, 97, 141, 238].

Einstein Boltzmann Equations at Early times Lets consider the Boltzmann equations at so early times that the cosmologically relevant scales are such that $k\tau << 1$, that is all they are super-horizon. Because these perturbations are super-horizon sized, they don't trigger any causal physics at all and the universe can be observed as uniform all over the sky. Applying the condition $k\tau \to 0$ to Boltzmann equations for photons and neutrinos (2.80) reduce to [97]

$$\dot{\Delta}_0 + \dot{\Phi} = 0, \tag{2.85}$$
$$\dot{\mathcal{N}_0} + \dot{\Phi} = 0. \tag{2.86}$$

Let us recall that dots denote derivatives with respect to proper time. Although at first, we expressed the perturbations equations in synchronous gauge, now we prefer to display them in Newtonian-conformal gauge in order to work with physical quantities directly. The first equation corresponds to equation (2.80). Let us consider the left terms of that equation, the first term is order Δ/τ while the second one is order $k\Delta$, therefore we can drop away the later. In a similar way we can drop away all terms multiplied by k at early times. Then a hypothetical observer would have seen a uniform sky since there's no causal physics producing any perturbation. Thus higher multipoles can be neglected since they are insignificant in comparison to the monopole. On the other hand, equations for baryons and dark matter under the same approximation reduce to

$$\dot{\delta}_m = -3\dot{\Phi}, \tag{2.87}$$
$$\dot{\delta}_b = -3\dot{\Phi}. \tag{2.88}$$

In the equations above, velocities are dropped away since they are order $k\tau$. Now, lets turn to see the form of the Einstein equations at early times. Given that radiation dominates the matter terms at the right of the first Einstein equation are negligible and $\dot{a}/a \sim 1/\tau$. Therefore the first equation describing the metric at early times is

$$\dot{\Phi}\tau - \Psi = 2\left([1 - f_\nu]\delta_0 + f_\nu \mathcal{N}_0\right) \tag{2.89}$$

where $f_\nu \equiv \rho_\nu/(\rho_\gamma + \rho_\nu)$ is the ratio of neutrino energy density to the total radiation density.

The second Einstein equation describes the mechanism by which higher-multipoles of photons and neutrinos make $\Phi + \Psi$ to be slightly different to zero, due to the

quadrupole of the photon and the neutrino. By neglecting such higher order multipoles, the second Einstein equation at early times is reduced to

$$\ddot{\Phi}\tau + 4\dot{\Phi} = 0, \tag{2.90}$$

which is solved by $\Phi = \tau^p$ with $p = 0, -3$. The first solution is the interesting one, $p = -3$ is a decaying solution, if it is excited early on it dies out and doesn't contribute at all. we'll see that the constant solution is justified by inflation in the following. Thus the gravitational potential is related to radiation as

$$\Phi = 2\left([1 - f_\nu]\Delta_0 + f_\nu \mathcal{N}_0\right). \tag{2.91}$$

Δ_0 and $\mathcal{N}_0$ are constant in time and equal since whatever causes perturbations it doesn't distinguish between photons and neutrinos. This implies

$$\Delta_0(k, \tau_{ini}) = \mathcal{N}_0(k, \tau_{ini}), \tag{2.92}$$

$$\Phi(k, \tau_{ini}) = 2\Delta_0(k, \tau_{ini}). \tag{2.93}$$

In the case of the equations for dark matter and baryons perturbations, they depend upon the nature of primordial perturbations. Combining the previous equations one obtains

$$\delta_m(k, \tau_{ini}) = 3\Delta_0(k, \tau_{ini}) + constant. \tag{2.94}$$

When the constant in the last equation is zero, perturbations are called *adiabatic* perturbations, otherwise they are *isocurvature* perturbations [97]. The last three equations displayed above are called the *adiabatic initial conditions* for perturbations.

Curvature Perturbation and Initial Conditions from Inflation The key clue to determine the initial conditions for the metric perturbations is to define the curvature perturbation which has the important feature that is conserved at super-horizon scales [13, 97]. In the context of slow-roll inflation the vacuum fluctuation of the inflaton $\delta\phi$ becomes classical at the time when it leaves the horizon, the point is that at least one of these perturbations should generate the curvature perturbation which can be observable when cosmological scales begin to re-enter the horizon. In order to make such definition it's important to remark that $\delta\phi$ is defined on what is known as flat slicing: when we consider fluctuations on the metric we allow the scale factor to become scale dependent, flat slicing is a restriction of this on the homogeneous case where the scale factor depends only on time locally. The curvature perturbation

arises when the energy-momentum tensor and the metric are smoothed on the shortest cosmological scale. The curvature perturbation is defined as follows [102]

$$g_{ij} = a^2(x,t)\delta_{ij}, \tag{2.95}$$
$$a(x,t) = a(t)e^{\zeta(x)}. \tag{2.96}$$

When the shortest mode of the curvature perturbation approaches the horizon ζ tends to take a constant value which determines the total energy density perturbation from which the initial conditions for the perturbations are determined inside the horizon and then it is accessible to be observed. If the tensor perturbation is neglected, ζ describes the curvature perturbation completely. It turns out that [13, 97]

$$\zeta = -aH\frac{\delta\rho}{\dot{\rho}}. \tag{2.97}$$

It can be shown that if and only if the pressure is only function of the energy density then ζ is a conserved quantity [13]. Now in the case of the scalar field the perturbation $\delta\phi$ is defined on the flat slicing and ζ is defined on the uniform energy density slicing. On the other hand the scalar is independent of position up to a function depending on time, hence its value at any instant gives the energy density (or the Hubble parameter). This implies that ϕ is also uniform on a slice of uniform density and hence we can replace the density by the scalar

$$\zeta = -aH\frac{\delta\phi}{\dot{\phi}^{(0)}}. \tag{2.98}$$

At this point we can connect (2.98) by using the vacuum fluctuations of the inflaton with to the curvature perturbation at late times. Because the curvature perturbation becomes a constant a few Hubble times after the horizon exit, it only remains to evaluate its value when that happens. The value of the curvature perturbation after inflation is given by [97]

$$\zeta = -\frac{3}{2}\Psi. \tag{2.99}$$

Therefore we can immediately relate the potential Ψ coming out from inflation to the inflaton fluctuation $\delta\phi$ at horizon crossing

$$\Psi_{post} = \frac{2}{3}\left[aH\frac{\delta\phi}{\dot{\phi}^{(0)}}\right]_{cross}, \tag{2.100}$$

where Ψ_{post} is the constant value of Ψ right after inflation and the *cross* subindex means evaluated after horizon crossing. Equivalently the power spectra are related as [97]

$$P_\Psi = \frac{4}{9}\left(\frac{aH}{\dot{\phi}}\right)^2 P_{\delta\phi}(k = aH, \tau) = \left[\frac{2}{9k^3}\left(\frac{aH^2}{\dot{\phi}^{(0)}}\right)^2\right]_{aH=k}. \tag{2.101}$$

Basically the calculation finishes here, however is important to repeat that in Newtonian-conformal gauge Φ corresponds to a physical, gauge invariant quantity and that fact has interesting implications. The Bardeen gauge-invariant variable, $\Phi_H = -\Phi$, can be geometrically interpreted. In particular, the curvature of the three-dimensional space at fixed time is equal to $4k^2\Phi_H/a^2$, hence perturbations in Φ_H can be thought as *perturbations in curvature*. This means that even if we live in space that is practically flat, perturbations give rise to curvature form place to place around the flat universe, as if it was a textured flat fabric with small curved weaves all around.

2.4 Cosmological Testable Observables from Perturbations

2.4.1 The Cosmic Microwave Background

A fraction of a million years after the Big-Bang the universe was hot, dense and turbulent as we already saw, around the time of recombination, photons and baryons were tightly interacting and the universe was obscure. After recombination (and re-ionization) when photons finally decoupled from baryons and electrons, electromagnetic radiation was free to travel through spacetime as the universe expanded until today. The accidental discovery of this residual radiation was due to Arno Penzias and Robert Wilson in 1964 [244]. According to the most recent report, it has a thermal blackbody spectrum peaking at a temperature of $2.72548 \pm 0.00057K$ [129].

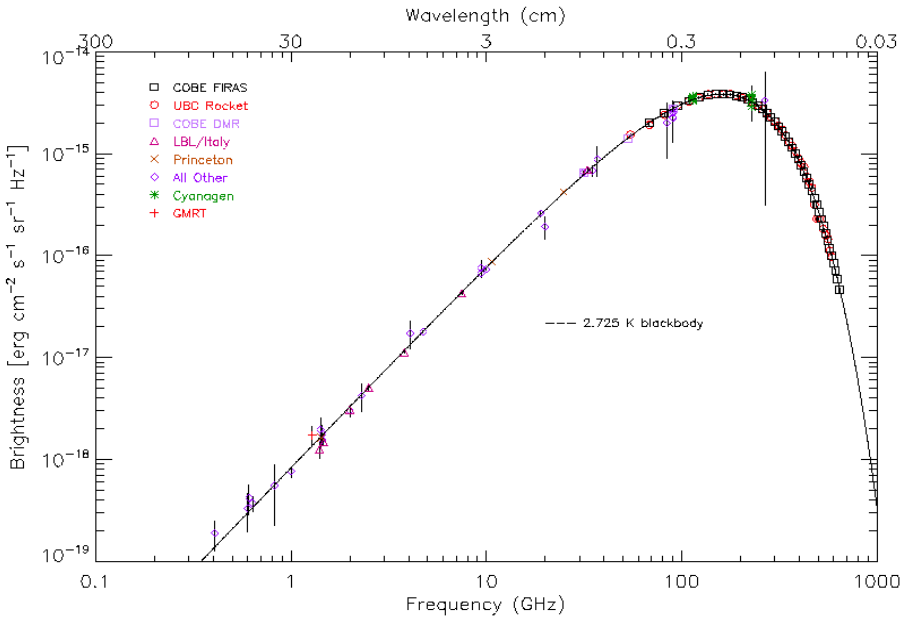

Fig. 2.2 The black body frequency spectrum of the cosmic microwave background with uniform temperature of $\sim 3^o K$ with an accuracy of one part in 10^4 measured by various groups. Figure taken from [278]

This discovery implies that the Universe was in thermal equilibrium when the radiation was released when the temperature of the universe was around $3000K$. It is a stunning fact that a part in 10^{-4} , this temperature is the same all over the sky. Assuming that before decoupling the universe was filled with radiation and neutrinos

mainly, this is surprising also because at the decoupling time the causal horizon of the universe (defined by the distance that light has traveled since the Big Bang) corresponded to $\sim 1^o$, as observed today, however the temperature of CMB is uniform even for patches larger than 1^o. The question on how could be possible that causally disconnected regions could reach mutual thermal equilibrium establishes the so called horizon problem [61, 212].

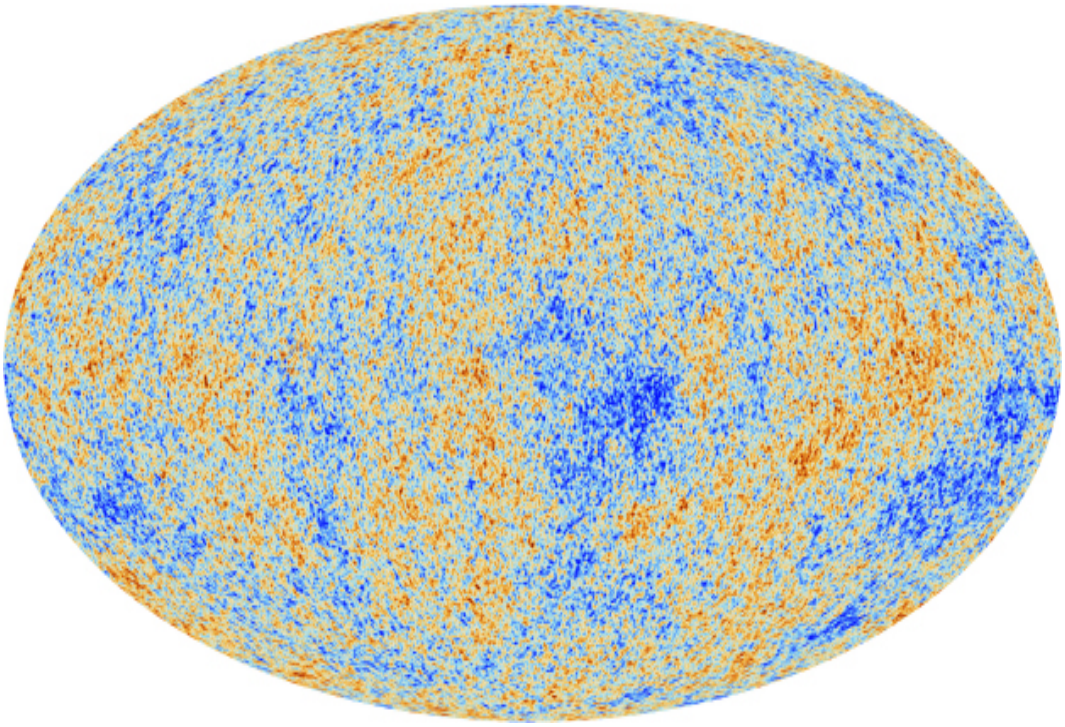

Fig. 2.3 The anisotropies of the cosmic microwave background as observed by Planck. According to the standard cosmological model, the CMB is a snapshot of the oldest light in our Universe, imprinted on the sky when the Universe was just 380 000 years old. It shows tiny temperature fluctuations that correspond to regions of slightly different densities, representing the seeds of all future structure: the stars and galaxies that surround us today. Figure taken from [302].

After the first discovery of the anisotropies of the CMB by the COBE satellite [286], they have become one of the most powerful observational probes of cosmology, particularly they have provided a tool to test inflation and to extract valuable information about the large scale structure of the universe [151].Very recently Planck has provided extremely accurate measurements of the CMB anisotropies which will bring deep insights to the subject.

To predict CMB anisotropies in any given model, we need to solve the set of coupled equations studied in previous sections in order to track the evolution of different species of particles present at different times in the universe and then determine

the spectrum of residual background radiation that reaches us today. Although the anisotropy formation is a very complicated process, an approximate analytical analysis may bring a good understanding of the physics driving the birth of the CMB anisotropy. In this section we intend to draw a clear and complete summary of the method to compute the CMB temperature and polarization anisotropies.

2.4.1.a Multipolar Decomposition

The CMB that reaches us from the sky has a complicated spatial structure. In order to handle it and to extract useful information from it we can decompose it into an infinite set of discrete moments which have a much simpler structure. Specifically the complex angular dependence of the CMB can be better handled by using special functions called spherical harmonics. To compute the anisotropy at a given point $\vec{x} = r\hat{n}$ we decompose the plane wave contributions with wavelength $\vec{k} = k\hat{k}$ (hat vectors have magnitude equal to 1) in the following way

$$\Delta(\vec{x},\hat{n},\tau) = \int d^3k \;\; e^{i\vec{k}\cdot\vec{x}}\,\Delta(\vec{k},\hat{n},\tau) \;\equiv \int d^3k\, e^{i\vec{k}\cdot\vec{x}} \sum_{l=0}^{\infty}(-i)^l\,(2l+1)\,\Delta_l(\vec{k},\tau)\,P_l(\hat{k}\cdot\hat{n})$$

The anisotropy at the origin may be expanded in spherical harmonics

$$\Delta(\hat{n}) = \sum_{l=0}^{\infty}\sum_{m=-l}^{l} a_{lm}\,Y_{lm}\,(\hat{n}) \tag{2.102}$$

where

$$a_{lm} = (-i)^l 4\pi \int d^3k \;\; Y^*_{lm}\,(\hat{k})\,\Delta_l(\vec{k},\hat{n},\tau). \tag{2.103}$$

The angular power spectrum of the anisotropy is defined as

$$\langle a_{lm}\, a^*_{l'm'}\rangle = C_l\;\delta_{ll'}\;\delta_{mm'}, \tag{2.104}$$

The angular two-point correlation function is

$$C(\theta) \equiv \langle\, \Delta(\hat{n}_1)\,\Delta(\hat{n}_2)\,\rangle = \frac{1}{4\pi}\sum_{l=0}^{\infty}(2l+1)\,C_l\,P_l(\hat{n}_1\cdot\hat{n}_2) \tag{2.105}$$

The anisotropy coefficients C_l are random variables which depend on the primordial power spectrum of perturbations. A consequence of this is that the angular power spectrum is related to the primordial power spectrum by [74].

$$C_l = 4\pi \int d^3k \; P_\Psi(\vec{k}) \, \Delta_l^2(k,\tau). \tag{2.106}$$

2.4.1.b Tight Coupling Limit

Before recombination the Compton scattering is quite effective because $\dot{\kappa}$ value is important. At this regime all multipoles Δ_l, $l > 1$ are negligible. Only the monopole and the dipole contribute to the total anisotropy. From here we can deduce that photons behave like a fluid. For perturbations with wavelength much smaller than the horizon at recombination smoothed out [97]. Combining the equations for photons and baryons at this regime a single equation for the photon monopole results

$$\Delta_0'' + \Phi'' + \frac{a'}{a}\frac{R}{R+1}(\Delta_0' + \Phi') + k^2 c_s^2(\Delta_0 + \Phi) = \frac{k^2}{3}[\frac{1}{1+R}\Phi - \Psi] \tag{2.107}$$

where the sound speed here is given by $c_s^2 = \frac{1}{3}\frac{1}{1+R}$. The equation above describes the so called acoustic oscillations in the photon-baryon fluid before recombination and from it we can read off the following three effects:

- Φ'' is responsible of the early Sachs-Wolfe effect on Δ_0'' which dominates at super-horizon scales $k\tau << 1$
- $k^2\Psi$, represents the gravitational infall which produces the adiabatic growth of the photon-baryon fluctuations, this effect is important near horizon scales $k\tau \sim 1$
- the $k^2 c_s^2 \Delta_0$ term accounts for the photon pressure which is important inside the sound horizon.

On the other hand, the gradient of the Newtonian potential induces a gravitational redshift on the photons as they travel through potential wells from recombination until today. The potential difference induces a temperature shift so the effective temperature of photons is $\Delta + \Psi$. This effect is called then the integrated Sachs Wolfe effect (ISW) [264]. Also the second effect mentioned above can be understood by looking the equations for baryons in the Newtonian-conformal gauge

$$\delta_b' = -\theta_b + 3\Phi', \tag{2.108}$$

$$\theta_b' = -\frac{a'}{a}\theta_b + c_s^2 k^2 \delta_b + \frac{4\bar{\rho}_\gamma}{3\bar{\rho}_b} a n_e \sigma_T (\theta_\gamma - \theta_b) + k^2 \Psi. \tag{2.109}$$

the Newtonian potential plays the role of a source in the velocity equation and it gives rise to the adiabatic growth of perturbations. Equation (2.107), in the fluid limit (at first order in $\dot{\kappa}$), is solved analytically by

$$\Delta_0(\tau) + \Phi(\tau) = [\Delta_0(0) + \Phi(0)] \cos(k r_s) + \frac{k^2}{3} \int_0^\tau d\tau' [\Phi(\tau') - \Psi(\tau')] \sin[k(r_s(\tau) - r_s(\tau'))]. \tag{2.110}$$

The sound horizon is defined as

$$r_s(\tau) = \int_0^\tau d\tau' c_s(\tau'). \tag{2.111}$$

The approximative solution above was first found by Hu and Sugiyama at [319]. This approximate solution has two interesting features: 1. it reproduces with high precision the position and height of the peaks of the exact solution. 2. It splits the calculation of the anisotropy in two simple steps, first compute the gravitational potentials generated by matter and afterwards integrate to get the temperature fluctuation. It is important to mention that the cosine mode is excited by the inflationary models since it involve non-zero initial conditions. When the first term dominates, this solution gives a quantitative way of determine the location of the peaks

$$k_p = \frac{n\pi}{r_s} \tag{2.112}$$

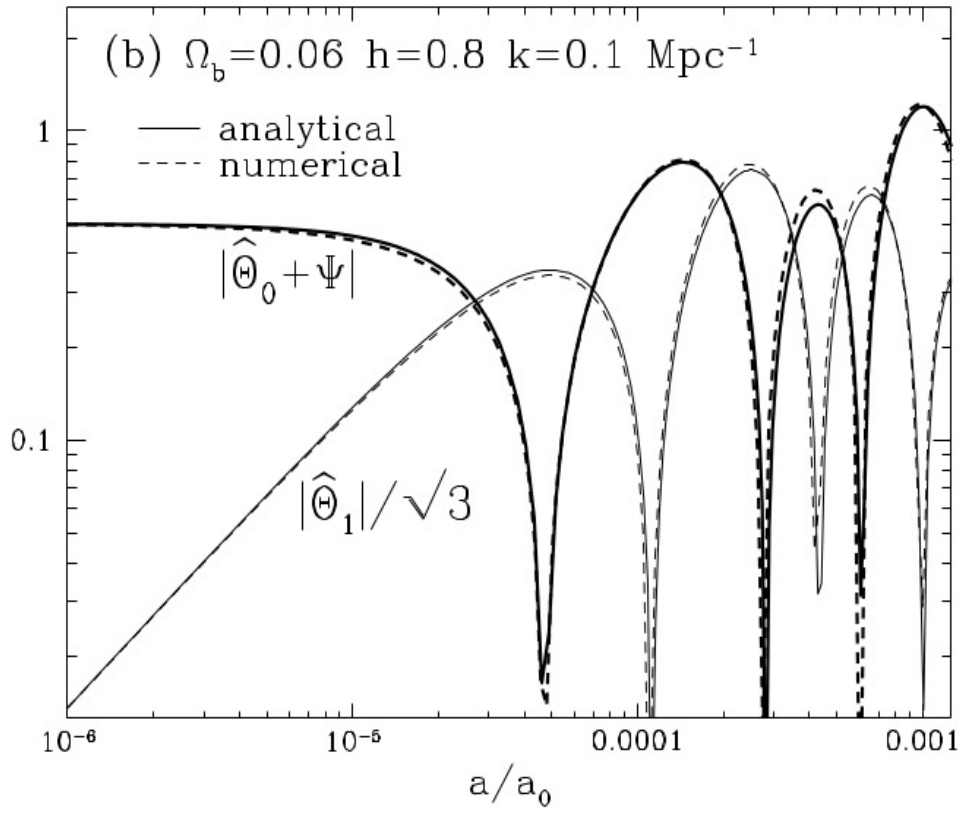

Fig. 2.4 Evolution of the photon anisotropy before recombination for a particular model. It is clear that the tight coupling approximation is very good. The numerical solution is for a universe which never recombines in order to eliminate the diffusion damping at recombination. The normalization is set such that $\Phi(0) = -1$. Figure taken from [319].

$$\Delta_1(\tau) = [\Delta_1(0) + \Phi(0)]\sin(kr_s) - \frac{k}{3}\int_0^\tau d\tau'[\Phi(\tau') - \Psi(\tau')]\cos[k(r_s(\tau) - r_s(\tau'))] \tag{2.113}$$

Note that the dipole and the monopole phases are shifted from each other. Accounting for the dipole rises the anisotropy spectrum, the shift between the monopole and the dipole turns the troughs of the spectrum more pronounced. So far, in the tight coupling regime we've ignored the high multipoles of the temperature fluctuation and only effects of the monopole and the dipole dominate. However at next order in the Compton scattering rate the quadrapole produces a small effect of diffusion [97, 242]. The damping of photons due to diffusion through baryons is related to the "finite thickness of the last scattering surface". Approximately, before recombination, photons and baryons form a perfect fluid, ideally this would be true if the rate of scattering of photons and electrons were infinite, however in reality this rate is finite and then photons travel a finite distance between scatters.

The resulting anisotropy in this limit is a damped tight coupling anisotropy that is

$$(\Delta_0 + \Psi) = (\hat{\Delta}_0 + \Psi) e^{-[k/k_D(\tau)]^2}, \tag{2.114}$$

where

$$\frac{1}{k_D(\tau)^2} = \frac{1}{6}\int_0^\tau d\tau' \frac{1}{\kappa'} \frac{R^2 + 4(1+R)/5}{(1+R)^2} \tag{2.115}$$

As a result anisotropies at scales $k >> k_D$ are exponentially damped by diffusion [277]. The presence of Ψ plays the role of the ordinary Sachs-Wolfe contribution due to the potential wells mentioned in before.

2.4.1.c The Anisotropy Today: Free-Streaming Solution

Just after recombination the temperature anisotropy of the CMB freezes because of the decoupling of photons from baryons. The remaining radiation travels free all along the way to us today [41, 42]. In consequence we observe this fluctuations in the sky almost as they were at the time of decoupling. Instead of solving the coupled system of differential equations that we studied above, one may use another mathematical method which results to be more economical. By this method one uses an integral method to find the solution of the anisotropies. Basically the perturbations for the photon are integrated out along the past light cone to obtain [309]

$$\begin{aligned}
\Delta_{P,T} &= \int_0^{\tau_0} d\tau e^{ik\mu(\tau-\tau_0)} S_{T,P}(k,\tau), && (2.116)\\
S_T &= g\left(\Delta_0 + \Psi - \frac{V_b'}{k} - \frac{\Pi}{4} - \frac{3\Pi''}{4k^2}\right) + e^{-\kappa}(\Phi' + \Psi') - g'\left(\frac{V_b}{k} + \frac{3\Pi'}{4k^2}\right) \\
&- \frac{3g'\Pi}{4k^2} && (2.117)\\
S_P &= -\frac{3}{4k^2}\left(g[k^2\Pi + \Pi''] + 2g'\Pi' + g''\Pi\right), && (2.118)\\
\Pi &\equiv \Delta_2 + \Delta_{P2} + \Delta_{P0}, && (2.119)
\end{aligned}$$

where μ has been eliminated by integrating by parts with respect to conformal time and $\tau_0 = \tau(a=1)$. By doing so only the monopole term is affected since the boundary terms vanish at early times today since they are unobservable. The terms above are called the sources of the anisotropy and the different contributions produce distinguishable effects of the observed anisotropy:

- The first two terms in (2.117) correspond to the effective anisotropy at the last scattering surface.

- The terms depending on the baryon velocity V_b are the Doppler terms.

- The term containing the gravitational potentials produce the so called integrated Sachs-Wolfe effect and it is important after recombination, especially if equality occurs close to recombination. In such case, the potentials are decaying by recombination and thus they act as enforcing agent that make the anisotropy to be enhanced.

- The terms containing Π affect the anisotropy at a 10% level and they are due to the photon polarization and anisotropic Thompson scattering [309].

It is worth to mention that the last equation is a generalization of the tight coupling limit, it reduces to it when the visibility function is a Dirac delta and Π can be neglected. In that approximation, one just needs to evaluate the sources at recombination and afterwards free-stream them to obtain the anisotropy today. In the general integration case contributions arisen during recombination and after are taken into account. When the tight coupling approximation breaks down at recombination, polarization and anisotropic stress must to be considered to compute the anisotropy.

The multipoles of the anisotropies observed today can be computed as well by using this integral method. For that propose, one needs to decompose the plane wave in the integrand into angular and radial eigenfunctions that is in a superposition of Legendre polynomials and spherical Bessel functions respectively as follows

$$\Delta_{(T,P)l}(k,\tau_0) = \int_0^{\tau_0} S_{T,P}(k,\tau) j_l[k(\tau-\tau_0)] d\tau, \tag{2.120}$$

where j_l is the spherical Bessel function. Note that the anisotropy is composed by two parts: the source which is independent of the multipole momentum l and the other geometrical j_l which is independent of the cosmological model. It is because of this feature that the integral method is quite convinient to save computational resources.

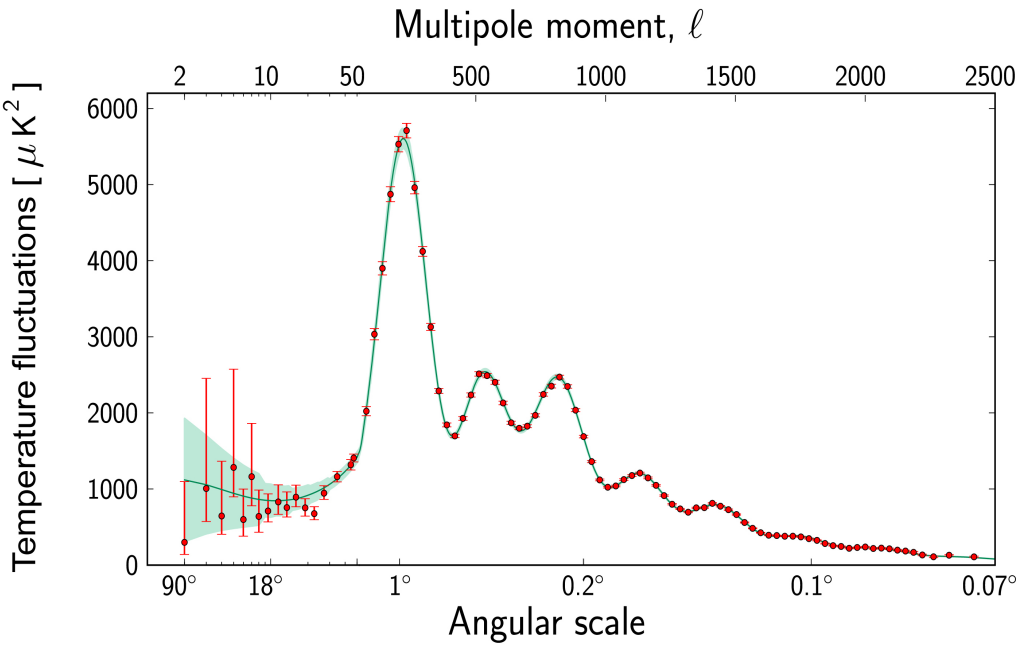

Fig. 2.5 The multipole spectrum of the CMB temperature anisotropy measured by the Planck Satellite. Figure taken from [4].

2.4.1.d The Cosmological Parameters and the CMB Anisotropy

The CMB is a powerful tool to determine cosmological parameters in a model, particularly for GR, thanks to the accurate measurements obtained during the last decades it has been possible to infer the values of the parameters with even better accuracy than one percent [6]. In this subsection we shall briefly analyse how the CMB is affected when the cosmological parameters in the standard model are varied.

Here we are going to take into account only a part of the whole set of cosmological parameters such that the resulting standard model considered is suitable to be compared to our models later on along the following chapter of this thesis. For example we are going to fix the curvature parameter to zero since we are studying a flat universe case, also we are going to set the neutrino's masses to zero.

Next we are going to analyse the effects that each relevant parameter has on the anisotropy. First, we will consider a subset that changes only the height of the peaks. Because these parameters affect the spectrum in the same way they are usually degenerate, then in order to determine them we need to consider different observations to discriminate each parameter from the others.

- **Tilt or spectral index-** According to inflationary theories, the primordial power spectrum of perturbations has a very simple form

$$P_0(k) = A_0 k^n$$

Where A_0 is the primordial amplitude and n is the spectral index. The value of A_0 is around 10^{-12}. The value $n = 1$ has a particular significance. It is called the Harrison-Zel'dovich scale-invariant spectrum. If the initial power spectrum has such form the perturbation have equal power at every scale. If $n < 1$ then the small scale anisotropies are smaller than when $n = 1$. From all the parameters in the subset, the characteristic effect of this one is the pronounced tilt that it produces and because of that the most easily extracted.

$$\frac{C_l(n)}{C_l(n=1)} \simeq \left(\frac{l}{l_{pivot}}\right) \tag{2.121}$$

l_{pivot} is determined by the normalization of the primordial spectrum.

- **Normalization** This parameter modulates the amplitude of the primordial spectrum and trivially changes the height of the peaks. It is the only parameter that can raise the amplitude of the entire spectrum.

- **Reionization** It is the name given to a late epoch in the history of the universe when it was almost ionized. This is inferred from the absorption spectra of high redshift-quasars where no evidence of neutral hydrogen is seen below $z \sim 6$ [125]. At this epoch the CMB returns to be in touch with electrons and if the scattering rate is sufficiently high isotropy is restored. If the CMB photons arrive to a region with optical depth κ, only a fraction $e^{-\kappa}$ will escape so the temperature that we see today is [97]

$$T[1+\Delta]e^{-\kappa} + T(1-e^{-\kappa}) = T[1+\Delta e^{-\kappa}] \tag{2.122}$$

This argument affects only scales inside the horizon at the epoch of re-ionization. Smaller scales will be suppressed by $e^{-\kappa}$.

Now we are going to study a subset of parameters which affect the CMB in various ways so they are not expected to be degenerate. All of them produce a shift in the locations of the peaks of the spectrum. To understand this lets recall a feature of the acoustic oscillation studied before. On one hand, inhomogeneities on scale k appear at an angular scale $l = k\tau_0$. On the other hand, from the solution for the monopole of the

anisotropy we can conclude that the peaks appear at $l_p = n\pi\tau_0/r_s(\tau^*)$. Since $r_s(\tau^*)$ depends on the matter density and the baryon energy density the positions of the peaks do as well.

- **Matter Density** $\Omega_m h^2$ Since l_p is quite sensitive to this parameter. When it is varied the positions of the peaks is importantly shifted. If matter density is low, equality occurs closer to recombination so the radiation density is considerable when computing perturbations at recombination. This also implies that the gravitational potentials are still decaying at recombination and they are a driving force for the oscillations. In consequence $\Delta_0(\tau^*)$ is larger than in a matter dominated universe. Furthermore, as we already mentioned, the time-varying potentials at recombination produce an early ISW effect which contribute to the spectrum, therefore the small-scales anisotropies increase if the matter density decreases.

- **Baryon Density** $\Omega_b h^2$ The sound horizon at recombination $r_s(\tau^*)$ is sensitive to this parameter but not as much as $\Omega_m h^2$, when varied the location of the peaks are shifted. In addition to this shift, changes in $\Omega_b h^2$ affect the height of the anisotropy, in particular the odd peaks are higher than the even peaks when the baryon density is large. This comes from the fact that the frequency of acoustic oscillations decreases when the mass of baryons increases. This modification to the spectrum is unique and is only produced by the baryon density parameter, so it is the easiest to extract from data.

- **Cosmological Constant** This parameter is relevant only at late times and it does not affect recombination at all. The only effects it can have are on the free-streaming and on the largest scales just entering the horizon today. It produces a small shift on the peak locations because it affects the conformal distance to recombination. The cosmological constant also has an important effect on the late ISW which enhances the anisotropy at large scales (small l) and increases the heights of the three first peaks.

2.4.2 The Large Scale Structure of the Universe

2.4.2.a Evolution of Matter Perturbations

One of the main problems that Modern Cosmology tries to describe is the formation of structure of matter under gravitational instability. Can structure in an expanding universe form from gravitational collapse of small fluctuations? If the answer is yes, then does the observed amount of structure agree with our theory? For the most part, these questions only deal with non-relativistic matter. Furthermore, most observable structure, for instance galaxies, is on scales much smaller than the cosmological horizon. Because of these two reasons, to describe structure formation in cosmology it is sufficient to use Newtonian perturbation theory mainly described by the continuity and Euler equations, which combined lead to

$$\ddot{\delta} + 2H\dot{\delta} + \left(\frac{c_s^2 k^2}{a^2} - 4\pi G\bar{\rho}\right)\delta = 0 \tag{2.123}$$

This equation mainly describes the so called gravitational instability that generates the formation of over-densities. This equation is similar to that of a static fluid with varying density. Notice that the expansion of the universe gives rise to a damping term which can be ignored if we consider that expansion is quasi-static in comparison to the evolution of the perturbation so the remaining system corresponds to an harmonic oscillator. In order to analyze the evolution of these matter perturbations lets define the Jeans scale as [78]

$$k_{Jeans} \equiv a\frac{\sqrt{4\pi G\bar{\rho}}}{c_s} \tag{2.124}$$

- if $k > k_{Jeans}$ we obtain oscillatory and stable solutions.
- $k < k_{Jeans}$: cannot be determined if the solutions grow or decay. Further information about H is needed.

The solutions of cosmological perturbations naturally split up in three stages. Looking at the solutions of the modes of the gravitational potentials for different scales we can observe that

1.- Early Times: all the modes are outside the horizon and the potential is constant.

2.- From radiation to matter domination epochs: the modes enter the horizon. The potential suddenly changes dramatically. The large scale mode which enters the horizon after equality falls down later and in less extent than the small scale mode which enters the horizon before equality.

3.- Late matter dominated epoch: the modes at different evolve in similar way remaining almost constant.

Consistently with such qualitative analysis formally it turns out that the solutions for the potential are given as

$$\Phi(\vec{k},a) = \frac{9}{10}\zeta(\vec{k})T(k)G(a) \tag{2.125}$$

where $\zeta(\vec{k})$ is the primordial random fluctuation determined by inflation, $T(k)$ is the transfer function describing the transition in the evolution of the modes at horizon crossing during the transition from radiation domination to matter domination eras. Finally $G(a)$ is the growth function which describes how perturbations grow coherently at late times.

The easiest way of probing the potential is determining the matter distribution mainly at late times which are related by

$$\delta(\vec{k},a) = \frac{k^2\Phi(\vec{k},a)a}{(3/2)\Omega_m H_0^2} = \frac{3}{5}\frac{ak^2}{\Omega_m H_0^2}\zeta(\vec{k})T(k)G(a) \tag{2.126}$$

At late times, when the potentials are inside the horizon the matter perturbation grows as time runs on. Intuitively, over-dense regions attract more and more matter becoming more overdense.

2.4.2.b Matter Power Spectrum

In practice the quantities that we determine by using perturbation theory are only expectation values rather than precise values of the perturbations. The situation can be thought as if we could have different inflationary situations and the perturbations would have phases additionally to the amplitude that is usually computed. This means that they are random variables generated by some random homogeneous and isotropic process. The quantity that can be computed for a given model that may be compared with observations is the power-spectrum, that is the Fourier transform of the two-correlation function. If the perturbations come from the generic prediction of inflation and then they are Gaussian then the power spectra contains the full statistical information of the model [102].

There is a difficulty about this picture, that we could never measure expectation values at all since we have only one universe, in other words only one realization of the stochastic process in question. However a way to approximately compute the power spectra is to determine the mean square fluctuation on a given scale k by averaging over many patches of size $1/k$ assuming that the spatial averaging is equivalent to

the ensemble averaging (the ergodic theorem is satisfied) . This works to scales smaller than the horizon otherwise the cosmic variance problem arises: the sum over independent volumes at a given scale may differ considerably from the ensemble average.

A generic power spectrum in Fourier space is defined as follows. Lets consider a scalar variable S at fixed physical time t_0 [102]

$$\langle S(\vec{k},t_0)S(\vec{k}',t_0)\rangle = (2\pi)^3\delta_D(\vec{k}-\vec{k}')P_S(k). \tag{2.127}$$

where δ_D denotes the Dirac delta. The average is assumed to be of ensemble type over random initial conditions in a given model. It is also assumed statistical isotropy since every direction has the same probability to occur. Also statistical homogeneity is assumed since every point in the Fourier space is equally preferred [102].

The power spectrum of matter observed today in terms of the the primordial power spectrum generated during inflation [97] $P_\Phi = (50\pi^2/9k^3)(k/H_0)^{n-1}\delta_H^2(\Omega_m/D_1(a=1))^2$ can be computed at late times in terms of the transfer function $T(k)$ studied below and the growth of matter perturbations $D_1(a)$ giving rise to

$$P(k,a) = 2\pi^2\delta_H^2\frac{k^n}{H_0^{n+3}}T^2(k)\left(\frac{D_1(a)}{D_1(a=1)}\right)^2 \tag{2.128}$$

where δ_H is related to the COBE normalization and corresponds to the matter density perturbation at the Hubble scale today. This convention is the following: since the potential is constant in the matter dominated epoch, the large-scale observations of COBE set the overall amplitude of the potential power spectrum today. The matter power spectrum above has dimensions of volume and $d^3kP(k)/(2\pi)^3$ corresponds to the power excess in a bin of width dk, so after being integrated over all direction of k the excess becomes $(dk/k)\mathscr{P}^2(k)$ with

$$\mathscr{P}^2(k) \equiv \frac{k^3P(k)}{2\pi^2} \tag{2.129}$$

At this point we can see that $\delta_H = \mathscr{P}^2$ and corresponds to a Harrison-Zel'dovich-Peebles spectrum of size equal to the horizon [144, 241, 343]. By looking at the figure we can observe some features of the power spectra, first at large scales $P \sim k$ where the transfer function is unity and $n = 1$. Second, at small scales the power spectrum bends downwards. This happens because on one hand at sufficiently small scales, the perturbations enter the horizon well before equality. On the other hand at the radiation era the potentials are decaying and then the transfer function is smaller than unity. The result is that the matter perturbations grow very slowly for a while just after matter onset. This suppression is stronger for smaller scales thus the power

spectrum decreases while the scale decreases (or k increases). So the turn over of the power spectrum occurs on the scale sized as the horizon at the time of equality. Another important scale is the one at which nonlinearities become important, that is about $k \sim 0.2hMpc^{-1}$ in most of the models

2.5 Summary of the Chapter

In this chapter we reviewed some aspects of the standard cosmological model which are relevant for rest of the Thesis. The contents of this chapter are the basis to develop and understand the same formalism applied to the simplest modifications of gravity: the Brans Dicke theory and a generalization of it, the effective scalar tensor theory studied along chapter 3 and chapter 4. There we try to extract the new physics carried by the new degrees of freedom leading to the modification, and this is achieved by contrasting the behavior of certain observables in such models with their already known features within the standard model.

Specifically , in this chapter we reviewed the standard paradigm that has allowed to draw a precise picture of our universe. As any physical theory, the basics in our palette are predictions of different types of observable quantities, which in principle are associated to quantities that can be measurable in the real world. In the previous chapter we had realised that the standard model based on general relativity and the cosmological principle, provides an excellent picture of the universe since its predictions agree with high accuracy with the cosmological observations so far in despite of bearing yet unsolved issues like the cosmological constant problem and the yet undetected dark matter.

Given the important and active moment of cosmology and the stream of observational data that comes out from various ultra-precise surveys, very specific observables arisen in a model can be strongly tested. For instance the CMB temperature and polarization anisotropies, direct measurements of distances of supernovae to test dark energy and observations of the distribution and structure of matter in the universe. In this chapter we introduced all the theoretical machinery, within ΛCDM, to derive the relevant observables to be tested in the next chapters. Although the basics we presented here are restricted to ΛCDM only, the set up of the model is also valid for other models based on different metric theories of gravity. The analysis of the physical implications is very similar at least in the theories we study in chapters 3 and 5.

CHAPTER 3

THE BRANS-DICKE COSMOLOGY

3.1 Historical Review of the Brans-Dicke Theory and its Generalizations

The Brans-Dicke theory of gravity (BDT)[46, 75] and its generalizations (gBDT), are among the simplest extensions of General Relativity depending on one free function $\omega(\phi)$. Historically the former has been an important model in which deep ideas were imprinted, it also inspired precise tests for general relativity and raised as the first viable alternative to it. It was first formulated by a number of people as an implementation of a varying gravitational coupling in General Relativity.

P. Jordan and his colleagues around 1959 in Germany [164] looked into Kaluza-Klein's first five-dimensional version of general relativity attempting to unify gravity with electromagnetism. Afterwards, it appeared the possibility of a 5th dimensional component of the metric, a scalar which might play the role of a dynamical Newton constant as suggested by Dirac [94]. In the original 5-dimensional GR, when the 5-dimensional spacetime is compactified to the 4-dimensions, the usual Einstein equations result coupled to the electromagnetic stress tensor and to the 5th component of the metric, in this case this Kaluza-Klein mode plays the role of a dynamical gravitational coupling. This result was the first hint of a varying G_N. Jordan and company, however, proposed purely 4-dimensional field equations for a scalar field related to Newton's constant. Shortly after Brans and Dicke [46] independently arrived at very similar result.

The starting point of Brans and Dicke in the early 1960's was Mach principle, that inertial frames of reference should be defined with respect to the whole mass of the universe. Thus the inertial masses of elementary particles must not be fundamental and absolute constants but they should rather represent the interaction of particles with some cosmic field coupled to the rest of the mass in the universe. This implies that the

absolute scale of elementary particles of the scalar field ϕ [321]. Because of these considerations Brans and Dicke proposed that in the correct equations of motion for gravitation G_N should be replaced by $\frac{1}{\phi}$ and, for consistency, they should also include the energy momentum tensor of the scalar field in the source of the gravitational field.

In order to implement explicitly the Mach's principle a cosmic non-canonical, dimensionless, massless scalar field ϕ is introduced which is coupled to gravity only. The action describing such a situation is given by

$$S = \frac{1}{16\pi G_N}\int d^4x\sqrt{-g}\left[\phi R - 2\Lambda - \frac{\omega}{\phi}(\nabla\phi)^2\right] + S_m, \tag{3.1}$$

where g is the metric determinant, R is the scalar curvature, ∇ is the covariant derivative corresponding to the metric, G_N is the Newton's constant and S_m the matter fields action. Note that this action is similar to that of GR, the only difference is that the scalar field normalizes the gravitational coupling. The scalar is only coupled to the metric and the metric is minimally coupled to the matter fields. Thus test particles travel along geodesics and then the weak equivalence principle is satisfied.

As in GR the curvature of the space-time is generated by the matter contained in it and the gravitational forces are purely geometric effects due to the curvature of the space-time. The strength of the coupling of this force is given by the inverse of the scalar field. This is achieved due to the weak equivalence principle.

In contrast to GR, the gravitational coupling varies in time and position. In this way, inertial masses of particles are not absolute quantities, instead they depend on the local value of the cosmic scalar field whose current value is related to the Newton constant that measure on earth.

A specific model is determined by a single parameter ω ,as we shall see below it modulates the value of the field and its variation. The natural conformal frame of this theory is the Jordan frame where the weak equivalence principle exclusively holds.

In later years, Bergmann [35], Nordtvedt [165] and Wagoner [317] proposed a generalized version of BDT by considering the most general scalar-tensor theory of gravity at the time, this was done by upgrading the only free parameter ω to a free function of the scalar field and allow the scalar field having an arbitrary potential.

As mentioned in the introduction, during the 1960's Dicke led a huge push to experimental tests of GR and its alternatives. This explosion of interest in relativity was in part due to the promotion of these viable alternative theories. The gap between the theory and the experiment was developed thanks to Will, Norvedt , Thorne among others [326]. For example, Nordtvedt used the BDT as an explicit case in which the gravitational free fall acceleration of massive bodies depends on their gravitational binding energy, and suggested testing the consequences of this possible violation of

the "strong equivalence principle" in the laser ranging data to the moon [226–228]. This led to one of our best current 'null' tests of Einstein's theory.

As we see, BDT has been useful as a contrasting theory of gravity, however the original BDT hardly differs from GR when confronted against observations. The BDT predictions fractionally differ from the general relativistic ones by around $1/\omega$, therefore the constraints from the Viking radar ranging data to Mars give $1/\omega < 2x10^{-3}$ at one sigma [326]. Furthermore, the measurement of the Parameterized Post-Newtonian parameter γ (see [326, 327]) from the Cassini mission gives $\omega > 40000$ at the 2σ level [2, 36, 327]). This raises the following questions concerning all alternative theories of gravity: Are there alternative relativistic theories of gravity which pass the various existing solar-system tests, but which differ appreciably from general relativity in the other regimes of strong or rapidly varying gravitational fields? And, if affirmative, is there a reasonably exhaustive way of parameterizing all the strong-field or rapidly-varying-field effects that distinguish those theories from general relativity? And as for BDT: Is it still worth studying it further?

Regarding the first two questions, we have good reason to think that the answers may be affirmative. As for the last question, we would like to convince the reader that the answer is affirmative as well.

In the more recent decades after the 1960's, BDT has turned out to be relevant since it appears as the special case or a limit of more sophisticated but also more realistic and physically-motivated theories. For instance, BDT is a close cousin of the so-called Galileon theories [223], recently proposed to explain cosmic acceleration while evading Solar System constraints. In other more theoretical grounds, the scalar-tensor action also arises as a special sector of the Plebanski action when the trace component of the simplicity constraints is relaxed in the absence of matter fields [31]. Finally as we discuss further below, BDT arises as a particular limit of Horndeski theory [93, 149], the most general scalar-tensor theory having second order field equations in four dimensions.

Although Solar System data provide a far superior bound on ω, on cosmological scales the story is somewhat different. In 2003 Nagata *et al.* [216] have reported that $\omega > \{50, 1000\}$ at 4σ and 2σ respectively using Wilkinson Microwave Anisotropy Probe (WMAP) first-year data (WMAP-1). However, as argued in [2], their 2σ result is not reliable as the reported χ^2 has a sharp step form, and rather, one should take the 4σ result as a more conservative estimate. Better constraints come from Acquaviva *et al.* [2] who report $\omega > \{80, 120\}$ at the 99% and 95% level respectively by using a combination of Cosmic Microwave Background (CMB) data from WMAP-1 and a set of small-scale experiments as well as Large-Scale Structure (LSS) data. Wu *et al.*in [337] report $\omega > 97.8$ at the 95% level using a combination of CMB data from 5

years of WMAP, other smaller-scale CMB experiments and LSS measurements from the Sloan Digital Sky Survey (SDSS) Release 4 [304]. Their constraint is weaker than in [2] even though newer data are used. Later [188] improve to $\omega > 181.65$ (95% level) using Planck data [4] with the same priors as [337]. Finally, as we shall find in chapter 4, we improved these constraints with Planck to $\omega > 890$ [19]. As we see, BDT has more chances of kicking in on linear cosmological grounds in contrast to complex small scales. Nowadays would be quite naive to seriously believe in BDT as a viable modification of GR that alleviates all the drawbacks of GR. Nonetheless, it might serve as a tool to test the viability of a host of theories which are indeed strong candidates to do so.

In this chapter we are going to study theoretical aspects of the Brans-Dicke theory which are going to serve to explore its phenomenology and to establish a framework to shed some light about the viability of more general modified theories of gravity in the later chapters.

3.2 The Model

In this subsection we present the setup and some technical aspects of the Brans-Dicke theories of gravity which are going to be useful in the following. As mentioned above we aim to create a theoretical framework rather than studying the BDT themselves as actual descriptions of phenomena.

The basic ingredients to construct the Brans-Dicke theory are the following

- Weak equivalence principle
- Mach's principle

As mentioned in the introduction, in order to implement the Mach's pricniple a non-canonical massless scalar field ϕ is introduced which is coupled to gravity only and it is described by action (3.1). For now we shall keep the original interpretation: the role of the scalar is that of a dynamical gravitational coupling within GR.

The equations of motion (e.o.m) resulting by extremizing the action are given by

$$\phi R_{\mu\nu} = 8\pi G_N T_{\mu\nu} + \nabla_\alpha\nabla_\beta\phi - g_{\alpha\beta}\Box\phi + \frac{\omega(\phi)}{\phi}\left(\nabla_\mu\phi\nabla_\nu\phi - \frac{1}{2}g_{\mu\nu}\nabla_\alpha\phi\nabla^\alpha\phi\right) \tag{3.2}$$

$$\phi R - \frac{\omega}{\phi}\nabla_\alpha\phi\nabla^\alpha\phi + 2\omega\frac{\Box\phi}{\phi} = 8\pi G_N T. \tag{3.3}$$

In the Jordan frame matter is minimally coupled to the metric, therefore test particle travel on geodesics and the energy momentum tensor is conserved

$$\nabla^{\mu} T_{\mu\nu} = 0, \tag{3.4}$$

where $T_{\mu\nu}$ is the energy-momentum tensor of the matter fields, T is its trace and $R_{\mu\nu}$ the Riemann curvature tensor. Note that the scalar couples indirectly to matter by means of the metric. If the metric equations (5.10) are traced and added to (5.11), the scalar curvature may be eliminated and obtain an equation for the field sourced by the metric as

$$\Box\phi = \frac{8\pi G_N}{2\omega+3} T. \tag{3.5}$$

The field is suppressed by $2\omega+3$, then for $\omega \to \infty$ the field is constant and GR is recovered. In the last equation the scalar couples to the trace of the energy-momentum tensor of matter. Note that for $\omega < -\frac{3}{2}$ the field is a ghost and thus physically pathological. It is interesting that BDT arises as a limit of more complex theories. For instance, it corresponds to the DGP braneworld model at subhorizon scales where the 5th dimension is not important with $\omega = \frac{3}{2}(\beta(t)-1)$ where $\beta(t) = 1 - 2Hr_c(1+\frac{\dot{H}}{3H^2})$, $\dot{H}$ is the time derivative of the Hubble rate and $r_c \sim \frac{1}{H_0}$ is the cross-over scale [104]. As mentioned before, equations of motion for matter are the same as in GR, however, since the metric might have a different solution due to the presence of the scalar, its final dynamics may also be modified. Notice that when $\omega \to \infty$, the scalar is constant and the theory is just GR. As suggested above, BDT is very similar to GR, with the only modification that the BDT field plays the role of a time-varying Newton's constant in order to implement the Mach's principle.

3.3 Background Cosmology

Assuming a flat, homogeneous and isotropic universe supported by observations of the galaxies distribution, the space-time geometry is described by the Friedmann-Robertson-Walker metric

$$ds^2 = -dt^2 + a^2(dx^2+dy^2+dz^2) = a^2(-d\tau^2 + dx^2 + dy^2 + dz^2), \tag{3.6}$$

where t is the synchronous proper time and τ is the conformal time. The average of the energy-momentum tensor of matter is given by

$$\begin{aligned} T_0^0 &= -\rho \\ T_i^j &= P\delta_i^j \end{aligned}$$

In order to preserve homogeinety, we consider an time-dependent scalar field upon which small perturbations may arise due to small perturbations of the metric

$$\phi = \bar{\phi} + \delta\phi. \tag{3.7}$$

The Einstein equations for the metric (3.6) become a modified version of the usual Friedmann and Raychaudhury equations [46]

$$3H^2 = \frac{8\pi G_N}{\bar{\phi}}\rho + \frac{\Lambda}{\bar{\phi}} + \frac{\omega}{2}\left(\frac{\dot{\bar{\phi}}}{\bar{\phi}}\right)^2 - 3H\frac{\dot{\bar{\phi}}}{\bar{\phi}}, \tag{3.8}$$

$$-2\dot{H} - 3H^2 - \frac{\ddot{\bar{\phi}}}{\bar{\phi}} - 2H\frac{\dot{\bar{\phi}}}{\bar{\phi}} - \frac{\omega}{2}\left(\frac{\dot{\bar{\phi}}}{\bar{\phi}}\right) = \frac{8\pi G_N}{\bar{\phi}}P - \frac{\Lambda}{\bar{\phi}}. \tag{3.9}$$

The scalar evolves in the FRW universe governed by the following equation

$$\ddot{\bar{\phi}} + 3H\dot{\bar{\phi}} = \frac{1}{2\omega+3}\left[8\pi G_N(\rho - 3P) + 4\Lambda\right]. \tag{3.10}$$

Where dotted letters denote derivatives with respect to proper time, e.g. $\dot{\bar{\phi}} = \frac{d\bar{\phi}}{dt}$ and $H = \frac{\dot{a}}{a}$.

Strictly speaking, the initial conditions must be fixed by the boundary conditions of the solution on small scales. On those scales observers in bound systems in the quasi-static regime like our solar system, would measure [46, 75][See subsection(6.3.2.a) equation (6.45)]

$$\bar{\phi}_0 \equiv \bar{\phi}(a=1) = \frac{G_N}{G_{eff}} = \frac{4+2\omega}{3+2\omega}. \tag{3.11}$$

in units where $\bar{\phi}_0$ is dimensionless. However, this assumption is quite strong since it would imply that BDT governs the physics at solar system. As we mentioned above, BDT is already not a good choice to describe gravity on that scales. If we aim to consider more general modifications of GR at the very large scales, $\bar{\phi}_0$ should be allowed to have different values, for that reason in this work we study models in which it is a free derived parameter. In our treatment we used as a primary free parameter the initial condition of the scalar at early times $\bar{\phi}_{ini}$ and derived $\bar{\phi}_0$ from it and the

evolution equations. From now on we'll call such models as "unrestricted models" (uBDT). For completeness, we also consider models which gravitational coupling is fixed as usual, we call them "restricted models" (rBDT).

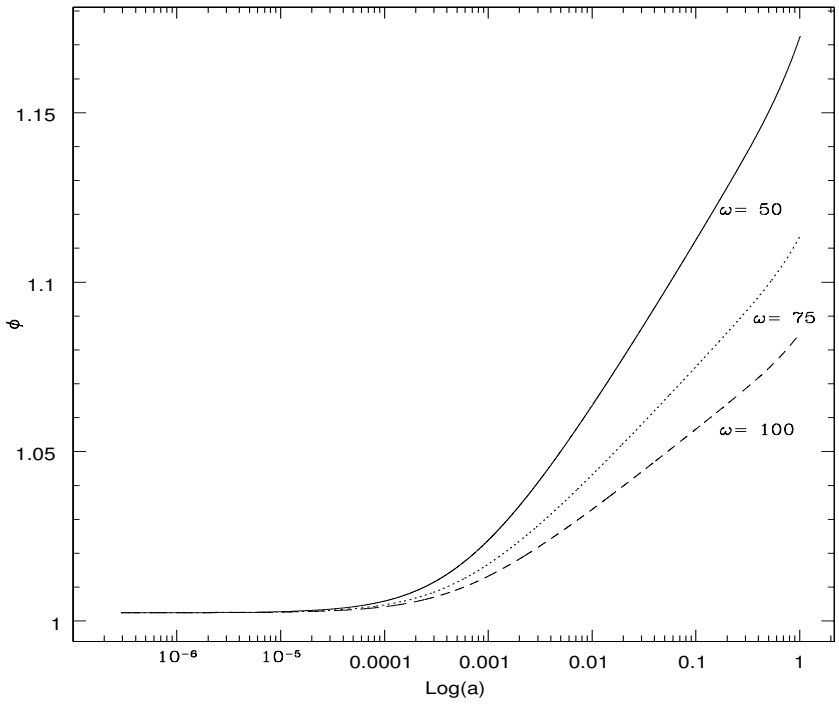

Fig. 3.1 Exact numerical solutions for the background scalar field $\bar{\phi}$ in the restricted models for a range of ω values. The plot shows the absence of growth during the radiation era and the logarithmic growth during the matter era. The larger ω the slower the growth.

As figure (3.1) shows, the field stays constant during the radiation era because (3.10) is sourced by $\rho - 3P = 0$ (since $P = \frac{1}{3}\rho$ for photons), resulting in $\bar{\phi}$ behaving like a massless scalar. As the Universe enters the matter era, however, $\bar{\phi}$ grows but only logarithmically with the scale factor a. Thus, the scalar field today, $\bar{\phi}_0$, is expected to be within a few percent of its initial value in the deep radiation era.

Now lets analyse the expansion history in these models. From equation (3.8) is straightforward to get

$$(H + \frac{1}{2}\frac{\bar{\phi}'}{\bar{\phi}})^2 = \frac{8\pi G_N}{\bar{\phi}}\rho + \frac{\Lambda}{\bar{\phi}} + f(\omega)\left(\frac{\bar{\phi}'}{\bar{\phi}}\right)^2 \tag{3.12}$$

where $f(\omega) = \frac{1}{4}(2\omega + 3)$. Typically, for realistic models the mean value of ω is large enough so the scalar is approximately constant then the Friedman equation is

nearly $3H^2 \approx 8\pi G_{\rm eff}\rho$ where the effective cosmological gravitational strength is given by

$$\xi = G_{eff}/G_N = 1/\bar{\phi}_0. \tag{3.13}$$

where $\bar{\phi}_0$ is the value of the scalar today. Thus, effectively ξ is a derived parameter which rescales the gravitational coupling measured in a bound system formed today. On the other hand, even for $\omega \sim 1$ (3.12) is just like in GR at very early times because the scalar is not coupled to radiation.

For the restricted BDT case, the larger value of ω is, the closer is universe to a FRW. As the scalar and its derivative are enhanced when $\omega \to 1$, the universe expands quicker due to the scalar's derivative contribution in the l.h.s of the Friedmann equation.

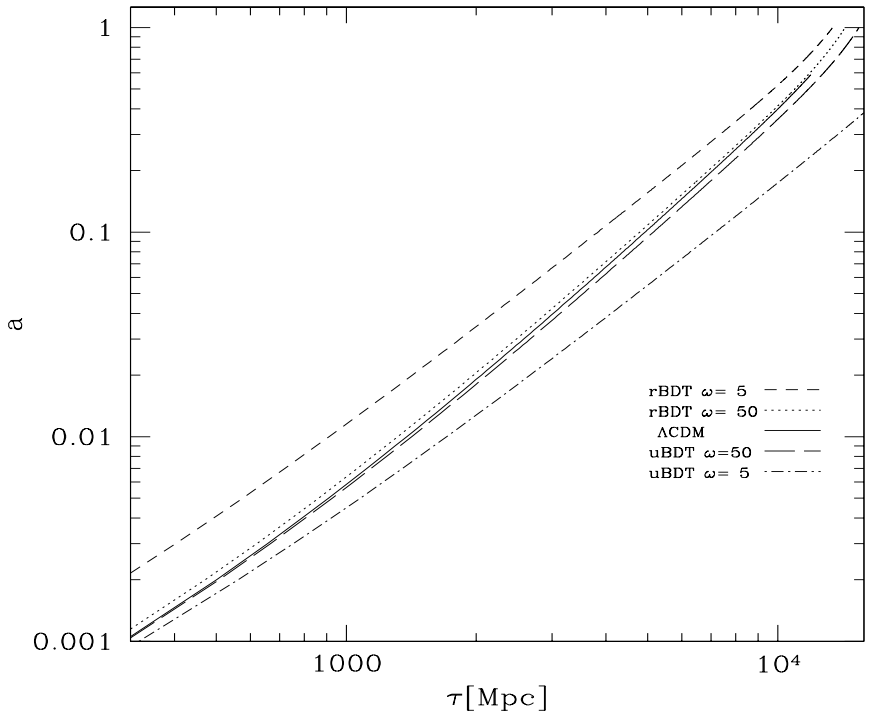

Fig. 3.2 The scale factor for uBDT ($\bar{\phi}_{ini} = 1$) and rBDT. When the effective G_N increases for the restricted case the scale factor increases as well because the universe expands more rapidly

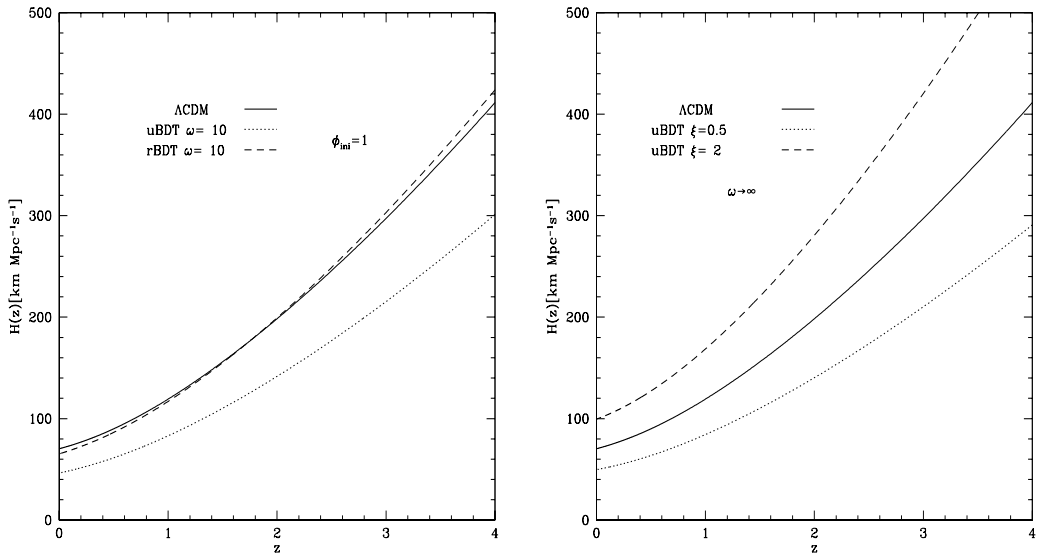

Fig. 3.3 Left: Variation of the Hubble rate as function of redshift with respect of ω for uBDT and rBDT models with $G_{eff} = 1.043$. The solid line corresponds to the ΛCDM model with $G_{eff} = 1$. In both cases the curve $H(z)$ bends upwards at early times and downwards at late times. Right: Variation of the Hubble rate as function of redshift with respect of ξ for uBDT. As expected, the expansion rate effectively increases when the gravitational strength is rescaled.

In the restricted case the mean value of G_{eff} decreases for smaller ω whilst it stays constant in the unrestricted case. Thus, the unrestricted models have an additional convenience over the restricted ones since the effects of $\bar{\phi}$ and $\dot{\bar{\phi}}$ over the expansion are uncorrelated since ω and ξ control each of them independently. We can observe such effects by looking how the Hubble rate depends on ω and ξ respectively as figure (3.3) shows.

The left panel displays $H(z)$ for different values of ω either for uBDT or rBDT with a fixed G_{eff}, notice that when ω decreases in both cases the curve of the Hubble rate bends upwards at early times and it does downwards at late times. The way in which the expansion history departs from the ΛCDM curve follows the same direction in both cases, however the modification of $H(z)$ for uBDT models is more pronounced than for the rBDT ones for large redshifts.

On the other hand, at late times, the Hubble rate for uBDT departs from the ΛCDM more than for rBDT. Since the turn over happens at relatively late times, the modification of the expansion rate at recombination time is more important in uBDT models. This difference is going to be important when we study the CMB of BDT. The right panel shows us how the Hubble rate, as function of redshift, changes when ξ

decreases. It is actually straightforward to realise intuitively the resulting effect: the expansion rate increases as the gravitational strength, controlled by ξ, increases.

Finally I'd like to mention roughly how distance measurements behave in BDT. Later, in section (3.7.5) of this chapter, we will study with more detail further measurements like the sound horizon and the acoustic scale. As expected, since the expansion history is modified in BDT, either the comoving distance as the angular diameter distance are sensitive to ω. As it decreases, distant objects appear further away from us in relation to the prediction of ΛCDM. Thus, it is a good idea to constrain BDT by using measurements of distance at cosmological scales as we do in the next chapter.

3.4 Conservative Bounds on the Horndeski's Subclass

Regardless of the simplicity of the BDT model, its importance relies in that it can approximate a wide subset of Horndeski theories, the most general second order scalar-tensor theories proposed in [93, 149], which their gravitational action is

$$S[g,\psi] = \frac{1}{16\pi G}\int d^4x\sqrt{-g}\sum_{I=0}^{3} L^{(I)} \tag{3.14}$$

where ψ is by convention dimensionless and $L^{(I)}$ are given by

$$\begin{aligned}
L^{(0)} &= K^{(0)} \qquad\qquad L^{(1)} = K^{(1)}\Box\psi && (3.15)\\
L^{(2)} &= K^{(2)}\,R + K^{(2)}_X\left[(\Box\psi)^2 - (D\psi)^2\right] && (3.16)\\
L^{(3)} &= -6K^{(3)}\,G^{\mu\nu}\nabla_\mu\nabla_\nu\psi \\
&\quad + K^{(3)}_X\left[(\Box\psi)^3 - 3(D\psi)^2\Box\psi + 2(D\psi)^3\right] && (3.17)
\end{aligned}$$

where $X = -\frac{1}{2}g^{\mu\nu}\nabla_\mu\psi\nabla_\nu\psi$, $D\psi = \nabla\otimes\nabla\psi$ and $K^{(I)}$ are functions of X and ψ. The general functions $K^{(I)}$ may be expanded as an analytical series and whose lowest order terms are

$$\begin{aligned}
K^{(0)} &\approx -2\Lambda + 8\omega X + \varepsilon_1\psi^2/\ell_*^2 + \varepsilon_2\ell_*^2X^2, && (3.18)\\
K^{(1)} &\approx \varepsilon_3\psi^2 + \varepsilon_4\ell_*^2X && (3.19)\\
K^{(2)} = &\approx \psi^2 + \varepsilon_5\psi^4 + \varepsilon_6\ell_*^2X && (3.20)\\
K^{(3)}/\ell_*^2 &\approx \varepsilon_7\psi^2 + \varepsilon_8\ell_*^2X. && (3.21)
\end{aligned}$$

These expressions are the approximate functional forms for $K^{(I)}$ corresponding to scales above some very large length scale ℓ_*. We have ignored the constant terms in $K^{(1)}$ and $K^{(3)}$ as they lead to total derivatives. The constant term in $K^{(2)}$ cannot be ignored in general but would lead to GR coupled to a massless scalar as $\varepsilon_i \to 0$ and is irrelevant to our work.

As the coefficients of the expansion $\varepsilon_i \to 0$ and further performing the field redefinition $\phi = \psi^2$ we recover the BDT. In other words, the leading order action is that for BDT, so this setup for the $K^{(I)}$ is restricted for theories that exclusively approximate to BDT at cosmological scales. We see that although the complete set of Horndeski theories is defined by four free functions of ψ and X, by restricting the set as above we get eight free constant parameters rather than functions. Thus our results hold for any Horndeski theory which can be approximated in the above form on cosmological scales.

In the next chapter we shall determine the limits on which ω lays according to observations, we will see they lay between $300 - 2500$. Choosing $\omega \sim 500$, $\ell_* \sim 1/16H_0$ (Hubble scale at recombination) and using the BDT background solution as $\dot{\bar{\phi}} = \frac{H}{\omega}$ and $\bar{\phi} \sim 1$ we find conservative estimates for the coefficients as

$$\varepsilon_i \ll \{10^{-2}, 10^5, 10, 10^5, 1, 10^3, 10^3, 10^5\}. \tag{3.22}$$

Theories within these limits might be approximated by BDT.

3.5 Big Bang Nucleosynthesis

We've already studied very carefully in the previous chapter how the light elements were formed at the time of nucleosynthesis. The details of this formalism work in almost the same way for BDT than for GR, the main modification arises only due to the different expansion history in both models.

As we know, since the rate of the interactions is determined by the rate of expansion which, at the same time, is affected by the strength of gravity, a different solution to ΛCDM would produce different rates of these reactions and different amounts of final species as well. Thus any observational evidence about the history of nucleosynthesis and recombination serves to constrain the evolution of the scale factor at those times. Actually, it is a typical practice to constrain the amount of baryons in the universe by fitting the abundances of light elements at nucleosynthesis estimated directly from nuclear and atomic physics.

However, in the context of modified gravity not only baryons might be constrained by these means but also the strength of gravity G_N, since dynamical G_N arises naturally in these models. Even though at early times BDT behaves similarly to GR and then these processes occur in very similar way than with FRW [See figure (3.4)], any tiny modification would allow us to accurately test some features this model. This test is particularly interesting for the unrestricted models since the modification of G_N at early times is important thanks to the rescaling of the initial conditions.

Moreover, it results an ideal test when it comes from a theory violating the strong equivalence principle just as BDT and their relatives. In chapter 4 we will present a review of different constraints of G_N by using BBN light element abundances. For now, we will focus on studying the effects due to the presence of the BDT scalar over the relevant quantities arisen from recombination history such as the visibility function, the ionization fraction and the light elements abundances.

It would be interesting to study the effects of a dynamical gravitational coupling during BBN and recombination. However, at BBN, the BDT's scalar field is coupled only to the small amount of newborn baryonic matter. So it is expected that the process of formation of atoms to be barely modified. Actually, in the classical restricted sort of BDT, the modification is basically null. However, as pointed below, it's straightforward to note that G_N in the unrestricted BDT might suffer rescaling even if its value stays steady at those early times. We called the rescaling constant as ξ, the effects on the abundances are shown by the following figures.

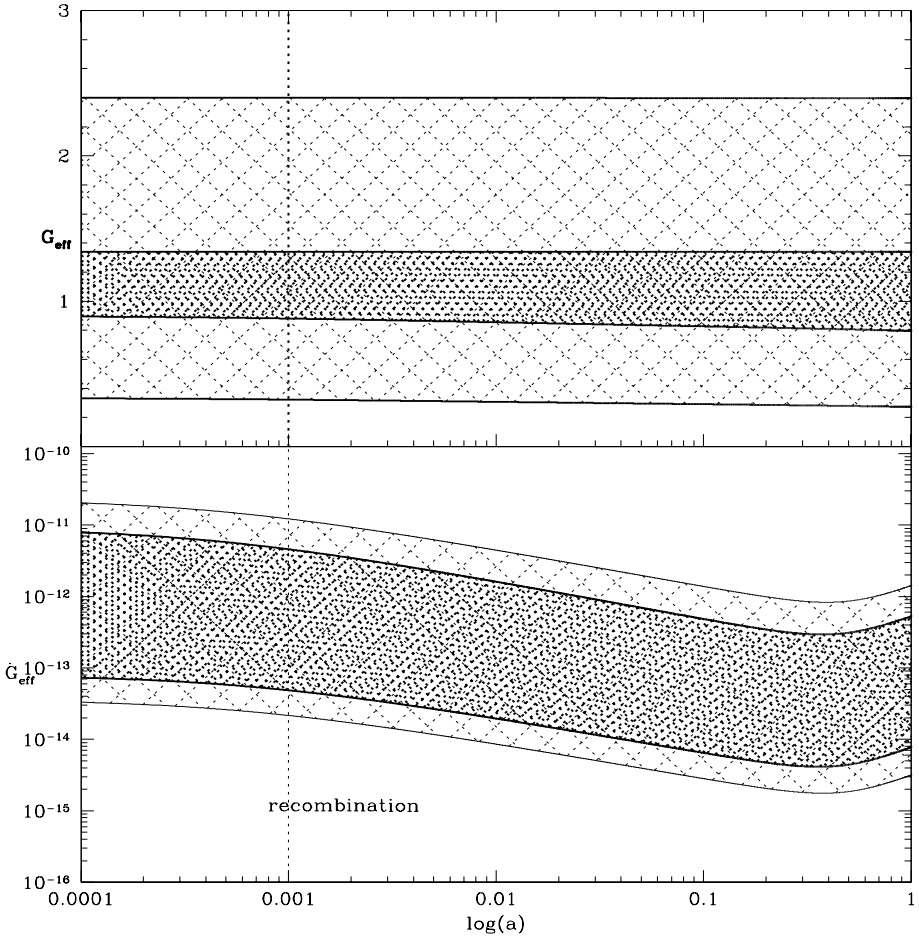

Fig. 3.4 Evolution of the scalar field and its variation along the universe's history for a set of models allowed by the data (CMB from Planck(dark band), WMAP7(pale band)plus BBN. For realistic models constrained by BBN and the CMB, G_N stays practically constant at BBN and recombination times. However, the stunningly accurate tests available today allow us to drop $\dot{G}_N$ below $O(10^{-12})$.

The stronger gravity is, the universe expands quicker and then the neutron-to-proton ratio increases since the reactions freeze out at higher temperature, then the resulting abundances increase as well as the figure (3.5) shows. Constraints on G_N by using light elements abundances measurements ($Yp = 0.2452 \pm 0.0015$ from [338], $DH = (2.78^{+0.44}_{-0.38})$ from [82] along with the CMB from WMAP1) have been firstly obtained by Umezu et al. in [307] in the context of GR. As it is shown forward in following chapters, Avilez and Skordis updated the result the last year by using more recent estimations of BBN abundances from [160] and the Planck data [6] in the context of unrestricted BDT models applying the same method than Umezu.

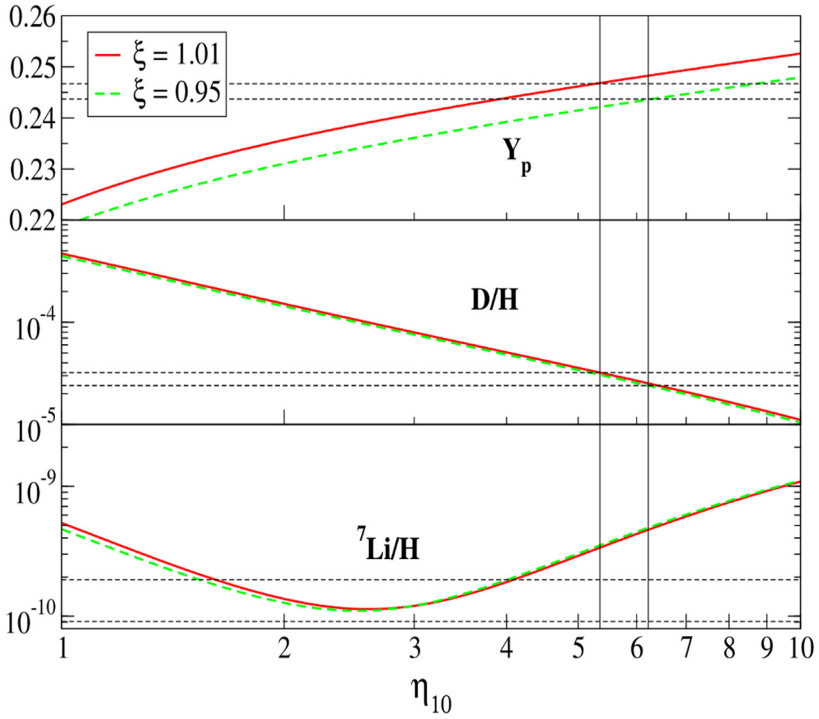

Fig. 3.5 Abundances of deuterium (DH), helium and lithium as functions of the amount of baryons quantified by η_{10} and the strength of gravity G_N, plot taken from [307]. The final abundance of an element depends not only of the amount of protons(baryons) but also on how strong gravity is.

3.6 Recombination History

Measurements of the temperature and polarization anisotropies of the cosmic microwave background tightly constrain the expansion rate of the universe during recombination. From what we have studied in chapter 2, we know that a change in the expansion rate modifies how the recombination of hydrogen is carried out. This change alters the shape of the acoustic peaks and the level of CMB polarization. This test is similar in spirit to the examination of abundances of light elements produced during big bang nucleosynthesis and it becomes a good ruler to measure possible departures from standard recombination.

The modification of the expansion history affecting the history of recombination is relevant at ($z \sim 1100$). In the context of BDT, as in nucleosynthesis, the most important effect is due to the normalization to the gravitational strength which is effectively significant in the unrestricted models rather the standard BDT. On one hand , since realistic models yield $\omega >> 1$ we could naively suspect (a priori) that the restricted

models behave basically like ΛCDM at these early times and any observational signature would come out. On the other hand, for unrestricted models G_N will suffer a rescaling and then important effects on the recombination history would be expected. Nonetheless, we will discover (a posteriori) that the slightly modified expansion history (even in the restricted case) carries interesting features of radiation at recombination era which are imprinted in the cosmic background radiation that we observe today.

The effects on recombination due to the rescaling of the Newton constant have been studied before by Zahn and Zaldarriaga [341]. Here we'll confirm what they point out: the main effect of increasing ξ (the rescaling factor of G_N) is to increase the width of the visibility function as shown in figure (3.6). If G_N were slightly different, all that would happen is that the universe would be expanding a bit faster or slower by a factor ξ.

Given that the problem of testing the Friedmann equation by using measurements of the CMB is more subtle than in the case of BBN because the dynamics of perturbations are also modified. The shape and position of the acoustic peaks of the CMB depend through the expansion rate on the size of the sound horizon and the angular diameter distance at recombination at early times and the ISW effect at late times, the effects produced by the single expansion rate at recombination can be isolated by studying the effects of the changing Newton's constant G_N as a rescaling.

$$G_N \to \xi G_N \tag{3.23}$$

BDT at early times is almost identical to FRW since $\dot{\phi}$ is negligible in comparison to radiation density. Thus the expansion rate gets just rescaled

$$H(a,\xi) = \xi f(a) \tag{3.24}$$

An interesting feature of this prescription is that we can translate the different G_N to a different recombination history only because gravity has no preferred scale and then we only measure angles when studying the CMB. The only way we can find out that such an alteration had occurred is by having an independent clock that measures the expansion rate. In our case this independent clock will be the physics of hydrogen recombination.

In order to understand the way in which the rescaling (3.23) affects the expansion rate we must note that the shape of H is unaffected by ξ. So the "expansion rate clock" is simply rescaled. As we saw in chapter 2 the anisotropies can be written as an line-of-sight integral over sources as equation (2.116) In order to see how the

anisotropy depends on ξ is better to use the expansion factor as a time variable rather than τ

$$\frac{d}{d\tau} = a^2 H \frac{d}{da} = \xi f(a) a^2 \frac{d}{da}. \tag{3.25}$$

So every time we change the time variables every time derivative introduces a factor of ξ. The dynamics of a mode with wave number k in a universe with $\xi \neq 1$ is equivalent to the dynamics of a mode with $k' = k/\xi$ in a universe with $\xi = 1$. This translates into

$$S(k, a, \xi) = S(k/\xi, a, \xi = 1) \tag{3.26}$$

The angular power spectrum of the anisotropy is given by

$$\Delta_l(k, \xi) = \int_0^1 da \;\; S_T(k, a, \xi) j_l(kD(a, \xi)) \; \tilde{g}(a, \xi) \tag{3.27}$$

where $\tilde{g}(a, \xi) \equiv -\frac{d}{da} \exp(-\kappa)$. The conformal distance is given by

$$D(a, \xi) = \int_0^1 \;\; \frac{da}{H(a) a^2} = \frac{D(a, \xi = 1)}{\xi}. \tag{3.28}$$

Suppose first that the visibility function would be independent of ξ. Then

$$\Delta_l(k, \xi) = \Delta_l(k/\xi, \xi = 1). \tag{3.29}$$

Then the power spectrum is calculated from Δ_T as

$$C_l(\xi) = \int \;\; \frac{dk}{k} \, P_0(k) \, |\Delta_T^l(k, \xi)|^2 = \int \;\; \frac{dk'}{k'} \;\; P_0(k\xi) \, |\Delta_T^l(k', \xi = 1)|^2, \tag{3.30}$$

P_0 is the primordial power spectrum. Thus, because the amplitude of the primordial power spectrum is adjusted then $C_l(\xi) = C_l(\xi = 1)$. Gravity introduces no preferred scale, so the dynamics of the perturbations remains the same when scales are measured in units of the expansion time. As a result, the angular power spectrum would not change as we rescale G_N. In conclusion ξ would not affect the perturbations if the visibility function remains the same. However the physics of recombination does introduce a preferred timescale, so the power spectra of the anisotropies will actually change. The important point here is that the only source of change is the difference in the way recombination proceeds as we change the expansion rate of the universe at early times.

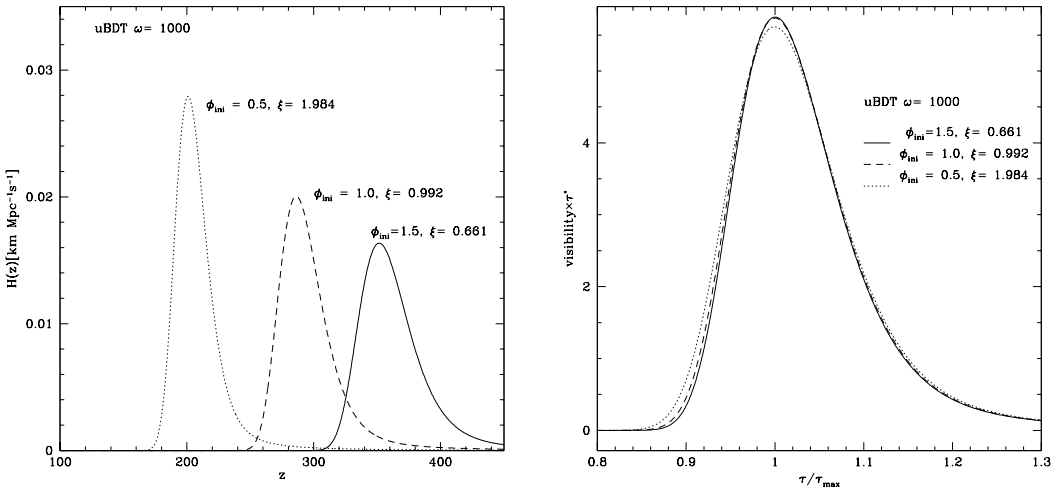

Fig. 3.6 Visibility function for different initial conditions of the scalar field. Effectively, changing the initial conditions translates in an increase of the scale factor by a factor of $\xi \sim \frac{1}{\dot{\phi}_0}$, and consequently recombination occurs before (left). If the universe expands quicker, it is more difficult for electrons to recombine and the process lasts longer since the visibility function is broader (right). Because conformal-time intervals scale differently for each BDT model, we use a more natural variable τ/τ_{max} instead of τ in order to compare the widths of the visibility for different models (right).

The visibility function changes with ξ, since the visibility function depends on the electron fraction $x_e = n_e/n_H$ and that at the same time depends on the strength of gravity and so on ξ. The faster the universe is expanding the more difficult it is for hydrogen to recombine and hence x_e is larger. This change in x_e leads to a change in the visibility function. As ξ increases the visibility gets broader. The thickness of the visibility function determines the extent to which the anisotropies at small scales get damped. We must mention that when one is aiming to calculate optical depths, this change almost cancels with the decrease in the time intervals between different redshifts due to the increased expansion rate. As a consequence, the locations and shapes of the acoustic peaks seem unaltered by ξ.

We first analyse how the expansion rate evolves and affects recombination in unrestricted models. As we pointed out above, the Friedmann equations of these models hold an interesting feature in contrast to the restricted ones: the effect of varying ω effectively decouples from the rescalings of G_N. As we saw in (3.3), the effect of ω on the Hubble rate is more pronounced in rBDT than in uBDT (ϕ_{ini}). For this reason the visibility takes its maximum at different times in both cases at a fixed ω as shown by figure (3.7). Given such initial condition for the scalar at early times, for sufficiently small ω, the resulting $\xi < 1$ whilst for large ω $\xi \sim 1$. Consequently, for larger ξ recombination occurs later.

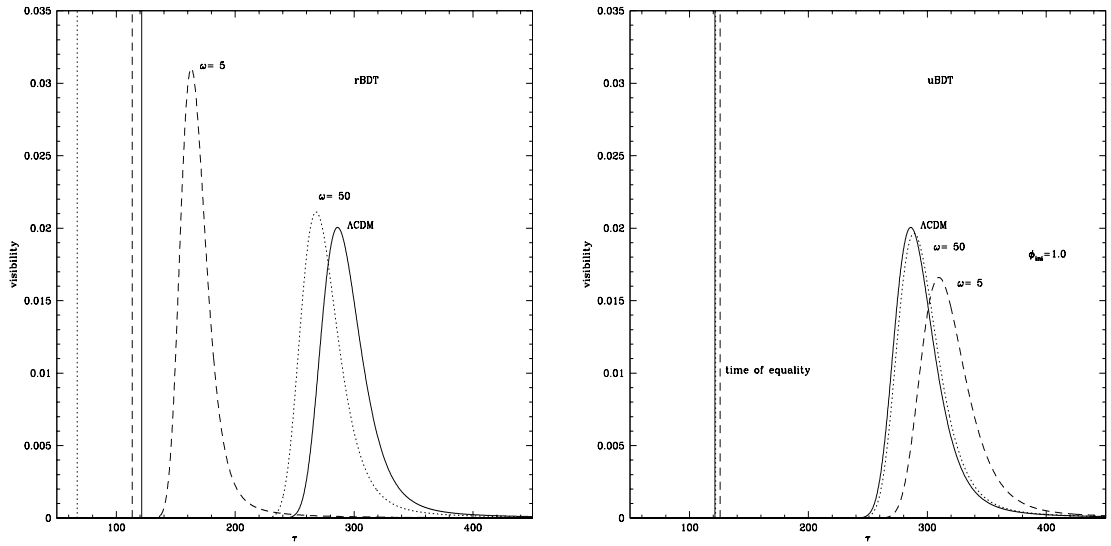

Fig. 3.7 visibility function depending on ω in restricted and unrestricted models. In both cases the visibility shifts because the expansion rate changes as ω varies. This is in agreement with figure (3.3), because the expansion rate at recombination within the restricted models increases as ω decreases recombination occurs before for those models. In turn, exactly the opossite happens within unrestricted models with $\phi_{ini} = 1$.

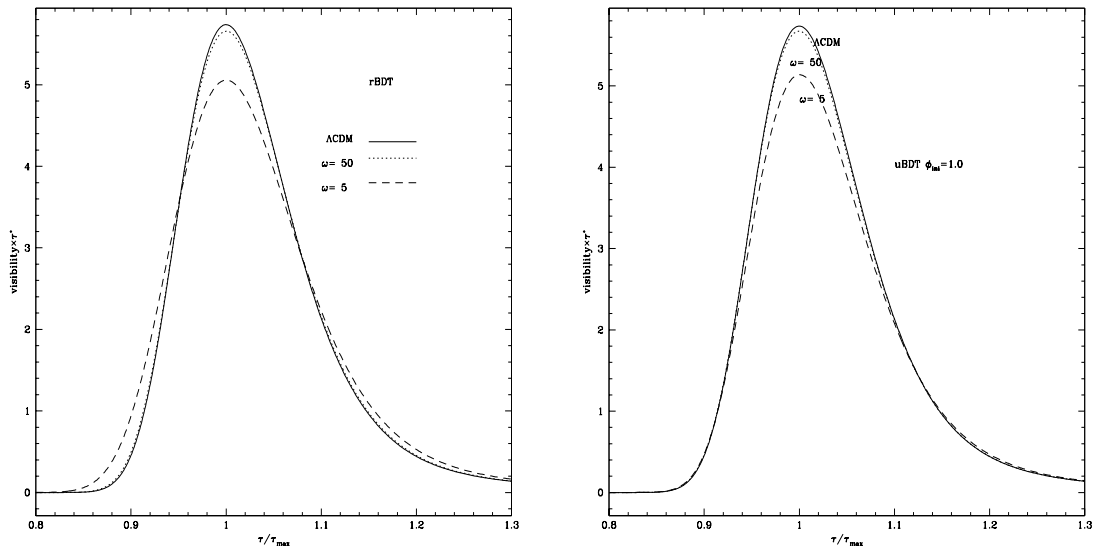

Fig. 3.8 Visibility function in uBDT and rBDT as function of τ/τ_{max}. This time variable is more natural to compare the thickness of the visibility functions arising in different models. As we see, the change in the thickness of the visibility happens in a similar way in both types of models. As the value of ω increases the visibility gets narrower and taller; this means that when the amplitude of the scalar is reduced as $\omega \to \infty$, it is easier for electrons to recombine.

Let us turn to see what happens within the rBDT models. On one hand, when ω decreases, the scalar grows efficiently leading the universe to expand quicker than in ΛCDM at recombination. This effect results from two joint contributions: the rescaling of G_N in the density term which increases as ω decreases and the contributions depending of $\bar{\phi}'$. The former increases the expansion rate and the latter only gets important when $\omega \sim 1$. Therefore, the rapid expansion achieved by making $\omega \to 1$ makes the universe reach 1 eV earlier, as a consequence, the width of the visibility function increases and then it is easier for electrons to recombine [See figure 3.8].

Notice in figure (3.8) that the way in which the shape of the visibility function is affected by ω is very similar in both rBDT and uBDT. Although for a fixed ω, recombination happens at different times depending on whether uBDT or rBDT model is being used, in both models the visibility is broader when ω decreases. Only for unrealistic models with $\omega \sim 5$, the visibility is wider in rBDT than in uBDT.

In summary, the differences in sensitivity of the visibility function in both rBDT and uBDT models are due to their differences in the expansion history of the universe. Therefore, tests of the recombination history are excellent means to detect these features.

3.7 Linear Cosmological Perturbation Theory

Given the wealth of data currently available , it is crucial to test our model by using cosmological observations, specially those testing features of cosmic fluctuations. The first part of this work (contained in chapters 2 and 3) is devoted to this a goal. Along with chapter 4, we are going to explicitly compare the theoretical predictions from BDT against observations of the CMB and Large Scale Structure. This section is devoted to studying linear perturbation theory for BDT. In order to efficiently test the model, it is essential to understand the physics behind and try to figure out observational signatures that will allow us to track effects of possible modifications to GR. First we are going to go through the mathematical formalism of the theory, after we will analyse the quasi-static limit of the exact equations at which some physics may be revealed more clearly. Finally we're going to study exact solutions of relevant perturbations in order to understand relativistic effects introduced by super-horizon perturbations.

3.7.1 Equations of Motion for Perturbations

Let us turn to a formal study of cosmological perturbation theory of BDT using the same reasoning as for GR studied in chapter 2 and similar to that of [74]. This is reasonable since it is also a metric theory of gravity and shares most of the basic principles of GR. Here we will use the synchronous gauge since it is convenient for computing perturbations, later on when we need to compute the CMB sources we will gauge transform to the conformal Newton gauge in order to use meaningful physical quantities. As we did before, we will depart from the line element of this perturbed metric given by (2.45)

Matter perturbations are described with exactly the same variables than GR in the corresponding gauge. Let us highlight that because matter is minimally coupled to the metric in the Jordan conformal frame that we use here, equations for matter are not modified at all so the GR conservation and Boltzmann equations describing the cosmological evolution of matter and energy perturbations hold in BDT. Although the equations are the same, these perturbations are affected by the scalar extra degree of freedom indirectly only by means of the metric perturbations which are directly coupled to it in this frame.

The corresponding independent modified Einstein equations (5.10) corresponding to this metric are given by

$$
\begin{aligned}
-2k^2\eta + \left(H + \frac{1}{2}\frac{\phi'}{\phi}\right)h' &= \frac{8\pi G_N}{\phi}\delta\rho + \left(\omega\frac{\phi'}{\phi} - 3H\right)\frac{\delta\phi'}{\phi} \\
&- \left[k^2 + 3H^2 + \frac{\omega}{2}\frac{\phi'^2}{\phi^2}\right]\frac{\delta\phi}{\phi} \\
2k^2\eta' &= \frac{8\pi G_N a^2}{\phi}(\bar{\rho} + \bar{P})\theta(Syn) + \frac{\delta\phi'}{\phi} \\
&- \frac{1}{\phi}\left(H - \omega\frac{\phi'}{\phi}\right)\delta\phi \\
\nu'' + 2\left(H + \frac{\phi'}{2\phi}\right)\nu' + 2\eta &= \frac{16\pi G_N a^2}{\phi}(\bar{\rho} + \bar{P})\Sigma + \frac{\delta\phi}{\phi}, \qquad (3.31)
\end{aligned}
$$

where $\nu = -6(\eta + h)/k^2$. The first two equations correspond to the time-time and space-time constraint equations and the third one the traceless component of the spacial equations contracted with the traceless derivative operator. Primed quantities are derivatives with respect to conformal time τ[1]. The last equations are written in Fourier space and k is the wave number of the corresponding perturbation.

The equation for the scalar perturbation is given by

$$
\delta\phi'' \quad + \quad 2H\delta\phi' + k^2\delta\phi + \frac{1}{2}\phi' h' = \frac{1}{3+2\omega}[8\pi G_N a^2(\delta\rho - 3\delta P)
$$

Now in order to devise a little bit of physics from this equations lets transform our variables to conformal-Newtonian gauge where the perturbations correspond to the gravitational potentials. If we were interested in studying the formation of large scale structure at cosmological scales only the modes with wavelength smaller than the causal horizon would be relevant. The dynamics of these scales happens on time scales much smaller than the expansion of the universe, so its effect may be negligible and the derivatives with respect to conformal time may be dropped out of the equations which reduce to

$$
\begin{aligned}
2\frac{k^2}{a^2}\Phi &= -\frac{8\pi G_N}{\phi}\delta\rho \\
(\Phi - \Psi) &= \frac{8\pi G_N a^2}{\phi}(\rho + P)\Sigma + \frac{\delta\phi}{\phi} \\
k^2\delta\phi &= \frac{8\pi G_N(\delta\rho - 3\delta P)}{2\omega + 3}
\end{aligned}
$$

[1] Lets recall that $d\tau = dt/a$ where t is proper time

The physical picture that this approximation brings up is that the universe is an homogeneous bound body whose gravity is merely described by the Newtonian prescription. The first equation reduces to the Poisson equation relating the Newtonian potential to the matter modes whilst the second one remains unchanged and shows that, unlike GR, $\Phi \neq \Psi$ when anisotropic stress vanishes and the scalar perturbation does not. This equation is important since leads to modifications on the way light is deflected gravitationally. The fact that it remains unchanged on all sub-horizon scales translates in that such effects on light might be produced by perturbations at every size and every time. Specifically, the early Sachs-Wolfe and lensing effects are in part due to this modification. Nevertheless, on very large scales such that $k\eta \to 0$, these super-horizon modes introduce relativistic effects coming from Hubble and primed terms in the set of equations. The integrated Sach-Wolfe effect, for instance, is imprinted in the CMB temperature spectrum on large scales and is due to the effect of modified potentials all along the track of light form the last scattering surface to the present. A more detailed analysis of perturbations in BDT can be found in [216]. In this work we solved the exact equations for all scales numerically by using two different codes: a modified and tested version of CAMB [186] and Dash [199]. In the following we will study the behavior of perturbations beyond the quasi-static limit by looking at such exact numerical solutions.

3.7.2 Scalar Perturbations And GR As A Late-Time Attractor

First, we are going to look at numerical solutions for the modes of the scalar perturbation. Solutions in the simplest case with $\omega = cte$ are shown at figure (3.9). We can observe that at any scale, the amplitudes of scalar modes are suppressed by ω. As firstly pointed out by [305], there exists an attractor behavior of the scalar perturbations toward GR at late times in gBDT. At very early times the field stays close to zero and starts to grow as the universe undergoes to the matter domination. Notice that the perturbation grows quickly just after equality, soon after it starts to have damped oscillations around an stationary point as matter sets on. At the later dark era, all the modes start to grow linearly. Notice that the perturbations tend to a constant as soon as the scalar background starts to grow. According to our cosmological constraints of ω derived in chapter 4, $\omega \sim 1000$ [19], for such models the perturbation takes values not higher than 10^{-3}.

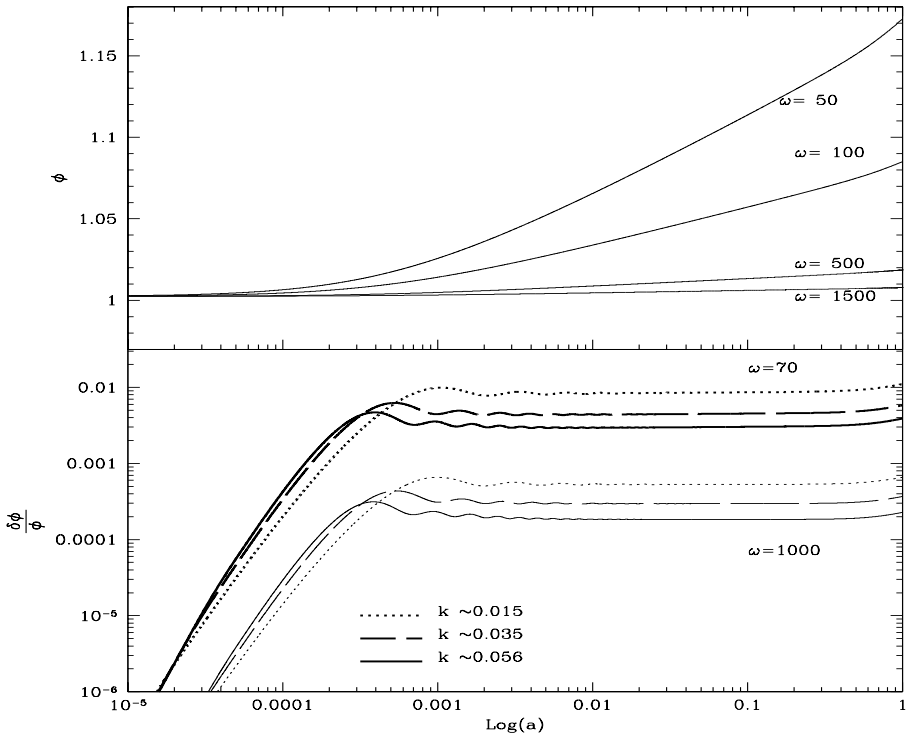

Fig. 3.9 Exact numerical solutions for the scalar perturbations $\delta\phi$ for two values of ω at different scales. For a given scale, the smaller ω is the field reaches earlier its stationary value. Also low energy perturbations tend to reach their equilibrium point at matter domination epoch later than those more energetic. Larger values of ω lead the perturbations to vanish, however they keep their attractor behavior along the time for any value of ω.

3.7.3 Matter Perturbations And Matter Power Spectrum

Although the evolution of matter perturbations is not the main matter of this work since the equations for matter and radiation are not directly coupled to the scalar, it can be effectively modified by means of the gravitational potentials. This indirect modifications can be tested with observations of the galaxy distribution in the universe so it is worth to wonder how this predictions are effectivelly affected by the BDT parameters.

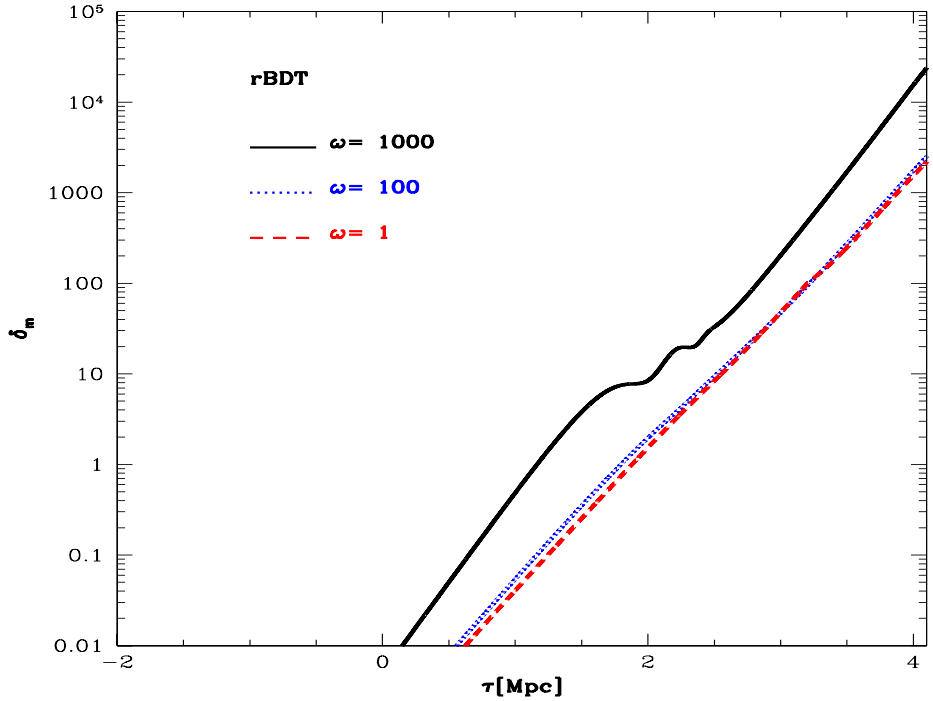

Fig. 3.10 Modes of total matter perturbations within different rBDT models for intermediate scale $k \sim 0.01$. The mode with $\omega = 1000$ presents some baryonic oscillations at times close to recombination. The modes for $\omega = 100, 1$ are comparable at this scale, however the at early times the amplitude of the mode with $\omega = 100$ mode is larger than the one with $\omega = 1$. At some point at late times their amplitudes are comparable and they start to grow at different rates. At very late times, the larger ω the model has, more rapid the growth of the corresponding mode is.

The main spirit of this part is to show the solutions for matter perturbations in order to understand the further effect of the BDT parameter on the matter power spectrum of inhomogeneities. When we were studying the matter power spectrum in chapter 2, we realized that it has a turn-over scale corresponding approximately to the size

of the horizon at the time of equality $k \sim 1/, \tau_{eq} \sim 0.01 Mpc$. This happens because matter perturbations grow very slowly for a while just after matter onset. So in order to see how the scalar affects the matter perturbations at this scale at which the power is maximized, figure (3.10) shows us matter perturbations solutions for different values of the BDT parameter ω within the restricted model. First, we analyse restricted models.

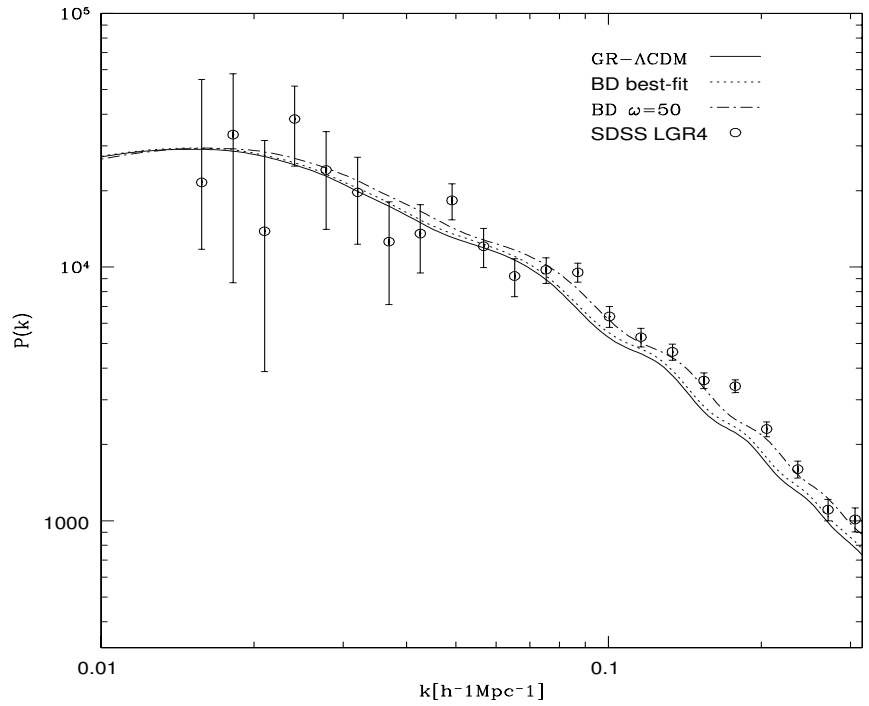

Fig. 3.11 The 3D matter power spectrum for BDT and GR best-fit models of the CMB + LSS measurements from WMAP7 and SDSS-R4. We can notice two different effects produced by the BDT scalar: shift of the turnover scale to smaller scales than for GR and an increment in the power at small scales. Although, by eye it seems that the BDT model with $\omega = 50$ fits well $P(k)$, it does not do since the total $\chi^2 = 3749.069$ whilst the best fit model has $\chi^2 = 3781.13$. However we must stress that on those scales non-linear physics is involved, therefore our linear predicted $P(k)$ may be not be thoroughly reliable.

Let us recall from section (3.6) that the effect of realistic large values of ω on the conformal distances is just a re-sizing caused by a rescaling of the Newton constant, this resizing is inherited to the primordial amplitude. So in summary we can foresee two main effects produced by ω on matter perturbations: 1. an overall increase in the amplitude of the matter perturbations. 2. a slight shift in the turn over point in the matter power spectrum due to the different sizes of the horizon at equality for different

ω. At the level of matter perturbations this translates as follows: the smaller ω the smaller scale at which matter perturbations start dimming [see figure (3.11)].

In turn, within uBDT, ξ affects $P(k)$ in very different way. On one hand the turn over scales remains unchanged when ϕ_{ini} varies (or ξ) and the amplitude of $P(k)$ is enhanced, specially at large scales [figure (3.12)]. On the other hand, at small scales the baryonic oscillations tend to disappear when ξ increases, as ξ increases gravity gains in its fight with the pressure of photons producing gravitational instability. In the linear regime scales above $k \leq 0.15$, ξ reescales the spectrum in a similar way than a linear bias. By realising this, we suspect that the bias parameter and ξ are going to be correlated.

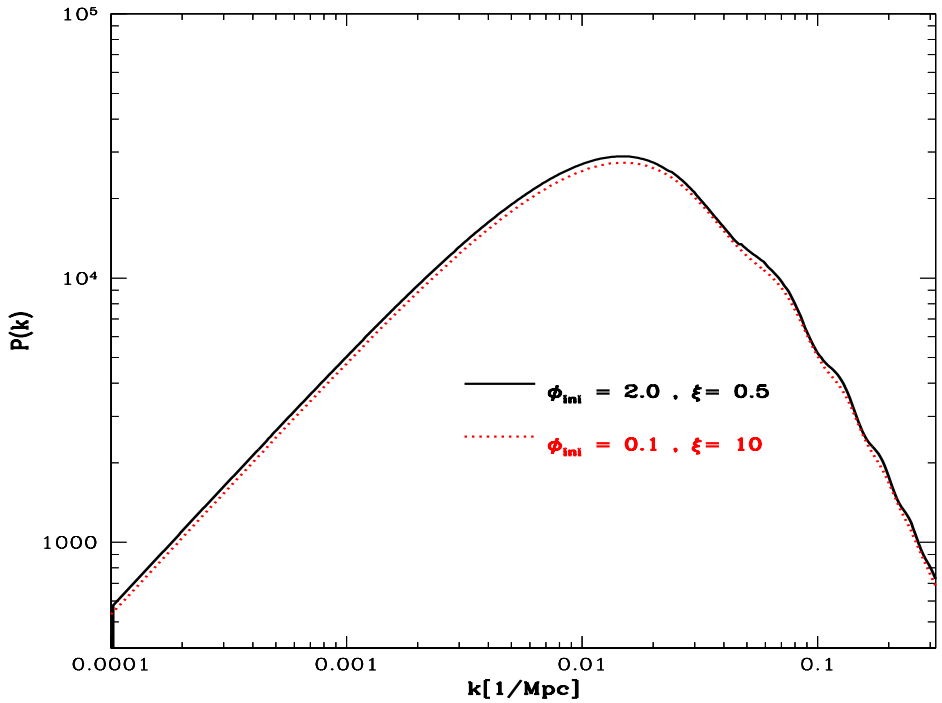

Fig. 3.12 The matter power spectrum today in BDT. Initial conditions of the scalar field $\phi_{ini} \rightarrow \phi_0 = 1/\xi$ rescale the matter power on large scales, in turn on small scales the baryon acoustic oscillations almost disappear when the strength of gravity increases.

3.7.3.a The Growth of Matter Perturbations

Since in this kind of models, we have ignored the self-interactions of the scalar, the perturbations are coherent [27]. Thus the growth of sub-horizon matter perturbations is scale independent and depend only on the background evolution. As we know the equations for matter perturbations are the same than GR so the time evolution of matter perturbations at late times only depend on the expansion history, which is equivalent to the fact that the matter perturbations grow coherently as in GR. However, because the background spacetime is not FRW in these theories, then the matter perturbations grow differently in BDT.

$$\delta_m \sim D_m(a)T(k)P_0. \tag{3.32}$$

Where $D_m(a)$ is precisely the growth, $T(k)$ the transfer function and P_0 is the primordial power spectra fixed at the end of inflation. From the equations for matter perturbations we can deduce the form of the growth [97, 238]

$$D_m = \frac{5\Omega_m H(a)}{2H_0}\int_a^1 da\frac{da'}{(H(a')a'/H_0)^3}. \tag{3.33}$$

In chapter 5 we shall compare the simplest BDT, with gBDT at their GR limit. It is possible to chose a set of parameters of gBDT such that the resulting models have an exact ΛCDM expansion history, but the growth of matter perturbations might still be modified. Thanks to this feature those theories are feasible candidates to break the degeneracy between GR and some modified theories of gravity by studying the growth. However, the simplest BDT case cannot be distinguished from GR by only studying the growth.

I would like to point that beyond trying to understand the matter perturbations by themselves, the growth is also associated with other observational features of the large scale structure formation, for example, when one aims to test effects due to peculiar velocities like the Alcock Pazcynski effect, the growth is needed to compute some observables associated with them. In other words, the growth might be constrained also by looking on these effects as we will see later on.

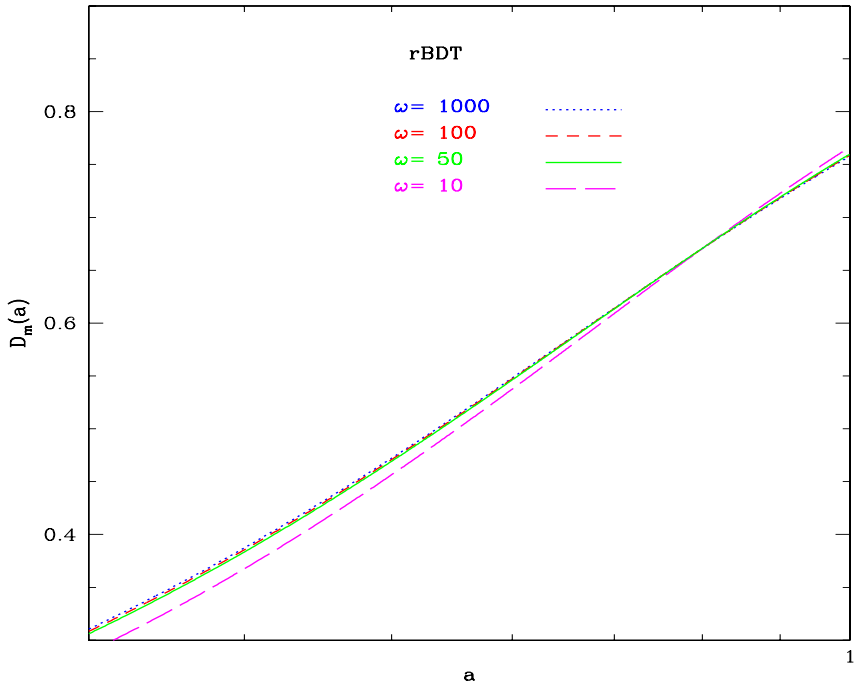

Fig. 3.13 Growth depending on ω. Relatively small values of ω leads straightaway to GR. more finely

3.7.4 Peculiar Velocities

In linear perturbation theory the velocities are related very simply to the over-densities. By measuring both the peculiar velocity field and the density field the matter density Ω_m can be inferred. Lets pick the continuity equation for subhorizon scales shown above and the solution at late times for δ then we get that peculiar velocities and the matter contrast are related by [97]

$$v(k,\tau) = \frac{i}{k}\frac{d}{d\tau}\left[\frac{\delta}{D_m}D_m\right] = \frac{i\delta(k,\tau)}{kD_m}\frac{dD_m}{\tau} = \frac{i}{k}faH\delta(k,a) \tag{3.34}$$

where we have defined the linear growth rate as

$$f \equiv \frac{d\ln D_m}{d\ln a} \tag{3.35}$$

In the standard ΛCDM model, the linear growth rate depends only on the matter density, however in the case of BDT where the strength of gravity measured by G_N is a dynamical variable, the new parameters also modify the linear growth rate. On one hand, since the peculiar velocities depend on the amount of matter, an over-density in a low density universe has less mass and therefore the gravity acting on infalling matter is weaker. On the other hand its gravitational pull depends also on the extra

parameters tunning the scalar field. The explicit dependence of the growth rate on ω is shown in figure (3.14)

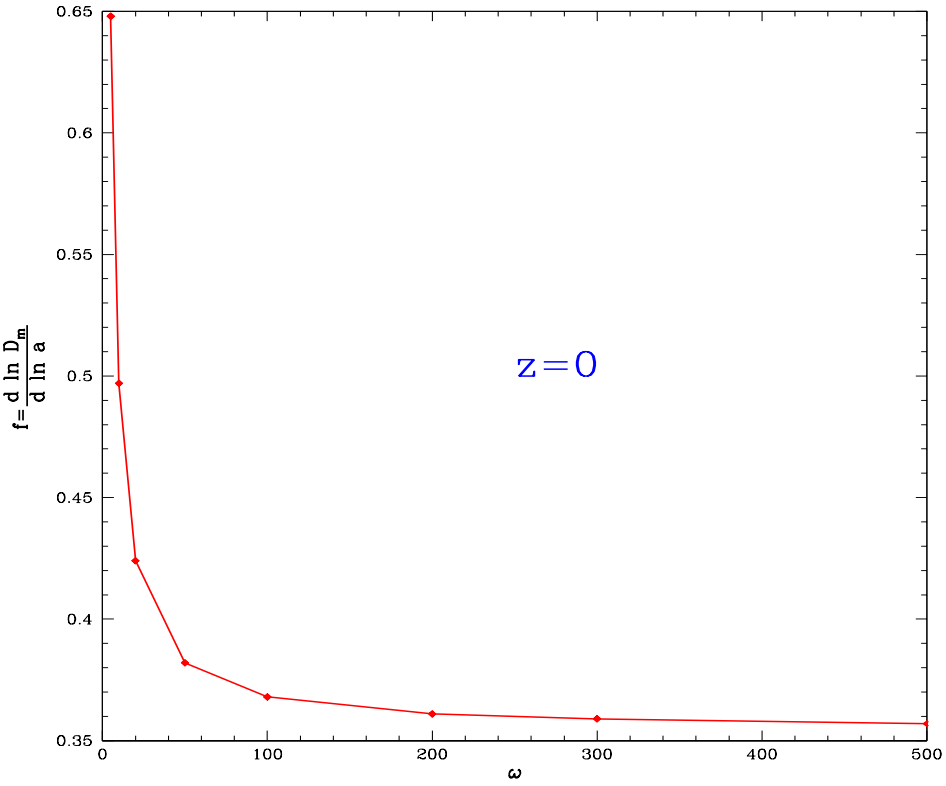

Fig. 3.14 The linear growth rate as function of ω in the restricted model. The values of the parameters are set using the best-fit ΛCDM model to WMPA7 and only varying ω. The smaller ω is the larger is the effect of the scalar, that is that gravity is stronger and consequently the infalling bodies towards an over-density have larger peculiar velocities.

The velocity is of course a vector, expression (3.34) is the component of the velocity along the $\vec{k}$ in Fourier space. Thus at low redshift (that is close to the present) the peculiar velocities are given by

$$\vec{v}(\vec{k}) = ifH_0\delta(\vec{k})\frac{\vec{k}}{k^2}. \tag{3.36}$$

In chapter 4 we are going to see that a number of surveys have directly measured peculiar velocities and that such observables are quite valuable since much cosmologically useful information about our models can be extracted from them. For example measurements of distance and the matter power spectrum can be induced as well. In

this work we use this measurements to set complementary constraints on our BDT and cosmological parameters, we also obtain some forecasts for constraints of ω from future velocity surveys by means of the detection of the Alcock-Pazcynski effect.

3.7.4.a Redshift Space Distortions

In redshift surveys the angular information about galaxies is supplemented with an estimation of its radial position given by its redshift. The radial distance from us of a galaxy with redshift z is estimated by

$$\chi_s(z) = \frac{z}{H_0} \tag{3.37}$$

This estimator of distance, however ignores the effect of peculiar velocities. An object that is assumed isotropic appears distorted in redshift space due to peculiar velocities. The effect is that a quadrupole moment contribution is induced in an otherwise circular over-density. If we were to measure the power spectrum in the redshift space we may ask How this distorted power spectrum is related to the true power spectrum in real space? Kaiser first solved the problem for linear theory. The starting point is to note that the number of galaxies in a region is the same in real and redshift spaces, therefore

$$n_s(\vec{x}_s)d^3x_s = n(\vec{x})d^3x \tag{3.38}$$

coordinates in both spaces can be related if by using the fact that the observed redshift is due to the actual expansion of the universe and also to the peculiar velocity of the galaxy so that $z = H_0 x + \vec{v}\cdot\hat{x}$. The redshift space coordinates are defined according to (3.37) therefore

$$x_s = x + \frac{\vec{V}\cdot\vec{x}}{H_0} \tag{3.39}$$

For modes with large wavelength $kx >> 1$ the Jacobian for this transformation is given by

$$J = 1 - \frac{\partial}{\partial x}\left[\vec{V}\cdot\hat{x}\right] \tag{3.40}$$

Thus, using (3.38) the number densities in both spaces at first order are related by

$$\delta_s(\vec{x}) = \delta(\vec{x}) - \frac{\partial}{\partial x}\left[\vec{V}\cdot\hat{x}\right] \tag{3.41}$$

In the distant observer approximation where $\hat{x}\cdot\vec{V}\rightarrow\hat{z}\cdot\vec{V}$ where $\hat{z}$ is the vector pointing to the center of the over-density, the Fourier transform of the number density perturbation is given by [97]

$$\delta_s(\vec{k}) = [1+f\mu^2]\delta(\vec{k}) \tag{3.42}$$

In the more general case for all scales, an observed galaxy power spectrum $\tilde{P}(k,\mu,z)$ in redshift space at linear regime is given by,

$$\tilde{P}(k,\mu,z) = P_{gg}^{\rm lin}(k,z) + 2\mu^2 P_{g\Theta}^{\rm lin}(k,z) + \mu^4 P_{\Theta\Theta}^{\rm lin}(k,z) \tag{3.43}$$

where the subscripts g and Θ denote the inhomogeneity of galaxy number density and the divergence of peculiar velocity measured in the units of the comoving Hubble velocity aH. $\mu\equiv\vec{k}\cdot\hat{n}$ is the projection of $\vec{k}$ on the line of sight. $P_{gg}^{\rm lin}=\langle|\delta_g(\vec{k})|^2\rangle$, $P_{g\Theta}^{\rm lin}=\langle\delta_g(\vec{k})\theta^*(\vec{k})\rangle$ and $P_{\Theta\Theta}^{\rm lin}==\langle\theta(\vec{k})\theta^*(\vec{k})\rangle$ denote the linear power spectra of density-density, density–velocity and velocity–velocity correlation functions. The subscript g denotes the perturbation of galaxy distribution. The density field $\delta_g(k,z)$ is given by

$$\delta_g(k,z) = b(k,z)\delta(k,z) \tag{3.44}$$

where $b(k,z)$ is the galaxy bias and it is assumed to be coherent through all scales at the linear regime [246]. In linear perturbation theory in an FRW metric, the application of the continuity equation implies that

$$P_{gg} = -fP_{g\theta} = f^2P_{\theta\theta} \tag{3.45}$$

where f is the growth rate. The Kaiser limit of power spectrum for very large scales is given by

$$P_{gg}(k,\mu) = b^2P_{\delta\delta}(k)(1+\beta\mu^2)^2 \tag{3.46}$$

where $\beta\equiv f/b$.

All this prescription works for coherent modified theories of gravity such as BDT, modifications to the standard predictions come in together from those in real-space matter power spectra studied before and from alterations to the growth rate. Figure (3.15) shows exact numerical solutions for the Kaiser power spectrum of matter perturbations in redshift space at different redshifts. It can be noticed that the overall effect of decreasing ω is a suppression in power which is more prominent at small angles and small scales.

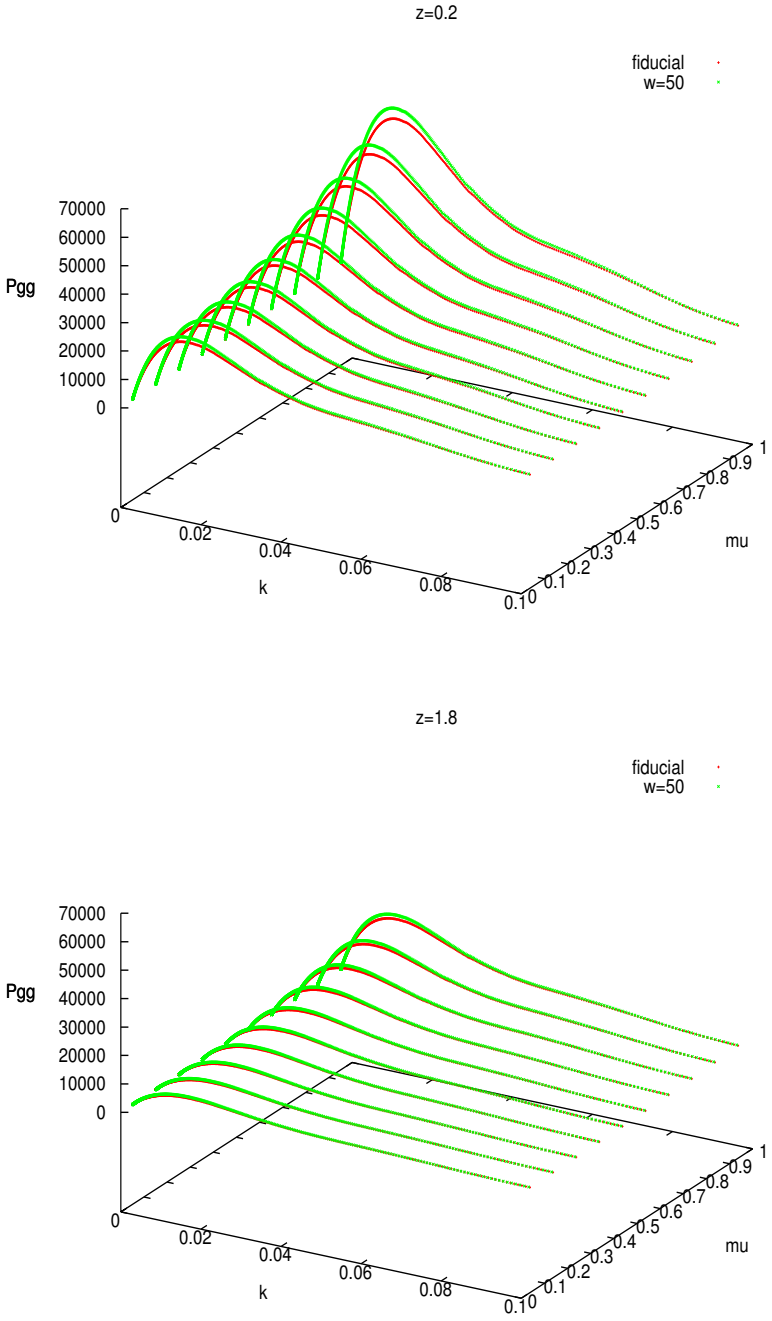

Fig. 3.15 The galaxy power spectrum observed in redshift space for BDT as function of the wavelength and the angle formed by the line-of-sight and the number vector of the mode. The maximum variation of power occurs at the turn over scale. As μ approaches to 1 the galaxy power becomes more sensitive to ω and also as the redshift takes low values.

3.7.5 Anisotropies In The Cosmic Radiation Background

3.7.5.a How does the BDT parameters affect the anisotropies?

We have already studied in previous sections of this chapter how the physics operates in BDT. In this section we will see how it is manifested into the CMB anisotropies. Such information is going to be very important when we aim to compare our predictions against observations during the next chapter. On one hand, we will demonstrate that if we were able to determine (even in a qualitative way) the features of the anisotropy that are affected when the BDT parameters are varied, that would help us to have an idea about the usefulness of the data to constrain our theory, in other words such information would helps us to decide whether the current measurements of the CMB anisotropies are enough to estimate the set of parameters of our theory or if further observations should be considered for that purpose. On the other hand, in the next chapter we are going to introduce the Fisher matrix method to estimate the parameters of a theory and one of its basic ingredients is a quantitative measure of the variation of the anisotropies with respect to each of the parameters to be constrained. Thus in this chapter we will derive that quantity and use it to analyse the sensitivity of the anisotropy to each of the BDT parameters. We will start analysing which effects coming from the background evolution which rise as a consequence of the modified expansion history, we will find out that these effects are the most important, afterwards we will go forth with perturbations which produce secondary effects which nonetheless are detectable.

Effects due to the Background Evolution

- **$\omega \rightarrow$Sound Horizon $\rightarrow$Location of the Peaks**

  In chapter 2 we have already analysed, in the context of GR, how the locations of the peaks in the angular power spectrum of the CMB anisotropy change depending on one background prediction: the ratio of the sound horizon to the angular diameter distance from today to the time of recombination which is usually named as the θ parameter. We saw that the location of the peaks are associated to scales with wavelengths with size equal to a multiple of the sound horizon as a result the peak structure of the CMB anisotropy measure the ratio of the angular diameter distance to last scattering surface, i.e. $\tau_0 - \tau_{lss}$ to the sound horizon at decoupling.

  In BDT the same history holds, however the modified expansion history bring different predictions. Specifically the sound horizon is quite sensitive to ω not the same to ξ [See figure (3.17)]. The way that this ratio depends on ω is shown

by figure (3.16). Thus if θ is measured somehow, then ω may be very well constrained. One of the main results of this thesis is that measurements of the CMB even yet from WMAP7 provides an accurate value of θ that allowed us to strongly constrain ω.

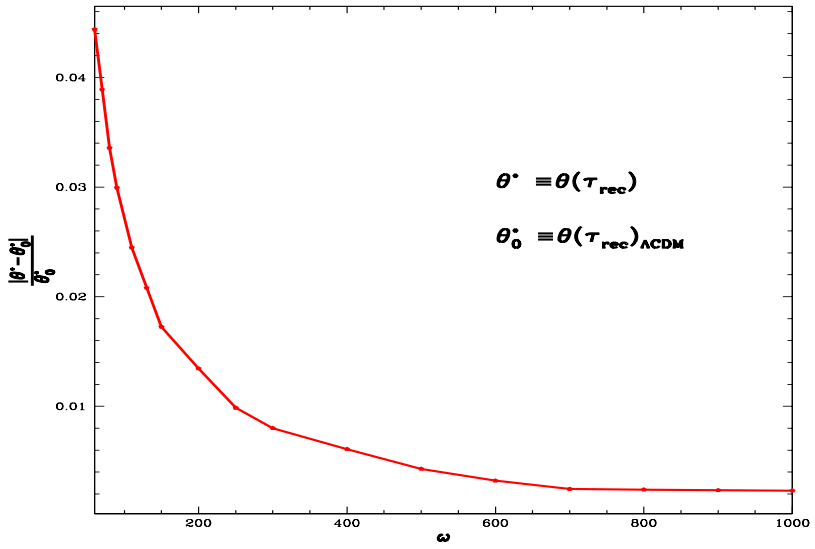

Fig. 3.16 Ratio of the sound horizon to the angular diameter distance from today to the time of recombination as function of ω within the uBDT models. All the other cosmological parameters are fixed to their fiducial values.

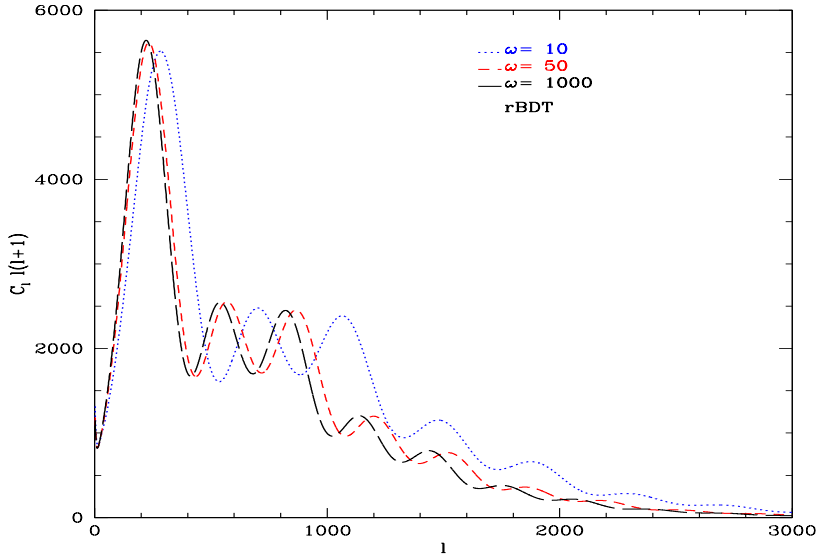

Fig. 3.17 The angular spectrum of the temperature anisotropy of the CMB for different values of ω. One of the main effects of the BDT parameters on the CMB temperature anisotropy come from the modified expansion history specially due to ω. The θ parameter is very sensitive to ω then the locations of the peaks and troughs are shifted as ω is varied.

- $\xi \rightarrow$ **Visibility Function** $\rightarrow$ **Heights of the Peaks**

  In order to see how ξ affects the CMB anisotropy we need to recall, on one hand, how the CMB anisotropy we observe today is built up from all the pieces of the cosmological model: background, recombination and perturbations, etc. At this point we can use for BDT the same treatment studied in chapter 2 for GR, because matter and radiation in BDT obey the same equations than in GR. On the other hand we must bring to mind the recombination history in BDT that we studied in relevant section of this chapter.

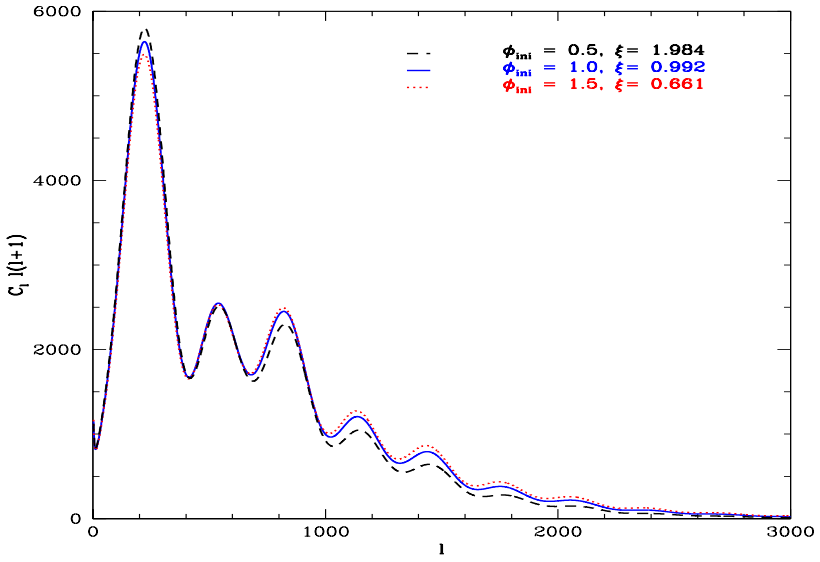

Fig. 3.18 The CMB temperature anisotropy depending on ξ (or ϕ_{ini}). The effect arises from the modified recombination history produced by ξ within the unrestricted models. Increasing ξ gives rise to a broader visibility function which translates in a diffusion damping of the temperature anisotropy on scales smaller than the damping scale k_D. This reduces the heights of the peaks at large angular multipoles.

Specifically, lets first recall that the visibility function can be thought as the probability of a electron to be scattered at the time of recombination to form neutral hydrogen. Following this interpretation, it is useful to remember that the tight coupling limit of the coupled equations is an idealized version of recombination at which the visibility function is as narrow as Dirac delta and electrons and baryons behave as a perfect fluid with a monopole and a dipole only.

The first order departure of this cartoon takes into account a boarder visibility function which leads to consider the next multipole moment, in this more realistic version of the photon-baryon fluid modes inside the horizon of acoustic oscillations get damped by diffusion and then their amplitude lowers down.

In summary the more boarder the visibility function is, the acoustic oscillations suffer more damping. In second place, the visibility function gets boarder as the gravitational strength, parametrized by ξ , increases. Thus, placing these pieces together we conclude that the effect of ξ on the anisotropy is: the heights of the peaks decrease as ξ increases for small scales as figure (3.18) shows.

The effect on large scales $l \sim 200$ is due in part to the rescaling of the expansion clock produced by increasing the value of the Newton constant [See section 3.6]. There's also a contribution from the ISW effect that has to do with perturbations rather than the history of recombination in BDT as we'll see later on.

Effects from Perturbations In order to extract only the effects due to perturbations it is useful to use a different parametrization for the background history, that is one at which θ is used instead ω_Λ. Thus in this paragraph every time we vary ω we fix all the other parameters including θ, by doing this we isolate the effects due to the background from those coming from perturbations. Lets recall that the overall effect of ξ on the temperature spectrum is to damp the heights of the peaks however the location of the peaks do not change. Thus to use this parametrization is only useful when one is after effects of ω on perturbations.

Among the effects of ξ over the CMB we can mention that ξ affects the polarization anisotropies through perturbations. The damping effect described above occurs on small scales, however, on large scales there's an enhancement on the amplitude of the perturbation. Since ξ turn the last scattering surface thicker, the amplitude of the local quadrupole increases, this produces a larger polarization signal as explained out in [341].

Now, using the parametrization described above, let us focus in the variation of the angular power spectrum of the temperature and *ee* polarization modes shown in figures (3.19) and (3.20).

The derivative of the spectrum with respect to ω carries valuable quantitative information about the sensitivity of the C_l to ω. We can clearly distinguish that the most important effect is due to the *ISW* effect at large scales, a lesser important effect arises at small scales due to perturbations in ϕ (indirectly through the effect of ϕ on the potential wells) and also due to a slight damping effect produced by the a small change in the Newton constant within the restricted model when ω is varied.

In the unrestricted case, if only ω is varied and ξ remains fixed this effect practically disappears. In conclusion a good measurement of the ISW effect at late times and the parameter θ promises to give rise a good estimate for ω.

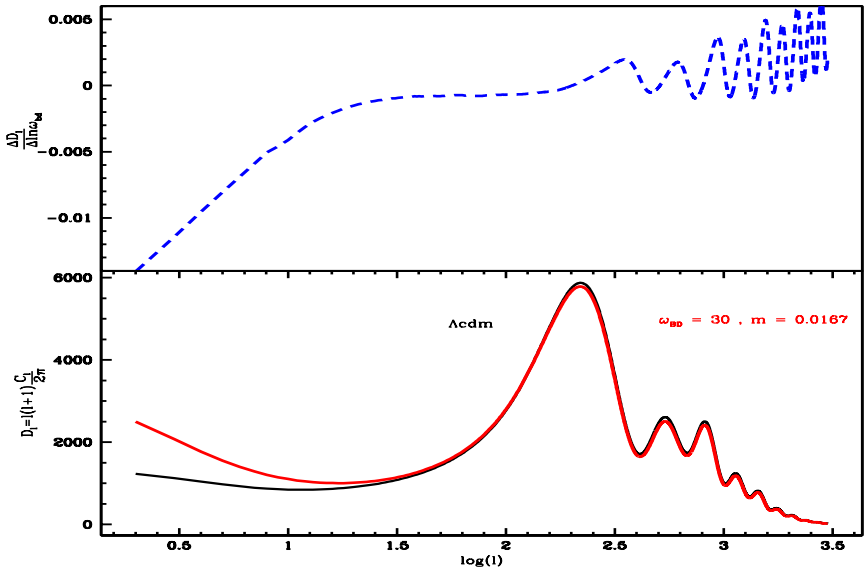

Fig. 3.19 The derivative of the temperature C_ls with respect to $\log \omega$. It is clear that the dominant effect of ω is through the ISW at large scales.

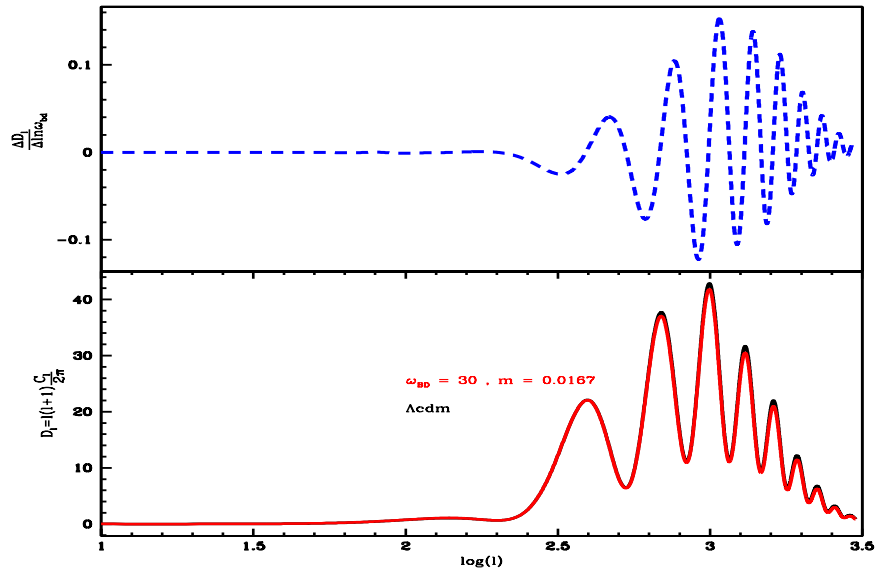

Fig. 3.20 The derivative of the EE polarization spectrum C_l with respect to $\log \omega$. A possible signature of ω is imprinted on the polarization spectrum on intermediate and small scales.

Without looking at further information about the underlying physics behind, the most important effect from varying ω at the level of perturbations over the temperature CMB spectrum is manifested at large scales (small multipoles). The temperature C_l's do also respond to ω at scales associated to the first three peaks. On small scales no significant change can be observed, so we can conclude that the only effect at such regime is that described before due to the wider visibility function carrying a modified envelope shape of the peaks when θ is allowed to vary. In turn, the polarization spectrum is fairly sensitive to ω at some range around $l \sim 1000$, as figure (3.20) shows.

In order to study the effects of ω on the polarization spectrum of the CMB, we follow an effective approach and quantify the overall sensitivity of the polarization spectrum to ω by computing its derivative shown by (3.20). we infer that measurements of the polarization spectrum at scales around $l \sim 1000$ could be a complementary source to constrain ω, however is not in a great extent as the measurements of the temperature spectrum.

Finally, within the uBDT models, the extra parameter ξ affects in great extent the small scale temperature anisotropy [Figure (3.21)]. Thus measurements of the damping tail are going to be essential to get a good estimate for ξ from the CMB.

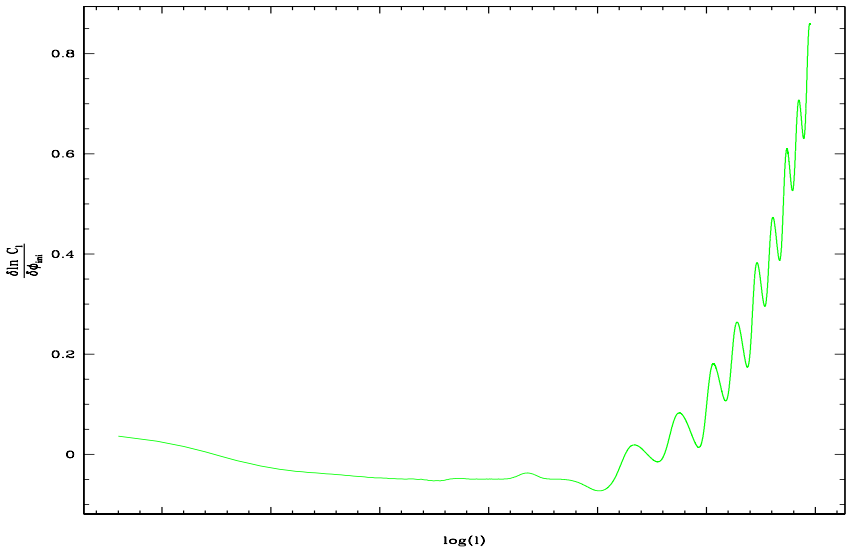

Fig. 3.21 The derivative of the logarithm of the angular spectrum of the temperature anisotropy with respect to ϕ_{ini}. The effect of this BDT parameter is more important as the multipole increases, thus we can have a better chance to measure it on small angular scales.

In order to talk about the physics behind these effects, it is convenient to split up the temperature spectrum into its distinct parts which can be read off from the line-of-sight integral expression of the anisotropy. By analysing how each of these pieces are affected by ω it is easier to figure out which physical aspects are modified in comparison to their peers in the standard model ones.

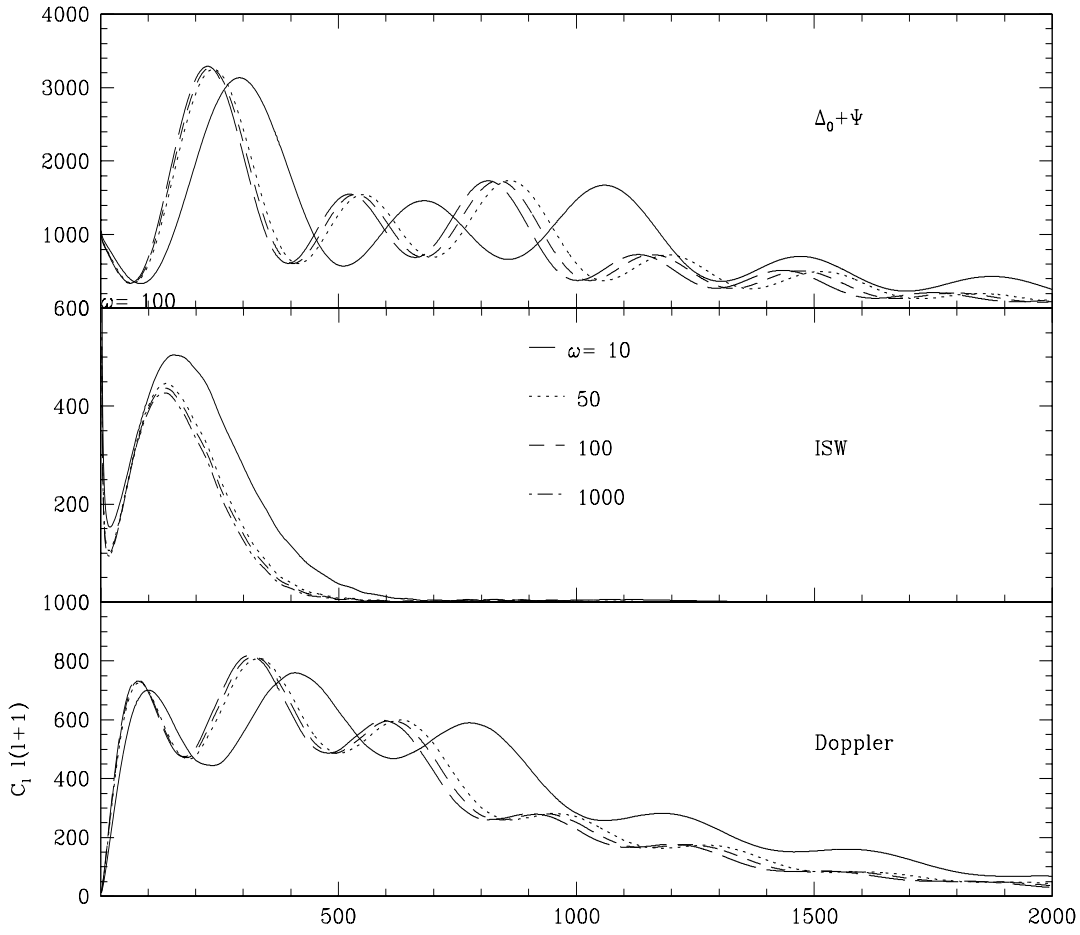

Fig. 3.22 Variation of different contributions to the source of the temperature CMB anisotropy with respect of ω. In the top panel the effective anisotropy is displayed, that is the monopole term plus the gravitational potential. The mid panel shows the ISW term depending on the time-variation of the gravitational potentials at recombination time. Finally the bottom panel plots the Doppler term due to the peculiar velocities of the overdensities.

In chapter 2 we studied the evolution of acoustic oscillations of the temperature perturbation, as we mentioned such a treatment is valid for BDT in the Jordan frame since matter is minimally coupled to the metric and the scalar extra degree of freedom added to the GR prescription modify these dynamics only through the potentials. Thus for BDT we use the same expression for the sources given by (2.117) and (2.118) can be used to compute the line of sight integral to determine the power spectra. If we drop the polarization contributions in (2.117) since its very small then it becomes

$$S(k,\tau) \simeq g(\tau)[\Delta_0(k,\tau)+\Psi(k,\tau)] + \frac{d}{d\tau}\left(\frac{iV_b(k,\tau)g(\tau)}{k}\right) + e^{-\kappa}\left[\Psi'+\Phi'\right] \quad (3.47)$$

and then the anisotropy is given by

$$\begin{aligned}\Delta_l(k,\tau_0) &= \int_0^{\tau_0} d\tau\ \ g(\tau)[\Delta_0(k,\tau)+\Psi(k,\tau)]j_l(k(\tau_0-\tau)) \\ &- \int_0^{\tau_0} d\tau g(\tau)\frac{iV_b(k,\tau)}{k}\frac{d}{d\tau}j_l[k(\tau_0-\tau)] \\ &+ \int_0^{\tau_0} d\tau e^{-\kappa}\left[\Psi'+\Phi'\right] \end{aligned} \quad (3.48)$$

The terms weighted by $e^{-\kappa}$ contribute at all times after recombination when $\kappa < 1$ and are proportional to the derivatives of the gravitational potentials then if the potentials are constant after recombination these terms do not contribute to the anisotropy at all. This happens for theories at which the time of equality occurs before decoupling. Though these terms are quantitatively important they do not change the structure of the CMB anisotropy. The dominant terms in the anisotropies which also determine its structure are those weighted by the visibility function $g(\tau)$. Remember that the visibility function has a sharp peak at recombination, qualitatively it plays the role of a Dirac delta, so the dominant terms in line-of-sight integral (3.48) are basically, as a good approximation, the integrands evaluated at recombination. This solution agrees with the exact one within the 10% of precision, so that is enough when we are after the physics behind the CMB.

First Term: The Effective Temperature Monopole The first term above encodes all the history about acoustic oscillations of the baryon-photon fluid enforced gravitationally described in chapter 2. The spherical Bessel function $j_l[k(\tau_0 - \tau^*)]$ is a measure of how much a plane wave with k contributes to the anisotropy on a given angular scale $1/l$. On very small angular scales $j_l \sim 1/l(x/l)^{l-1/2}$ it is tiny for large l when $x < l$. This means that $\Delta_l(k, \tau_0) \to 0$ for $l > k\tau_0$. In summary, a perturbation with wavenumber k contributes mainly on angular scales of order $l \sim k\tau_0$.

As shown by the first panel in figure (3.22), the monopole of the effective temperature anisotropy given by $\Delta_{T0} + \Psi$ is affected by ω only by means of the background. As we already explained, the change in the θ parameter produced by the modified expansion history produces a shift in the location of the peaks. We can also note a slight decreasing in the heights, since G_N is rescaled by a $(2\omega+3)/(2\omega+4)$ hence the visibility function is slightly widen and consequently $\Delta_{T0} + \Psi$ gets damped at some degree.

Last Term: Late Integrated Sachs-Wolfe Effect Because at the time of recombination subhorizon scales we observe today were far outside the horizon and so they were completely disconnected from causal physics at that time, the large scale anisotropy we observe today do not depend on the micro physics occurring before decoupling at all. On this large scales only the monopole is relevant when computing the anisotropy today. The first determining this were Sachs and Wolfe in 1967 [264], they found that a solution in this case is given by [97]

$$\Delta_0(k \to 0, \tau^*) + \Psi(k \to 0, \tau^*) \sim \frac{\Psi(\tau_0)}{3D_m(a=1)} \tag{3.49}$$

In order to understand how the ISW works is BDT lets see the second panel of figure (3.22). The ISW spectrum gets strongly enhanced when the BD field increases as ω drops down. The reason why this happens has two sources which can be unveiled by looking at the evolution of the gravitational potentials at large scales shown by figure (3.23).

First the larger is the amplitude of the BDT scalar the negative potential is slightly enhanced so the anisotropies pass through deeper wells along their way toward us. Second, in contrast to what happens in GR, in BDT the potential at large scales do not stay completely constant at matter domination era, by effects of the scalar dynamics, it is time dependent even at late times. This feature produces the main contribution to the ISW at low ω.

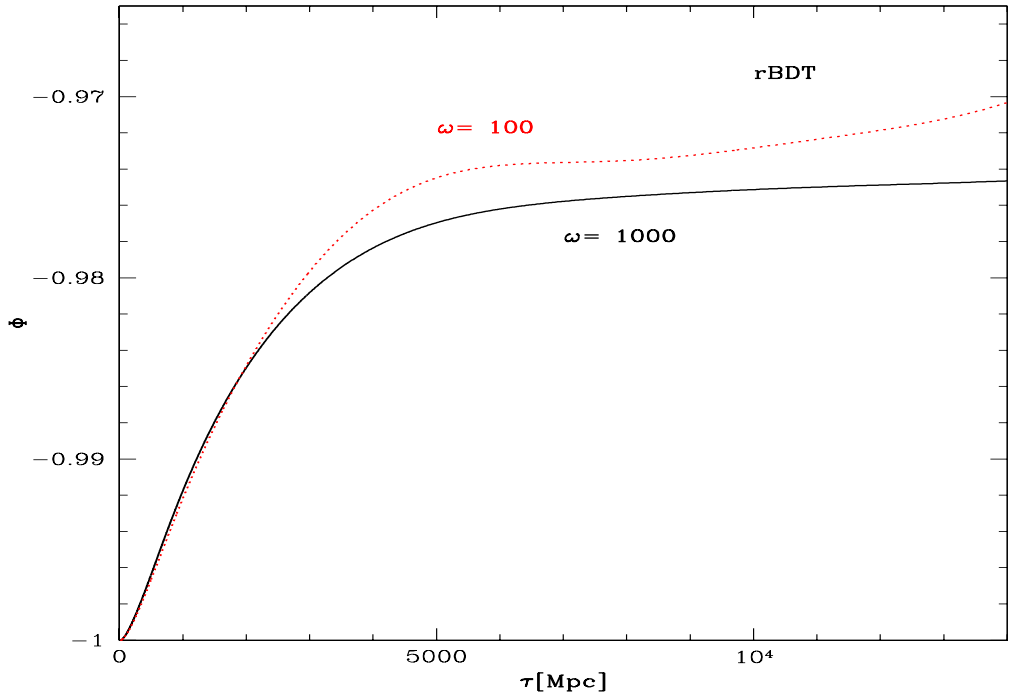

Fig. 3.23 Modes of the gravitational potential for two different rBDT models corresponding to $k \sim l/(\tau_0 - \tau_{rec}) \sim 0.05$ which lies between the first two peaks of the temperature spectrum. The potentials for small ω are clearly time-varying leading to an early ISW effect.

Doppler Term This term is the contribution due to the peculiar velocities of baryonic matter. Naively, velocity fields of order $v \sim 10^{-3}$ (see e.g. [208] for a review) and optical depths of a few percent would imply a Doppler effect that rivals the acoustic peaks themselves. Since the Doppler effect comes from the peculiar velocity along the line-of-sight, it retains no contributions from linear modes with wave vectors perpendicular to the line-of-sight. But as we have seen, these are the only modes that survive cancellation. Consequently, the Doppler effect from reionization is strongly suppressed and is entirely negligible below $\ell \sim 10^2$ unless the optical depth in the reionization epoch approaches unity .

3.7.5.b CMB Lensing

As photons travel through potential wells generated by galaxies these act like gravitational lenses producing an deflection on the original trajectory of photons. This deflection affects the temperature spectrum in about 2% level and around 10% the polarization spectrum. The effect is that the peaks get shallower without changing their position.

On one hand, the characteristic size of potential wells given by the scale of the peak of the matter power spectrum is around $300Mpc$ in comoving coordinates, and the distance to last scattering is about $14000Mpc$, so the number passed through is around 50 this leads to a deflection of ~ 2 arcminutes [15] which correspond to $l > 3000$.

Although lensing would dominate at such scales if not secondary anisotropies were present, indeed the power is small due to damping. On the other hand lensing can also have an important effect on the scale of the primary acoustic peaks. The reason why is that the deflection angles will be correlated over the sky by an angle given by the angular size of a characteristic potential which is 2 degrees.

Now lets get an non-rigorous derivation of the lowest order result for deflection angle produced by such potential wells. Consider a weak lensing of a photon with velocity $\mathbf{V}$ by a point mass M within Newtonian theory. By weak lensing we should understand that the deflecting angles are small perturbations and so they can be treated accurately using the first order results. The acceleration of the photon due to the mass is given by the gradient of the potential Ψ causing a small transverse acceleration [15]

$$\dot{V}_T = -\nabla_T \Psi = GM\cos\theta/r^2 \tag{3.50}$$

where θ is the angle between the photon trajectory and the relative vector joining the points of the mass and the photon $\vec{R}_0$. Then the deflection angle is given by

$$\frac{V_T}{|\mathbf{V}|} = \frac{2GM}{R_0} \tag{3.51}$$

In order to generalize this to the GR case the acceleration can be associated to the covariant derivative of the velocity of the photon along the photon world line. By doing this we take into account the curvature of space. The effect is a local deflection angle of the photon's world line given by

$$\delta\beta = -\delta\chi\nabla_T(\Psi + \Phi) \tag{3.52}$$

where $\delta\chi$ is a differential distance along the photon path. The comoving distance that the source appears to have due to lensing is $(\chi_* - \chi)\delta\beta = \chi_*\delta\theta$. Then the deflection in the image oberved due to the source at χ is

$$\delta\theta_\chi = \frac{(\chi_* - \chi)}{\chi_*}\delta\beta = \frac{(\chi_* - \chi)}{\chi_*}\delta\chi\nabla_T(\Psi + \Phi) \tag{3.53}$$

Integrating all the contributions from the source to us the total deflection is given by

$$\theta = -\int_0^{\chi_*} d\chi \ \frac{(\chi_* - \chi)}{\chi_*}\nabla_T(\Psi + \Phi)(\chi\mathbf{n}; \tau_0\hat{} - \chi). \tag{3.54}$$

where $\tau_0 - \chi$ is the conformal time of the photon when it passes closest to source producing the potential well. From this we can define the *lensing potential* just as

$$\psi = -\int_0^{\chi_*} d\chi \ \frac{(\chi_* - \chi)}{\chi_*}(\Psi + \Phi)(\chi\mathbf{n}; \tau_0\hat{} - \chi). \tag{3.55}$$

so that the deflection angle is $\theta = \nabla_T\psi$. In order to compute the lensed CMB temperature in a direction $\hat{\mathbf{n}}$ we can use the fact that it is given by the unlensed temperature in the deflected direction, that is [15]

$$T_{lens}(\hat{\mathbf{n}}) = T(\hat{\mathbf{n}} + \theta). \tag{3.56}$$

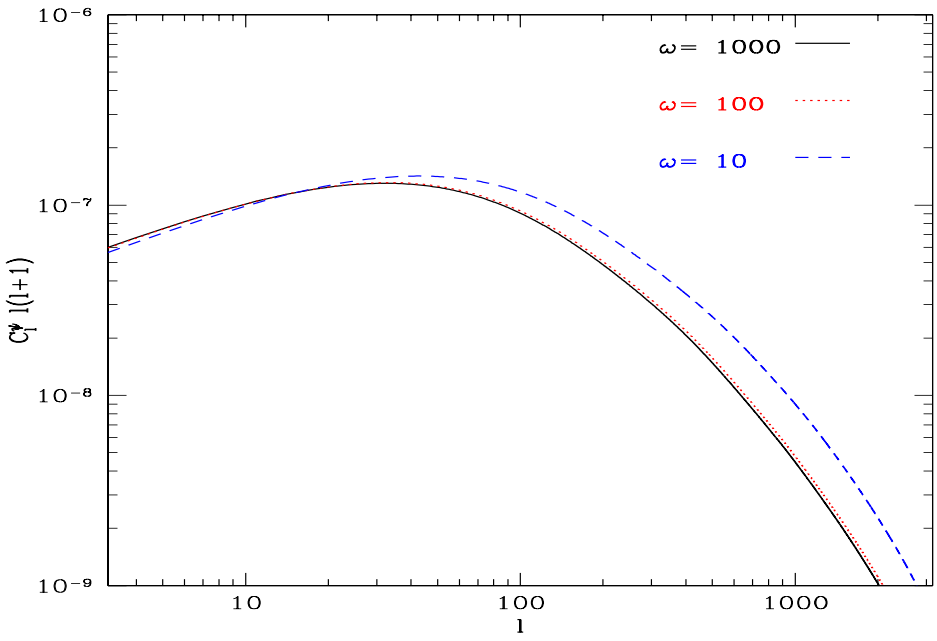

Fig. 3.24 The angular power spectrum for the lensing potential ψ for three values of ω. The lensing potential is directly related to the BDT scalar field perturbation $\delta\phi$.

The lensing potential in BDT might be a very important physical quantity since the only modification to the standard Einstein equations in this theory is directly related to the BD field perturbation. By looking at the perturbations equations above and using the gauge transformation to go from synchronous to Newtonian gauge we can notice that the last equation is equivalent to

$$\Phi - \Psi \sim \frac{16\pi G_N a^2}{\phi}(\bar{\rho} + \bar{P})\Sigma + \frac{\delta\phi}{\phi} \tag{3.57}$$

Hence in absence of anisotropic stress the $\Psi = \Phi + \frac{\delta\phi}{\phi}$, thus the lensing potential above gets an extra term equal to the scalar perturbation. Figure (3.24) show us the power spectrum of the lensing potential for different BDT models. At small scales, the scalar perturbation enhances the lensing potential importantly, in contrast at large scales its power is reduced in less extent. For large realistic values of ω, the lensing potential is not affected significantly so we don't expect that data related to these observation to be very useful to constrain our simple BDT. However, for smaller values of ω, potentially associated with self accelerating theories with shallow potential $V(\phi)$, lensing might set strong constraints on the model.

3.8 Conclusion and Summary of the Chapter

In summary, in this chapter we made a wide study of the cosmology derived from the massless Brans-Dicke theory which is the simplest alternative model to ΛCDM. The motivation of taking this model is not only its simplicity but rather the fact that it arises as a limit at very large (cosmological) scales of other more realistic and physically motivated theories involving a scalar such as DGP, Galileons and F(R). In our setup we consider to types of models rBDT and uBDT. The first type corresponds to the classic BDT with a cosmological Newton coupling equal to the one measured at a Cavendish like experiment and a single parameter ω while the second type a rescaling of the cosmological Newton coupling is an extra free parameter ξ and then it is not restricted to match with the measurements at solar-system scales as it happens in more realistic theories.

As a starting point of a future work motivated in the idea that BDT approximates more general theories. We constructed the very specific subclass of Horndeski theories that degenerate into Brans-Dicke theories at very large scales ℓ_*. The way we built up this class was simply by expanding the general free functions defining a general Horndeski theory around their specific functional form for BDT. By using explicit BDT solutions for realistic values of $\omega \sim 500$, we set very conservative limits of the coefficients of the Horndeski's analytic expansion. We argue that the subset of Horndeski theories defined within such region of parameters, actually approach to BDT at large cosmological scales. However this assertion stands to be verified in further research work.

Although the resulting background cosmology of both models behave in almost the same way, the very small discrepancies have important effects on the history of recombination and henceforth on the CMB anisotropies. Also another discrepancy that should be highlighted is that in the uBDT the physical effects can be better extracted, thanks to the extra parameter. In both sorts of models, varying ω affects the rate of expansion and consequently alters the measurements of distance like D_A, r_s, etc. On the other hand in both models there is an effect due to a rescaling of the Newton constant which is more significant in the uBDT while in rBDT it lies around 1. This produces a rescaling in the expansion rate, it is probed that this effectively changes the thickness of the visibility function at recombination producing that the CMB anisotropies to be even more damped than in ΛCDM.

We also studied some features of perturbations. First, as it is well known, the scalar perturbations present an attractor behavior in time: starting from zero at early

times they grow considerably once matter domination sets on and freezes to a constant value at very late times. Metric perturbations are coupled to this scalar perturbation and then they present some small but detectable symptoms mainly as a late ISW. Matter perturbations were also considered, which are found not particularly sensitive to the BDT parameters except for very extreme values at which the model is not viable, however even these effects on $P(K)$ are small, measurements of LSS still have a chance to set complementary constraints on BDT. Another observable considered and briefly studied was the Alcock-Paczynski distortion, we concluded that for viable values of the parameters (those which stick the observables close to ΛCDM) a detectable APD may arise only for a very high redshifts which the current surveys haven't reach. Finally we briefly studied the lensing potential in BDT which is directly coupled to the scalar perturbation, again we discovered that at large scales it is not affected significantly by the scalar, however at small angular scales a small effect appears.

In conclusion, this results are very useful to plan how to constrain this theory using cosmological observations along the next chapter. We can reasonably expect that measurements of the anisotropies of the CMB might strongly constrain the BDT. First, the ISW imprinted in the CMB anisotropies at large scales might importantly constrain ω. Second, the locations of the acoustic peaks would provide a precise measurement of ω while their heights would be sensitive to ξ specially at small scales in the case of uBDT. Finally, polarization may constrain ω considerably at intermediate and small scales so it is a good idea to include this dataset. Also, the APD is not particularly sensitive to ω however it can be compared with measurements of H_0 as a complementary test of the expansion with the advantage that APD provides a model-independent probe whilst the H_0 reconstruction from the distance measurements is made in the context of ΛCDM.

CHAPTER 4

COSMOLOGICAL TESTS OF BRANS-DICKE THEORY

4.1 Introduction

We already know that the 1960's was a golden decade for general relativity since it was placed under strong theoretical and experimental tests regarding to the physics of our solar system. Although cosmology had been a popular line of research at the time due to the discovery of expansion of the universe by Hubble and the cosmic microwave background, it was until the 1990's that is turned to become in important tool to accurately check the predictions of any theory of gravitation.

This era of Precision Cosmology started when Cosmic Background Explorer (COBE) was launched in 1989 [40]. A couple of years later the Wilkinson Microwave Anisotropy Probe (WMAP) provided accurate measurements of anisotropies and inhomogeneities and placed the standard model of cosmology based on general relativity as the best description of the universe as a whole [32, 34]. During the later years, smaller but nonetheless important surveys were launched in order to measure inhomogeneities and anisotropies at large scales such as the Sloan Digital Sky Survey (SDSS) [58], the 2dF Survey [204] and the WiggleZ Survey. All of them brought valuable observations of structure of matter in the universe different scales and redshifts. As time goes on, the cosmological precision tests become stunningly accurate, this becomes our times in a golden era for cosmology and gravitation and it is crucial time not only for general relativity, but moreover for fundamental physics.

Current and future surveys overtake the accuracy of previous ones. The huge extrapolation of GR made in the early 1920 is farly being placed under tough tests. In despite of the flaws of the model to bring complete predictions at the level of the background, namely the need of assuming dark elements in the matter- energy contents of the universe to obtain the right predictions, the standard model has best fitted the observations as any other cosmological model so far. At the level of perturbations there are still plenty of tests for GR to overcome due to the size of our ignorance about

the structure formation at very large scales. Furthermore,the healthier stand point to have when one aims to test the large scale structure is to use a model-independent theoretical framework in order to reproduce observations. This sounds appealing, however the huge number of degrees of freedom to be constrained overwhelm the number of measurements available so far. A remaining solution is to consider into the test not only the standard model but also a wide set of candidates to reliable describe the observations. Thus at this precision era, alternative theories of gravity must be passed through test and they must share the same status than GR as far as observations lead us.

As we already know, the main goal in this chapter is to compare the predictions of the simplest modified theories of gravity: BDT. In order to go forth in this direction, for both models, we use the very standard method Markov-Chain-Monte-Carlo in order to compute the likelihood function and the posterior distributions in the space of parameters. This method is a powerful tool to derive good estimations of the most likely values of the parameters within some level of confidence according to a given dataset. We also use the Fisher matrix method to constrain and forecast its parameters using the latest data and future surveys.

In particular, we aim to compare the theoretical predictions of BDT in first place to the latest observations of the CMB anisotropies from WMAP and Planck. Nonetheless, in order to take advantage of all the phenomenology behind these models -which in despite of its simplicity its implications are important- we use complementary data to derive better estimations of some of the parameters, specially when degeneracies appear. Among the most important we should mention small scale measurements of the CMB from SPT and ACT; measurements of the expansion rate as HST, Alcock-Paczynski test, etc. Only for the unrestricted model in BDT, we obtain constraints for the Newton constant by using actual values of light-elements abundances at BBN. For BDT we also obtain complementary constraints ω by using direct observations of the matter-power-spectrum from SDSS-R4 along with WMAP7.

The main goal in the first section of this chapter is to introduce the tools required to accomplish such comparison between theory and observations. We summarize the basics that enable us to understand how each method works without going into full details. The goal here is just to prepare the ground and give a general ideas about the methods used to derive our estimations which are going to be presented with more detail along the next sections. There we specify technical aspects on the particular way of using the methods presented within this section.

The structure of this chapter is simple to follow, in section 2 a discussion of different ways of testing a theory in general is presented, with this we aim to set a context in which it is possible to classify the methods that we describe in the latter

subsections. In that last part of section 2 definitions and tools relevant for this work are briefly described. In section 2 we present the explicit analysis of data for BDT, in the first subsection we describe the specific methodology used to compare the BDT predictions of the CMB with measurements from WMAP7 and Planck mainly and some other complementary data. In further subsections, we present further estimations using complementary data appart of the CMB in order to constrain some special features of BDT.

4.2 Theory v.s. Data: Some Tests And Methods

4.2.1 Parametric And Phenomenological Approaches

One can distinguish two complementary approaches for testing the experimental validity of any given theory of gravitation, usually they are termed as the "phenomenological" one, and the "theory-space" one, respectively. In order to understand the logic behind each of them lets denote T a theory and C one of the predicted observations. It is well known in elementary logic that "T implies C" is equivalent to "no C implies no T". Althought, a scientist would like to be able to have a way to verify a given theory , it is much more common that an experiment gives negative results for a given theory and in this way they tell us something about the theories only when they are wrong. This is the basis of the phenomenological approach . The only logical way of verify a theory is, first to consider the subset of all theories and the subset of theories which predict the same C as T. In this way, experiment might tell us that the common features of TC are "true". This is the basis of the theory-space approach [84].

4.2.1.a Phenomenological Approach

Lets consider a "kinematical" model containing a set $\{p_i^{pheno}\}$ of free parameters for describing the evolution of a determined physical system. By fitting somehow the experimental observations, we can "measure" the phenomenological parameters: $p_i^{obs} \equiv (p_i^{pheno})_{best-fit}$. with in an error bar corresponding to a confidence level including both statistical and systematic errors. The final outcome of the testing process is a set of questions: $p_i^{theo} = p_i^{obs}$ which should be stated in probabilistic terms. Indeed, the theory never predicts the exact values of the parameters but gives them in terms of theoretical parameters $p_i = F_i(\lambda_a)$.

As an example we can think of the Newtonian theory of gravitation and the Einstein one being tested by the observation of the precession of perihelion of mercury. By testing both theories by the phenomenological approach the Newtonian prediction

differs from observation up to 90σ while the Einsteinian prediction lies within one sigma. So Newton's theory turns to be false while the Einstein one is simply not ruled out. In other words, the philosophy behind this approach is that a given theory remains true as long the contrary is not probed to happen.

The problem of this approach is that it does not tell us anything about which elements of the theory are being tested. It does not give us a clue on what parts of the structure of GR have been tested or which of them simply do not play any role in the test [84].

4.2.1.b Parametric Approach

The idea behind this approach is to embed the currently preferred theory within a continuous set of alternative theories. The point of doing this is that the inner structures present in a theory are better distinguished if one contrasts them to a theory which is similar but different in some way. A usual way of charting the continuous set of alternative theories is by means of a continuous finite set of real parameters $\{a_k\}$. In this approach one has, on one hand, the set of the labeled alternative theories S and on the other hand the set of observations to compare with, what follows is to ask: Which subset of S is in better agreement with the observations? A standard quantitative measure of the extent of agreement between the subset of theories and the experimental observations is the "goodness of fit" statistics defined as follows.

Lets consider the set of theoretical predictions $\{x_i^{theo}\}$ and the set of observational data $\{x_i^{obs}\}$ with its respective error bars $\{\sigma_i^{obs}\}$. Then the "goodness of fit" statistics for a given experimental data, can be computed as

$$\chi^2(a_k) \equiv \sum_i \left(\frac{x_i^{obs} - x_i^{theo}(a_k)}{\sigma_i^{obs}} \right)^2 \tag{4.1}$$

The best agreement between observations and theory corresponds to the minimum of χ^2. Thus if one imagines the χ^2 function as a hypersurface in the space of theories parametrized by a_k, the most likely theory to describe the observed parameters is that for which the hypersurface χ^2 has a hollow and its surrounding. In order to illustrate this, lets imagine a space with $\{a_1, a_2\}$ in which case χ^2 can be thought in a third direction. If this hypersurface is sliced by a plane in $\chi^2 = cte$, the points inside the level contours correspond to theories more likely to agree with observations as the plane approaches to the minimum. Therefore, to each difference in level above the minimum we can associate a "level of confidence" which depends also on the number of fitted parameters.

In summary, the theory-space approach associates to each independent set of experimental data some confidence region in theory space. It remains to address the following questions: does the collection of confidence regions corresponding to the various data sets admit a non-empty intersection? And, if there exists a non-empty intersection what is its shape in theory space, in other words, what are the common features of the theories that pass the considered tests? As we see from the last question, the theory-space approach is giving us a handle on what theoretical structures are being actually probed by some sets of observations [84].

4.2.2 Tools For Comparing Predictions v.s. Data

4.2.2.a The Analysis Techniques

The issue on how to analyse the data in the best possible way has started to be of great importance in the last decades [97]. The reason for this is that the amount and quality of data have improved dramatically in the last decade and this huge data sets create new challenges in the analysis. The likelihood function is one of the foundations among the techniques that we have at hand to handle this analysis. It is defined as the probability that a given experiment would obtain the data it did given a theory. Even though the simplicity of its definition, the likelihood function is very powerful. Once we have this function we can determine which set of parameters of a given model better fits the data and also the error of such estimate.

In order to set a precise definition lets assume we have a set of values x_i^{obs} associated to observed data (it could be a set of observables or parameters to uniquely label them) and x_i^{theo} a set of values associated to predictions of a model (it could be specific values of the set of parameters of the model or the respective predicted observables). The probability of getting x_i^{obs} from an observation given x_i^{theo} fixed values from a theory can be interpreted as the likelihood $\mathscr{L}(x_i^{obs}|x_i^{theo})$. The interpretations is especially obvious when x_i^{obs} is fixed and x_i^{theo} is allowed to vary [202].

The fundamental tool for analysing CMB data is indeed the likelihood function. It has been used since the early days of anisotropy searches [43, 96, 255]. Brute force likelihood analyses [200] were carried out even on the relatively large COBE data set, with six thousand pixels in its map. Present data sets are a factor of ten larger, and this factor will soon get larger by yet another factor of a hundred. Therefore, the brute force approach no longer suffices. In response, analysts have devise a multitude of techniques that move beyond the primitive brute force approach.

The simplicity of CMB linear physics is manifested in analysis by the apparent Gaussianity of both the signal and various sources of noise. In the Gaussian limit, optimal statistics are easy to identify. These compress the data so that all of the

information is retained, but the subsequent analysis becomes easier to perform. Many of these techniques first intended to study the CMB, have been proposed for studying: the 3D galaxy distribution [206], the 2D galaxy distribution [111, 159] the Lyman alpha forest [158], the shear field from weak lensing [155], among others. Indeed, these techniques are now indispensable, powerful tools for all cosmologists.

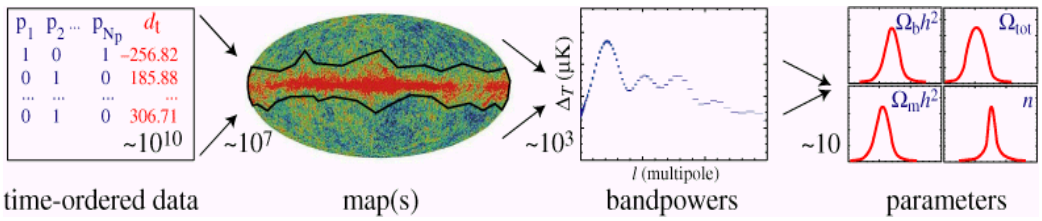

Fig. 4.1 Analysis of data time-line.

Figure (4.1) summarizes the way by which the data is usually analyzed from starting point: a time-stream of data points, to the end, the determination of cosmological parameters. Each step radically compresses the data by reducing the number of parameters used to describe it. Although this data pipeline and our discussion below are focused on temperature anisotropies, similar steps have been interpreted for polarization [49, 187, 303].

4.2.2.b Estimating Parameters

Given a set of data, our main goal is to interpret them in terms of a model that we assume is true. Of course this model usually has some parameters x_i^{theo} which we wish to determine at the end. The goal of parameter estimation is to obtain estimates of the parameters and their errors at least and furthermore the whole probability function of x_i^{theo} given the data x_i^{obs}. This is called the posterior probability distribution and it's the probability that the parameters of our theory take certain values after doing the experiment.

$$P(x_i^{theo}|x_i^{obs}) \tag{4.2}$$

From this distribution one is able to calculate the expectation values of the parameters, and their errors. In this definition we are taking a Bayesian view of probability, as a degree of belief, rather than a frequency of occurrence in a set of trials. The opposite distribution $\mathscr{L}(x_i^{obs}|x_i^{theo})$ is usually what we look for, since usually having the collected data from an experiment we want to know what is the probability that

our parameters to take a value given the data. Both distributions are easily related by the Bayes theorem [250]

$$P(x_i^{theo}|x_i^{obs}) = \frac{\mathscr{L}(x_i^{obs}|x_i^{theo})P(x_i^{obs})}{P(x_i^{theo})} \tag{4.3}$$

$P(x_i^{theo})$ is called the prior, and expresses what we know about the parameters prior to the experiment being done. This may be the result of previous experiments, or theory. In the absence of any previous information, the prior is often assumed to be a constant and it is called flat prior. $P(x_i^{obs})$ is not important since it plays the role of the normalization of the distribution and then it can be safely ignored. As a consequence a flat prior the likelihood and the posterior distributions are proportional,

$$\mathscr{L}(x_i^{obs}|x_i^{theo}) \propto P(x_i^{theo}|x_i^{obs}). \tag{4.4}$$

Lets assume that we have a posterior distribution that has a single peak, the first estimate for the parameters is given by those for which the likelihood is maximum x_{i0}^{theo} and usually is equal to the mean. Assuming a flat prior, the posterior is proportional to the likelihood then close to the peak the likelihood the distribution can be approximated by a Gaussian in the space of parameters. This can be seen if the logarithm of likelihood is Taylor expanded as follows

$$\ln\mathscr{L}(\mathbf{x}^{obs};\mathbf{x}^{theo}) = \ln\mathscr{L}(\mathbf{x}^{obs};\mathbf{x}_0^{theo}) + \frac{1}{2}(x_i^{theo} - x_{i0}^{theo})\frac{\partial^2\ln\mathscr{L}}{\partial x_j^{theo}\partial x_i^{theo}}(x_j^{theo} - x_{j0}^{theo}) + ... \tag{4.5}$$

where $\mathbf{x}_{i0}^{theo}$ are the true values of the model parameters. The matrix $F_{ij} \equiv \partial^2\ln\mathscr{L}/\partial x_j^{theo}\partial x_i^{theo}$ encodes the correlations between parameters. If it's diagonal, the estimates are uncorrelated.

4.2.2.c Marginalization

If we are interested in the probability distribution for a single parameter x_1^{theo} taking into account all the possible values of the remaining parameters, we should compute the 1D marginal distribution for x_1^{theo}. To compute it we just need to sum over all the possible values of the parameters different to x_1^{theo}

$$p(x_1^{theo}) = \int dx_2^{theo}...dx_N^{theo}P(\mathbf{x}^{theo}). \tag{4.6}$$

This process is called marginalization. Often it is useful to analyse the marginal distribution of two parameters in order to study their correlations, in such case the

process is the same so we just left the pair of variables out of the integration. The plots of such errors are named contours at some specific confidence level. In the case when the marginal distribution is a Gaussian the confidence level agrees with an specific numbers of σ's which depends on the dimension of the space of the marginal distribution, the standard conventions to tell about the confidence region of a marginal distribution are shown in the following table [147, 210]

σ	c.l. %	$\Delta\chi^2$, $d=1$	$\Delta\chi^2$, $d=2$	$\Delta\chi^2$, $d=3$
1σ	68.3%	1	2.30	5.35
2σ	95.4%	4	6.17	8.02
3σ	99.73%	9	11.8	14.2

where $\Delta\chi^2 \equiv \chi^2 - \chi^2_{min}$ and d is the dimension of the parameters space. Note that in some of the results shown above we assume the likelihood (or posterior) is well-approximated by a gaussian. We should say that this may not be so. However, a Gaussian likelihood is useful to compute marginal errors for this rather general situation. The simple result is that the marginal error on parameter x_i is

$$\sigma_i = \sqrt{F^{-2}_{ii}}. \tag{4.7}$$

One has to be careful since in the previous expression the repeated indices denote the diagonal components rather than sum. In practice, this result is often used to estimate errors for a future experiment, where we deal with the expectation value of the Fisher matrix. This error is always at least as large as the expected conditional error. This result holds for Gaussian-shaped likelihoods, and is useful for experimental design. For real data, you would do the marginalization a different way [147].

4.2.2.d Fisher Matrix Analysis

Suppose that our data set consists in N real numbers x_1^{obs} , x_2^{obs} , ..., x_N^{obs} , which we arrange in an N-dimensional vector $\mathbf{x}^{obs}$. These numbers could for example be the measured temperatures in the N pixels of a CMB sky map or the counts-in-cells of a galaxy redshift survey. Before collecting the data, we think of $\mathbf{x}^{obs}$ as a random variable with some probability distribution which depends in some known way on a vector of M model parameters $\mathbf{x}^{theo} = x_1^{theo}, x_2^{theo}$, ..., x_N^{theo}.

Lets denote by $\mathbf{x}^t_0$ the true value of the vector of parameters and $\mathbf{x}^t$ the estimates. Since $\mathbf{x}^t$ is a function of $\mathbf{x}^o$ it is also a random variable. For it to be a good estimate,

we would of course like it to be unbiased i.e. $\langle \mathbf{x}^t \rangle = \mathbf{x}_0^t$ and give as small error bars as possible. In order to get the unbiased estimator a key piece is the Fisher information matrix defined as

$$F_{ij} = \langle -\partial^2 \ln \mathscr{L} / \partial x_j^{theo} \partial x_i^{theo} \rangle \tag{4.8}$$

Another key quantity is the maximum likelihood estimator, defined as the parameter's vector $\mathbf{x}_{ML}^t$ that maximizes the likelihood function. A number of powerful theorems have been probed using the previous definitions, among the most important

1. *Cramer-Rao Inequality*: for any best unbiased estimator $\Delta x_i^t \geq 1/(F_{ii})$.

2. If an unbiased estimator satisfies the lower Cramer-Rao bound , it is the ML estimator.

3. The ML estimator asymptotically corresponds to the best unbiased estimator.

The first theorem places a lower limit on the error regardless of which method is being used to estimate the parameters from the data. The second theorem shows that maximum likelihood estimates have quite a special status: if there is a best method, then the ML-method is the one. Finally, the third result basically tells us that in the limit of a very large data set, the ML-estimate for all practical purposes is the best estimate, the one that for which the Cramer-Rao inequality becomes an equality. The normal case the minimum standard deviation is given by

$$\Delta x_i \leq (F^{-2})_{ii}^{1/2} \tag{4.9}$$

and it is called the marginal error and normally this is the relevant error to deal with. Notice that marginal and conditional errors are equal if F is diagonal, otherwise the estimates for the parameters are correlated.

I just want to make a final comment about the Fisher matrix when different experimental data is used. If the data is independent then the Fisher matrix is just the sum of fisher matrices corresponding to each set of data. It is important to mention that the marginal error contours in the combined dataset can be much smaller than you might expect, given the marginal error ellipses for the individual experiments, because the operations of adding the experimental data and marginalizing do not commute. I will not show the probe here and it can be found in detail at [147].

4.2.2.e Particular Case: Likelihood Function for the CMB

Now lets translate the previous to the CMB. The true temperature anisotropy in a given spot in the sky will be denoted by Δ while the data point, which is the resulting average of multiple measurements, $\bar{\Delta}$. The variance of this estimator C_N represents the spread of the measurements is also given from the experiment. To compare the observed $(\bar{\Delta}, C_N)$ lets assume that the signal in a given spot on the sky has a Gaussian profile distribution, this is a prediction from simplest theories based on inflation as is the case in this work. The probability that the temperature of the background radiation observed in the sky falls between the interval $\Delta + d\Delta$ is given by

$$P(\Delta)d\Delta = \frac{1}{\sqrt{2\pi C_S}} exp\left[-\frac{\Delta^2}{2C_S}\right] d\Delta \tag{4.10}$$

C_S is the expected variance due to the signal alone without including the contribution of any noise. After we take the convolution of the previous probability with the likelihood function of the signal, the final expression for the likelihood function to the realistic case with a measurement of N_p pixels is given by [97]

$$\mathscr{L} = \frac{1}{(2\pi)^{N_p/2}\sqrt{\det C}} exp\left[-\frac{1}{2}\Delta^T C^{-1}\Delta\right] \tag{4.11}$$

where the vector Δ is a data vector formed with N_p measurements and C is the full covariance matrix defined as $C \equiv C_S + C_N$ the sum of the variances due to the signal alone and to the noise. In general the noise covariance matrix is fairly close to a diagonal matrix, however the theoretical or signal covariance is not. This makes the evaluation of the likelihood computationally very expensive when taking the determinant and the inverse of the $N_p \times N_p$ full covariance. However a couple of simplification can be done. Any given theory is associated with a full set of C_l's, and these can be used to construct C_S. The second simplification is that most of the experiments are not sensitive to individual C_l's but only to the average power over a range of l's which is usually named as band-powers. So the fitting in question requires fewer parameters to be determined.

A useful rule of thumb for estimating the signal in a CMB experiment is to calculate the variance of the data points and compare it with the average noise per signal If the data has larger variance than the noise then the theoretical signal is simply given by the difference of the two. To compute the error of C_S by using the fact that the error is given by the second derivative of the log of the likelihood which after being computed

explicitly and replacing the theoretical values of the anisotropy in the maximum of the log of the likelihood , leads to

$$\sigma_{C_S} = \sqrt{\frac{2}{N_p}}(C_S + C_N) \tag{4.12}$$

This equation is useful to assess how accurately a given experiment will determine parameters in a theory using the theorems shown just below (4.8). A more general expression of this gives the corresponding error when the free parameters are the C_l's themselves

$$\sigma_{C_S} = \sqrt{\frac{2}{(2l+1)f_s}}(C_l + C_{N,l}) \tag{4.13}$$

the number of independent measurements has been replaced by $2(l+1)f_s$, where f_s is the fraction of the sky covered. When the full sky is covered one can sample the distribution characterized by C_l at most $2l+1$ times and this is a fundamental limit of accuracy to measure C_l's . Even without C_N there's a remaining uncertainty in the theoretical parameters due to the fact that we only have one sky on which to take measurements. This limit is called cosmic variance in a full-sky survey.

4.2.2.f Sampling The Space Of Parameters Via Monte-Carlo-Markov-Chain Method

Markov Chain Monte-Carlo is essentially Monte-Carlo integration using Markov chains. When we need to integrate over high-dimensional probability distributions to make an inference about a model with free parameters given a set of data. Mote-Carlo integration draws samples from the required distribution and then forms sample averages to approximative expectations. The specific Markov Chain Monte Carlo samples the space of parameters by running a Markov chain for a long time. Along 40 years, MCMC penetrated the statistical practice. In the last years to date, MCMC is oriented towards Bayesian inference [134, 219].

The aim of MCMC is to construct a random walk in the space of parameters whose distribution function is the same as the target density, in this case the likelihood or the posterior. MCMC sampler moves in the space of parameters in a Markov process. The main feature of a Markov process is that the next sample depends on the present one, but not on the previous ones.

The resulting Markov chain samples the posterior, such that the distribution of the points in the random walk within the parameter space is proportional to the target distribution at least asymptotically and then we can estimate all the quantities of

interest as the mean an the variance of different parameters. The number of steps required to obtain good estimates scales linearly with the dimension of the space of parameters.

Thus this process is much more efficient than the grid-based evaluation as the number of parameters decreases. Direct grid–based evaluations of the likelihood have computation time and storage requirements which rise exponentially with the number of parameters. In consequence, in cosmology people usually deals with 10-20 parameters, so MCMC has been a very powerful tool and variety of implementations have been developed [71, 101, 173, 185]. Among the various ways of constructing these chains there's the special case of the general Metropolis-Hasting (MH) method first developed by Metropolis in the 50's [207] and generalized by Hastings in the 70's [145].

One popular construction principle within the Metropolis-Hastings context, is the Gibbs sampler, a specific MCMC method that samples iteratively from each of the univariate full conditional posterior distribution $p(\theta_i|x,\theta_1,...,\theta_{i-1},\theta_{i+1},...,\theta_n)$. Given arbitrary initial values $\{\theta_i^{(0)}\}$ the algorithm proceeds as follows [70, 250]

$$\begin{aligned}
\theta_1^{(1)} &\sim p(\theta_1|x,\theta_2,...,\theta_n)\\
\theta_2^{(1)} &\sim p(\theta_2|x,\theta_1,\theta_3...,\theta_n)\\
&\ .\quad .\quad .
\end{aligned}$$

and yields $\theta^{(m)} = (\theta_1^{(m)},...,\theta_m^{(m)})$ after m iterations. This defines a Markov chain that converges to the target distribution as its equilibrium distribution [134, 219].

One of the basic concepts of the MH algorithm is that of generating a density with the simulation technique *rejection sampling*. However, the *proposal distribution* $q(y|x)$, can now depend on the current state x of the sampling process, and instead of rigorously accepting or rejecting a new candidate y , it is accepted with a certain acceptance probability $\alpha(y|x)$ also depending on the current state x such that the transition probability specifying the Markov chain $p(x,y) = q(y|x)\alpha(y|x)$ satisfies detailed balance [71]. This is met by imposing

$$\alpha(y|x) = min\left\{\frac{f(y)q(x|y)}{f(x)q(y|x)},1\right\} \tag{4.14}$$

here f denotes the target distribution and x and y are multidimensional vectors defined in the parameter space. Then the main steps of MH algorithm are

- Start form an arbitrary point x_0 in the space of parameters.

- Generate y from $q(.|x_i)$ and $u \in (0,1)$

$$\text{If } u \leq \alpha(y|x_i) \text{ set } x_{i+1} = y \qquad \text{(acceptance)}$$

$$\text{If } u > \alpha(y|x_i) \text{ set } x_{i+1} = x_i \qquad \text{(rejection)}$$

The outcome from the MH algorithm can be regarded as a sample from the invariant density only after a certain 'burn-in' period (or initial set of dependent samples in the Markov chain). In order to perform convergence diagnostics of the random walk different techniques have been developed which have been reviewed and summarized by Cowles and Carlin [198] and have been implemented in cosmology via CosmoMC, for example, in [185] (see also [101]).

4.3 Cosmological Constraints On Brans-Dicke Gravity

In this section, we aim to determine the regions of the parameter space of the Brans-Dicke theory whitin which this model is in agreement with cosmological observations like the CMB and LSS. In order to do so, we use the MCMC tool to sample the parameter space within the context of the parametric approach described in the previous section. This will allow us to compute the desired likelihood and the posterior distributions from which we can carry out the corresponding statistical analysis to finally determine the most likely values for the parameters and their error bars. The following subsections explain in detail such a procedure.

4.3.1 MCMC Constraints From The CMB Anisotropies

4.3.1.a How the BDT Parameter Tickles the CMB?

In the relevant chapter, we have already look at the variation of the CMB anisotropies when the BDT parameters were varied since we were interested in understanding the new effects in BDT upon the standard model based on GR. Now we are ready to use that information to design a strategy to analyse the viability of our theories according to the observations of the CMB anisotropies. In order to do so, we must keep in mind an important fact when we aim to constrain a theory.

It is well known that the standard ΛCDM model has been the best fitting model of the CMB anisotropies and then the predictions of any alternative theory must lay close to the ΛCDM prediction.

Therefore, observable quantities, such as the CMB spectra, whose theoretical prediction depart considerably from ΛCDM correspond to a good source to constrain the model in question. In order words from looking at the variation of the observables with respect to the parameters we can figure out the sensitivity of the theory to the data and viceversa.

We already have explicitly studied the sensitivity of the CMB anisotropies to ω and ξ within BDT in chapter 3. Here we only are going to summarize such analysis. On one hand, the ratio of the sound horizon to the angular diameter distance to the last scattering surface is very sensitive to ω (not so ξ). On the other hand, we know that such quantity is well measured by the locations of the peaks of the anisotropies as we demonstrated in chapter 2. Therefore, ω is sensitive to θ.

However, It has been probed that there's a one to one relation between θ and ω_Λ as primary parameters when all the other parameters are fixed. Thus, choosing

the $\theta-$parametrization one can vary ω and extract other effects beyond those due to modified background evolution. Figures (3.19) and (3.20) show how temperature and polarization anisotropies change when ω varies and their explicit derivative in this new parametrization. This derivatives provide valuable information in order to determine in which extent the observations are capable to constrain our model.

4.3.1.b Methodology and Analysis

In order to obtain accurate theoretical observables within BDT, we numerically solved the BDT background (3.12) and the linearized equations for perturbations (3.31) in the Jordan frame presented in chapter 3. Lets recall that in this frame matter is minimally coupled to the metric hence the equations for different components of the matter-energy in the universe remain the same than those in GR. This feature ensures that the effective gravitational strength is correctly implemented in the code.

To test our numerical results we implemented the synchronous gauge equations for scalar modes in a modified version of the CAMB package [186] and compared with our own Boltzmann code (derived from CMBFast [274] and DASh [167]) in which both the synchronous gauge and the conformal Newtonian gauge were used. Also, to test the background solutions of the BDT scalar we performed the computation in both Jordan and Einstein frames and compared the results by means of the corresponding dictionary [75].

I would like to add a comment here about the task of modifying CAMB. Usually it is argued that only few lines in the code are needed to be added or changed in order to implement modified theories of gravity properly. However, I'd like to point that one has to be careful about some subtleties which determine in great extent the reliability of the estimates.

For example, in the standard CAMB code the expressions for the sources (2.117) and (2.118) needed to compute the CMB temperature anisotropy by using the line-of-sight integral and the lensing potential are only valid for ΛCDM. We rewrote completely these sources using the general expressions presented in [309] in terms of the solutions of perturbations valid for any theory. Other subtlety that is important is the parametrization, in the standard CosmoMC, the Hubble H_0 constant and the non-physical parameters (e.g. Ω_b instead $\Omega_b h^2$) are used as primary parameters. However, this is not general, because the computation of H_0 is model-dependent and hence a derived parameter. In general, for a cosmological model different to ΛCDM a more natural primary parametrization is made of the physical parameters and ω_Λ instead of H_0.

Also, the algorithm to compute the real θ (the ratio of the sound horizon to the angular diameter distance to the last scattering surface) from the theory is not general at all neither. Remember that this observable is well tested by the CMB, therefore if we aim to measure the real θ from the locations of the acoustic peaks in the temperature spectrum, this part of code needs to be modified necessarily. The modification that we used to estimate the parameters of BDT take all these points and also other minor arrangements.

In order to carry out a Bayesian analysis for BDT using available data of the CMB, we use the MCMC approach described above to sample the BDT parameters space. We used the popular code CosmoMC to handle the MCMC implementation in cosmology. We generated multiple chains for various combinations of models and data sets by means of the Metropolis-Hasting algorithm. Our chains were long enough to pass different convergence diagnostics processed by the GetDist program. The convergence diagnostics that we used are mainly the Gelman and Rubin "R= variance of chain means/mean of chain variances" statistic for each parameter using the second half of each chain [48]. Also the Raftery and Lewis convergence diagnostics were used [253].

The main datasets we used are from the Planck satellite[4], WMAP-7/9 [175], the South Pole Telescope (SPT) [269] and the Atacama Cosmology Telescope(ACT) [100]. We also use data from Big-Bang Nucleosynthesis (BBN) light element abundances [160].

The chains were generated for the two types of models described before, rBDT and uBDT models. The rBDT models have 7 parameters which are the dimensionless baryon and dark matter densities ω_b and ω_c respectively, the ratio of the angular diameter distance to the sound horizon at recombination θ, the reionization redshift z_{re}, the amplitude and spectral index of the primordial power spectrum A_s and n_s respectively and the BDT parameter ω. The Hubble constant H_0 and the (dimensionless) cosmological constant density ω_Λ are derived parameters.

The uBDT models have one additional parameter which is the initial condition ϕ_{ini}. When generating likelihoods for the Planck data, 11 astronomical parameters to model foregrounds and 3 instrumental calibration and beam parameters (3) were used as described in [4]. When ACT and SPT were also included with Planck, 17 more calibration parameters were used [4]. In order to sample efficiently the large number of "fast" parameters, we used the speed-ordered Cholesky parameter rotation and the dragging scheme described by Neal and Lewis [184, 220] implemented in the latest version of CosmoMC.

We now turn to the issue of priors. For the non-BDT parameters we assume the same priors as for ΛCDM since the two types of cosmological evolution are very

similar. A "prior" on H_0 (HST) from the measurement of the angular diameter distance at redshift $z = 0.04$ [3] is also imposed for some chains[1].

It is worth of mentioning that when WMAP data is used the question on whether the prior on ω is important or not comes to be relevant. Since WMAP does not constrain ω too tightly this check should at least be done. In this work, for the BDT parameters we impose flat priors on $\bar{\phi}_i$ and on $-log(\omega)$. In [337] flat priors on $y = \ln(1+1/\omega)$ were used, in order to accommodate negative ω. However, since $\omega < -\frac{3}{2}$ is a ghost we see little reason for this. Furthermore, since $dy \approx -d\ln\omega/d\omega$, using y rather than $\ln\omega$ penalizes models with large ω (explains the weaker constraints found in [337]) which we feel is rather artificial. Therefore, the prior on $-\ln(\omega)$ is more convenient for sampling the chains [2]. However, the choice of prior is not important when Planck is included after all, as our constraints strongly improved compared to past experiments.

For sake of completeness, in order to address the issue of whether our results are dependent on the prior in the case of the $log(\omega)$ parametrization, we used three cutoffs of different order of magnitude and verified that the results were independent. The reason why the choice of a cutoff may give rise to different results is the following. Since the data prefer models close to ΛCDM, the 1D posterior distribution for $log(\omega)$ has a single tail. Because of the error in the data, the distribution is flat at the high likelihood region $log(\omega) \to \infty$. Therefore, the confidence limits calculated for this prior are potentially invalid. At first glance, the position of the upper limit depends on the cutoff for $log(\omega)$. Nevertheless, the choice of a cutoff is not as arbitrary as we may initially think if we restrict ourselves to consider a realistic range of values for ω. In order to be more explicit, let us pick for example as cutoff the constraint from the solar system $log(\omega) \sim 10^5$. A large set of models within this prior stand in the flat, high-likelihood-region. The order of the corresponding confidence limits for this cutoff would be the same even if we increase the cutoff by one or two orders of magnitude. Given the accuracy of current and near future surveys, models above such a cutoff are in practice indistinguishable. Therefore, we can easily realise that we are safe to choose any cutoff with an order of magnitude lying around the solar-system constraint.

[1] Remember that H_0 is a derived parameter here so the H_0 prior is rather a further constraint

4.3.1.c Results and Discussion

BDT parameters We first discuss the restricted models, which contain only ω as an additional parameter to ΛCDM. Using WMAP7 alone, we find $\omega > \{90, 51\}$ at 95% and 99% level respectively while for WMAP7+HST we improve to $\omega > \{126, 62\}$. This is a significant improvement over [2], driven mainly by the inclusion of polarization data which break the degeneracy between z_{re} and n_s and allow the measurements of the damping tail to improve the determination of the other parameters and limit the freedom of ω to vary. For WMAP7+SPT+HST data, this changes to $\omega > \{157, 114\}$ at the same confidence levels.

The use of Planck Temperature (PlanckTemp) data greatly improves the measurement of the damping tail and together with WMAP 9yr polarization [WMAP9(pol)] further improves the constraint to $\omega > \{1808, 692\}$. This is in line with the forecasting of [64]. Our results, including more data combinations, are summarized in table I.

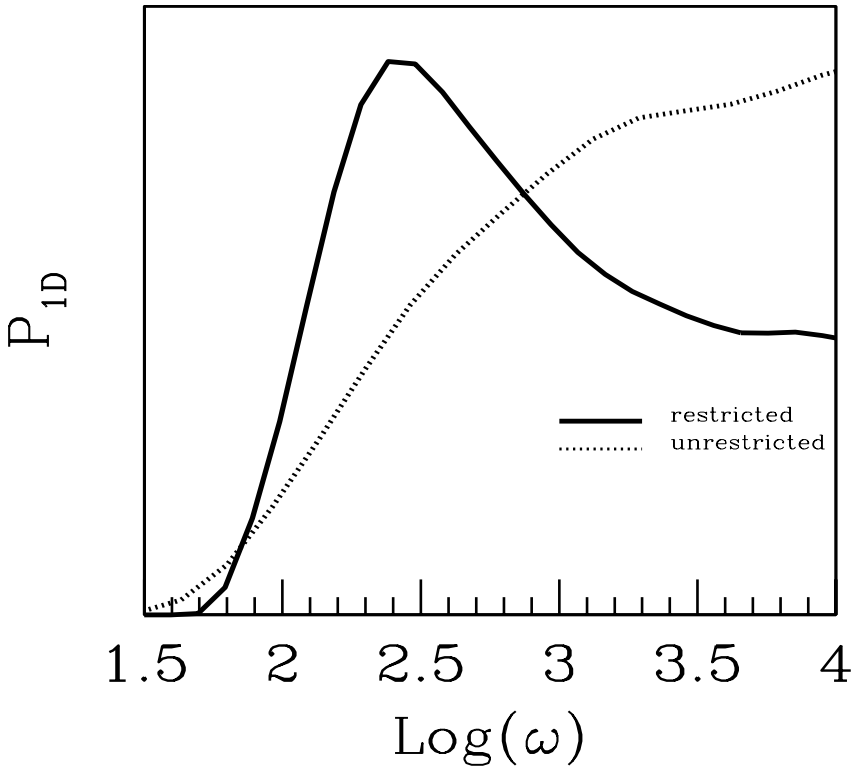

Fig. 4.2 The 1D marginalized posterior of $\log_{10}\omega$ for the rBDT(solid) and uBDT(dashed) models using WMAP7 + SPT.

Constraints on uBDT models, which contain ξ as a further parameter, have not been presented before. As discussed in [341], the main effect of increasing ξ is to increase

the width of the visibility function which in turn increases photon diffusion and damps the CMB temperature anisotropies on small scales. Thus the main constraints on ξ from CMB temperature come from fitting the damping envelope with measurements of the CMB at small scales from ACT, SPT and Planck. Increasing ξ has a slightly different effect on polarization. The same damping effect occurs on small scales but on large scales we get an enhancement as a thicker last scattering surface increases the amplitude of the local quadrupole, producing a larger polarization signal [341].

Using WMAP7 alone, we find $\omega > \{99, 55\}$ and $\xi = \{0.98^{+0.67}_{-0.55}, 0.98^{+0.98}_{-0.63}\}$ at the 95% and 99% level respectively which changes to $\omega > \{269, 148\}$ and $\xi = \{1.10^{+0.13}_{-0.14}, 1.10^{+0.17}_{-0.19}\}$ at the same confidence levels with WMAP7+SPT+HST data. Using PlanckTemp+WMAP9(pol) improves the constraint to $\omega > \{1834, 890\}$ and $\xi = \{1.12^{+0.11}_{-0.11}, 1.12^{+0.16}_{-0.14}\}$. These results and more data combinations are summarized in table I.

Why do restricted models become less constrained than the unrestricted models which have one more parameter? In fact, our WMAP7+HST results are compatible with the forecasting of [64] but given that they expect ω to be constrained close to ~ 1000 with Planck, it is reasonable to expect values around $500 - 700$ with the inclusion of SPT data, contrary to what we find in practice. The reason we see no improvement with the inclusion of SPT data is uncovered by figure (4.2). The marginalized distribution of $\ln \omega$ exhibits a peak around $\omega \sim 400$, however, the difference in likelihood between the GR limit and this peak is very small which renders this "detection" insignificant. However, its presence makes it difficult to improve the lower bound of ω unless a different data set is included. When we use PlanckTemp+HL data the peak is washed out, however, a small effect still remains.

In order to understand this better, lets recall that in the unrestricted model the preferred value of ξ deviates from unity at around 10%. However, as in the restricted model $\xi \approx 1$ this discrepancy in ξ between the two types of models, cuts-off a large portion of good likelihood in parameter space. In order to verify this assertion we consider a fictitious restricted model where $\bar{\phi}_i$ is fixed so that ξ today is the best fit from the unrestricted model. As expected, the best-fit sample for this fictitious model lies in the ΛCDM large ω limit and the constraint on omega becomes $\omega > 471$ at the 95% level which is notably stronger than both the realistic models and also in line with the forecasting of [64].

In both types of models, constraints on ω using PlanckTemp+WMAP9pol improve by a factor of six over WMAP7+SPT+HST. We can notice that the fact that in the restricted models, ω is less constrained than in the unrestricted class still stands when Planck data is added. Furthermore, this is more pronounced when other data combinations with PlanckTemp are used. The reason why is because the extra parameter

ξ helps to fit the data better; i.e. the best-fit sample for the unrestricted model has a slightly better χ^2 than the restricted model.

PlanckTemp together with lensing potential reconstruction (PlanckLens) gives the tightest constraint on ω. However, PlanckLens displays small discrepancies from PlanckTemp [4] and once again we opt for not using it when we report our final result. Interestingly when HL data is added, both PlanckTemp+PlanckLens and PlanckTemp+WMAP9(pol) give very similar constraints.

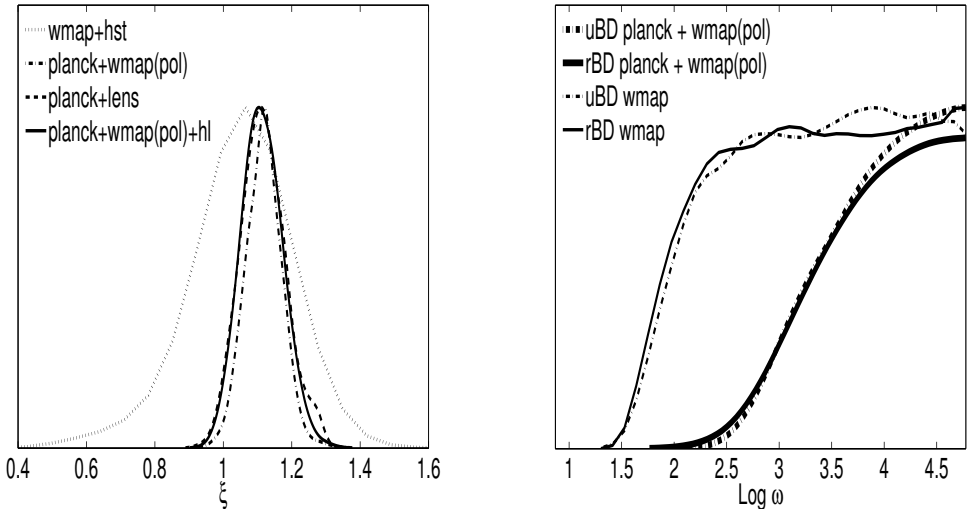

Fig. 4.3 Left: 1D marginalized posterior for $\xi = G_{\rm eff}/G$ with Planck+WMAP9(pol). Right: The 1D marginalized posterior of $\ln\omega$ for different BDT models.

The following table shows our main results in this subsection derived with different data sets. The first row labels the parameters constrained, $CMB + BBN$ means previous constraints plus BBN. U and R, in the second row denote unrestricted and restricted models respectively. The percentages shown in the third row are the corresponding confidence levels.

	ω				ξ		ξ from CMB + BBN	$\dot{\xi} \times 10^{-13}\ years^{-1}$	
	U		R					upper	
	95%	99%	95%	99%	95%	99%	1σ	95%	99%
WMAP7	99	55	90	51	$0.98^{+0.67}_{-0.55}$	$0.98^{+0.98}_{-0.63}$	1.113 ± 0.156	2.45	3.37
WMAP7 + HST	126	62	177	120	$1.07^{+0.22}_{-0.24}$	$1.07^{+0.40}_{-0.43}$	0.991 ± 0.036	2.85	3.59
WMAP7 + SPT + HST	269	148	157	114	$1.10^{+0.13}_{-0.14}$	$1.10^{+0.17}_{-0.19}$	0.996 ± 0.029	1.92	2.81
PlanckTemp + WMAP9pol	1834	890	1808	692	$1.12^{+0.11}_{-0.11}$	$1.12^{+0.16}_{-0.14}$	1.006 ± 0.018	0.93	1.78
PlanckTemp + WMAP9pol + High-l	1923	843	1326	213	$1.11^{+0.13}_{-0.11}$	$1.11^{+0.17}_{-0.14}$	1.009 ± 0.014	0.74	1.75
PlanckTemp + PlanckLens	2441	1033	1901	420	$1.12^{+0.10}_{-0.14}$	$1.12^{+0.16}_{-0.17}$	0.998 ± 0.029	0.63	1.51
PlanckTemp + PlanckLens + Hight-l	1939	829	1408	330	$1.07^{+0.11}_{-0.10}$	$1.07^{+0.14}_{-0.13}$	0.999 ± 0.024	0.36	0.83

Cosmological Constraints on ξ Cosmological constraints on the Newton constant from the CMB can be found in [307] where $0.74 \leq \xi \leq 1.66$ is found from WMAP-1 alone at 95% of confidence level while by including BBN data the tighter bounds $0.95 \leq \xi \leq 1.01$ are obtained at 1σ. In this paragraph we report equivalent constraints for ξ for both sort of measurements, however we update the result since we use more recent data from Planck and BBN. As we'll see in short, our BBN-alone constraints are nothing but an update of the ones reported by Umezu et. al. However those resulting from an MCMC analysis using only CMB data hold the extra feature that are valid only within the BDT context.

Within BDT the extra scalar field plays the role of the Newton strength G_N which is a dynamical entity. Moreover, lets recall that a motivation to consider the uBDT models was to consider possible variations of the value of G_N today at cosmological scales (which may be in principle different than in GR).

Indeed, along chapter 6 we shall see that G_N within the cubic galileon theory at large scales within the PPN approach, actually bear a dynamical G_N at cosmological scales. A way to bridge both regimes would be to set the constraints on cosmological G_N as boundary conditions for the galileons. For that reason we consider is important to constraint G_N as much as possible. We already realised in chapters 2 and 3, that the abundances of light elements at the BBN epoch are quite sensitive to G_N. Thus tight constraints on ξ can be achieved fitting this set of data.

Lets first regard to the BBN-alone estimations. In order to constraint G_N within uBDT using BBN we follow the same methodology as in [307]. As we already studied in the BBN section in chapter 3, at early times G_N does not evolve in time it just adjust its value due to rescalings when the initial conditions for the BDT scalar change from one model to another. Thus one basically deals with GR and includes possibles rescalings of G_N. Basically what we did is to update the treatment used in [307] by using the latest estimations of Deuterium and 4-Helium abundances from [160].

In summary the drill goes as follows: we used the Kawano code to solve the coupled system of Boltzmann equations describing the abundances of components involved in the nuclear reaction occurring during nucleosynthesis [168]. As the rate of the reaction decreases in relation to the expansion rate, the process comes out of equilibrium and the abundances of final products tend to a constant. The final values of these freeze-out abundances of light elements right after the process of nucleosynthesis depend on the following parameters: the amount of baryons Ω_b which is quantified by the baryon-to-photon ratio η, the strength of gravity G_N and the neutron-lifetime which by default in the code is given by 888.54 seconds, however we updated that value to 882.1 according to [307]. In our treatment as in [307], we keep the number of neutrino species fixed to 3 and a possible cosmological constant to 0.

Our final goal was to derive the lower and upper 1σ 2D constraints for allowed values of ξ and $\eta_{10} \equiv 10^{10}\eta$ corresponding to the 1σ measurements of Deuterium and 4-Helium abundances reported in [160]. In order to accomplish that task, we multi-ran the Kawano code for all different combinations of values of η and G_N in the relevant ranges so that the final abundances were fixed to its lower and upper 1σ bounds. The set of values giving rise to the desired abundances are shown in figure (4.4), the region square-shaped enclosed by the curves, corresponds to the values for G_N and η^{10} that give rise to abundances laying inside the latest estimation.

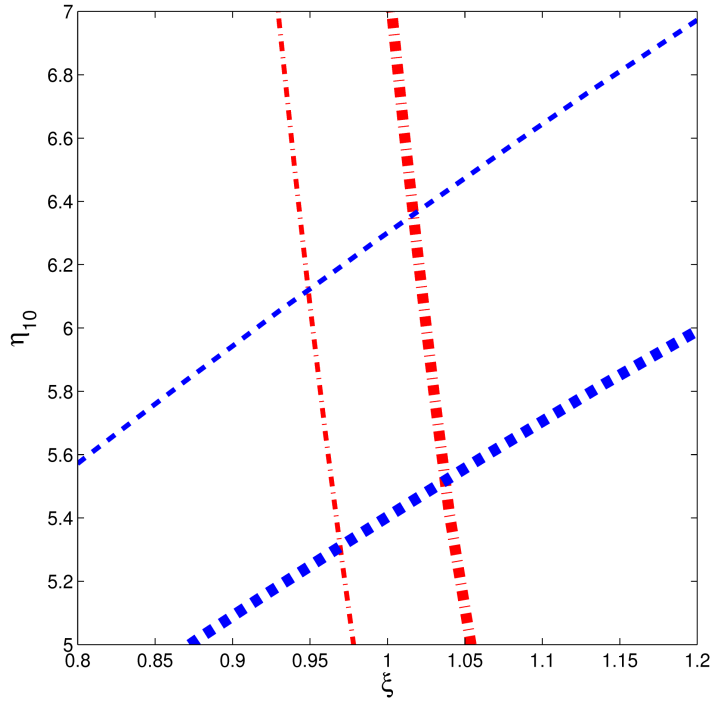

Fig. 4.4 Required values of baryonic matter and G_N to obtain an amount of a given element. The lower(thin) and upper(thick) values of each element correspond to the latest limits from different observations of Helium-4 (red/dashed-dotted) $Y_p = 0.250 \pm 0.003$ and Deuterium (blue/dashed) $D/H = (2.17 \pm 0.29) \times 10^{-5}$ abundaces from [160].

The projected estimation for G_N within this approach results to be very tight $\xi = 0.995 \pm 0.035$. The corresponding constraint for the baryon-to-photon ratio is also very tight and consistent with other measurements [6] $\eta_{10} \in (5.25, 6.30)$.

Lets turn to derive further constraints combining BBN plus CMB data. Again, we follow the same procedure than Umezu to combine the data, independent 1σ constraints from CMB and BBN respectively are overlapped and the joint region gives rise to a fairly good estimation for ξ [see figure (4.5)]. We find $0.998 \leq \xi \leq 1.024$ at 1σ with PlanckTemp+WMAP9pol+BBN and further results can be found in table

I. As expected, our results improve on [307] and further put them in the context of a realistic theory. In a more recent work by [188] constraints for G_N are obtained in the context of the restricted BDT, however in their analysis they left out a possible rescalings. We also report a strong upper bound on the time-variation of G_N from the CMB alone around $\sim 10^{-13}/year$, as in table I.

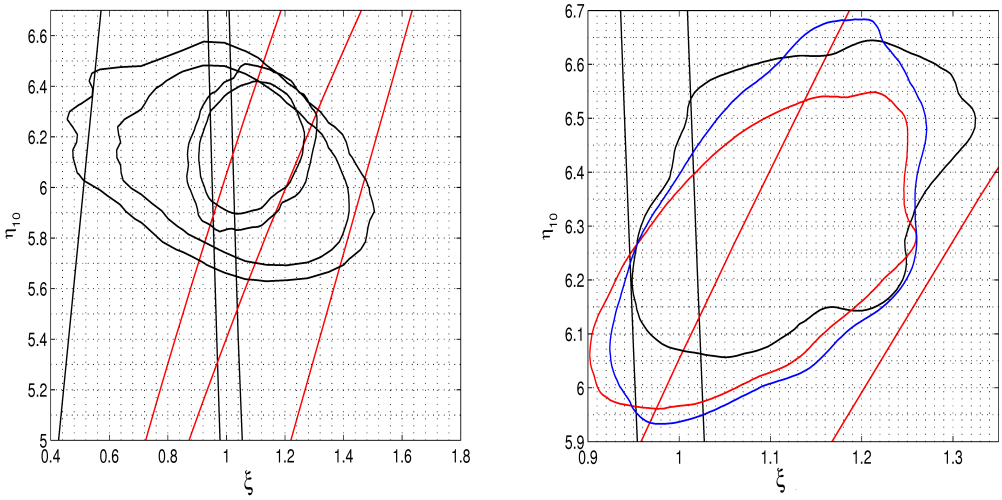

Fig. 4.5 Independent 2D constraints of $\xi - \eta_{10}$ from CMB at 1σ and/or 2σ are overlapped with those from BBN at 1σ. The Joint region corresponds to the constraints corresponding to combined data. Left: WMAP7+HST and WMAP7+SPT+HST. Right: Closed lines: red$\rightarrow$ planck + lensing, blue $\rightarrow$ planck + lensing + high-l, black: $\rightarrow$ planck + wmap9(pol). Right: Closed lines: red$\rightarrow$ planck + lensing, blue$\rightarrow$ planck + lensing + high-l, black:$\rightarrow$ planck + wmap9(pol)

Estimates of ω, Ω_Λ and ξ Estimations for the restricted model using WMAP7+SPT brings up a degeneracy between ω_Λ and ω which consequently gives rise to a weak constraint for the BDT parameter. Interestingly, this degeneracy is less important for the unrestricted model and further more completely alleviated when the value of G_{eff} is fixed to the its best fit [See figure (4.6)]. Therefore when G_{eff} (or ξ) is allowed to take different values than the solar system, ω and ω_Λ are better determined. We can understand why this happens thinking in the way these parameters move the temperature CMB anisotropy. On one hand ω and ω_Λ move the CMB in similar directions, both affect the distances and then they change importantly the locations of the peaks and in a lesser extend affect the heights as well. This explains the degeneracy given the resolution of WMAP7. On the other hand, ξ barely changes the location of the peaks, in turn it affects more importantly their heights. Thus at the level of the background evolution, ξ helps to gain control when fitting the CMB in this direction.

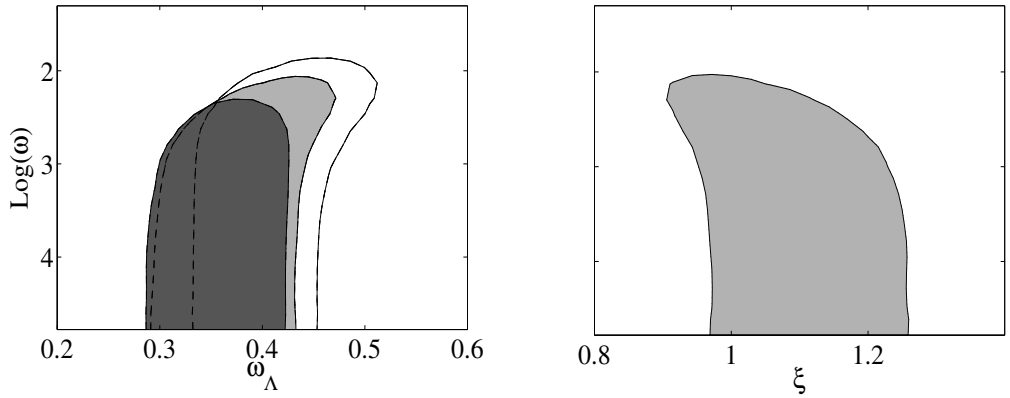

Fig. 4.6 The 2D marginalized posterior distributions for $\omega - \omega_\Lambda$ and $\omega - \xi$ are shown in the left and right panels respectively at 95% confidence level with WMAP7 + SPT data. The left panel, the contours in the back are for the restricted model, the contours in the middle are for the unrestricted and the front ones for a fictitious restricted case where G_{eff} today was fixed to be the best fit from the unrestricted case.

This story changes with the inclusion of Planck. The great improvement in quality and accuracy of the measurements of the spectrum from Planck over WMAP suffices to break down this degeneracy even in the restricted models where the effects ω and Ω_Λ are fully distinguished as figure (4.6) shows.

Cosmological Parameters As expected the best fit model in BDT for any combination of data lay very closely to the best fit of ΛCDM. Actually our constraints are compatible with ΛCDM within 1σ [4]. The following table shows our resulting estimations for the cosmological parameters for both of models restricted and unrestricted at 1σ for different data combinations.

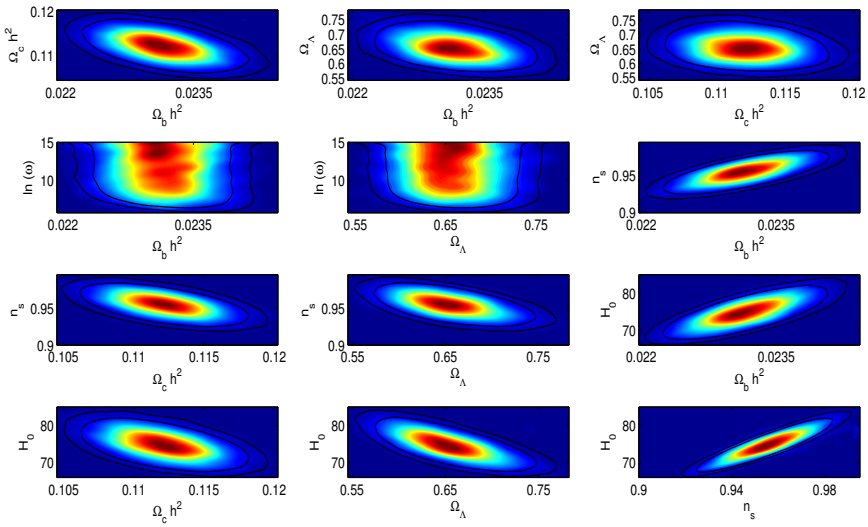

Fig. 4.7 2D marginal posteriors(solid contours) and the projection of the likelihood(scatter-color plot) for the set of most correlated parameters with the dataset uBDT Planck + WMAP9(pol) + ACT+SPT: the 1σ estimations of cosmological parameters of uBDT are compatible with estimations for ΛCDM at the same confidence level. Some degeneracies can be spotted in 2D marginal distributions corresponding to H_0, n_s and cosmological parameters.

	URESTRICTED 1σ			
	$\omega_b h^2$	$\omega_c h^2$	ω_Λ	H_0
	lower, mean ,upper	lower, mean, upper	lower, mean, upper	lower, mean, upper
W7	0.0211, 0.0222, 0.0234	0.0960, 0.111, 0.0127	0.520, 0.716, 0.970	69.92, 73.78, 77.71
W7SP	0.0216, 0.0224, 0.0232	0.0106, 0.114, 0.0122	0.564, 0.667, 0.791	70.68, 74.65, 78.67
PLW9(pol)	0.0224, 0.0232, 0.0231	0.108, 0.112, 0.117	0.593, 0.652, 0.717	69.39, 74.75, 80.13
PLLS	0.0221, 0.0229, 0.0237	0.109, , 0.1140.120	0.568, , 0.646, 0.720	68.46, 73.82, 80.65
PLW9(p)HL	0.0225, 0.0232, 0.0239	0.108, 0.112, 0.117	0.593, 0.657, 0.726	69.18, 74.58, 80.46
PLLSHL	0.0221, 0.0229, 0.0237	0.109, 0.113, 0.118	0.614, 0.673, 0.736	67.34, 72.27, 77.32
	RESTRICTED 1σ			
	$\omega_b h^2$	$\omega_c h^2$	ω_Λ	H_0
	mean, lower, upper	mean, lower, upper	mean, lower, upper	mean, lower, upper
W7	0.0211, 0.0222, 0.0233	0.101, 0.111, 0.122	0.677, 0.747, 0.849	69.59, 72.72, 76.10
W7SP	0.216, 0.0223, 0.230	0.102, 0.110, 0.119	0.717, 0.756, 0.793	70.18, 73.33, 76.96
PLW9(p)	0.0222, 0.0228, 0.0234	0.108, 0.113, 0.118	0.692, 0.720, 0.745	67.27, 69.62, 71.99
PLLS	0.0219, 0.0226, 0.0232	0.110, 0.113, 0.118	0.690, 0.715, 0.740	66.88, 69.12, 71.39
PLW9(p)HL	0.0222, 0.0227, 0.0233	0.108, 0.113, 0.118		
PLLSHL	0.0220, 0.0226, 0.0233	0.109, 0.113, 0.118	0.691, 0.718, 0.743	67.21, 69.38, 71.69

Acoustic Scale It is defined as the characteristic angular size of the anisotropies in the CMB. We already know that this quantity is quantified by the θ parameter. With accurate measurement of seven acoustic peaks, Planck determines the observed angular size within BDT as it is shown in the following table:

model	$\theta(\tau_{rec})$ (rBD/uBD) 2σ	$\theta(\tau_{rec})$ in ΛCDM 1σ [6]
planck+wp+hl	1.03939 ± 0.00064/1.039867 ± 0.00067	1.04132 ± 0.00068
planck+lensing+hl	1.03934 ± 0.00062/1.03954 ± 0.00065	1.04132 ± 0.00068

The agreement of our measurement with the standard model is only achieved at 2σ and the mean is underestimated in the case of rBDT whilst its closer within uBDT. Nevertheless, as it happens within the standard model, since this parameter is constrained by the positions of the peaks but not their amplitudes, it is quite robust; the measurement is very stable to changes in data combinations and the assumed cosmology [4]. Tight constraints on $\theta(\tau_{rec})$ also implies strong constraints on other cosmological parameters which determine distance measurements as the sound horizon and the angular diameter distance.

Hubble Parameter, Matter densities and Cosmological G_N In the standard ΛCDM model the Hubble constant, H_0 , and matter density parameter, Ω_m , can only be tightly constrained by using a special combination arisen from principal component analysis [4][2]. However the extent of the degeneracy is limited by the effect of the physical matter density on the relative heights of the acoustic peaks. Within BDT, G_N is introduced as an extra parameter and it takes part in this game. First, the main effect of ξ is on the amplitude of the peaks so one can anticipate a degeneracy with all these parameters and also the spectral index [figure (4.8)]. Second the surface $\theta^* = constant$ lives in a larger parameter space where ω and ξ are now included, and hence the degeneracy between these parameters is more significant. The degeneracy between H_0 and G_N in BDT is analogous to the degeneracy between H_0 and $\Omega_m h^2$ in ΛCDM. The source of correlation between H_0 and G_N is the same than for H_0 and $\Omega_m h^2$ and it can be understood by looking at the Friedmann equation today. To vary either ξ or $\Omega_m h^2$ may produce a similar Hubble rate of expansion. Consequently the constraint for H_0 and G_N has the same shape as that for H_0 and Ω_m [4] (Figure (4.8)).

[2]Parameter combinations that fit the Planck data must be constrained to be close to a surface of constant θ^*. This surface depends on the model that is assumed. For the base model this surface is straightforwardly determined and then Ω_m is well constrained.

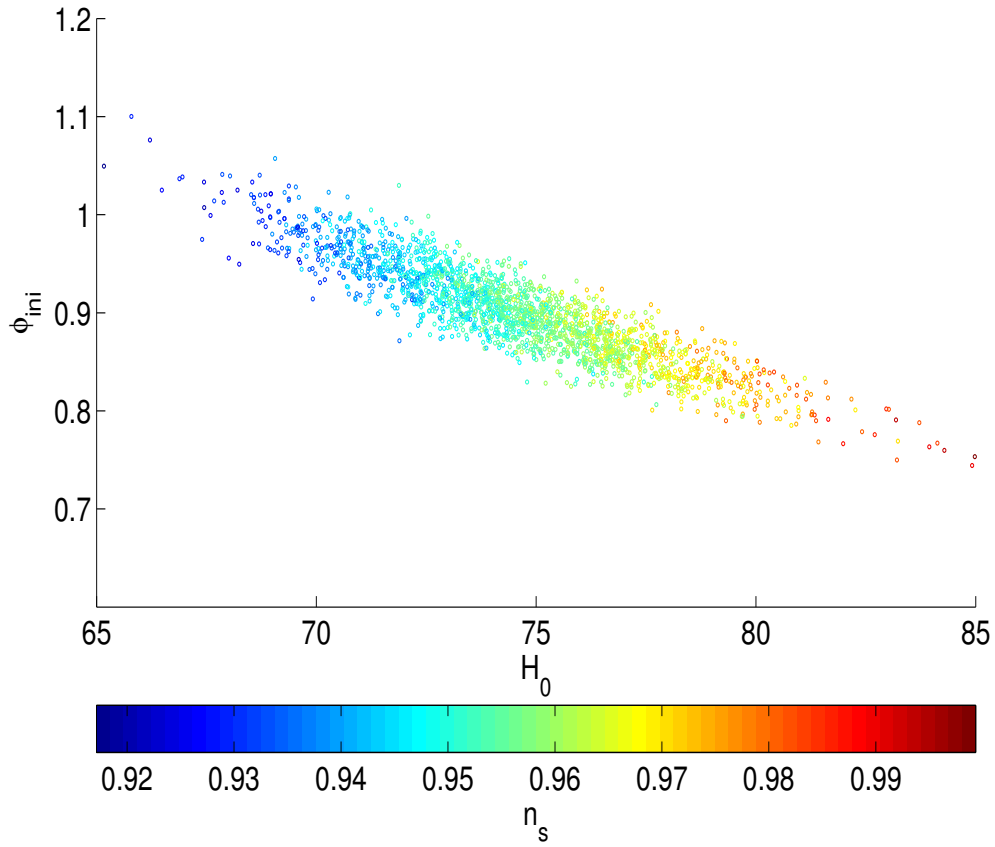

Fig. 4.8 3D marginal distribution for ϕ_{ini}, H_0 and the spectral index n_s at 1 σ. Colored points show samples from the Planck+WP+act+spt posterior, different colors correspond to different values of the spectral index n_s. Clearly there is a degeneracy between these three parameters, however there is a very well constrained direction set by the acoustic scale.

The constraint for H_0 results from the projection of the 2D posterior onto the relevant axis. We find a 4% for the Hubble parameter within BDT by Planck at 1σ

$$69.18 < H_0 < 80.46 \qquad H_0^{mean} = (74.5 \pm 2.9) km\, s^{-1}\, Mpc^{-1} \tag{4.15}$$

Althought this estimation of H_0 is not as precise as for the ΛCDM model due to the degeneracy with the spectral index and other parameters , it has the great advantage that it is compatible with other probes of H_0 like SN or local probes in contrast to the results from ΛCDM using the latest Planck data [4].

Spectral Index and Matter Densities The temperature spectrum of the CMB measures the matter densities in baryons and dark matter from the relative heights of the acoustic peaks. However, the degeneracies of the matter densities with the spectral index and other parameters sacrifices accurate estimations. Nonetheless, with Planck there are enough well measured peaks the extent of degeneracy is limited. On the other hand the spectral index is also correlated to the optical depth since it affects the relative power between large scales and intermediate and small scales. However, this degeneracy can be reduced by the inclusion of $WMAP$(pol) [4].

4.3.2 MCMC Constraints from the CMB and LSS

The most basic results of this chapter have been already presented in the previous section. Along the following sections we are going to analyze BDT using complementary cosmological data apart to the underlying CMB in order to extract further information about specific phenomenological implications of our theory. Specifically, in this section we are going to set further constraints on BDT using observations of features of the large scale structure. Along the first part, we will make the analysis using observations of the galaxy power spectrum in order to constrain the theoretical matter power spectrum. I must mention, that in contrast to the previous section, our goal here is not to get the best-as-possible constraints using latest data but rather investigate on the sensitivity of the data to the BDT parameter and vice versa. For this analysis, our baseline CMB data is WMAP7 and upon it we add measurements of the galaxy power spectrum $P(k)$ from SDSS Release 4 and detections of the Alcock-Paczynski effect using galactic peculiar velocities measurements from WIGGLEZ. It turns out that restricted and unrestricted models have to be treated somehow differently when we aim to constrain them using galaxy power spectrum observations. To deal with unrestricted models, one need some care with the statistical methods used to compute the likelihoods. Thus in this work we only point out the need of further analysis in this case without actually addressing the issue. In consequence we shall constraint the restricted case, only.

4.3.2.a Methodology

In the same way than for the CMB alone case, we used our own modified version of CAMB to calculate the matter power spectrum within BDT. Apart of the baseline parameters used to fit the CMB, we introduced a linear bias parameter to our set in order to fit observations of $P(k)$ from SDSS-R4 [304]. Lets recall that indeed we don't know which is the configuration of the overdensities in the universe, the galaxy power spectrum that we observe does not correspond necessarily with the theoretical

matter power spectrum. In order to parametrize this ignorance the bias $b(a,k)$ is introduced and hence both spectra are related by $\delta_g(k,z) = b(k,z)\delta_m(k,z)$. In the linear case, the bias is independent of the scale and furthermore, in this work we only use measurements for $z = 0$ so the bias is a simple constant.

In first place, lets describe how the bias is usually handled in CosmoMC. Since the bias is assumed to be completely undetermined from the theory it is marginalized over analytically following [47], as long as the likelihoods are Gaussian, and the prior on the amplitude parameter is Gaussian or flat [185].

$$L \propto \int d\alpha P(\alpha) exp[-(\alpha \mathbf{v} - \mathbf{d})^T C_N^{-1} (\alpha \mathbf{v} - \mathbf{d})/2] \tag{4.16}$$

where $\mathbf{v}$ and $\mathbf{d}$ are vectors and C_N is the noise covariance matrix and $P(\alpha)$ is the prior. For example with the 2dF data $\mathbf{v}$ would be the predicted matter power spectrum values, and α would be the unknown amplitude relative to the galaxy power spectrum at $z = 0$. Then the best-fit χ^2 is given by

$$\chi^2_{best-fit} = \mathbf{d}^T \left(\mathbf{N}^{-1} - \frac{\mathbf{N}^{-1}\mathbf{v}\mathbf{v}^T\mathbf{N}^{-1}}{\mathbf{v}^T\mathbf{N}^{-1}\mathbf{V}} \right) \mathbf{d} \tag{4.17}$$

The marginalized result is only "correct" if the assumed flat prior is correct; it is an advantage of the maximization technique that the result does not depend on the prior.

In contrast to ΛCDM, the case of BDT , as in other modified theories of gravity, the dynamics driving the large structure formation is characterized by a dynamical Newton coupling. At the level of the matter power spectrum physics, this dynamical G_N might be strongly correlated to the bias because both of them rescale the overdensities at a given scale and redshift. In other words, the bias and G can not be distinguished by $P(k)$ observations alone. Additionally, G_N is a parameter not completely unknown and can be determined by the theory (other physics apart of $P(k)$), thus given this possible correlation of G_N with the bias, we consider that is safer not to apply the analytical marginalization, or at least not assume a priori that the analytic marginalization holds for a correlated parameter.

Thus, in our version of CAMB we added a constant linear bias with flat prior to compute the $P(k)$ of galaxies and removed the analytic marginalization from CosmoMC so that the bias is allowed to be sampled numerically by the MCMC process. Anyway we considered both sort of procedures: run with/without analytic marginalization algorithm to check if the results are affected. Specifically we sampled the space of parameters of this model in three ways for comparison purposes:

1. The default CosmoMC algorithm: a scale-dependent bias with flat prior is assumed which is analytically marginalized when calculating the χ^2 corresponding to the $P(k)$ data.

2. To assume a scale-independent bias with flat prior and keeping the analytical marginalization turned on.

3. To introduce a constant bias with flat prior as a theory parameter, turn off analytical marginalization and calculate χ^2 as usual. The marginalization of the bias is carried out numerically after the space of parameters is sampled.

In the following we will make our analysis using these different methods of marginalization to derive the corresponding posteriors for different parameters and sort of models. This check is important since the extent of accuracy and reliability of our estimations depend on the quality of the statistical method used.

4.3.2.b Results and Discussion

(Un)Restricted Models and the Bias As we saw above, ξ and the bias are strongly correlated. This brings up some issues when trying to obtain reliable estimates for the parameters of different BDT models. In particular, the uBDT models are specially sensitive to the method used to handle the bias as coordinate in of the parameter space. Usually, the bias is assumed to be uncorrelated to the other parameters and then when implementing the MCMC sampling method into a code it is marginalized analytically in order to cut down on computing resources.

In the standard CosmoMC code, the already described analytic marginalization is carried out by default so care has to be taken when it is being used to sample the space of parameters. In this subsection, we will show that as expected, the results are affected by this procedure only in the uBDT. Thus, at the end of the day in order to get good estimates for our parameters from CosmoMC we have two choices: first, stick to the rBDT or second, modify the code to get rid of the analytic marginalization of the bias in order to take into account possible correlations between the bias and other parameters.

The results for the rBDT are illustrated in figure (4.9). It can be noticed that the posteriors are independent of the method used to marginalize the bias. The reason why this happens is that $\xi \sim 1$ within rBDT then the correlation with the linear bias is practically negligible. However, it still leaves tiny a footprint in the statistics of ω.

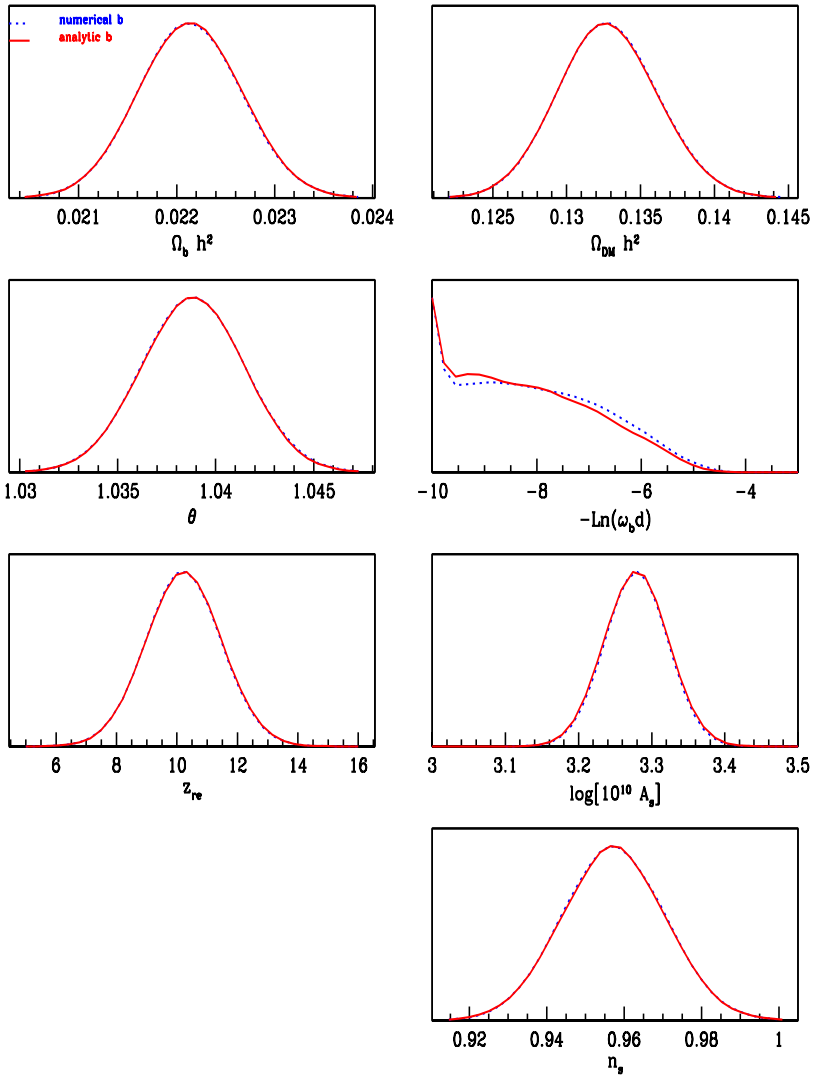

Fig. 4.9 Restricted model's parameters from WMAP7+SDSS-R4. The resulting 1D posterior distributions for cosmological parameters are independent of the method of marginalizing the bias. However, the BDT parameter is slightly sensitive to the method used, as we can see the analytical method produces stronger constraints.

For rBDT we obtained a very tight constraint of $\omega > 592.4$ with WMAP7+SDSS-R4 at 95% of confidence level which is independent of the method of marginalization of the bias [see figure (4.9)] and the posterior distributions for the cosmological parameters as well and they are consistent with ΛCDM figure up to 1σ .

In turn, within the uBDT models, the posterior distributions change depending on whether the marginalization of the bias is made numerically or analytically. In

addition, the resulting distributions for different sets of data have some issues that we are going to discuss in short. Of course the main cause of these issues is the mentioned degeneracy between the linear bias and ξ at the matter power spectrum level. It doesn't suffice to fit the CMB and LSS using the unrestricted model, it is necessary to include further data in order to break such degeneracy. Small scale CMB data, measurements of distance to test the expansion history and measurements of BAO of course, are sensitive to ξ and thus they can help to distinguish it form the bias.

In addition, as we know, the uBDT models are interesting since they take into account different values of the Newton coupling at cosmological and solar-system scales and so they can be a very-large-scale limit of more general and better physically motivated theories. So it might be worth to overcome this degeneracies in order to use BDT as a more general framework to study modified gravity at cosmological scales.

As ξ fits only the heights o the temperature CMB spectrum and its damping tail, the small scale CMB from SPT is sensitive to the second effect, however the first one is produced also by other cosmological parameters, thus ξ introduces a great extent of degeneracy affecting the reliability of estimations of $\Omega_m h^2$, θ and n_s. In despite of this issue, we can see in figure (4.11), in this uBDT case, setting the default analytic marginalization in CosmoMC is risky. The resulting posteriors differ importantly depending on how the bias is handled, particularly in the case of the degenerated parameters the posteriors depend even more on the method of marginalization. Finally, the inclusion of SPT, does not help too much, on the contrary, estimations of θ, $\Omega_{DM} h^2$ and n_s are incompatible with ΛCDM and constraints on ω get weaker.

The following table shows the extent in which constraints for ω using WMAP7+SDSS within uBDT rely on the way of handling the bias

case	$\omega >$ at 95%
1: k-dependent marbias	156
2: k-indpendent marbias	471
3: k-independent numbias	696

In summary, in order to constrain uBDT one has to deal with important degeneracies of various parameters and it is recommendable to assume a linear bias as a primary parameter which should be marginalized out only after having sampled the space of parameters.

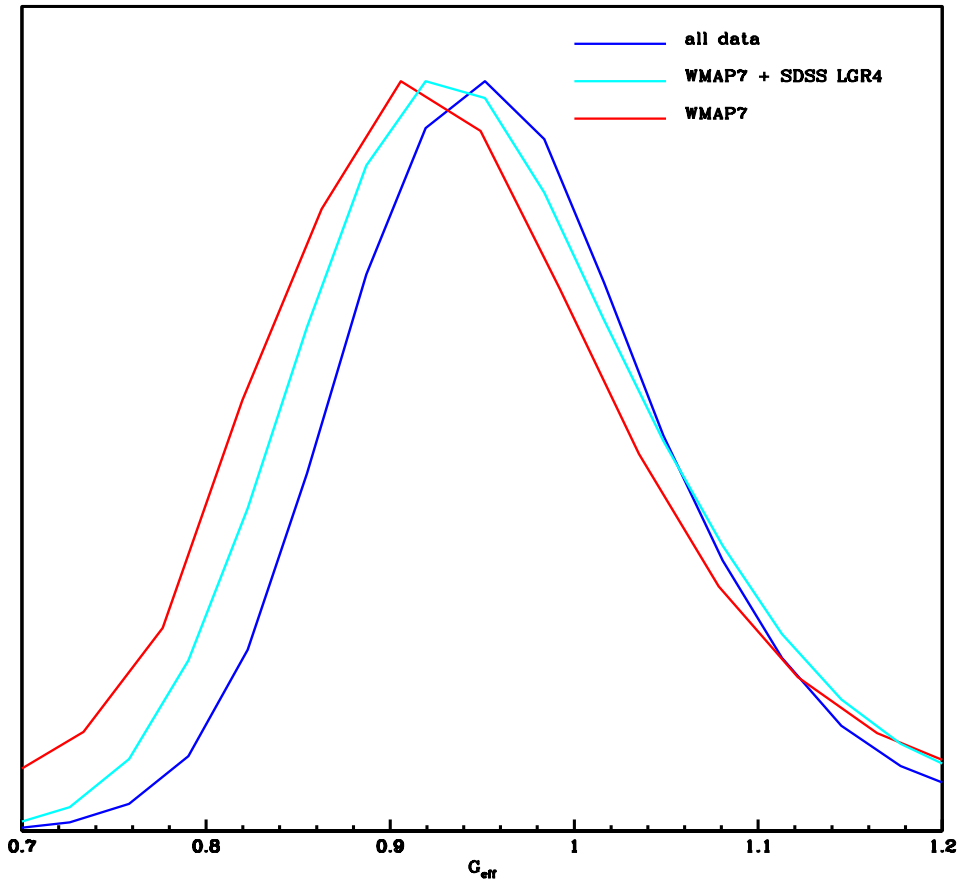

Fig. 4.10 Constraints on ξ with WMAP7+SDSS-R4. WMAP7 alone prefers lower values of G_N while SDSS pushes its value closer to $\xi = 1$. "*All data*" means WMAP7+SDSS+SPT

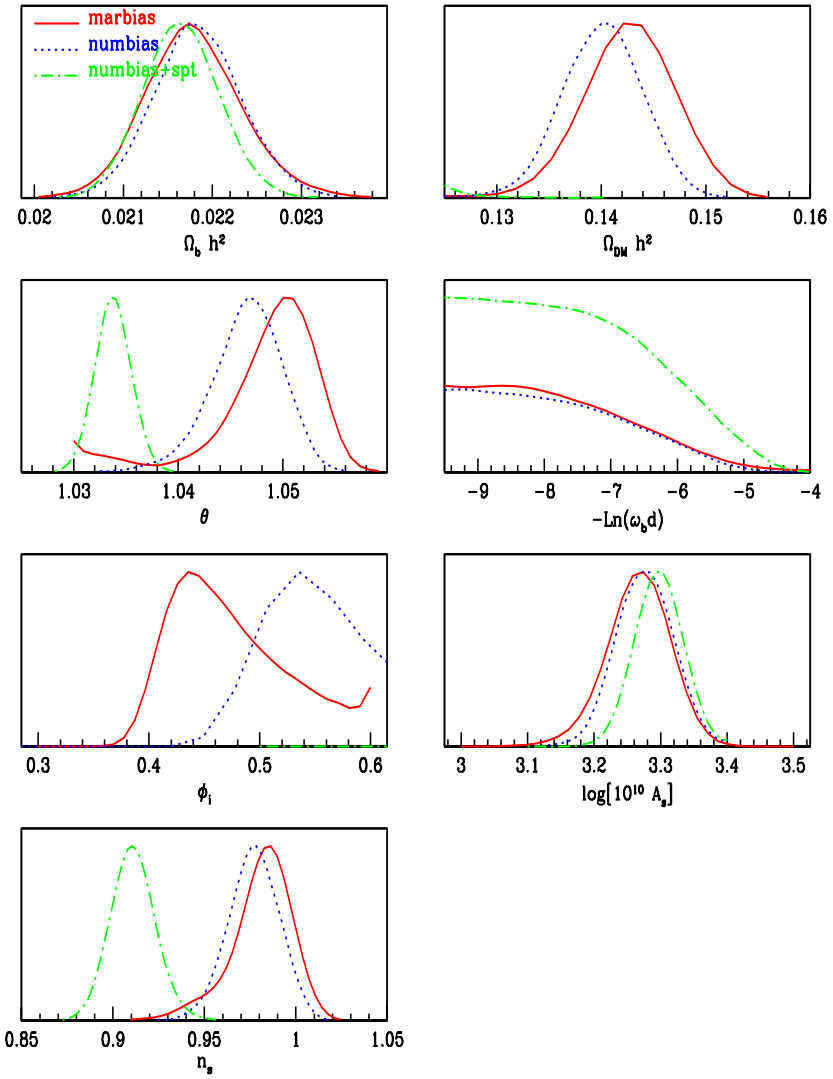

Fig. 4.11 Marginal posterior distributions for cosmological parameters within the uBDT for three different cases: Red: WMAP7 + SDSS data. The bias is used to fit $P(k)$ and it is marginalized numerically(numbias). Green: WMAP7+SDSS+SPT data used. The bias is introduced as primary parameter and marginalized over numerically. Blue: WMAP7 + SDSS data, the bias is marginalized over analytically (denoted marbias).

4.3.3 Constraints from WMAP7 and The Alcock-Paszynski Test

4.3.3.a How Does the Alcock-Paczynski Test Work?

The expansion rate as a function of time has proven very difficult to measure directly. However, recently it has been proposed in [68] a new way to determine the cosmic expansion history in a model independent, non-parametric way by combining distant supernovae observations with a geometrical analysis of large-scale galaxy clustering within the WiggleZ Dark Energy Survey, using the Alcock-Paczynski test (APT) to measure the distortion of standard spheres.

In the standard cosmological analyses, involving datasets such as distant supernovae [76, 124, 247, 257], galaxy surveys [245] and the Cosmic Microwave Background radiation [175], the expansion rate of the Universe at different look-back times is not measured directly, but rather, by fitting the noisy observed luminosity distances using a parametric frameworks and making prior assumptions about the components of the Universe and their evolution with redshift. However, the unknown physical nature of dark energy implies that we cannot yet be certain that any particular parametric model is correct.

The Alcock-Paczynski effect arises as a consequence of the peculiar velocities of galaxies. Spherical objects i.e. those possessing equal co-moving tangential and radial sizes L_0, appear distorted in the redshift space [9]. The observed tangential dimension is the angular projection given by

$$\Delta\theta = \frac{L_0}{(z+1)D_A(z)} \tag{4.18}$$

The observed radial dimension is given by the redshift projection

$$\delta z = L_0 H(z) \tag{4.19}$$

It is no need to know L_0 in order to make the measurement since the observable is given by

$$F(z) \equiv \frac{\Delta z}{\Delta\theta} = (1+z)D_A(z)H(z)/c \tag{4.20}$$

this measurement is independent of any assumption about spatial curvature. It is usually called the Alcock-Paczynski parameter or distortion (APD). Measurements of APD can be applied to cosmological "objects" and to any isotropic process such as the 2-point statistics of galaxy clustering [24, 203].

Actually, general analysis of the tangential/radial galaxy clustering pattern in the presence of baryon acoustic oscillations demonstrates how the information may be

divided into an overall scale distortion, quantified by a distance parameter $(D_A/H)1/3$, and a warping, quantified by the Alcock-Paczynski distortion factor $D_A H$, enabling the disentangling of D_A and H [234, 299]. Such approaches are just becoming possible with the current generation of large-scale galaxy surveys, [117].

In this work we use the technique proposed in [68] to determine the expansion rate $H(z)$ using the Alcock-Paczynski effect, it consists of two steps: First they apply an Alcock-Paczynski measurement [9] to the large-scale clustering of galaxies in the WiggleZ Dark Energy Survey [236], by measuring the distortion parameter $F(z)$ defined above. Second they combine this measurement with the supernovae luminosity distances $D_L(z)H_0/c$, using the equivalence of distance measurements $D_L(z) = D_A(z)(1+z)^2$, to infer the value of $H(z)/H_0$.

The result is an accurate non-parametric reconstruction of the cosmic expansion history. They report individual measurements of $H(z)/H_0$ in four redshift bins within the redshift range $0.1 < z < 0.9$.

Here we use the measurements of $H(z)$ derived in [68] to get complementary constraints of the cosmic expansion history in BDT. Standard measurements of $H(z)$ from HST used in the standard CosmoMC in order to test the expansion rate of the fitting model are also implemented in our code, however, we use more recent observations of SN obtained by the SHOES team [258]. Nevertheless, I would like to mention that, strictly speaking, using such dataset is not valid for modified gravity since it has been derived in a model-dependent manner.

4.3.3.b Behavior of the Alcock-Paczynski Parameter in BDT

In this work, besides of fitting the $H(z)$ measured by [68], we also do fit the direct measurement of APD above at 4 redshifts bins: $\{z_1 \in (0.1,0.3),\ z_2 \in (0.3,0.5),\ z_3 \in (0.5,0.7),\ z_4 \in (0.7,0.9)\}$.

In particular the APD in BDT is not sensitive to a constant ω with values lying inside the 95% limits, we can foresee a very slight enhancement of the WMAP7 constraints by adding the APT from WiggleZ, since the highest redshift at that survey is less around 1. This is verified after sampling explicitly the space of parameters since the WMAP7 constraints of ω are not affected by fitting APD. However, we think is worth to have a look to the explicit values of the APT parameter since future high redshift surveys are expected to yield up to $z = 2$.

Interestingly, in the case studied in chapter 5 where $\omega = -3/2 + ma^n$ is not a constant, the APD is sensitive to the exponent n, specially when ω is globally small for appropriate values m. As we will see in the next chapter, $m \sim 50$ is actually very likely, so the APT is a great test to be applied in that case. Unfortunately, in this work we didn't have time to get that far, but the problem stands in our list as a future project.

4.3.3.c Results

The resulting posterior distributions within rBDT and uBDT have different features.

1. In rBDT the inclusion of either HST and APT doesn't improve significantly the thickness of the error bars, different measurements of the expansion rate lead to shifted mean values for the estimates. However we can notice that the estimate for $\Omega_m h^2$ is the same in both cases. On the other hand, the shape of the 1D posterior for ω is clearly different in both cases. Althought with HST, there is shift of the tail to the good likelihood region the bump compensates the apparent improvement.

2. In the case of uBDT, the 1D posteriors of the matter densities take almost the same values either with HST and APT, however the estimate for $\Omega_{DM} h^2$ is better for HST since the 1D is narrower than for APT. In a similar way, a much better measurement of θ is obtained with HST. In rBDT case the bump in the posterior of ω disappears when HST is included and the resulting 95% percent constraint for APT is slightly better than in the rBDT case.

3. $\xi \sim 1$ within a small error according to HST, however lets remember that in order to reconstruct HST, the standard model is granted to be the correct model describing measurements of distances. Thus, in despite that the APT measurement of ξ is not as good, it raised from a model independent measurement of the expansion rate.

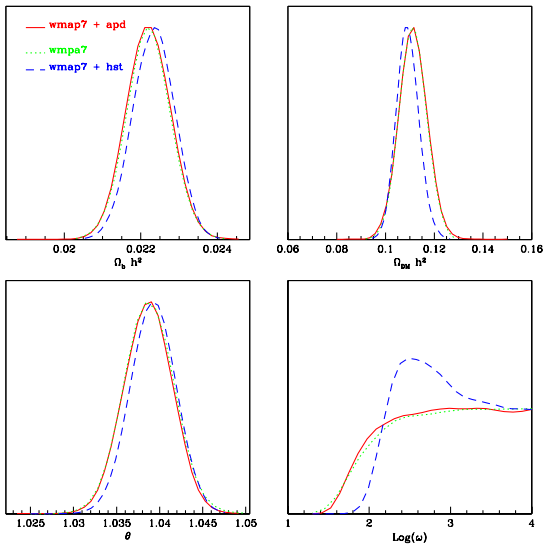

Restricted Model			
param	mean	lower(95%)	upper(95%)
$\Omega_b h^2$	0.221996E-01	0.211224E-01	0.233037E-01
$\Omega_{DM} h^2$	0.111439E+00	0.102393E+00	0.120512E+00
θ	0.103866E+01	0.103331E+01	0.104401E+01
ω	—	112.8	—
$log[10^{10} A_s]$	0.319090E+01	0.311135E+01	0.326779E+01
n_s	0.965779E+00	0.938040E+00	0.994952E+00

Up: 1D posteriors for rBDT with WMAP7 and complementary tests of the expansion history from HST and APT respectively. Down: Cosmological parameters for the restricted model according to WMAP7 + APT.

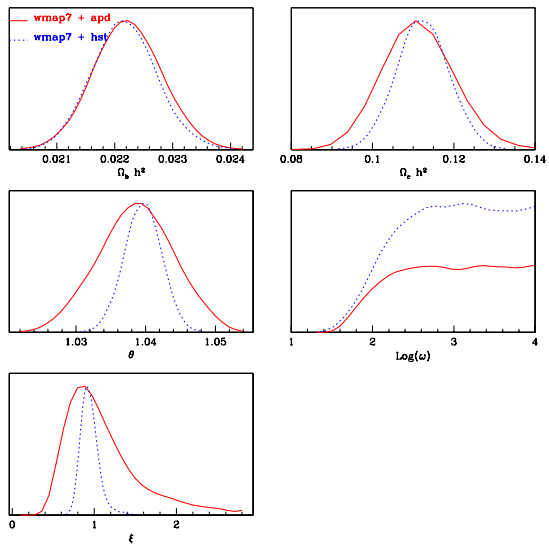

Unrestricted Model			
param	mean	lower(95%)	upper(95%)
$\Omega_b h^2$	0.222297E-01	0.210934E-01	0.233963E-01
$\Omega_c h^2$	0.111243E+00	0.987990E-01	0.124600E+00
θ	0.103864E+01	0.102806E+01	0.104893E+01
ω	—	126.1	—-
ξ	0.903016074	0.48189	0.171774E+01
$log[10^{10}A_s]$	0.318675E+01	0.310841E+01	0.326421E+01
n_s	0.966448E+00	0.936992E+00	0.995975E+00

Up: 1D posteriors for uBDT with WMAP7 and complementary tests of the expansion history from HST and APT respectively. Down: Cosmological parameters for the unrestricted model according to WMAP7 + APT.

4.4 Forecasts on BDT from Redshift Space Distortions

4.4.1 Theoretical models and upper bound of the detectability

On large scales, the observed large-scale structure is basically described by a small perturbation to the homogeneous universe. Ignoring the higher-order contributions, the two-dimensional power spectrum in redshift space, $\tilde{P}(k,\mu,z)$, given as function of the wavenumber k and the directional cosine μ between line-of-sight direction and the wavenumber $\vec{k}$ of the perturbation, is only characterized by the Kaiser equation already described in chapter 3. In reality, the observed redshift-space power spectrum suffers significantly from nonlinear corrections even at large scales. One important effect is the gravitational evolution along the expansion. Furthermore, the random motion of galaxies is known to cause a non-linear redshift distortion which is the so called Finger-of-God (FoG) effect. An approximate prescription to describe these nonlinear effects was proposed by Scoccimarro [271], and it is expressed as

$$\tilde{P}(k,\mu) = \left[P^{\rm lin}_{\delta\delta}(k) + 2\mu^2 P^{\rm lin}_{\delta\Theta}(k) + \mu^4 P^{\rm lin}_{\Theta\Theta}(k)\right] G(k,\mu,\sigma_p). \tag{4.21}$$

where $\sigma_{\rm p}$ is the one-dimensional velocity dispersion. Nonlinear corrections due to the random motion is described by the FoG effect encoded in the G distribution.

Beyond a simple model prescription, one crucial aspect of the redshift distortions may be that the linear squeezing and nonlinear smearing effects on distorted maps are not separately treated. Taking into account this fact, Taruya, Nishimichi & Saito proposed an improved model of the redshift-space power spectrum, in which the coupling between the density and velocity fields associated with the Kaiser and the FoG effects is perturbatively incorporated into the power spectrum expression [298]. The resulting expression is similar to equation (4.21), but includes nonlinear corrections consisting of higher-order polynomials. In addition, we need to properly take into account the effect of nonlinear gravitational evolution for the self and cross-power spectra $P_{XY}(k)$. Since the standard perturbation theory is known to produce ill-behaved expansion leading to the bad UV behavior, a consistent calculation of the correlation function should be carried out using the improved perturbation theory with an appropriate UV regularization.

At scales in which the first order term of FoG dominates, the assumption of FoG effect is valid through fitting σ_p with datasets. However, beyond this quasi-linear cut-off, our statistical model breaks down. The measurement of $P^{\rm lin}_{\Theta\Theta}$ is limited by the uncertainty of FoG effect at higher orders. In figure (4.12), we show the detectability of the linear spectra at $z = 0.35$, 1, 2 and 3 from the top to bottom

panels. Using the simulated maps at $z = 0.35$, we find this upper bound of wavelengths $k_{\max} = 0.11\,h\,\mathrm{Mpc}^{-1}$ in which our assumption is valid . Additionally, we test the detectability against higher redshift data at $z = 1$, 2 and 3. As expected, the upper bounds of corresponding to these redshifts are larger than the one of low redshift $z = 0.35$, since the damping scale of FoG effect becomes milder at higher redshift. We found that the linear velocity spectra $P^{\mathrm{lin}}_{\Theta\Theta}$ are precisely measured up to $k_{\max} = 0.12$, 0.14 and $0.18\,h\,\mathrm{Mpc}^{-1}$ at $z = 1$, 2 and 3, respectively.

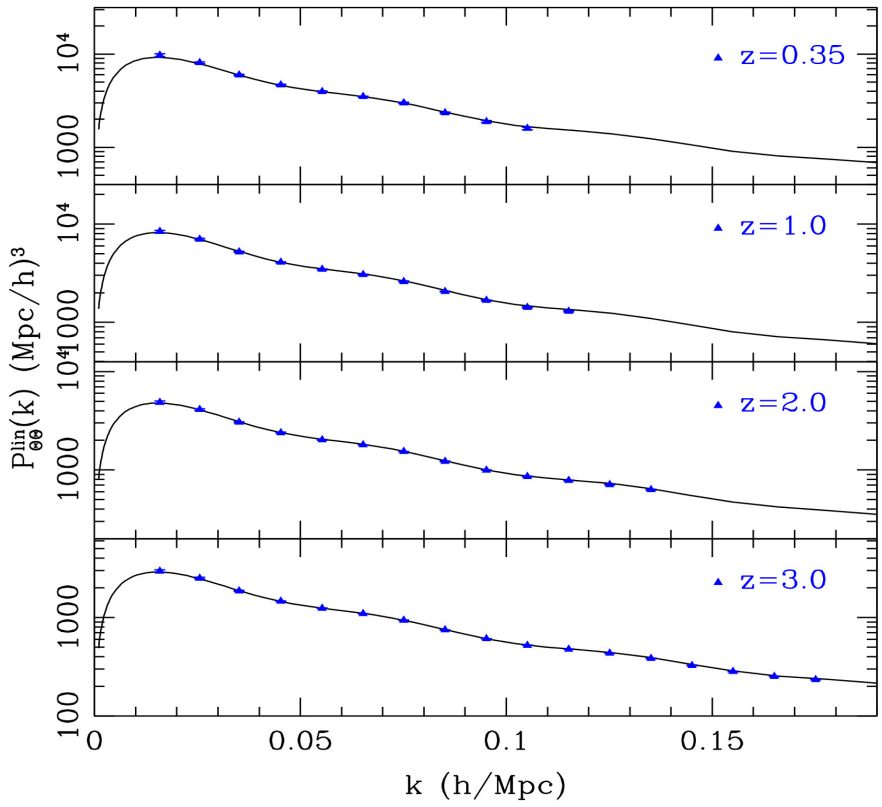

Fig. 4.12 Decomposed spectra of peculiar velocities $P_{\theta\theta}(k)$ are presented for different redshifts. The linear spectra are measured in precision up to $k_{max} = 0.11hMpc^{-1}, 0.12hMpc^{-1}, 0.14hMpc^{-1}$ and $0.18hMpc^{-1}$ at $z = 0.35, 1, 2$ and 3 respectively

4.4.2 Alcock-Paczynski Effect from RSD

The following two subsections are product of the joint research work with Costas Skordis and Yong-Seon Song not published yet. As we already mentioned, the transverse and radial distance components of an assumed isotropic distribution are given by D_A and H^{-1}. Each galaxy is located using angular coordinates and redshift in galaxy redshift surveys. Because the clustering function is measured in comoving distances, the fiducial cosmology should be applied to generate maps in comoving space. The transformation depends on the transverse and radial distances. Instead of recreating maps in comoving space, we obtain the approximate fiducial maps by rescaling the transverse and radial distances. This Alcock–Paczynski effect at the level of the maps can be described by the relation between $(D_A^{\rm fid}, H^{-1\,\rm fid})$ and $(D_A^{\rm true}, H^{-1\,\rm true})$, where 'fid' and 'true' denote the fiducial and fitted distances with BDT, respectively. The observed spectra are transformed by variation of distance measures through correspondent coordinate components in Fourier space. With the plane wave approximation, k and μ are given by $k_\perp$ and $k_\parallel$ as,

$$k = \sqrt{k_\perp^2 + k_\parallel^2} \tag{4.22}$$

$$\mu = k_\parallel / k. \tag{4.23}$$

Given the observational quantities, such as $k_\perp D_A$ (i.e., an angular scale) and $k_\parallel H^{-1}$ (i.e., a scale along redshift), different distance measures (D_A and H^{-1}) result in a feature of power spectra in different wavenumbers $k_\perp$ and $k_\parallel$. When we have prior information on the location of a feature in $k_\perp$ and $k_\parallel$, then we can determine D_A and H^{-1}. Additionally, the volume effect is added as,

$$\tilde{P}(k_{\rm ref}, \mu_{\rm ref}; z)/V_{\rm ref} = \tilde{P}(k, \mu; z)/V \tag{4.24}$$

where V is a volume factor given by $V = D_A^2 H^{-1}$. If we define projected spectra $\mathscr{P}$ as,

$$\mathscr{P}(k, \mu, z) \equiv \tilde{P}(k, \mu, z)\,[V_{\rm ref}(z)/V(z)]\,, \tag{4.25}$$

then the logarithmic derivatives of $\mathscr{P}$ in terms of D_A and H^{-1} are given by,

$$\frac{d\ln \mathscr{P}(k,\mu)}{d\ln D_A} = \frac{d\ln \tilde{P}(k,\mu)}{d\ln D_A} - 2, \tag{4.26}$$

$$\frac{d\ln \mathscr{P}(k,\mu)}{d\ln H^{-1}} = \frac{d\ln \tilde{P}(k,\mu)}{d\ln H^{-1}} - 1. \tag{4.27}$$

We invite the reader to review the analysis that we did along chapter 3. On one hand, the behavior of the galaxy power spectrum in redshift space for various values of the redshift and the angle μ in BDT. On the other hand, the study on how the measurements of distance behave within BDT, specially those given by $H(z)$ and D_A which characterize the longitudinal and transversal directions of the spectrum.

4.4.3 Forecasting Constraints From Future RSD Surveys

The specific application of the material described above in this work was to derive conservative errors for the BDT parameters using the Fisher matrix method that we describe right below. We use a Fisher-matrix calculation to investigate whether the effects of BDT to determine in which extent forthcoming CMB and $\tilde{P}(k,\mu,z)$ maps might be able to distinguish Brans-Dicke and general-relativistic cosmology.

The Fisher matrix arisen from redshift distortions would be fully determined by the following expression,

$$\begin{aligned} F_{\alpha\beta} &= \int \frac{d^3k}{2(2\pi)^3} \frac{\partial \tilde{P}(k,\mu)}{\partial p_\alpha} \frac{f_{sky}V_0}{[\tilde{P}(k,\mu)+1/\bar{n}_{\rm gal}]^2} \frac{\partial \tilde{P}(k,\mu)}{\partial p_\beta} \\ &\sim \sum_{k_i=0}^{k_{\rm max}} \bar{k_i}^2 \frac{\Delta\bar{k}_i}{(2\pi)^2} \sum_{\bar{\mu}_j=0}^{1} \Delta\bar{\mu}_j \frac{\partial \tilde{P}}{\partial p_\alpha} \frac{f_{sky}V_0}{[\tilde{P}+\bar{n}_{\rm gal}^{-1}]^2} \frac{\partial \tilde{P}}{\partial p_\beta} \end{aligned} \tag{4.28}$$

where $\tilde{P}_{gg}(k)$ is the spectrum of galaxy described above. We assumed that the galaxy bias $b(z)$ is scale–independent. Here, it is set to be $b(z)=1$. We use the Fisher matrix with discrete bins of equation 4.28. The μ bins are divided into 100 bins. The k bin runs from $k_{\rm min}=0.001\,h\,{\rm Mpc}^{-1}$ to $k=k_{\rm max}(z)$ and the redshift from $z_{\rm min}=0$ to $z_{\rm max}=2$. The maximum k space is given by simulated work described in figure (4.12).

4.4.3.a Results

Our starting point, is to derive a primary constraint of ω using the latest measurements of the temperature anisotropy of te CMB. Upon this base, we derive a forecasts for the constraints of ω using the corresponding f_{sky} and bounds of the Fisher matrix and covariances of EUCLID . This test would allow us to restrict further the range of validity of the BDT in agreement to this survey. To accomplish our first step, we used the Fisher matrix method described above, we estimate the error at 1σ using measurements of the unlensed angular spectrum of the temperature anisotropy of the CMB taken by the Planck satellite. The set of cosmological parameters which we marginalized over is, $(n_s, \omega_m, \omega_b, z_{reion}, \theta, A_0, b)$, where b denotes the constant bias. The resulting error for $\frac{1}{\omega}$ is

$$\sigma(\frac{1}{\omega}) = 1.17 \times 10^{-3} = |\frac{1}{\omega_{fid}} - \frac{1}{\omega_{lower}}| \tag{4.29}$$

where $\omega_{fid} = 10^6$, σ is the resulting 1σ error for $1/\omega$ which corresponds to $\omega_{lower} > 588$. According to the latest forecasts for ω [64], Planck would lead to a limit of $\omega \sim 1000$ which is consistent with our result. On the other hand, the resulting limits for ξ according to this dataset is

$$\sigma(\xi) = 2.2 \times 10^{-3} \tag{4.30}$$

where $\xi_{fid} = 1$ thus leading to $\xi = 1 \pm 0.0022$. The second step is to put both sets of data together and apply the same method than above to get the forecasted limit for BDT resulting to be a stringent constraint

$$\sigma(\frac{1}{\omega}) = 6.0 \times 10^{-5} \tag{4.31}$$

$$\sigma(\xi) = 1.8 \times 10^{-3} \tag{4.32}$$

where $\xi_{fid} = 1$ thus leading to $\xi = 1 \pm 0.0018$. As above, the same ω_{fid} has been used, this error corresponds to the lower limit $\omega_{lower} = 1.7 \times 10^4$ which is fairly large. Furthermore, we found out that this limit can be further improved if we make the following changes in our setup: 1. increase cut-off as $k_{\max} = 0.2$, 2. increase the redshift range to $z_{\min} = 0$ and $z_{\max} = 3$ and 3. refine the redshift bins to $dz = 0.2$. This set up leads to a very tight constraint of $\omega_{lower} \sim 10^5$. However, figure (4.13) can help us to understand why such a strong constrain is obtain from this dataset. On one hand, the line corresponds to the variation of the expansion rate as function of the redshift $H(z)$ with respect to ω evaluated at the fiducial model. On the other hand, the bars correspond to the estimated error of $H(z)$ derived from the measurement of radial component of $\tilde{P}(k, z, mu)$ which has been affected by the Alcock-Paszynski effect.

As we see, the variation of the expansion rate is comparable to the sensitivity of the error bars derived from the measurement of radial component which is sub-percentage level. So ω has such a huge boost in order to fit such small variation. As long as a better detection of $H(z)$ is achieved at some future survey, we can not expect a realistic constraint for ω.

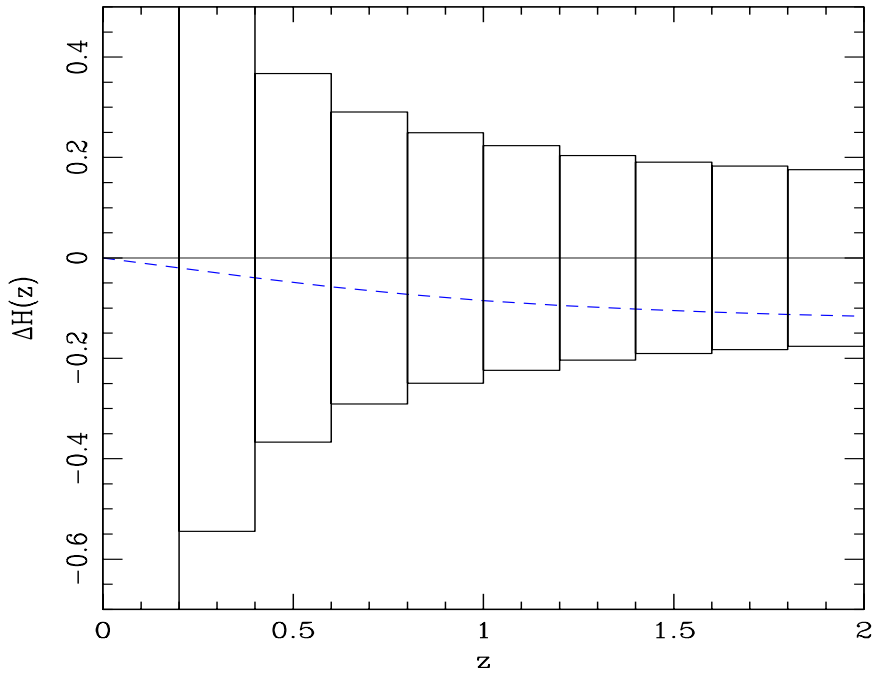

Fig. 4.13 The line corresponds to the derivative of the expansion rate with respect to the reciprocal of ω, $dH/d(1/\omega)$ as function of redshift. The bars correspond to the total error estimation of the $H(z)$ at each redshift bin derived from the measurement of radial component of the matter power spectrum in redshift space.

In summary, by simply using the baseline CMB dataset from Planck and applying the Fisher's matrix technique, we obtain the lower bound for uBDT, $\omega > 588$ and $\xi = 1 \pm 0.0022$. The result for ω is in agreement with recent forecasts from [64] and the constraint for ξ is compatible with our MCMC constraints up to 1σ, using the same data set. Furthermore, in addition to the baseline, our analysis incorporates the estimated covariance matrices of measurements of RSD of matter power spectra in redshift space, from Euclid. We consider measurements on scales within bounds of detectability where the FoG effect does not introduce significant uncertainty. We derive a forecast for this dataset given by $\omega_{lower} = 1.7 \times 10^4$ and $\xi = 1 \pm 0.0018$. We found out that, if the cutoff of detectability is increased, a tight constraint $\omega_{lower} \sim 10^5$ might be accomplished. However, this possible reduction of non-linear effects at

small-scales is just unobserved at this point. On the other hand, even with a small cutoff, the reconstruction of $H(z)$ from RSD measured by Euclid is expected to have narrow error bars so BDT is expected to be sufficiently constrained to reach such predictions as figure (4.13) shows.

4.5 Summary and Conclusions of this Chapter

Let us to start summarizing our results from the MCMC analysis using CMB data. Because this work was started before Planck data was available, we started our analysis using WMAP7 data. Before the first Planck data had been launched, we improved the existing constraints of $\omega > 120$ at 95% of C.L. using WMAP7 + SDSS-R4 derived by Acquaviva in [2] to $\omega > 269$ at the same C.L. using WMAP7+SPT within the uBDT. Constraints for the rBDT are not fully reliable because of the peak appearing in the 1D distribution of ω. Though we have probed the results might be correct due to the tension between the measurements of θ_{rec} from SPT and WMAP we prefer to report the constraint arisen in uBDT also because in this context BDT can be thought as a large-scales limit of more general theories with self-interactions. Constraints for the Newton constant today with the same data set are $1.10^{+0.13}_{-0.14}$ at 95% of confidence level.

Now, using measurements of the temperature anisotropies of CMB from Planck, we found strong constraints on the BDT parameter. Our better results are with Planck+WMAP9(pol) $\omega > 1834$ at 95% of C.L. and with Planck+PlanckLens $\omega > 2441$ at 95% of C.L. both within the uBDT. Interestingly, contrary to our expectations, results within rBDT are weaker than within uBDT even when the parameters space of the latter is larger. What happens is that the ξ parameter helps to fit better the CMB, for example in the case with Planck+WMAP9(pol) $-\log(\mathscr{L}) = 4905.94$ for uBDT whilst $-\log(\mathscr{L}) = 4991.32$ for rBDT (where remember $\mathscr{L}$ is the likelihood). Planck+PlanckLens gives the best result for ω however in the case of ξ the best constraints are obtained for Planck+WMAP9(pol) $\xi = 1.12^{+0.11}_{-0.11}$ at the 95% confidence level , significantly improving on previous work. In order to set stronger limits on ξ, we also fitted primordial BBN abundances of Helium-4 and Deuterium using the uBDT models. Our best constraint using Planck + WMAP9(pol) + ACT + SPT + BBN is given by 1.009 ± 0.014, notice that the error bar for ξ improves in one order of magnitude and the mean value of ξ is pushed from larger values to 1.

Let us recall that the BDT is usually used as a consistent implementation of GR with a time-varying effective gravitational strength G_{eff}, in this context, limits on $\dot{G}_{eff}$ can be imposed according to a given dataset. We determined such limits for various

sets, the worst value given by $2.45 \times 10^{-13}\ years^{-1}$ accordingly with WMAP alone and the best improved almost one order of magnitude $3.6 \times 10^{-14}\ years^{-1}$ according to PlanckTemp + PlanckLens + HL.

Now we turn to summarize our results from the MCMC analysis with CMB+LSS. When one is aiming to constrain BDT using LSS one needs be careful when handling the bias parameter. Since the standard assumption of CosmoMC that the bias is an uncorrelated parameter does not hold for uBDT due to its correlation with ξ. In turn within the rBDT models the analytic marginalization formula of in the algorithm to compute the likelihood is justified as $G_{eff} \sim 1$. We also changed the standard assumption of a scale-dependent bias by a constant one more suitable for a coherent theory like BDT. To probe explicitly this statements, we implemented the different possibilities to handle the bias into our code to run the chains and compare the results. As expected, constraints on ω within uBDT using LSS are dependent on the different assumptions about the bias, in contrast, for rBDT the results are independent. Thus we conclude that when one aims to constraint BDT using $P(k)$ data is recommendable to use rBDT rather that uBDT. The resulting constraint for ω within rBDT using $P(k)$ measurements at redshift $z = 0$ from SDSS-R4 is $\omega > 592.4$ at 95% of confidence level. The result from WMAP7 has been importantly improved along with the constraints for the cosmological parameters. All these results together are consistent with ΛCDM up to 1σ.

From the part of this chapter at which we compare tests of the rate of expansion from Alcock-Pazcynski distortion and H_0 reconstructions we can conclude that, even though our goal goes in a different direction than trying to explore the nature of dark energy, we are concerned about which tests of this type are suitable as a complementary source to set limits on our models. We found out that measurement of H_0 from SHOES has significant power to constraint the BDT and cosmological parameters rather than APT at the given redshifts. This is not a surprise, in chapter 3 we found out that ω barely tickles the APD at low redshifts. Anyway we expected the APD reconstruction from WiggleZ RSD to have a better resolution to feel ω, however we were wrong. On the other hand, we should keep this choice in mind in the near future since more precise measurements of the APD and at higher redshift are about coming.

Finally, in relation to our CMB + RSD forecasts for the BDT parameters, by using the Fisher-matrix estimator, we derive forecasts of the minimum lower bounds of ω according to expected covariance matrices of forthcoming observations of the CMB from Planck and of the power spectra in redshift space by Euclid. The procedure consisted in using the CMB to derive a baseline constraint for the BDT parameters which was subsequently tightened by including the estimates of the covariance matrix

of $\tilde{P}(k,\mu,z)$ from Euclid. The resulting constraint for both datasets resulted to be very strong, even being close to the order of the limits from solar system, $\omega_{lower} = 1.7 \times 10^4$. By increasing the cutoff and the number of redshift bins leads to a even tighter constraint $\omega \sim 10^5$. Nonetheless, we figured out that this happens because the variation of the expansion rate and the sensitivity of the error bars derived from the measurement of radial component are sub-percentage level. So ω has such a huge boost in order to fit such small variation. In conclusion, measurements of RSD with the resolution of Euclid would be more than powerful enough to constrain the BDT ω parameter. In conclusion, the expected values ω should be greater than $\sim 10^4 - 10^5$ in order to be in agreement with Euclid according to our forecasts.

CHAPTER 5

THE EFFECTIVE SCALAR-TENSOR THEORY AT COSMOLOGICAL SCALES

5.1 Introduction

In the previous chapter we have studied the simplest modified theory of gravity, the Brans-Dicke theory. The BDT can be directly generalized to the Bergmann-Wagoner scalar-tensor theories [35] by upgrading the single parameter ω to a function $\omega(\phi)$ and considering a more general potential $V(\phi)$ than the cosmological constant playing the role of dynamic dark energy driving the expansion of the universe. Along this chapter we are going carry out almost the same analysis as we did for BDT above along the previous two chapters for a special case of the scalar-tensor set of models. This subset arises in an effective model from a phenomenological setup for generalized modified theories of gravity at linear cosmological scales as we describe in what follows. From now on we are calling this class of models the *effective scalar-tensor theories*.

The $\omega(\phi(a))$ function associated to the effective scalar-tensor theory is given by a power law of the scale factor. As we explain below, the phenomenological setup considered here was originally motivated as a framework to constrain modifications to the growth of the large scale structure. Since within this framework the origins of the expansion of the universe are not being investigated, we consider that the standard cosmological constant plays the role of dark energy in order to keep things simple.

Originally the motivation of the phenomenological setup of a model arises from quite popular parametrization of the growth of subhorizon linear perturbations in GR [10, 178]. The particular setup used here was the implementation of the former to make it suitable for modified gravity, it was first proposed in [288]. The basic idea behind the general framework is to parametrize the equations describing the dynamics of sub-horizon perturbations in the Newtonian-Conformal gauge in the quasi-static limit. The main purpose of doing this was to take into account possible modifications

to the growth of matter perturbations for bounded systems at very large scales. In other words, the lack of knowledge about the growth of structure in the universe at every scale and redshift is parametrized at the level of equations for the perturbations that affect the dynamics of this process. As shown in [10, 178, 288], such parameterizing functions are related to specific observables and if we were able to measure them (e.g. the growth) at every scale and redshift, we could determine the specific theoretical model to describe the exact growth of the LSS inhomogeneities. However, given the available surveys, this task is difficult if not impossible so far [288]. A shortcut would be to reduce the space of models by taking a wide set of parametric models based in a particular modified theory and swap the initial undetermined functions by specific functions with undetermined parameters to be constrained. In this way the particular setup used here arises.

More specifically, the particular model resulting from such setting is actually the effective scalar-tensor theory studied here (gBDT). Originally, the main goal was to establish an approximative way to constrain the growth of LSS of any general modified model of gravity with an extra scalar degree of freedom regardless of the expansion history. In order to fill the gap between the most general scalar-tensor theory and the modest gBDT they make two basic assumptions: first, the self-interactions are negligible except a linear mass term which is tightly constrained and second, that matter couples minimally to the metric. This are reasonable assumptions as long as one lies on cosmological linear scales. Self-interactions only play the role of screening the scalar at small scales and they may still have considerable effect at large scales (LSS formation like clusters of galaxies) but only due to non-linear effects.

Another important input in the original phenomenological setup is that the growth is assumed to behave as a power law of the scale factor. This assertion is motivated observationally and theoretically. On one hand, it is expected that the predictions of our model lie close to those of the standard model (which are well constrained by observations), thus since the growth in the standard model behaves as a very specific power law given by $\Omega_m^{0.6}$ [97, 238] it is reasonable to consider a more general form of a yet power law for gBDT. On the other hand, such functional form of the growth ensures that perturbations in this model to be coherent as in the standard model which is consistent with ignoring the non-linearities since they are the source of possible incoherent growth of LSS.

An important resulting feature of this setup is that any specific form of the growth corresponds to a specific function $\omega(\phi(a))$ which uniquely defines the effective gBDT. Therefore, we can establish a correspondence between the growth and the parameters of gBDT: to derive constraints of the growth within the framework gives rise to constraints of the parameters of gBDT. However, the line-of-thought in this work goes

actually in the opposite direction: we start from a gBDT defined by an ω behaving as an undetermined power law and our goal is to constrain its parameters by means of diverse cosmological observations and these parameters would give us an estimate for possible modifications of the growth. We aim to set bound for the growth indirectly by means of the effective gBDT.

In this chapter we study the cosmological theoretical implications of gBDT beyond the original motivation. Specifically, we are going to follow the same structure that we did for BDT , however we make our analysis with less detail. As in the previous chapter we'll review the whole cosmology of gBDT , however we try to focus on the differences with BDT in order to draw up the new features arisen in this generalization. As we did before, apart of solving this academic problem, our goal is to figure out observational signatures which lead us to test the theory with sensible data.

In the next section we will constrain gBDT using a variety of data, we sample the space of parameters by the well-known Monte-Carlo-Markov-Chains (MCMC) method in order to compute the likelihood function and the posterior distribution for our theories, after that we would be able to study the viability of these specific models at the light of the current observations.

5.2 A Phenomenological Setup for Modified Gravity

As we already explained previously in order to explain the formation of structure (or the evolution of inhomogeneities) at sufficiently small scales it suffices to study the dynamics of sub-horizon perturbations in the quasi-static limit. In that limit, the dynamics of perturbations can be fully described by the standard Newtonian prescription. A quite popular way to take into account possible modifications to the growth of subhorizon perturbations is achieved by parameterizing the standard Newtonian equations introducing undetermined functions η and Q as follows [1]

$$\begin{aligned} k^2\Phi &= 4\pi G_N a^2 Q(a,k)\rho_m\Delta_m, \\ \Phi+\eta\Psi &= 0. \end{aligned} \tag{5.1}$$

A merit of this parametrization is that the undetermined functions are directly related to observable quantities and hence, ideally, they could be constrained straightforwardly if such quantities were measured for every scale and redshift. As a consequence, this framework stands as a powerful method to test the standard description of

[1] if no anisotropic stress at late times is assumed to exist.

the growth of structure. On one hand, measurements of the newtonian potential Φ (and then Q) can be obtained directly from galaxy distribution, however this is difficult due to the bias of galaxies. On the other hand, weak lensing and ISW effect are sensitive to $\frac{\Phi-\Psi}{2} \sim \frac{Q}{2}(1+\eta^{-1})$ which is an unbiased quantity. Additionally, peculiar velocities are proportional to $\Psi \sim \frac{Q}{\eta}$.

In principle, Q, Σ and η might be constrained in a model-independent way, however a quite large number of degrees of freedom are to be constrained by fitting a much small number of observational data. A way of overcoming such a drawback is to abandon (to some extent) the model-independent approach by using a still general class of parametric models. Regarding to physically viable theories in which a modification to GR is accomplished by an scalar degree of freedom, the Horndeski theory represents a large class of this kind. Strictly speaking, the goal would be to constrain the whole set of parameters of the Horndeski theory by testing the growth according to the parametrization shown above, however from the phenomenological point of view, this cumbersome task at cosmological scales happens to be unnecessary.

It is well known that, at the level of the background, there exists a degeneracy between ΛCDM and other models like DGP, Galileons, dark energy models , etc. since all of them predict considerably well the observed expansion of the universe. Thus we must go after a different set of phenomena in order to break down this degeneracy. As suggested in [288], observations of the dynamics of coherent sub-horizon linear perturbations still stand as a wealthy source available, not only to test GR, but furthermore to bring insights about the reliability of its modifications. In this work, as in [288] it is aimed to set a phenomenological framework to test a large class of modified theories of gravity which at very large scales behave like gBDT

In that particular case the equations describing the dynamics of sub-horizon perturbations reduce to

$$\begin{aligned} \Phi - \Psi &= \delta\phi \\ k^2\Phi &= 4\pi G_N a^2 \rho_m \delta_m + \frac{k^2}{2}\delta\phi, \\ (2\omega+3)k^2\delta\phi &= -8\pi G_N a^2 \rho_m \delta_m - \mathscr{I}(\delta\phi) \end{aligned} \tag{5.2}$$

where

$$\mathscr{I}(\delta\phi) = M^2\delta\phi + \int \frac{d^3k_1 d^3k_2}{(2\pi)^2}\delta(k-(k_1+k_2))M(k_1,k_2)\delta\phi(k_1)\delta\phi(k_2).$$

These interactions are important only at the non-linear regime at very small scales, however they are not relevant for linear cosmological perturbations. Though the linear M^2 term may be important, it has been strongly constrained [128]. It is imporant to point out that effectively G_N and ω can be functions of the scale factor. However, in the quasi-static limit the gBDT equations are the same as in BDT because the time derivatives [2] are neglected since the time scale of the formation of structure is adiabatically small related to H_0^{-1}.

From the previous equations we can obtain analytically η and Q

$$Q(k,a) = \frac{2+2\omega+M^2a^2/k^2}{3+2\omega+M^2a^2/k^2} \tag{5.3}$$

$$\eta(k,a) = \frac{2+2\omega+M^2a^2/k^2}{4+2\omega+M^2a^2/k^2} \tag{5.4}$$

$$\mu(k,a) = \frac{Q}{\eta} \tag{5.5}$$

$$\Sigma(k,a) = 1 \tag{5.6}$$

Though it sounds obvious, we want to state clear that the parameterizing functions reduce to 1 in the case of GR. For gBDT there are two ways to recover GR : $\omega >> 1$ or $\frac{M^2a^2}{k^2} >> 1$. From the previous equations we can notice that because $\Sigma = 1$ either the ISW effect and the lensing potential remain the same as in GR.

On one hand, it's a well know result in GR that $\mu_0 \sim \Omega_m^{0.55}$ [97, 238] . On the other hand we only expect slight deviations from the GR predictions within gBDT, thus is yet quite reasonable to assume that overdensities grow as in GR plus a small modification behaving as a power law of the scale factor as well

$$\mu = \mu_0(1+ra^s) \tag{5.7}$$

For the coherent case considered here we assume that $M^2 \sim 0$, anyway it is strongly constrained and its effects can be neglected. By plugging the power law ansatz for μ into (5.5) we obtain a specific for of ω given by

$$\omega(a) + \frac{3}{2} = \frac{1}{2r\mu_0 a^s} = ma^n \tag{5.8}$$

where $m = 1/2r\mu_0$ and $n = -s$. Thus, for every specific modification of the growth corresponds an unique scalar-tensor theory defined by (5.8)

[2] notice that the corrections to the BDT e.o.m. to give rise to the gBDT ones are proportional to the variation of ω.

As mentioned in the introduction, in contrast to the YS work, our goal in this work is to test the growth indirectly by constraining the effective scalar-tensor theory defined above using measurements of the anisotropies of the CMB. We start blindly from a scalar tensor theory whose ω is defined above. However we aim to explore the cosmological implications of this theory beyond the original conditions in which it was setup. Specifically we'll go beyond the quasi-static limit and study the perturbations of this theory for a full range of scales and hence take into account relativistic effects as well. Considering that in the following we'll be using such extrapolation some points should be considered

- For sub-horizon perturbations it turns out that $\Sigma = 1$, this means that the lensing potential and ISW are not modified. However this changes when considering super-horizon perturbations, as we'll see in the following chapter. When exact solutions are being considered ISW and the lensing potential are sensitive to the scalar at these scales.

- μ parametrizes the linear growth and can be interpreted alternatively as a classical "running" G_N constant at the level of the equations shown above. However, within the context of Horndeski-like theories the dynamics of the Newton constant is much more than that, and even in the simplest cases like BDT and gBDT such interpretation of the growth is not valid. Actually such dynamical G_N encodes much richer phenomenology further beyond the growth as we already saw in chapter 3 when we studied the simplest case. Furthermore, in more complicated frameworks such as the Horndeski-like theories screening mechanisms arise naturally and the GR predictions at small scales are recovered, in turn, at cosmological scales the scalar extra degrees of freedom show up and G_N becomes dynamical and it affects not only the growth but the whole set of cosmological predictions. Indeed, in the specific case of gBDT the scalar plays the role of such dynamical coupling.

- Peculiar velocities of galaxies are also sensitive to μ, so we expect that testing this theories by Alcock-Pazcynski effect would bring interesting results. Since we are dealing with coherent growth, the expansion history allows us to predict the different features of the power spectra of galaxies in redshift space at different spatial directions, these anisotropies caused by the peculiar velocities give rise to the observable Alcock-Pazcynski effect. For such reason we think it is worth to constraint the expansion history of gBDT using such a test.

- As pointed out in [288] the massless case is a good approximation at cosmological scales since the scalar is suppressed by the mass in a Yukawa way. However

if we were interested in accounting for the small effects from this coupling, we would have to constrain non-coherent perturbations by non-linear contribution of the matter power spectra and the CMB at small cosmological scales, However that purpose lies beyond of the goals of this work.

5.3 Cosmological Implications of The Effective Scalar-Tensor Theory

The general scalar-tensor theories arise as a generalization of the original BDT first purposed by Bergmann [35, 227] and Wagoner. They considered the most general scalar-tensor theory of gravity at the time (gBDT) by upgrading the only free parameter ω to a free function of the scalar field and allow the scalar field having an arbitrary potential.

5.3.1 The Model

In this subsection we shall study theoretical aspects of the the effective scalar tensor theory constructed before. The starting point is going to be the general scalar-tensor theories described by the following action

$$S = \frac{1}{16\pi G}\int d^4x\sqrt{-g}\left[\phi R - 2\Lambda(\phi) - \frac{\omega(\phi)}{\phi}(\nabla\phi)^2\right] + S_m, \tag{5.9}$$

All the symbols involved in the previous action mean the same as in BDT, and it is basically a direct generalization as mentioned before. Still matter couples minimally to the metric and the scalar affects matter only indirectly by means of the metric, so the evolution of matter is determined by the conservation equations. All the features of BDT are conserved, still the local value of the gBDT scalar field is related to the Newton constant that we measure on earth in order to implement the Mach principle.

A specific model is determined by the functions $\omega(\phi)$ and $\Lambda(\phi)$, the role of the first one is to determine the conformal factor by which the modification of gravity is yielded and the second one plays as a dynamical form of dark energy. A popular special case is $F(R)$ defined by $\omega(\phi) = 0$. When it is constant is nothing but a cosmological constant which will be the case in this work since we are interested in modifications of the gravitational sector rather than in dark energy models.

The equations of motion (e.o.m) resulting by extremizing the action are given by

$$\phi R_{\mu\nu} = 8\pi G_N T + \nabla_\mu\nabla_\nu\phi - g_{\mu\nu}\Box\phi + \frac{\omega(\phi)}{\phi}\left(\nabla_\mu\phi\nabla_\nu\phi - \frac{1}{2}g_{\mu\nu}\nabla_\alpha\phi\nabla^\alpha\phi\right) \tag{5.10}$$

$$\phi R - \frac{\omega}{\phi}\nabla_\alpha\phi\nabla^\alpha\phi + 2\omega\frac{\Box\phi}{\phi} + \frac{d\omega}{d\phi}\nabla_\alpha\phi\nabla^\alpha\phi - 2\phi\Lambda' = 8\pi G_N T \tag{5.11}$$

as in BDT, primed quantities are derivatives w.r.o ϕ

$$\nabla^\mu T_{\mu\nu} = 0 \tag{5.12}$$

where $T_{\mu\nu}$ is the energy-momentum tensor of the matter fields, T is its trace and $R_{\mu\nu}$ the Riemann curvature tensor. Note that the scalar couples indirectly to matter by means of the metric. This indirect coupling between the scalar and matter can be achieved if the metric equations (5.10) are traced and added to (5.11), the scalar curvature may be eliminated and obtain an equation for the field sourced by the matter

$$\Box\phi = \frac{1}{2\omega+3}\left(8\pi G_N T - \frac{d\omega}{d\phi}\nabla_\alpha\phi\nabla^\alpha\phi + 4\Lambda - 2\phi\frac{d\Lambda}{d\phi}\right). \tag{5.13}$$

The field is suppressed by the local quantity $2\omega+3$, then for $\omega\to\infty$ the field is constant and GR is recovered. In the last equation the scalar couples either to the trace of the energy-momentum tensor of matter, to the Λ and its derivative and the derivative of ω.

Note that for $\omega < \frac{-3}{2}$ the field is a ghost and thus physically pathological. A special case of gBDT corresponds to the DGP braneworld model at subhorizon scales where the 5th dimension is not important with $\omega = \frac{3}{2}(\beta(t)-1)$ where $\beta(t) = 1 - 2Hr_c(1 + \frac{\dot{H}}{3H^2})$, $\dot{H}$ is the time derivative of the Hubble rate and $r_c \sim \frac{1}{H_0}$ is the cross-over scale [104]. As mentioned before, equations of motion for matter are the same as in GR, however since the metric might hold a different solution due to the presence of scalar, its final dynamics may also be modified.

5.3.2 Background Cosmology

The modified Einstein equations describing the dynamics of the FRW metric, lead to a modified version of the usual Friedmann and Raychaudhury equations given by [97]

$$3H^2 = \frac{8\pi G_N}{\bar{\phi}}\rho + \frac{\Lambda}{\bar{\phi}} + \frac{\omega}{2}\left(\frac{\dot{\bar{\phi}}}{\bar{\phi}}\right)^2 - 3H\frac{\dot{\bar{\phi}}}{\bar{\phi}}, \tag{5.14}$$

$$-2\dot{H} - 3H^2 - \frac{\ddot{\bar{\phi}}}{\bar{\phi}} - 2H\frac{\dot{\bar{\phi}}}{\bar{\phi}} - \frac{\omega}{2}\left(\frac{\dot{\bar{\phi}}}{\bar{\phi}}\right) = \frac{8\pi G_N}{\bar{\phi}}P - \frac{\Lambda}{\phi}. \tag{5.15}$$

The evolution of the gBDT background scalar $\bar{\phi}$ in a flat FRW universe is governed by the following equation

$$\ddot{\bar{\phi}} + 3H\dot{\bar{\phi}} = \frac{1}{2\omega+3}\left[8\pi G_N(\rho - 3P) + 4\Lambda - \frac{d\omega}{d\bar{\phi}}(\dot{\bar{\phi}})^2 - 2\bar{\phi}\frac{d\Lambda}{d\bar{\phi}}\right], \tag{5.16}$$

recall that $\dot{\bar{\phi}} = \frac{d\bar{\phi}}{dt}$ and $H = \frac{\dot{a}}{a}$.

In the particular case we are concerned of, $\frac{d\omega}{d\bar{\phi}} = \frac{Ha}{\dot{\bar{\phi}}}\frac{d\omega}{da} = \frac{Ha}{\dot{\bar{\phi}}}\, nm\, a^{n-1}$. For $n = 0$ we clearly have the original Brans-Dicke theory, in gBDT ω is allowed to change its value locally, m plays the role of omega today ω_0 and n modulates its local value as function of time.

We consider restricted and unrestricted models, as in BDT. In the former models, the initial conditions are fixed either using the restriction over the Newton constant measured solar system experiments given by

$$\bar{\phi}_0 = \frac{1}{G_N}\frac{4+2\omega_0}{3+2\omega_0}, \tag{5.17}$$

where $\omega_0 = \omega(a=1) = m$. In the unrestricted case, $\bar{\phi}_0$ is a free parameter. Again we'll distinguish such models by calling them "*restricted models*" (rgBDT) and "*unrestricted models*" (ugBDT) respectively.

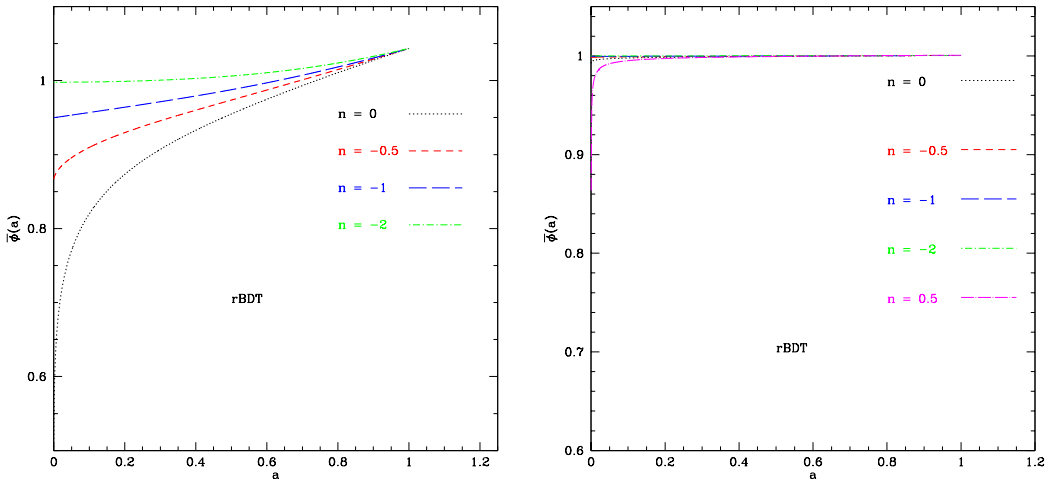

Fig. 5.1 The scalar field solutions for $\omega(a) = ma^n$. As m increases the variation of the field decreases, it determines the value of the gravitational current strength. Negative values of the exponent suppress the scalar while positive ones enhance it.

In contrast to BDT where the field stays approximately constant during the radiation era, gBDT might lead to a dynamic solution. Although, during radiation domination the field stays unaffected by matter era because (5.18) is sourced by the trace of the energy-momentum tensor, it might hold a non trivial solution since it obeys the following equation

$$\frac{d(a^3\dot{\bar{\phi}})}{da} + \frac{nm\, a^{(n-1)}}{2\omega+3}(a^3\dot{\bar{\phi}}) = 0 \tag{5.18}$$

Striclty for $n \neq 0$, the solution for the first derivative of the scalar is

$$\dot{\bar{\phi}} \sim a^{-\left(3+\frac{n}{2}\right)} \tag{5.19}$$

Notice that $\dot{\bar{\phi}}$ appears in the right hand side of the Friedmann equation, so it can be thought that it plays the role of an extra component of the matter-energy density. If the exponent is negative as $a \to 0$ the field variation tends to infinity. In particular, for theories near to the BD limit $n \to 0$ the derivative of the scalar behaves as a matter term density, for larger $n \sim 2$ it behaves as such as the radiation density does. For larger positive values of n the ϕ' would be dominant at early times, however for such large values of $|n|$ the theory is not physically feasible at late times so those effects at early times are not going to be considered.

Figure (5.1) shows us numerical solution for the scalar over the whole history of the universe within the restricted model. Clearly, the trend of the field is the same for a wide range of n values, it grows monotonically along with time. The overall variation of the field is larger as n increases.

In order to illustrate better how the field grows at late times, we'll make an approximation of (5.18) for low redshifts $z << 1$. In that case $\omega(z) = m(1-nz)$ and the scalar equation (5.18) is

$$\left(4 - mn\frac{1}{(2m+3)\phi_0^{-2}(m)}(1+\frac{2nz}{2m+3})\right)H\dot{\bar{\phi}} = \frac{8\pi G}{2m+3}\Omega_m\left(1+\frac{3(2m+3)+2n}{2m+3}z\right). \tag{5.20}$$

Since $z \sim 0$, the approximation works only if we set $\frac{1}{z} >> |n|$ so that the last term in the r.h.s is small. Within this bounds if $|n| >> 1$ and $m \sim 1$, then the first term in the left hand side can be neglected and then $\dot{\bar{\phi}}_{z=0} \simeq -\frac{\Omega_m \bar{\phi}_0^2(m)}{m}\frac{H_0}{n}$. If $n < 0$ the field's variation increases at late times and vice versa for $n > 0$. Since the field evolves monotonically, and its derivative is suppressed by n, then this parameter also suppresses the field, as shown in the figure. It is clear that for large fixed values of m, negative n suppresses more efficiently the scalar. Thus we can expect these two parameters to be strongly correlated. In summary, at the level of the background, at a given small redshift z the GR limit is accomplished at least in two ways: $(m > 1, -\frac{1}{z} \sim n << 0)$ or $(m \to \infty, n = 0)$.

Now lets analyse the expansion history in these models. By looking at the solution of the scalar we can see that it is more relevant at late times so we'll stick to that regime. From equation (3.8) is straightforward to get

$$(H + \frac{1}{2}\frac{\dot{\bar{\phi}}}{\bar{\phi}})^2 = \frac{8\pi G_N}{\bar{\phi}}\rho + \frac{\Lambda}{\bar{\phi}} + f(\omega)\left(\frac{\dot{\bar{\phi}}}{\bar{\phi}}\right)^2 \tag{5.21}$$

where $f(\omega) \sim 1$. Lets consider $m, |n| > 1$ and ignore the radiation term. We already know that $\frac{\dot{\bar{\phi}}}{\bar{\phi}} \sim \frac{H_0}{nm}$ at late times so the left hand side correction term FRW equation is a $O(\frac{1}{nm})$ whilst the one at right hand side can be neglected. It is worth of mentioning that for an heuristic analysis both terms may be neglected, however the l.h.s should be taken into account if we aim to test the theory with high accuracy as it will be when we try to set strong constraints on the parameters. A more significant correction comes up from the normalization on G_N in the matter term in the right hand side as it happens in BDT.

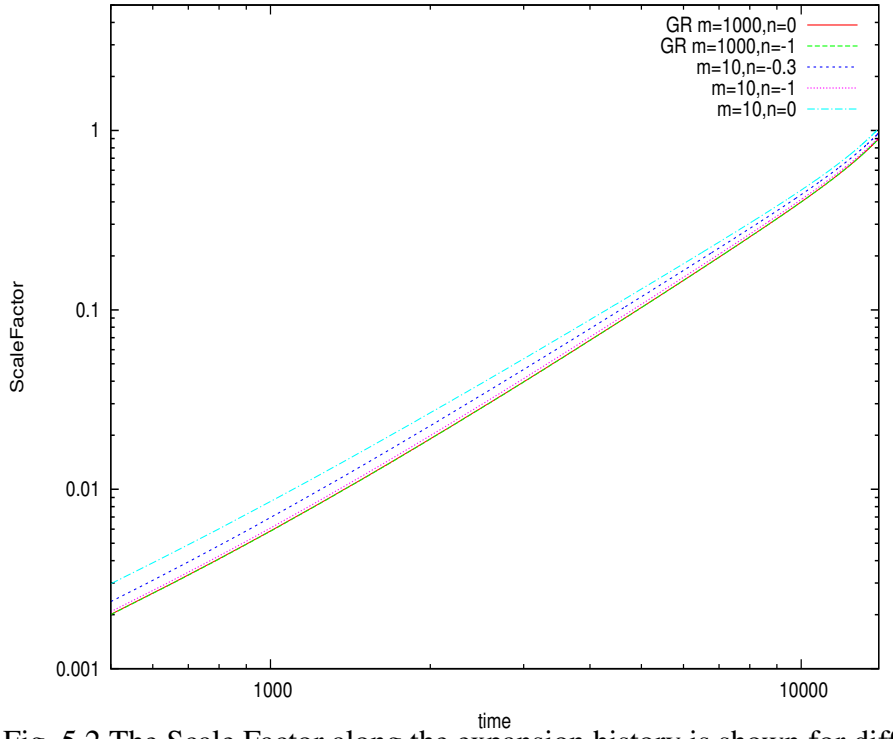

Fig. 5.2 The Scale Factor along the expansion history is shown for different values of n and small m. For large values of m the scale factor remains as for ΛCDM regardless the value of n. For m small we see that for relatively small values of n (not at infinite at all) the scale factor tends to ΛCDM. In summary, the ΛCDM limit is reached for relatively small values of ω.

For the restricted gBDT case, the larger the mean value of ω is, the closer is universe to a FRW ΛCDM. As the scalar and its derivative are enhanced as $\omega \to 1$, the universe expands quicker due to the scalar's derivative contribution in the l.h.s of the Friedmann equation. The mean value of ω in gBDT should be understood as its average over time.

In the restricted case, the mean value of G_N varies for smaller ω whilst it stays constant in the unrestricted case. Thus, as BDT, the unrestricted models have an additional convenience over the restricted ones because the effects of $\bar{\phi}$ and $\dot{\bar{\phi}}$ over the expansion are uncoupled since ω and ξ modulate each of them independently.

Now lets turn to study how distance measurements behave in gBDT. The comoving distance as the angular diameter distance are sensitive mainly to m, as it decreases distant objects appear far away in relation to the prediction of ΛCDM. For a fixed value of $m \sim 1$ increasing the absolute value of the exponent n makes objects appear closer regardless its sign. Therefore, it is a good idea to constrain BDT by using measurements of distance but not so gBDT since the parameters m and n are degenerated.

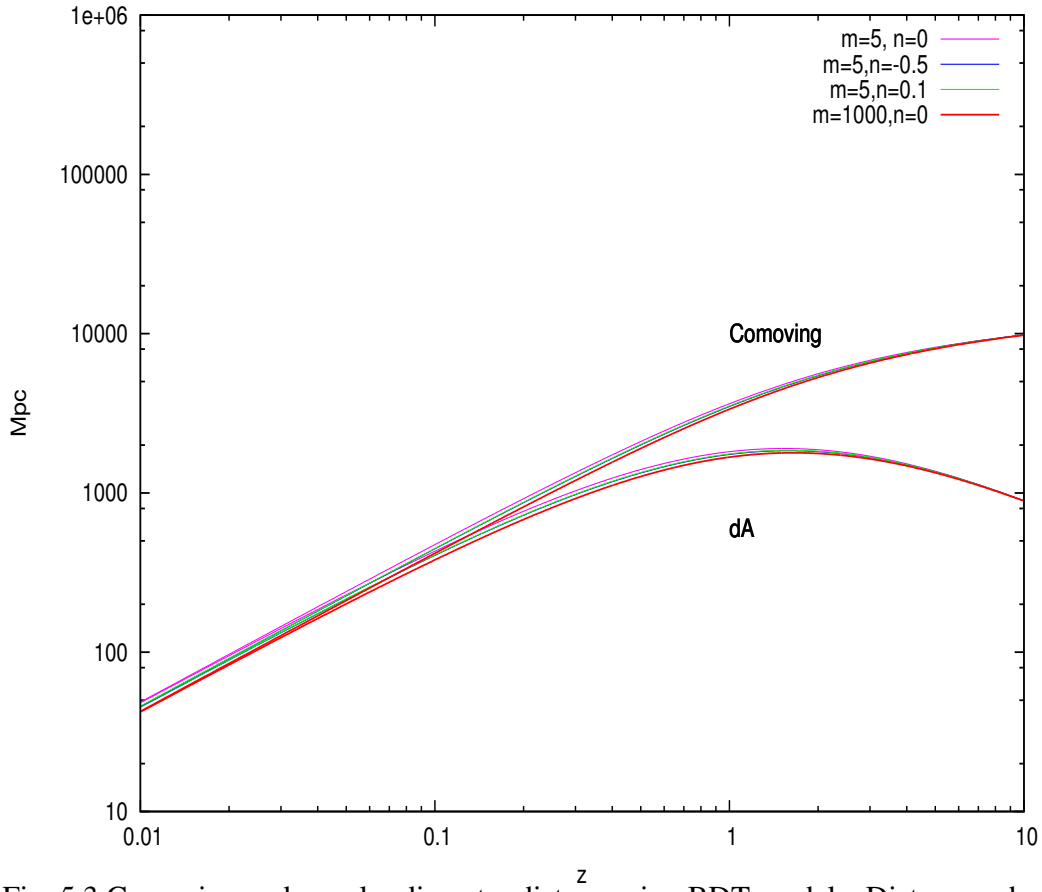

Fig. 5.3 Comoving and angular diameter distances in gBDT models. Distances change when the overall value of ω is varied, for fixed $m \sim 1$ distances remain the same when the exponent is changed.

5.3.3 Linear Cosmological Perturbation Theory

5.3.3.a Equations of Motion for Perturbations

Lets turn to formally study the cosmological perturbation theory of gBDT. We have already studied precisely the basic principles and framework of cosmological perturbations theory for BDT and GR in chapters 3 and 2 respectively. Therefore, in order to be concise and avoid repetition, in this part we only present the relevant equations arisen using the same framework as above. The same variables and setup established before will be used and the equations in conformal-Newtonian gauge will be casted as well. Special emphasis will be done in the new features of gBDT in contrast to BDT and GR. The corresponding independent modified Einstein equations (5.10) to the metric in conformal-Newtonian gauge are given by

$$\begin{aligned}\frac{2}{a^2}\left\{3H^2\Psi+3H\Phi'+k^2\Phi\right\} = & -\frac{8\pi}{\phi}\delta\rho-\frac{\delta\phi}{2a^2}\left(\frac{\phi'}{\phi}\right)^2\frac{d\omega}{d\phi}\\ -\frac{1}{a^2\phi}\left\{(6H\Psi+3\phi')\phi'-3H\delta\phi'/k^2\delta\phi\right\}+ & \frac{\omega}{a^2\phi}\{\frac{\delta\phi}{2}\left(\frac{\phi'}{\phi}\right)^2-\left(\frac{\phi'}{\phi}\right)\delta\phi'\\ +\frac{\phi'^2}{\phi}\Psi\}+ & \frac{3}{a^2}\frac{\delta\phi}{\phi}H^2, \end{aligned} \tag{5.22}$$

$$\begin{aligned}\frac{2}{a^2}\left\{H\Psi+\Phi'\right\} = \frac{8\pi}{\phi}(\rho+P)\theta- & \frac{1}{a^2\phi}\left\{H\delta\phi+\phi'\Psi-\delta\phi'\right\}\\ + & \frac{\omega}{a^2}\frac{\phi'}{\phi}\frac{\delta\phi}{\phi}\end{aligned} \tag{5.23}$$

$$\begin{aligned}&\frac{2}{a^2}\{[H\Psi'+(2H'+H^2-\frac{k^2}{3})\Psi+\Phi''+2H\Phi'+\frac{k^2}{3}\Phi\}=\frac{8\pi}{\phi}\delta P\\ +\ &\frac{\delta\phi}{a^2\phi}(2H'+H^2)+\frac{1}{a^2\phi}\{2\phi''\Psi+\phi'(\Psi'+2H\Psi+2\Phi)-\delta\phi''-H\delta\phi'\\ -\ &\frac{2}{3}k^2\delta\phi\}+\frac{\delta\phi}{2a^2}\left(\frac{\phi'}{\phi}\right)^2\frac{d\omega}{d\phi}-\frac{\omega}{a^2\phi}\{\frac{\delta\phi}{2}\left(\frac{\phi'}{\phi}\right)^2-\left(\frac{\phi'}{\phi}\right)\delta\phi'+\frac{\phi'^2}{\phi}\Psi\},\end{aligned} \tag{5.24}$$

$$\Phi-\Psi=\frac{8\pi a^2}{\phi}(\rho+P)\Sigma+\frac{\delta\phi}{\phi}. \tag{5.25}$$

Equations (5.22) and (5.23) correspond to the time-time and space-time constraint equations, (5.24) is the trace component of the spatial equations or pressure perturbation equation and (5.25) is the traceless component of the spacial equations contracted with the traceless derivative operator. The equation for the scalar perturbation is given by

$$\begin{aligned} \delta\phi'' + 2H\delta\phi' &+ k^2\delta\phi - 2\phi''\Psi - \phi'\left(\Psi' + 4H\Psi + 3\Phi'\right) = \\ \frac{1}{3+2\omega}[8\pi^2(\delta\rho - 3\delta P) &- \frac{d^2\omega}{d\phi^2}\phi'^2\delta\phi - 2\frac{d\omega}{d\phi}(\phi'\delta\phi - \phi'^2\Psi + \phi''\delta\phi \\ &+ 2H\phi'\delta\phi)]. \end{aligned} \tag{5.26}$$

For modes of perturbations inside the horizon the effect of the expansion is small and derivatives with respect to conformal time may be neglected and then the equations reduce to the same equations than in BDT since all time-derivatives are dropped away in the quasi-static limit.

A more detailed analysis of perturbations in gBDT can be found in [216]. In that work they study a particular set up for $\omega(\phi)$, which differs from gBDT. However, both frameworks imply the same physics. Here we solved the exact equations for all scales numerically using an extended version of the CAMB code described above suitable to gBDT with $\omega(a) = ma^n - 3/2$.

5.3.3.b The Late-Time Attractor behavior of Scalar Perturbations

First, we are going to look at numerical solutions for the modes of the scalar perturbation. In order to illustrate the evolution of the scalar perturbation in the effective scalar-tensor lets have a look to exact numerical solutions for different scales shown in (5.4) and compare them to the solutions for BDT.

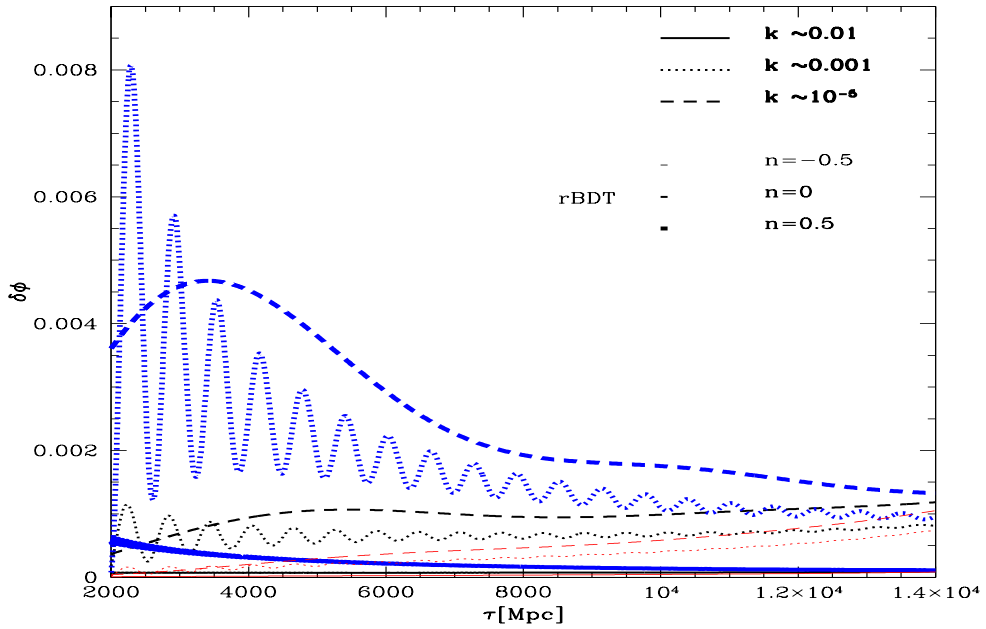

Fig. 5.4 Scalar perturbation for fixed current value of $\omega(a=1)=1000$ and different exponents for its growth along the expansion history. In contrast to the constant ω case, when its value evolves in time the shape of the perturbations is modulated.

In BDT the scalar perturbations have the same shape regardless the scale and value of ω. They grow as matter grows in the universe and tend to bound their track around a stationary point by making damping oscillations, they remain steady there while matter dominates and they turn on again growing monotonically. In contrast, in gBDT the attractor behavior is more complex since the stages of damped oscillation and linear growth overlap and at some scale the growing effect wins [see figure (5.4)].

5.3.3.c The Growth of Matter Perturbations

Since in this kind of models, we have ignored the self-interactions of the scalar, the perturbations are coherent. Thus the growth of sub-horizon matter perturbations is scale independent and depends only on the background evolution. As we are in the Jordan conformal frame, the matter is not coupled to the scalar and the energy-momentum tensor is conserved. Technically speaking this means that the equations for matter perturbations are the same than GR. In general, the background spacetime

is not FRW in this theories, then the matter perturbations grow differently in these models.

In the regime where the growth would tend to behave like in general relativity (if $m \to \infty, n = finite$ and $m = finite, n \to -\log\infty$). Although the expansion history is just FRW, the growth of matter perturbations still might be modified. Thanks to this feature these theories are feasible candidates to break the degeneracy between GR and MG by testing the growth of matter perturbations. For example, as the figure (5.2) shows, for $n \sim -\frac{1}{2}$, from redshifts $z < 2$ to the present time, the expansion history is just FRW, however considerable modifications of the growth are allowed in this model. Let's highlight that at the moment the planned deep redshift surveys would not go further than $z = 1$, Euclid for example is planned up to $z = 2$.

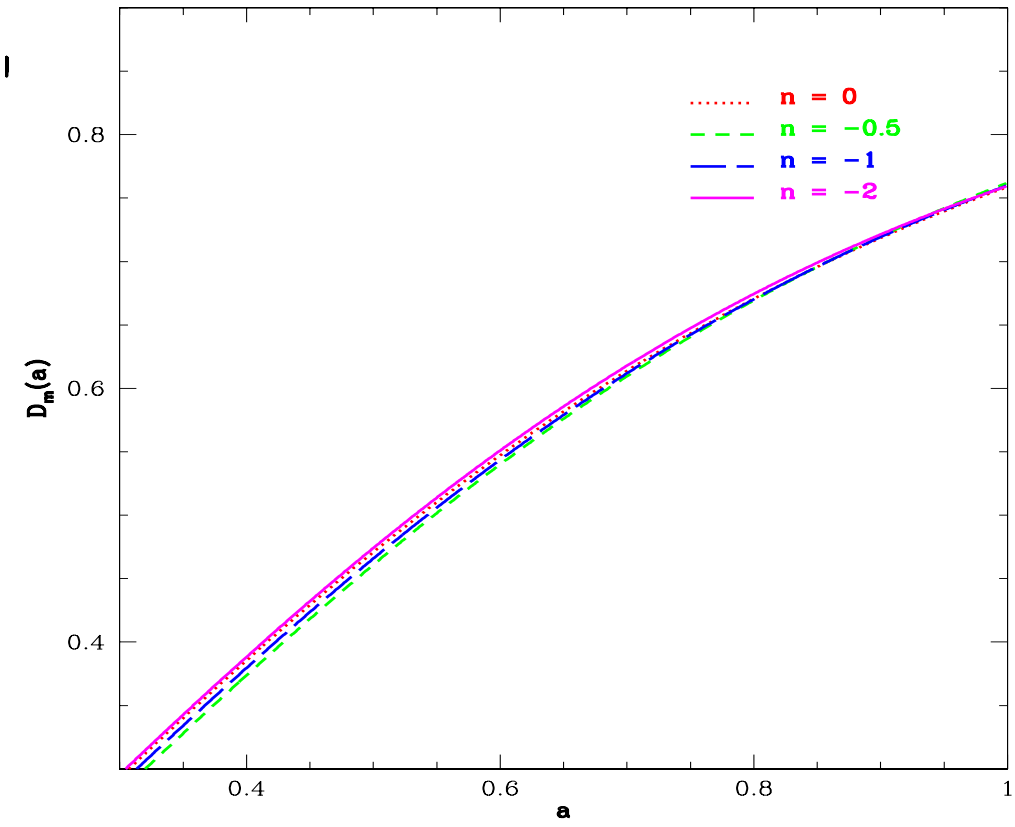

Fig. 5.5 The growth of matter for various values of n. Even when $m = 10$ is not too large, relatively small negative values of n help to approach GR.

5.3.4 The Alcock-Paczynski Distortion in *gBDT*

In this small section I just want to make a brief comment about the relevance of the Alcock-Pazcynski test applied to BDT and gBDT. As we'll see in short, the test does not bring important insight when applied to BDT. In contrast, since the measure associated with the mentioned effect is sensitive to the extra parameter introduced in gBDT, it is a interesting probe to be applied to this model.

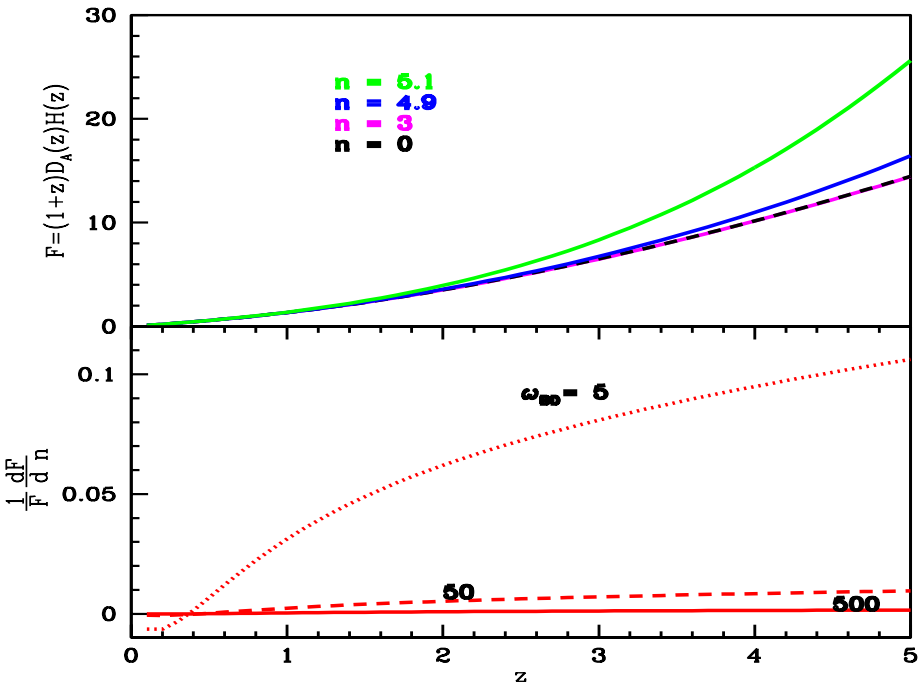

Fig. 5.6 Up: The Alcock-Paczynski parameter for different values of the exponent n and $m = 100$. The sensitivity of APD to the exponent is almost abscent today, however it increases as the redshifts increases as well, this tell us that high-redshift surveys are more capable of detecting a possible AP effect in BDT. Bottom: Variation of the APD with respect to the exponent for different gBDT models. As we see if $m \to 1$ the sensitivity of APD to the exponent is larger. For the extreme case of $m = 5$ APD is detectable even at relatively low redshift.

As figure (5.6) shows, the APD for in gBDT starts to be more sensitive to n from $z > 1$ onwards. As expected such sensitivity is reduced as m increases. As mentioned in previous chapters, $m \to 0$ may be associated with self-accelerating theories when a potential $V(\phi)$ plays the role of dark energy, thus if it is true that our $m \sim 0$ model is an approximation for a shallow-potential case, we can imply that the APD is a powerful test for these self-accelerating theories, such like DGP in the decoupling limit and some $F(R)$.

5.3.5 Anisotropies in the Cosmic Microwave Background

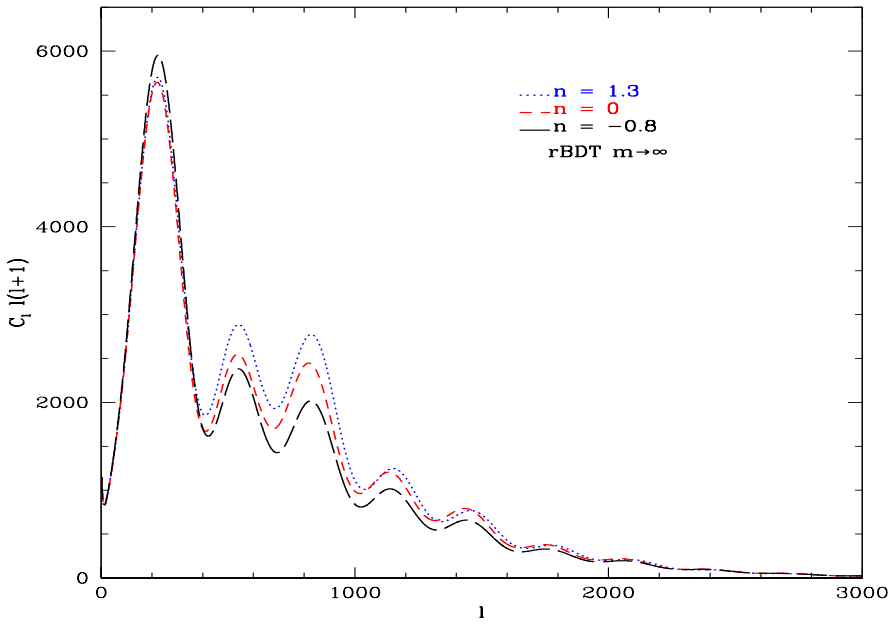

Fig. 5.7 Temperature spectrum in the limit $m \to \infty$ for extreme values of n within the restricted model.

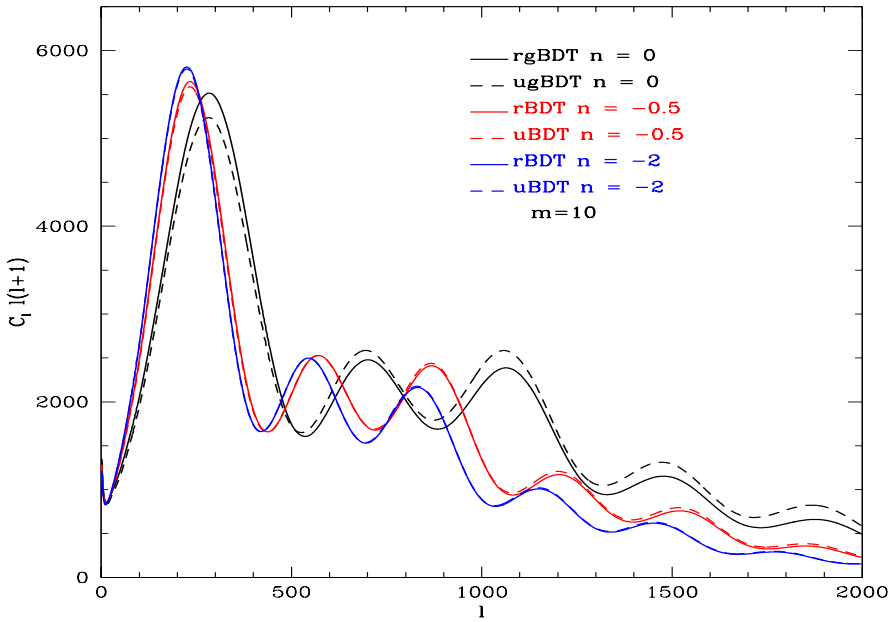

Fig. 5.8 Restricted and unrestricted ST models are contrasted for small $m(= 10)$ and a range of values of n.

As with BDT in this part we aim to figure out how the CMB anisotropies behave in gBDT. In order to disclose the new signatures due to the time-varying nature of ω, the idea is to contrast features of the BDT's CMB spectrum against gBDT's.

Now we shall analyse the effects coming from the background evolution, afterwards we shall continue with the effects due to perturbations which in contrast to BDT, carry some new interesting observational signatures.

5.3.5.a Effects from the Background Evolution and Recombination

As within BDT, the modified expansion history in gBDT have some effects on the history of recombination ($z \sim 1100$). All the effects studied in chapter 3 are inherit by gBDT, thus now we shall focus on the new effects due to the local time variation of ω tuned by the n parameter.

On one hand, since it is likely that realistic gBDT models yield global $1 << \omega$, we might naively suspect (a priori and wrongly) that restricted models would behave basically like ΛCDM at early times when recombination occurs [3].

Similarly, for unrestricted models, we could expect naively recombination to be the same as in BDT. However, we already found that in gBDT the expansion history is slightly different than for BDT at early times (even in the restricted case). Therefore, we can probe (a posteriori) that recombination is significantly affected by the gBDT field and so the cosmic background radiation that we observe today as well.

On one hand, the effect on recombination produced by the rescaling of G_N is similar as within gBDT: increasing ξ makes the visibility function wider. On the other hand, we can understand the effect of m as we did for $\omega =$constant within BDT. By decreasing m the overall value of $\omega(a)$ decreases, this makes the universe to expand quicker and then the universe reaches the temperature ~ 1 eV earlier, this also explains why the visibility function shifts to earlier times when ω decreases. Figure (3.7) in chapter 3 illustrates this effect for restricted and unrestricted models both with equal initial conditions $\phi_{ini} = 1$.

Therefore, the new effects are introduced by the n parameter as can be observed in figure (5.2). In order to understand how the visibility function is affected, let us consider the following two regimes

[3] because the main effect is due to a change on G_N which is ~ 1 for large ω within rBDT and because photons do not couple to the scalar.

1. **Figure (5.9).** $m = 1000$ **is large but not as much to reach the** ΛCDM **limit**

   For large m the model today is close to ΛCDM and then it is a viable model, if $n < 0$ the whole ω is large all along the expansion history and the visibility approaches to that of GR. Otherwise, when $n > 0$, the scalar is enhanced all along and so the expansion history is greatly modified unless m is sufficiently large to counter the effect.

   As shown by (5.9), the width and height of the visibility remains the same for negative values of the exponent. The shift in τ_{rec} can be understood by the same argument used for BDT, changes in the expansion rate makes that the temperature $\sim 1eV$ to be reached at different time.

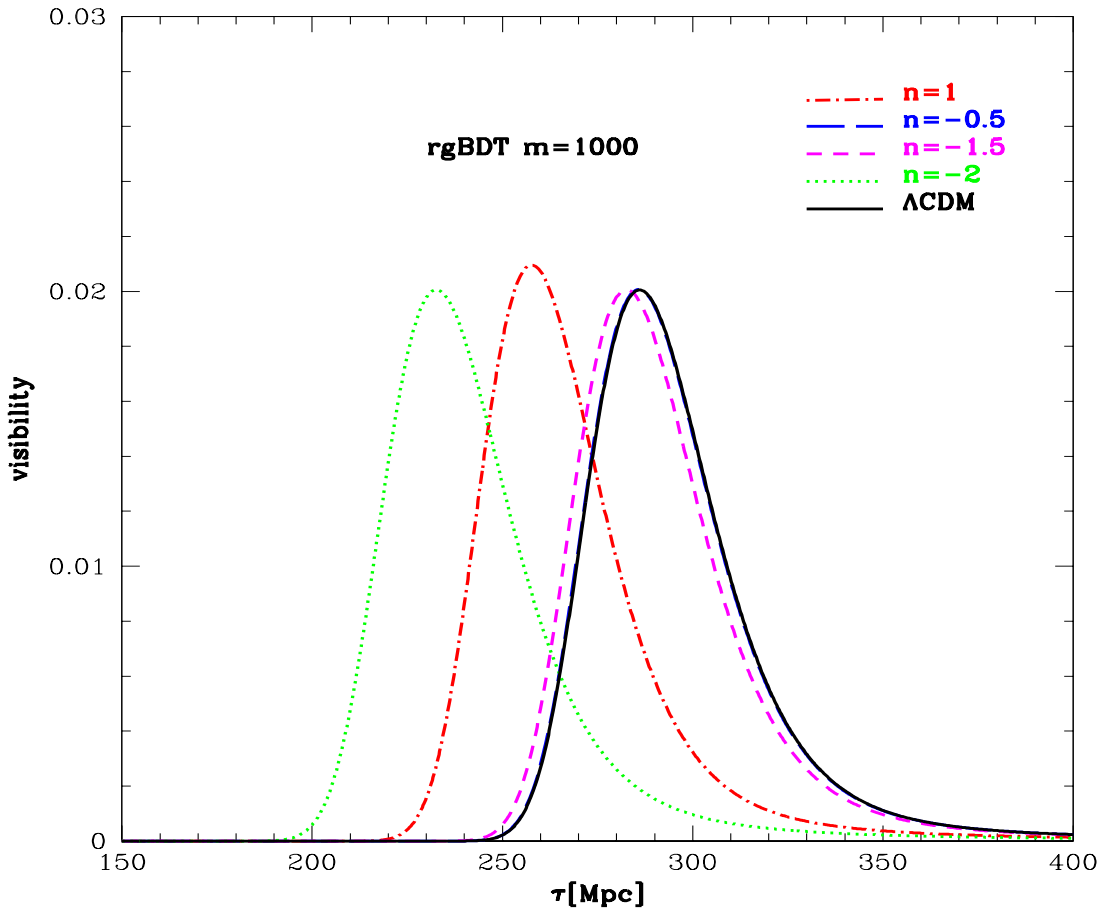

Fig. 5.9 Visibility fuction for large m and a range of values of n within rgBDT.

2. **Figure (5.9). Small** m. In this case, unless the exponent is negative and large, the effects due to the scalar field are important. Notice in figure (5.9) that increasing the absolute value of the exponent affects the visibility in the same way as in figure (5.10), as expected the exponent only helps to approach the ΛCDM limit, as a result the visibility is sensitive only to the overall value of ω and the same argument for BDT works here. It's worth to mention that for $n > 0$ even for small values of n the visibility departs in great extent from ΛCDM then, as we confirm later, they are very likely to be rejected by data as preferred models.

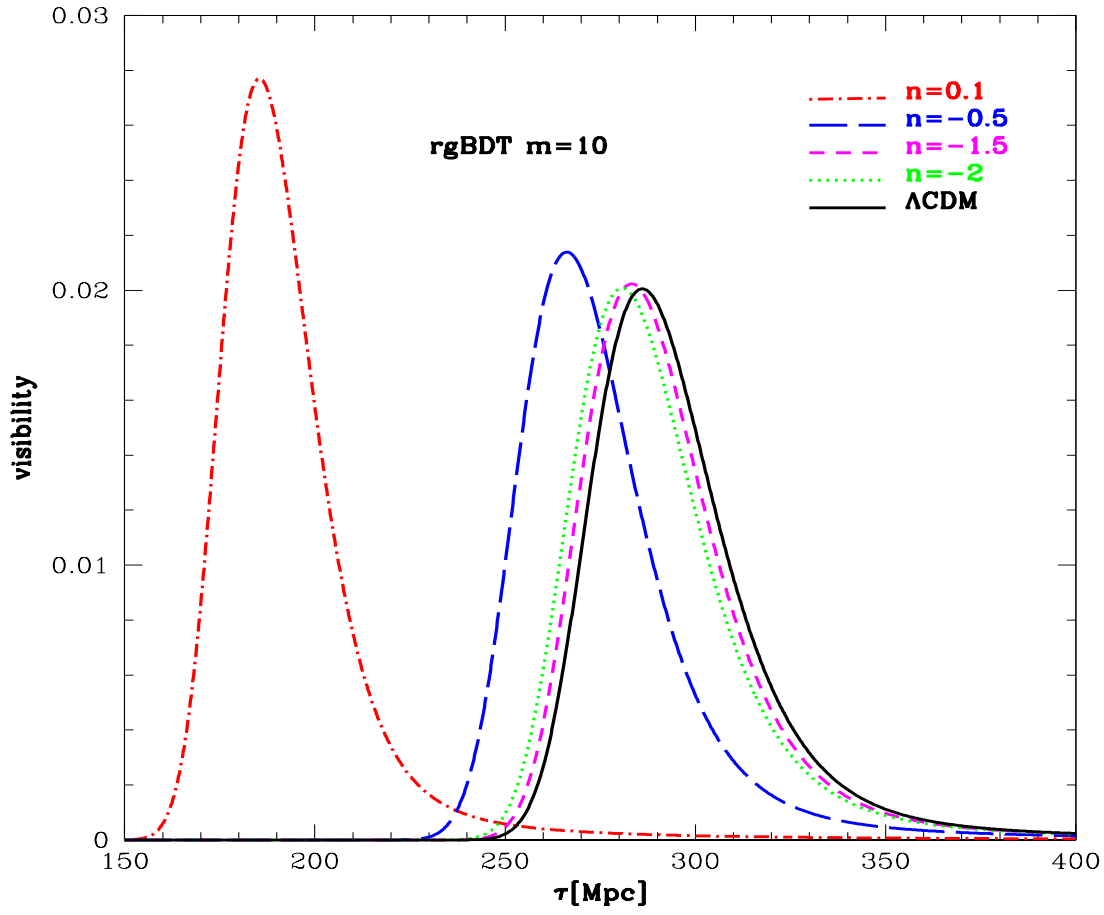

Fig. 5.10 Visibility function for gBDT with $m = 10$ and different values of n within rgBDT.

The following table shows the values of ω at the time of recombination for relevant values of m and n within rgBDT models.

$\omega(\tau_{rec})$			
	$m = 10$	$m = 100$	$m = 1000$
$n = 0.1$	4.96	49.7	496.9
$n = 0$	10	100	1000
$n = -0.5$	330.5	3301.7	33013.8
$n = -1$	1×10^4	1×10^5	1×10^6

Unrestricted vs. Restricted at Recombination As we can see in figure (5.11), very different visibility functions arise for rgBDT and ugBDT when n varies for a fixed m and ϕ_{ini}. Within ugBDT, for small $m \sim 10$, as n increases the visibility function takes its maximum earlier, at the same time, the visibility function becomes narrower and then the anisotropies turn to be more damped as the model approaches to the ΛCDM limit ($n << 0$). In turn, within unrestricted models with $\phi_{ini} = 1$ the tendency is the contrary, figure (5.11) makes clear this behavior.

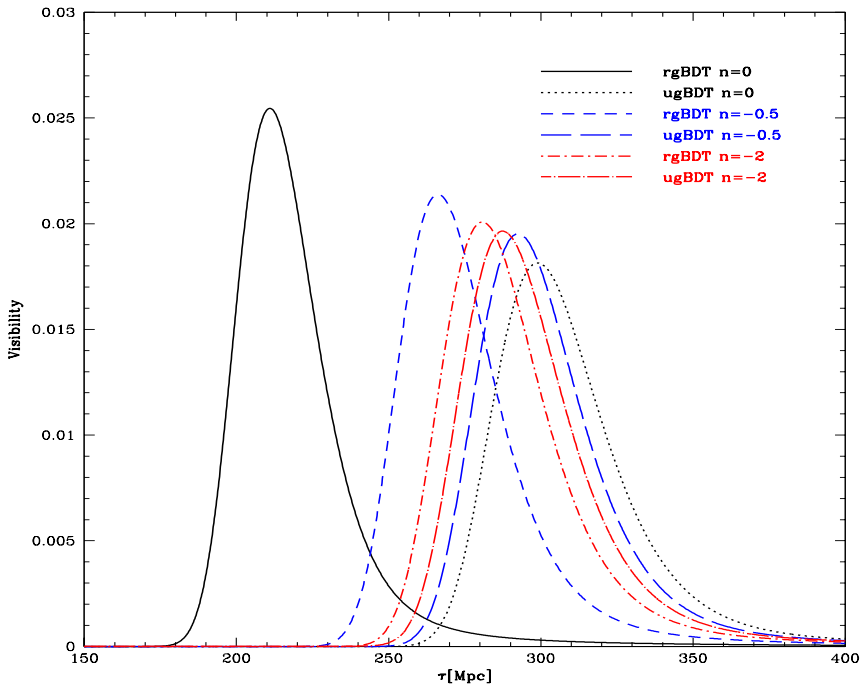

Fig. 5.11 Visibility function for ugBDT and rgBDT models for SMALL fixed $m = 10$. For negative values of n the larger $|n|$ more similar are the visibility functions in both cases. Also, for ugBDT models, the visibility is wider as a consequence is more difficult for electrons to recombine into neutral hydrogen.

As we shall explain below, the visibility within both types of models tend to approach to each other for $n << 0$. As a consequence, within both models, the heights of the peaks of the temperature spectrum become similar as $|n|$ increases ($n < 0$), as shown in figure (5.8). Besides, for very large m and $n <\sim 0$ the visibility is shifted to earlier time as $|n|$ increases without changing too much its width and thus the damping effect on the anisotropy is less prominent than for small m as shown in figure (5.7), also a damping effect on intermediate scales still happens.

Because the visibilities of rgBDT and ugBDT models with $m \to \infty$, $\phi_{in1} = 1$ and $n << 0$ approach to each other, their temperature spectrum tend to be indistinguishable. On the contrary, even for small values of positive n the visibility of both types of models differ significantly.

This feature will be important when we test gBDT using the CMB since it lead us to reasonably suspect that the negative n are likely to be preferred by data as $\omega(\tau_{rec})$ (5.3.5.a)is pushed to the ΛCDM limit. Therefore, we expect similar results from restricted against unrestricted models.

Second, to find out why the recombination history of rgBDT and ugBDT are too different for small $\omega(\tau_{rec})$, we need to recall that they have different expansion rates [See (3.3)]. Regarding the rgBDT models, since $\omega(\tau_{rec})$ gets large if $n < 0$ [See table for $\omega(\tau_{rec})$], the rescaling factor $(2\omega+4)/(2\omega+3)$ of the Newton constant easily tends to be equal to 1 at early times. Otherwise, if $n > 0$ then $(2\omega+4)/(2\omega+3) > 1$ then the rgBDT model would have weaker Newton's constant than ugBDT, an then it would reach the time of recombination before giving rise to a slightly narrower visibility function than in ugBDT.

Measurement of the Acoustic Scale by means of the Peaks Location Lets recall that in BDT the sound horizon is quite sensitive to ω constant which is the case of gBDT corresponds to the overall value of ω integrated along the expansion history. Depending on the value of m, the extent of sensitivity of θ to n changes. The larger m is the lesser θ changes when n is varied. Such dependence is shown in the following table

$\theta(\tau_{rec})$		
n	$m = 1000$	$m = 10^6$
1	0.933639	1.035941
0.1	1.032737	1.037637
0.0	1.034614	1.037319
-0.3	1.036291	1.037173
-0.5	1.036713	1.036639

This shows us that the measurement of θ from the CMB would not provide a good measurement of n unless m is not too large. As expected, because both parameters are degenerated at the level of the background evolution, only if m is independently measured by other means, n could be well constrained. In the case a measurement of m is provided such that $m \to \infty$, although the first peak is placed in the same location for all n [figure (5.8)], the peaks at smaller scales suffer a further shifting, if this effect is well constrained the measurement of θ would be even better.

5.3.5.b Effects due to Perturbations

The effects due to perturbations on the CMB anisotropy can be better understood by studying each component of the source in the line-sight integral as we did in chapter 3. As usual, we are going to see how the new parameter n affects each of the components and try to figure out the physics behind the effect. In order to discriminate the effects due to the background (and hence to recombination) and only keep those due to the perturbations as much as possible, it is useful to work in the limit $m \to \infty$ where the effects of n on perturbations are more visible.

Integrated Sachs Wolfe Effect As explained in previous chapters, usually the ISW effect at late times on the temperature anisotropy can be understood as follows: the temperature anisotropy of photons traveling from the last scattering surface towards us, is modified by a considerable number of well potentials of galaxies formed at late times. Another source of ISW is due to the possible temporal variation of the potentials at late times. The former effect is manifested in the monopole of the temperature perturbation of the photon analysed in the next item, by now, we are concerned about the second type of late ISW. We have already probed that at large scales the gravitational potentials, even in BDT are actually time varying and that is going to produce an important signature of the gBDT parameters on the large scale temperature anisotropy shown in figure (5.12)

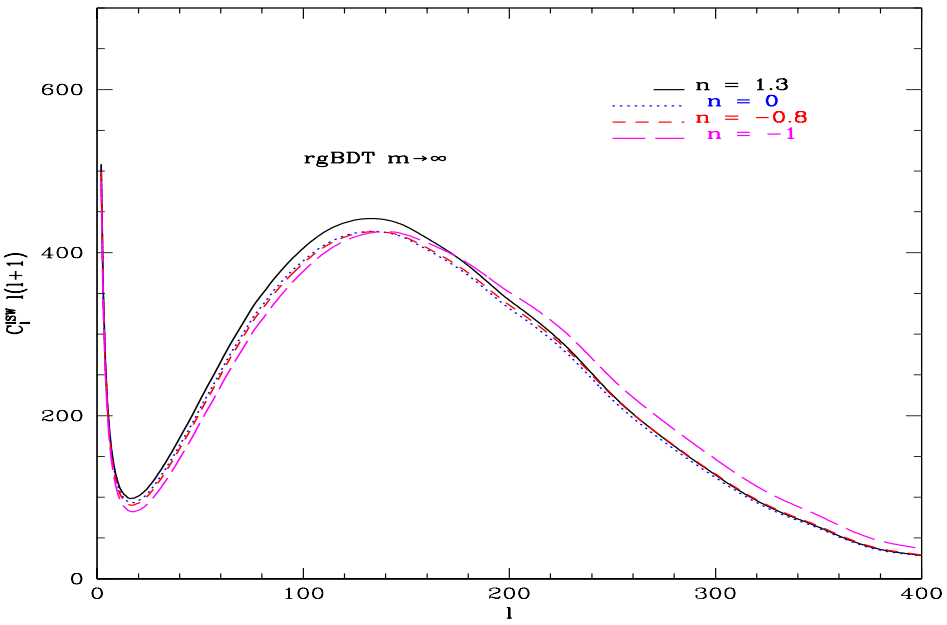

Fig. 5.12 Effect of the gBDT parameters on the late ISW contribution to the temperature spectrum. For negative values of n the ISW spectrum shifts with respect of $n = 0$ due to different expansion histories while for positive n the ISW is enhanced.

Notice that for $|n| \sim 0$ the ISW is unimportant, this means that it is more sensitive to the BDT m rather than n, however for sufficiently large $n > 0$ it gets enhanced and the scale at which it takes its maximum remains unaffected. In turn for $n < 0$ the spectrum is lowered and it takes its maximum on smaller angular scales.

Temperature and Doppler terms: Silk Damping and Acoustic Driving First of all, by inspection of figures (5.13) and (5.14), we can extract much of the information about the effects of gBDT perturbations on the temperature spectrum of the CMB.

Notice that the local time variation of ω carries much wealthier phenomenology in contrast to the BDT one. In the latter, the shape of the temperature and Doppler components of the spectrum is not significantly altered when constant ω is varied. In turn in gBDT one can identify singular effects at different scales which alters dramatically the shape of the dominant components of the temperature spectrum that we study right below.

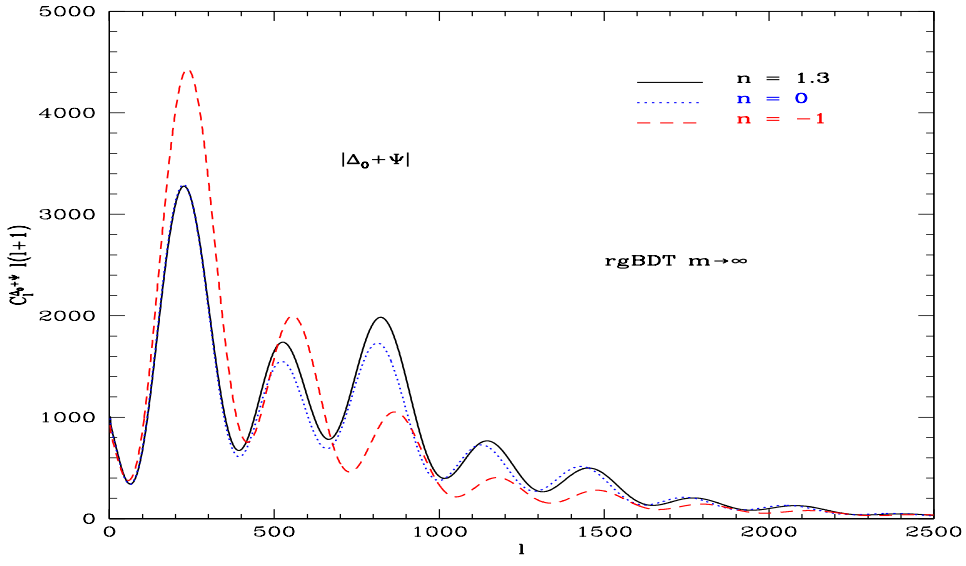

Fig. 5.13 Angular spectrum of the monopole of the effective temperature perturbation of photons corresponding to terms in the source in gBDT in the limit $m \to \infty$.

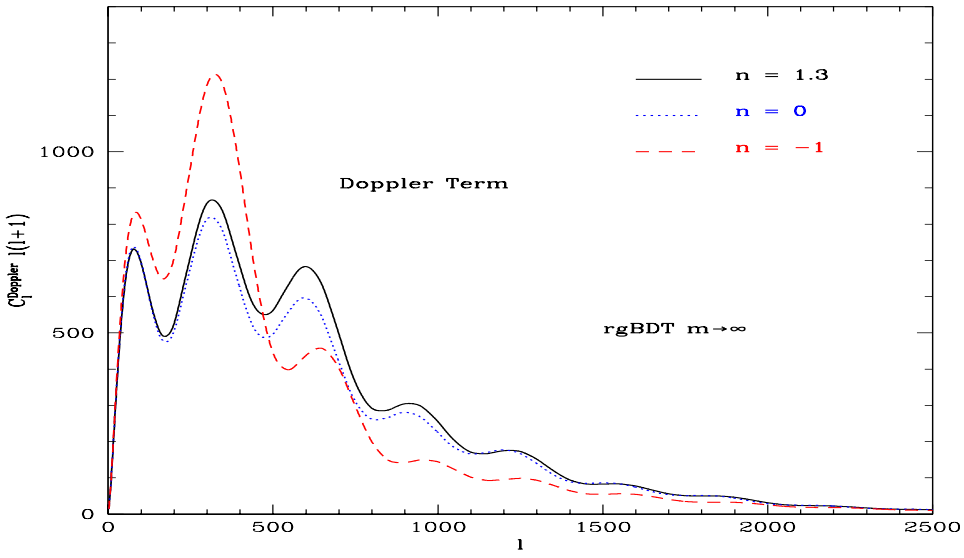

Fig. 5.14 Angular spectrum of the Doppler term in the source S_T within gBDT in the limit $m \to \infty$.

We can notice straightaway that, effectively, the shape of both spectra change dramatically for different signs of n. When $n > 0$, on one hand, the spectrum stays within its 10% at scales larger than $l = 400$. On the other hand, for $500 < l < 1000$ the spectrum is boosted upwards (more significantly in the second and third peaks). At smaller scales $l > 1500$ the spectrum is not particularly sensitive to n.

For $n <\sim 0$ the predominant effect is owing to damping oscillations, however a special signature can be spotted in the first two peaks of the monopole and Doppler spectra. When $|n|$ takes a more extreme value, the first two peaks get greatly enhanced whilst the next ones get importantly damped. This effect at large scales may be happening due to a combination of the ISW effect, Silk damping and acoustic driving. It is interesting that, in this last case, the CMB looks like one without CDM.

In order to understand these effects, we can recall from chapter 2 that before decoupling photons and baryons are tightly coupled due to Compton scattering. Approximately the system can be considered as a fluid because only the monopole and the dipole of the fluctuations survive, this limit occurs when $n_e\sigma_T \to \infty$. In this fluid, competing forces due to pressure and gravitation give rise to a series of acoustic oscillations of the temperature fluctuations of photons (and baryons as well). When photons and baryons decouple, these oscillations freeze at the last scattering surface. At this point, modes with wavelengths such that have a crest or a well coincides exactly with the size of the last scattering surface, appear as a peak or an through in the angular temperature power spectrum of the CMB. These acoustic oscillations

within this idealized picture are governed by (2.107), if in this formula the potentials are time-dependent then an extra effect apart of the oscillatory forcing sources appears and it is normally called *acoustic driving*.

In gBDT this acoustic driving actually happens since in the potentials are time-varying (5.15) on the relevant scales, this has the effect of increasing the oscillation amplitude for the modes relevant to the time where the potentials are time varying. Notice in the left panel of (3.7) that for small ω_{rec} ($n > 0$ given a finite m lead to small $\omega(\tau_{rec})$), the last scattering surface is not far from the radiation to matter equality and so there are modes for which the potentials are still time varying to some extend. We can spot in (5.13) that around the 3rd peak there's a boost in the amplitude of the monopole of Δ_0 due to this effect.

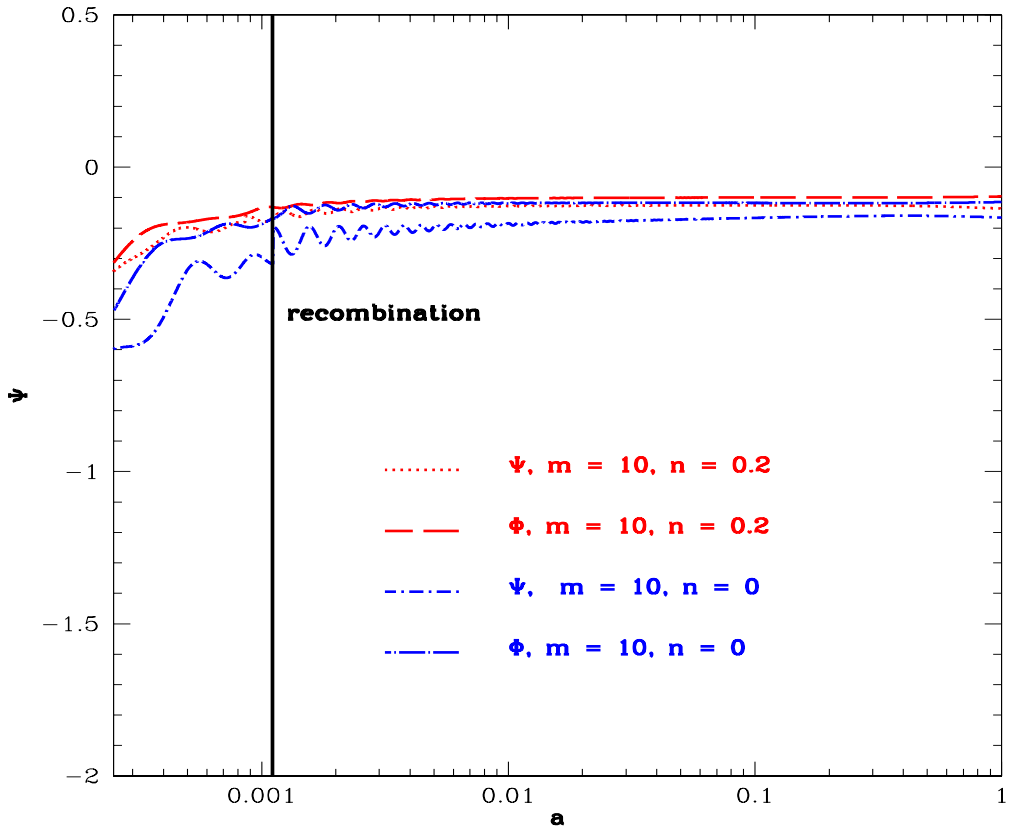

Fig. 5.15 This plot shows the variation of the gravitational potential Ψ within the rgBDT for fixed m at the scale corresponding to the first peak in the temperature CMB spectrum. Also the acoustic driving affecting the third peak for positive n are produced by these time-varying modes of the potentials.

The tight coupling limit described above breaks down in a real situation since $n_e\sigma_T$ is finite, as a consequence, the photons diffuse through the baryon fluid as a random walk leading to a diffusion damping or Silk damping of their perturbation [277]. The average distance that a photon goes across is given by $\lambda_D \sim \frac{1}{\sqrt{n_e\sigma_T H^{-1}}}$ and it is called the diffusion lenght. The effect of this photon diffusion is to wash out anisotropies with wavelengths smaller than λ_D. In chapter 2 we have introduced the damping coefficient k_D given by (2.115) which quantifies more accurately the scale of damping. The following table shows the values of k_D depending on the gBDT model.

k_D			
	$m = 10$	$m = 100$	$m = 1000$
$n = 0.1$	0.1834	0.1426	0.1385
$n = 0$	0.1698	0.1412	0.1384
$n = -0.5$	0.1457	0.1388	0.1381
$n = -1$	0.1408	0.1383	0.1381

The physics governing the effects on the Doppler term carried by the variation n can be understood easily. As we know from (3.7.5), this term is the contribution due peculiar velocities of galaxies along the line-of-sight. Therefore, before recombination the velocity of matter is proportional to the dipole of the baryon-photon fluid whilst after decoupling the more matter the universe contains the larger is the doppler effect since the velocity of matter increase as the density of matter does. Thus if decoupling happens right after the time of equality, the Doppler term gets enhanced. The following table displays the time of equality happens for different gBDT models. By using it along with figure (5.10), we can understand how the Doppler term is affected by n: On one hand, if $n < 0$ the larger is $|n|$ the closer are the times when recombination and equality of matter happen. On the other hand, if $n > 0$ as it increases either recombination and equality happen earlier so the effect is less important in this case.

τ_{EQ}			
	$m = 10$	$m = 100$	$m = 1000$
$n = 0.1$	75.77	115.03	120.76
$n = 0$	87.96	117.25	120.99
$n = -0.5$	113.09	120.56	121.34
$n = -1$	118.34	121.13	121.36

Early Sachs-Wolfe Effect An early ISW effect occurs right when decoupling has ended and it is stronger if decoupling takes place closer to the radiation era. Typically this happens for theories at which equality occurs before decoupling. In such case the

potentials are decaying to their constant values during matter domination [see figure (5.16)]. The early ISW effect affects scales around the first and possibly second peak. This has the effect of raising the 1st peak substantially higher.

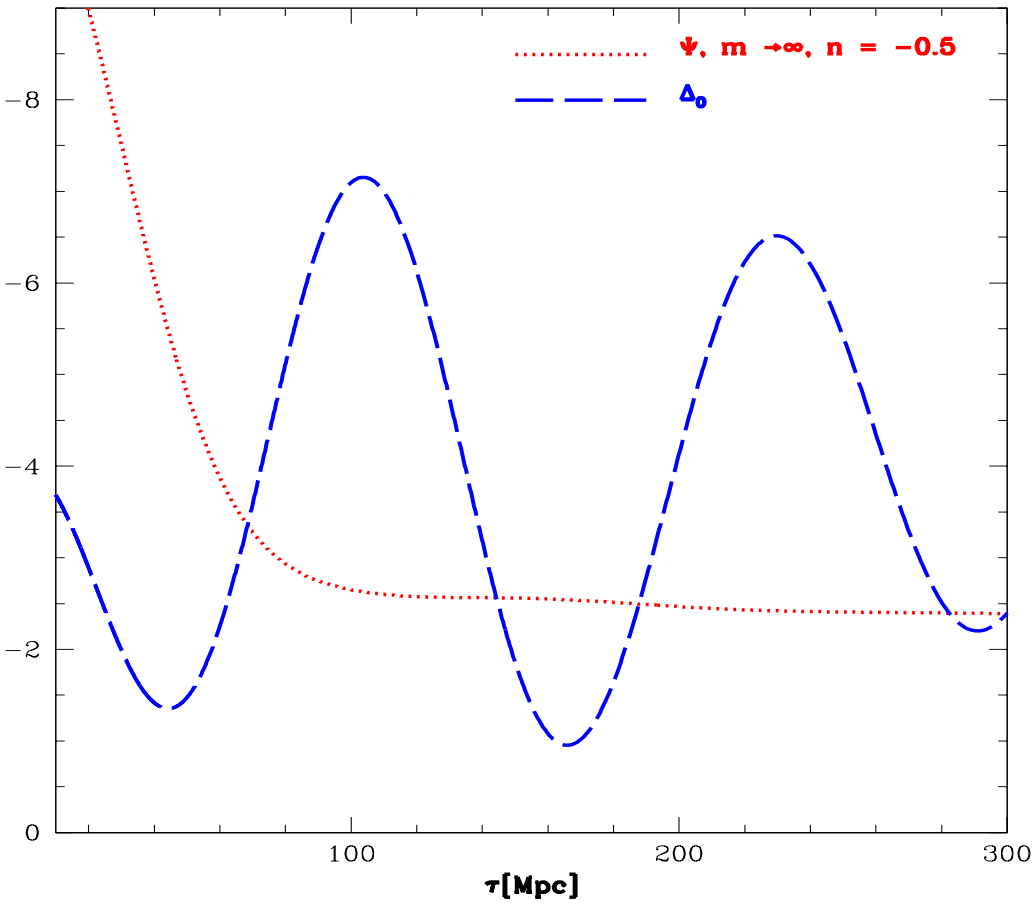

Fig. 5.16 Exact solutions for the potential Ψ and the monopole of the photon fluctuation for the restricted gBDT model with $m \to \infty$ and $n = -0.5$ on the scale k_1 corresponding to the first peak. At early times, the time-varying potentials produce the early ISW effect, this variation couples to the photon mode which behaves as a forced oscillator.

5.4 Constraints On The Effective Scalar-Tensor Theory

5.4.1 Methodology and Analysis

Basically we simply adjust the methodology used in the previous chapter for BDT to be suitable for gBDT. We properly modified the last version of our BDT CAMB for gBDT. The gBDT background was solved exactly and also the linearized equations in the Jordan frame using synchronous gauge variables as with BDT, we carried out our numerical results using a modified version of the CAMB package [186]. We used suitable modification of the first version of CosmoMC including the Planck data to sample the space of parameters of gBDT.

Our chains were long enough to pass the various convergence diagnostics provided in the package and give very accurate 1D and 2D marginalized posteriors. The main datasets we used are from the Planck satellite[4], WMAP9(pol) [175], the South Pole Telescope (SPT) [269] and the Atacama Cosmology Telescope (ACT) [100].

As usual, the chains were generated for both rgBDT and ugBDT models. In both cases the two gBDT parameters m and n were implemented in addition to the basic 6 already described for BDT. The Hubble constant H_0 and the (dimensionless) cosmological constant density ω_Λ are derived parameters as in BDT. Exactly as before, the ugBDT models have one additional parameter which is the initial condition $\bar{\phi}_{ini}$. It turns out that the constraints for the derived parameter ϕ are quite similar to those in BDT. All the other parameters including foreground astronomical parameters, fast parameters, calibration and beam parameters remain the same as in the original code.

We now turn to the issue of priors. For the non-BDT parameters we assume the same priors as for ΛCDM since the two types of cosmological evolution are very similar. A prior on H_0 (HST) from the measurement of the angular diameter distance from SHOES [258] is also imposed for some chains. The priors for the gBDT parameters are flat on $\bar{\phi}_i$, $\ln(m)$ and n. In order to determine the allowed ranges we used the information obtained in the previous chapters about the regions where gBDT resembles to GR. We left a wide range around these central values where these parameters are allowed to vary.

5.4.2 Results and Discussion

Let us first discuss the results for the restricted models, which contain m and n as additional parameters to ΛCDM. We already proved in previous sections that for regions in parameters space of interest, it is reasonable to expect that the restricted and unrestricted models are going to behave similarly. Nevertheless we did sample the space of parameters and obtained estimations for the parameters of both models in order to infer this conclusion a posteriori as we do below.

In the relevant chapter above I already analyzed in detail the effects of these parameters on the CMB at different levels. Now we are going to summarize the different effects studied along the last chapter: at the level of the background, varying m and n changes the expansion rate H in a similar way than in BDT when ω is varied.

In this context, both parameters are degenerate since the change in the expansion history depends on the overall value of ω rather than on each parameter separately. As in BDT, the effective result is a shift of the peak locations and peak heights. In order to single out the effect over the perturbations, we distinguish two regimes at which the theory approximate ΛCDM, the first one is characterized by $m \sim 1$ and $n < 0$ and the other one consists of models with $m \to \infty$ and n taking any value. The second region is theoretically preferred since it corresponds to a very small correction to the growth of LSS in the phenomenological setup of gBDT. In this region, when n is varied two main effects arise: at large scales the temperature anisotropy is enhanced due to the ISW and at intermediate scales, there is a combined effect due to acoustic driving and silk damping affecting intermediate scales which is manifested as a boost in the amplitude of the second and third peaks. Other peaks for higher multipoles feel this effect in less extent.

It turns out that using Planck + WMAP9(pol) alone is not enough, in such case even if the number of samples is huge, the posterior distributions fail to pass the convergence diagnostics within an acceptable level. This lead us to the conclusion that further data was needed to constrain the parameters space. In order to get better results, we added HST and BAO. However, as we will see in short, some remaining degeneracies are still present.

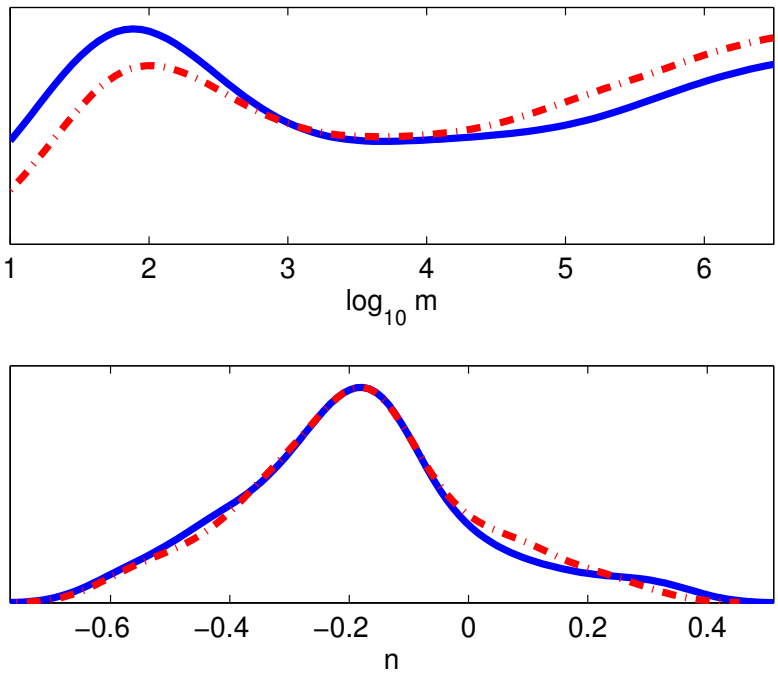

Fig. 5.17 1D marginal posterior distributions for ugBDT(red-dashed) and rgBDT(blue-solid) models with Planck+WMAP9(pol)+BAO+HST. Both sort of models have well defined regions of good likelihood: $m \sim 1$ and $m \to \infty$. According to Planck, the exponent n prefers small negative values which lead to a big integrated value of ω along the expansion history.

In despite that our focus is pointed towards the analysis for the rgBDT models, I am going to compare the posteriors in both types of models only for the baseline data set: Planck+ WMAP9(pol)+BAO+HST only for verify our expectations. We can see that ugBDT and rgBDT 1D marginal posteriors have similar shape [See figure(5.17)]. It is nice to notice that the high-likelihood regions that we foresee in previous sections, clearly are picked by the data in both kind of models.

However we can spot a very small difference: ugBDT prefers the BDT region ($m \to \infty$) while the restricted models get on well with smaller m. This place rgBDT in an interesting place over ugBDT: if we keep in mind the indirect measure of modifications to the growth motivating the phenomenological setup of gBDT, it can be concluded that, according to combined measurements of the CMB by Planck and the expansion history by BAO and HST, a modification of the growth in GR is allowed and it would be of order $(1/m)$ today within 68% of confidence level. Thus, since smaller values of m lead to larger value of the modification to the growth, according to Planck, it is possible to detect deviations which are lesser suppressed in rgBDT than in ugBDT.

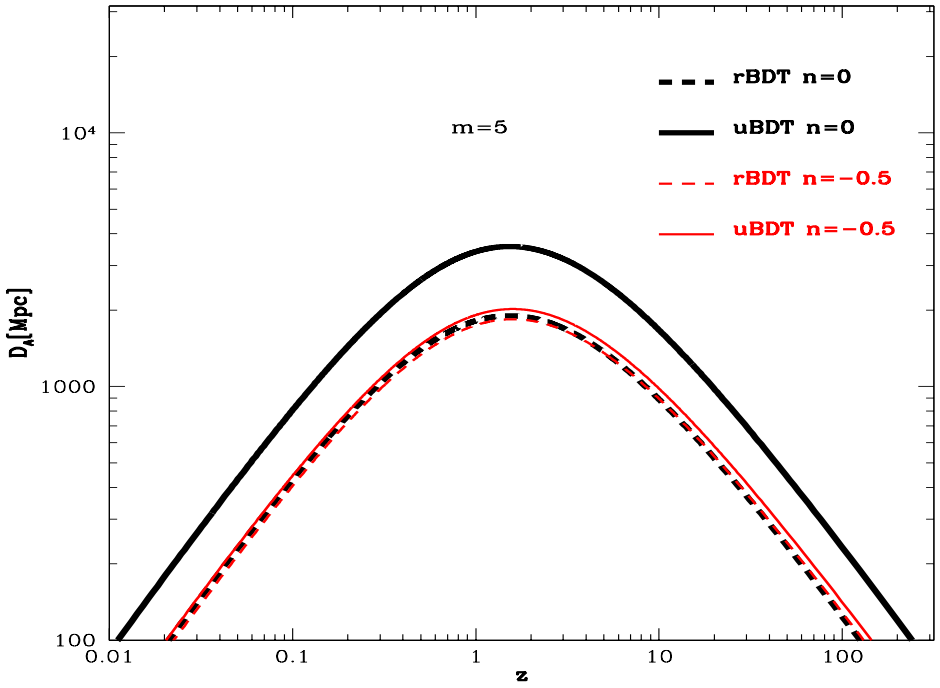

Fig. 5.18 Angular diameter distance as function of the scale factor for different gBDT models.

Different preferred regions of ugBDT and rgBDT are closely related to the different sensitivities of the angular diameter distance to the n parameter of each type of model. Figure (5.18) shows the predicted D_A in both types of models. A possible explanation would be that, once the CMB alone is fitted, the restricted case fits better the D_A measurements from BAO and HST than the unrestricted one.

In order to have a better idea on the features and quality of the 2σ and 1σ estimations for the gBDT parameters, lets have a look to their 2D marginal posteriors. The first outstanding characteristic is a considerable correlation between m and n. At 2σ such the well-constrained direction is well determined, however at 1σ two disconnected constraints arise at different degeneracy directions.

Above $m > 10^4$, the extent of correlation is the same as for 2σ, in turn for $10 < m < 10^3$ the 1σ region(mild orange) bends in complicated way leading to a large correlation between the parameters. From projecting the l.h.s region of the 1σ constraint on vertical axis gives us an estimate for n (table 1). Notice that at 2σ the upper bound moves to larger values due to the leaning shape of the constraint.

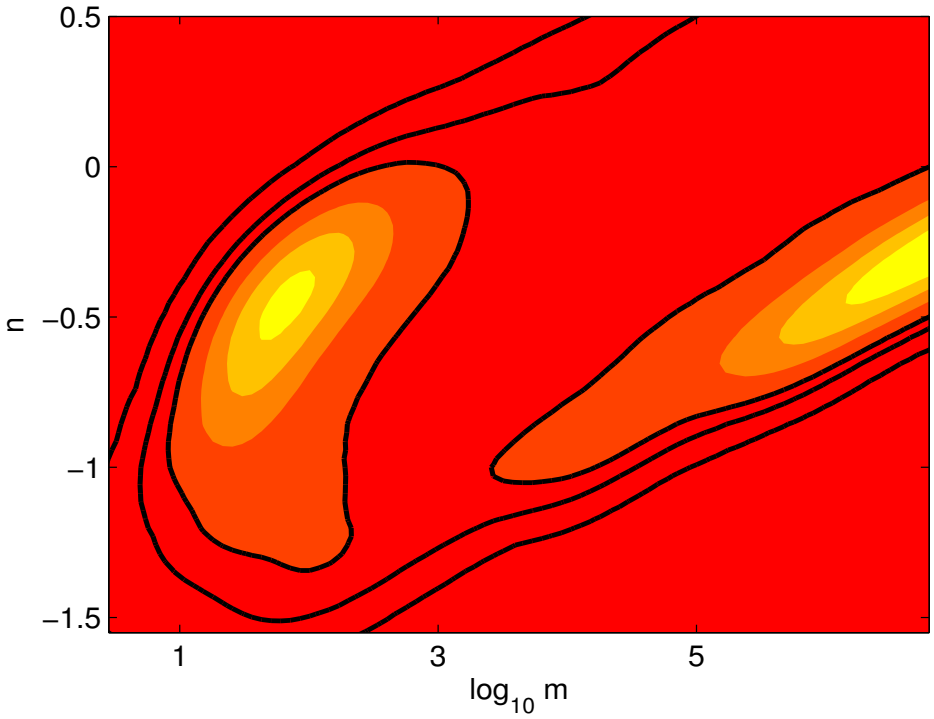

Fig. 5.19 2D constraints of the gBDT parameters with Planck+WMAP9(pol)+BAO+HST.

Constraints of n with Planck+WMAP9(pol)+HST+BAO

CL	mean	lower	upper
68	-0.47	-0.94	-0.15
95	""	-1.39	0.57
99	""	-1.45	0.84.

Results with Planck and other data different than WMAP(pol) give rise to very different constraints. Lets start from analyzing the 1D posteriors (Figure (5.20) for the restricted model for the following datasets: Planck + WMAP9(pol) + High-l and Planck + lensing.

As it happens small scales measurements of the CMB strongly constrain the gBDT parameters, the inclusion of high-l data dramatically changes the shape of the 1D marginal posteriors in comparison to Planck + WMAP9(pol). The well-spotted preferred low-high-m regions vanish for this dataset and the model gets strongly constrained, the lower limit of m is pushed up to the $m \to \infty$ limit while n firmly sticks to the $-1/2$ value and rejects positive values.

For Planck + lensing , the distribution shows us that a wide range of models with intermediate values of m are picked by the data and even though the exponent prefers

negative values, $n < 1$ are not fully rejected as SPT does. It is interesting that lensing does not prefer the limit $m \to \infty$ as expected at first place. The fact that posteriors for Planck + WMAP9(pol) + SPT are tighter than for Planck + lensing tells us something about the extent of sensitivity of this datasets to the gBDT parameters.

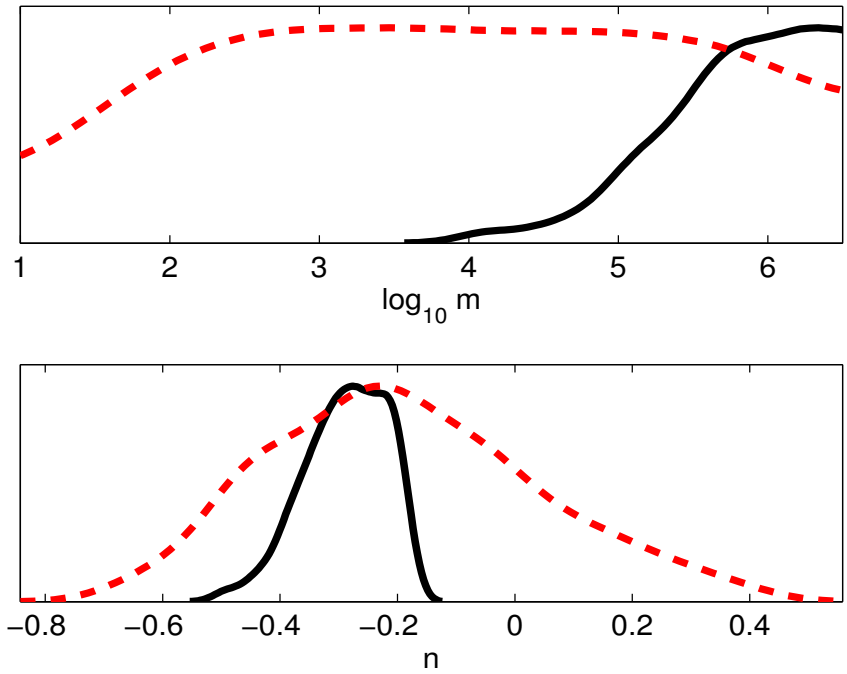

Fig. 5.20 1D posterior for m and n respectively within the restricted model with Planck + WMAP9(pol) + BAO + HST+ LENSING (red) and Planck + WMAP9(pol) + BAO + HST + ACT+SPT (black). Bottom: The inclusion of lensing gives rise to weak estimates of n whilst by adding the high-l data from ACT and SPT, the constraints become very strong. Top: the inclusion of lensing doesn't improve significantly the lower limit for m. Models with very large m, which were in principle expected to be close to ΛCDM, seem to be less likely than others with lower m; further analysis is needed in order to determine the reason why this happens. In contrast, when small-scales measurements are included, the lower limit of m is very well constrained.

5.5 Conclusion

The growth of LSS assumed in the phenomenological setup for modified theories of gravity considered here is assumed to behave as a power law $\mu = \mu_0(1 + ra^s)$. There is a correspondence between this setup and the effective scalar-tensor theory with $\omega(a) + 3/2 = m\, a^n$ where $m = 1/2r\mu_0$ and $n = -s$. We tested indirectly the free parameters involved using cosmological observations different to LSS. The main data set is the CMB anisotropies from Planck and tests of the expansion history from BAO and HST, that give rise to the 1σ constraint of $n = -0.47^{+0.32}_{-0.47}$ and two regions for m: $m = 50.1 \pm 11.2$ and $m > 3.2 \times 10^3$. The fact that the first of these regions is likely has an interesting consequence: according to the CMB, BAO and HST, the growth of LSS is allowed to hold a modification today of order $\sim 10^{-3}$ which is not negligible.

CHAPTER 6

THE PARAMETRIZED POST NEWTONIAN-VAINSHTEINIAN FORMALISM

6.1 Introduction

First of all, I would like to acknowledge that great part of this chapter is product of the joint research work with Costas Skordis, Antonio Padilla and Paul Saffin to be published soon. General Relativity (GR) is a very successful theory since it passes all the solar-system tests with great accuracy [330, 331]. Any other theory of gravity is strongly challenged to agree with this predictions. However, the question of whether GR is the correct theory for describing all gravitational phenomena in nature still stands without a satisfactory answer. Indeed, experimental gravitation is a very active field in physics nowadays, to goal is to increase the precision of gravitational tests and also to push the boundaries where these tests have been carried out.

Since the whole "space" of gravitational theories is vast, perhaps infinite, it is convenient to construct a "master theory", a framework, which comprehend a wide range of theories. Different theories would then correspond to a specific set of parameters of this framework. Examples are the Parametrized Post-Newtonian (PPN) [229, 329, 332], the Parametrized Post-Keplerian (PPK) [85], and the Parametrized Post-Einsteinian (PPE) [79, 192, 340] formalisms. In the cosmological regime we also have the various simplified parametrized approaches [279, 345], the small-scale parametrized approach [11] as well as more complete frameworks such as the Hu-Sawicki Parametrized Post-Friedmannian formalism [153, 154], the Parametrized Post-Friedmannian (PPF) formalism [22, 23, 280] [1], the effective fluid [29, 30] and effective field theory formalisms [39, 138, 248].

[1] Although [154] and [23] use the same acronym, the two formalisms are widely different.

Tests of gravity in the solar system have achieved astonishing precision. With the help of the PPN formalism, solar system tests such as lunar laser ranging and Doppler tracking of the Cassini spacecraft have set strong bounds on the PPN parameters around $10^{-3} - 10^{-5}$ for curvature effects and $10^{-7} - 10^{-20}$ for preferred frame effects [331]. However, the PPN formalism (as well as the PPE formalism) has as a basic assumption that the spacetime away from a source is asymptotically flat. Typically, metric theories of gravity treated with the PPN formalism, have a classical strong field regime characterized by the Schwarzschild radius. For compact relativistic sources like neutron stars or black holes, the strong gravitational fields arise at scales $\sim r_s$ close to the massive source whilst the geometry of spacetime is asymptotically flat far away from it. However, there are other metric theories for which this basic assumption cannot be implemented directly.

Those theories have the property that the additional degrees of freedom to the metric become classically strongly coupled at some distance away from the source. This makes it impossible to construct a perturbative expansion (as the PPN requires) valid all the way towards infinity. The importance of such theories has been put forward in chapter 1, let us briefly recall that they arise in an intend of introducing departures from GR in the cosmological regime, i.e. in the limit of ultra-low curvatures and potentials. They aim to explain cosmic acceleration as a modification of gravity. One possibility to explain cosmic acceleration is to modify the theory of gravity on cosmological scales by including new degrees of freedom which make gravity behave rather differently from GR on ultra low curvatures. However, since the solar system data indicate that gravity is described by GR to a very good approximation, these degrees of freedom must somehow be hidden on the scale of the solar system.

A way to accomplish this is to make these degrees of freedom become strongly coupled close to massive sources. The mechanism by which this happens is called the Vainshtein mechanism [20, 313]. We saw in chapter 1 that examples of such theories are the so-called Galileon Theories and the massive gravity theories. However, the "screening" of these new degrees of freedom is not perfect, and some residuals can in principle be detected. In this chapter we aim to present an extension of the PPN framework, the Parametrised Post-Newtonian Vainshteinian (PPNV) framework which is able to handle Vainshteinian corrections and thus establishing the way for determining the compatibility of such theories with solar system and other strong-field data.

We should mention that this work is not the only attempt to explore the physics behind these theories at the solar system and strong-field regimes. For instance, in

other context different to PPN, first works towards this direction were made in [50] in the particular case of the static spherically symmetric source. Other more general approach to the problem of gravitational radiation in these models was proposed in [14, 72]. Finally within the PPN conditions, in [163] they deal with low-density stars with slow rotation and static relativistic stars by applying a perturbative approach, this proposal is similar to our PPNV approach, however it is restricted to the static spherically symmetric source and it is only developed up to the corresponding $O(2)$ in PPN.

This chapter is organised as follows. We first describe the PPN framework followed by a short description of the Vainshtein mechanism. We then outline how the PPN formalism has to be modified in order to include Vainshteinian corrections. As we will show further below, there are two separate perturbative regimes, one inside the Vainshtein radius and one outside, which must be handled separately. We then take the cubic galileon theory as an example and perform the calculation in the two regimes. We finish by considering spherical symmetry as a special case.

6.2 The PPNV Expansion: Vainshteinian Correction to the PPN Formalism

6.2.1 The Standard Post-Newtonian Approximation

The PPN formalism is a prescription for a perturbative expansion of the gravitational, matter and additional field equations of motion in successive orders of a small parameter, the velocity of matter V (in units of the speed of light). Such expansion is valid in the weak field regime for non-relativistic sources for which the spacetime geometry is nearly Minkowskian. In this prescription, small but detectable relativistic effects are introduced by the corrections in terms of V. It was developed by Nordtvedt[229] and later expanded refined by Will [329] and Will and Nordtvedt [332].

In PPN, one assumes that gravity is a geometric phenomenon and is described by a metric $g_{\mu\nu}$ and that matter only "sees" this metric $g_{\mu\nu}$ and follows its geodesics. Specifically this means that if $T_{\mu\nu}$ is the stress-energy tensor for matter then

$$\nabla_\mu T^\mu_\nu = 0 \tag{6.1}$$

where ∇_μ is the covariant derivative compatible with $g_{\mu\nu}$. However, the metric $g_{\mu\nu}$ may not be the only gravitational field. For instance, there may be additional scalar

fields to the metric that mediate the gravitational force (as is in our case), however, these fields are not involved in the equations of motion for matter.

To carry out the formalism, one starts by expanding the metric $g_{\mu\nu}$ around Minkowski spacetime $\eta_{\mu\nu}$ as

$$g_{\mu\nu} = \eta_{\mu\nu} + h_{\mu\nu} \tag{6.2}$$

When doing explicit calculations, we shall adopt the convention that the metric has signature $+2$. Lets recall that the Newtonian theory of gravitation suffices to explain all the phenomena in most of the solar systems for an accuracy less than about 10^{-5}. The metric perturbation $h_{\mu\nu}$ is further expanded in successive orders dictated by a small parameter: the velocity of matter v (we will assume units where the speed of light is unity). Thus, the PPN is a small velocity expansion and is valid for gravitational fields generated by slowly moving matter in comparison to the speed of light.

The first correction to Minkowski spacetime is the Newtonian potential

$$U \equiv \int \frac{\rho(\mathbf{x}',t)}{|\mathbf{x}-\mathbf{x}'|} d^3x' \qquad \Leftrightarrow \qquad \vec{\nabla}^2 U = -4\pi\rho \tag{6.3}$$

generated by the rest-mass density of matter ρ. This potential generates acceleration $\mathbf{a} = G_N \vec{\nabla} U$ where G_N is the measure Newton's constant by an experiment on the Earth. Thus, virial relations lead to the relation $v^2 \sim U$, implying that the Newtonian potential has a PPN order $O(2)$. In particular for spherical symmetry, we have that $2G_N U = \frac{r_s}{r} \ll 1$ where $r_s = 2G_N M$ is the Schwarzschild radius of a source with mass M. Moreover the acceleration equation gives the PPN order for derivatives, i.e. spatial derivatives leave the PPN order unchanged while time derivatives have a PPN order $\frac{\partial}{\partial t} \sim O(1)$.

Matter variables are also associated with a PPN order. The matter rest-mass density ρ has a PPN order $O(2)$ as is implied by (A.2). In addition to the density, matter sources may also have specific energy density Π (equal to the ratio of the matter total energy density to its rest-mass density ρ) and pressure P. In this prescription matter is assumed to behave as a perfect fluid so that the matter stress-energy tensor is given by

$$T_{\mu\nu} = (\rho + \rho\Pi + P) u_\mu u_\nu + P g_{\mu\nu} \tag{6.4}$$

where the velocity four-vector is normalized as $g_{\mu\nu} u^\mu u^\nu = -1$. Since the pressure is generally smaller than the gravitational energy of matter $\sim \rho U$ then we associate it with a PPN order $P \sim O(4)$. Similar considerations apply to the specific energy density Π which is associated with a PPN order $\Pi \sim O(2)$.

The evolution of the matter fluid is determined by the continuity and Euler equations of motion which are obtained from (6.1) by expanding in PPN orders.

Clearly, (6.4) implies that $O(4)$ terms would appear in the (generalized) Einstein equations, thus we need to include these terms in the metric perturbation. The required order for the metric perturbation components is found to be [326]

$$\begin{aligned} h_{00} &= h_{00}^{(2)} + h_{00}^{(4)} \\ h_{0i} &\sim O(3) \\ h_{ij} &\sim O(2) \end{aligned}$$

where the superscript number in the parenthesis denotes the PPN order of a particular term. In the standard PPN formalism one has that $h_{00}^{(2)} = 2G_N U$, however, as we shall see further below, in the PPNV framework the Vainshteinian corrections contribute to $h_{00}^{(2)}$ in the form of new Vainshteinian potentials. Furthermore, in the standard PPN gauge, one has $h_{ij} = 2G_N \gamma U \delta_{ij}$ where γ is one of the PPN parameters. In the PPNV example we consider below, one still has that $h_{ij} \propto \delta_{ij}$, however, h_{ij} is no longer proportional to $h_{00}^{(2)}$ as in PPN due to the appearance of new Vainshteinian potentials. We shall show that PPNV introduces new parameters which are not part of the standard PPN parameters.

In general, the PPN formalism starting point is the action of a neutral single particle given by

$$\begin{aligned} I_p &= -m_0 \int dt \left(g_{\mu\nu} \frac{dx^\mu}{dt} \frac{dx^\nu}{dt} \right)^{\frac{1}{2}}, \\ &= -m_0 \int dt (-g_{00} - 2g_{0j} v^j - g_{jk} v^j v^k)^{\frac{1}{2}}. \end{aligned} \tag{6.5}$$

(6.6)

Thus, in order to add first order corrections to the newtonian leading order description, we need to compute different components of the metric (and consequently the corresponding components of the Einstein equations as well) up the following orders

$$\begin{aligned} g_{00} &\quad \text{Up to} \quad O(4), \\ g_{0j} &\quad \text{Up to} \quad O(3), \\ g_{ij} &\quad \text{Up to} \quad O(2). \end{aligned}$$

We also shall require some components of the matter-energy tensor. T_{00} is required up to $O(4)$ which corresponds to

$$T_{00} = \rho(1+\Pi+v^2-2GU) \tag{6.7}$$

and T_{0i} to $O(3)$ given by

$$T_{0i} = \rho v_i \tag{6.8}$$

We shall also need the trace $T = T^{\mu}_{\mu}$ which to $O(4)$ is

$$T = -\rho(1+\Pi)+3P. \tag{6.9}$$

We need the R_{00} equation and Riemann tensor up to $O(4)$, the R_{ij} ones up to $O(2)$ and the R_{0i} up to $O(3)$. Thus the following quadratic expansions are going to be useful

$$R_{00} = -\frac{1}{2}\left(\nabla^2 h_{00} + (h_{jj,00} - 2h_{0j,0j}) - h_{00,j}(h_{jk,k} - \frac{1}{2}h_{kk,j}) + \frac{1}{2}(\nabla h_{00})^2 - h_{jk}h_{00,jk}\right), \tag{6.10}$$

$$R_{i0} = -\frac{1}{2}\left(\nabla^2 h_{0i} - h_{k0,ik} + h_{kk,0i} - h_{ki,0k}\right), \tag{6.11}$$

$$R_{ij} = -\frac{1}{2}\left(\nabla^2 h_{ij} - h_{00,ij} + h_{kk,ij} - h_{ki,kj} - h_{kj,ki}\right). \tag{6.12}$$

The framework uses a nearly Lorentz coordinate system in which the coordinates are (t, x_1, x_2, x_3). Three dimensional Euclidean vector notation is used throughout. The coordinate arbitrariness or gauge freedom is usually removed by specification of the coordinates by the standard PPN gauge [see appendix (A)] In the standard PPN formalism, arbitrary PPN parameters are introduced in front of each post-Newtonian term in the metric. Ten parameters are needed and they are denoted as : $\gamma, \beta, \hat{\xi}, \alpha_1, \alpha_2, \alpha_3, \zeta_1, \zeta_2, \zeta_3$[2]. In terms of them the metric reads

[2]One needs to be careful so not to confuse $\hat{\xi}$ with ξ denoting the rescaling of G_N along the previous chapters.

$$
\begin{aligned}
g_{00} &= -1+2GU-2\beta G^2U^2-2\hat{\xi}\Phi_W+(2\gamma+2+\alpha_3+\zeta_1-3\hat{\xi})\Phi_1 \\
&+ 2(3\gamma-2\beta+1+\zeta_2+\hat{\xi})\Phi_2+2(1+\zeta_3)\Phi_3+2(3\gamma+3\zeta_4-2\hat{\xi})\Phi_4 \\
&- (\zeta_1-2\hat{\xi})\mathscr{A} \\
g_{0j} &= -\frac{1}{2}(4\gamma+3+\alpha_1-\alpha_2+\zeta_1-2\hat{\xi})V_j-\frac{1}{2}(1+\alpha_2-\zeta_1+2\hat{\xi})W_j, \\
g_{ij} &= (1+2\gamma GU)\delta_{ij}. \qquad (6.13)
\end{aligned}
$$

The PPN solutions of the metric of a wide set of metric theories of gravity can be written in terms of these PPN potentials whose definitions are displayed in appendix (A). Particular PPN parameters are obtained for different metric theories. In any case, these parameters are fully written in terms of the corresponding theoretical parameters involved in the model. Since, different linear combinations of the PPN parameters are directly related with measurable quantities involved in different tests, the PPN formalism provides a powerful tool to set constraints on the theoretical parameters by using measurements of the PPN parameters, see [326] for further details.

Let us now discuss the Vainshtein mechanism and the modifications it introduces to the standard PPN formalism, leading to the PPNV expansion.

6.2.2 Vainshtein Mechanism for a Spherically Symmetric Source

As we already discussed in the previous subsection, the metric theories treated with the standard PPN formalism (e.g. GR or Brans-Dicke [326]) have a single expansion parameter given by $v^2 \sim \frac{r_s}{r}$. In contrast, the non-linearities of the scalar field in theories with a Vainshtein mechanism (such as the Galileon theories) introduce new regimes that must be handled along with PPN. These Vainshteinian thresholds are associated with an extra expansion parameter $\frac{r}{r_V}$ which accounts for new physical effects associated with the new scale introduced in these theories, the Vainshtein scale r_V.

There is a simple way of thinking about this different regimes. The ratio $\frac{r_s}{r} \ll 1$ accounts for the non-relativistic nature of the matter sources considered in the PPN approximation while the ratio $\frac{r}{r_v}$ determines whether the observer is placed either inside or outside the Vainshtein radius r_V and how far from the source (or close to r_v) and consequently how important the Vainshteinian corrections are. Clearly, we must then consider two regimes: inside the Vainshtein radius so that $\frac{r}{r_V} \ll 1$ and outside the Vainshtein radius where $\frac{r}{r_V} \gg 1$. These two regimes must be treated separately.

In order to illustrate how the Vainshtein mechanism operates let us consider static spherically symmetric solutions in the cubic Galileon theory in the Einstein frame. The metric $g_{\mu\nu}$ that enters (6.1) is a combination of the Einstein metric $\tilde{g}_{\mu\nu}$ and the scalar field χ (assumed dimensionless) as $g_{\mu\nu} = e^{2\chi}\tilde{g}_{\mu\nu}$. Thus, considering weak fields on Minkowski spacetime the effective gravitational potential would be $h_{00} = \tilde{h}_{00} - 2\chi = \frac{2GM}{r} - 2\chi$. The scalar equation of motion for a spherically symmetric source of mass M centered at $r = 0$ is

$$\frac{2\omega+3}{r^2}\frac{d}{dr}\left[r^2\chi'\right] + \frac{8\alpha}{r^2}\frac{d}{dr}\left[r(\chi')^2\right] = GM\frac{\delta(r)}{r^2} \tag{6.14}$$

where

$$\alpha = \frac{M_p}{8\Lambda^3} \tag{6.15}$$

Now (6.14) can be integrated once to give

$$(2\omega+3)r^2\chi' + \alpha r(\chi')^2 = GM. \tag{6.16}$$

Thus, solving for χ' we find

$$\chi' = \frac{2\omega+3}{16\alpha}r\left[-1+\sqrt{1+\frac{32GM\alpha}{(2\omega+3)^2r^3}}\right] \tag{6.17}$$

where the plus sign in front of the square root is chosen so that no divergence appears when $\alpha \to 0$. We can distinguish are two limiting cases. First, as $\alpha \to 0$, or , when $\frac{32GM\alpha}{(2\omega+3)^2r^3} \ll 1$ then

$$\chi = -\frac{GM}{(2\omega+3)r} + \frac{(GM)^2}{(2\omega+3)^3}\frac{2\alpha}{r^4} + \ldots \tag{6.18}$$

Second, the opposite limit as $\alpha \to \infty$, or in other words, when $\frac{32GM\alpha}{(2\omega+3)^2r^3} \gg 1$ then

$$\chi = \sqrt{\frac{GM}{2\alpha}}r^{1/2} \tag{6.19}$$

where the integration constant is ignored as it can be rescaled away by a coordinate transformation. The turning point from one limit to the other, occurs when $\frac{32GM\alpha}{(3+2\omega)^2r^3} = 1$, i.e. at a radius $\frac{1}{(2\pi)^{1/3}(3+2\omega)^{2/3}}r_V$ where r_V is given by

$$r_V = \frac{1}{\Lambda}\left[\frac{M}{M_p}\right]^{1/3} \tag{6.20}$$

r_V is called the Vainshtein scale and will play a fundamental role in what follows. The Vainshtein mechanism is now clear. For small distances away from the source, $r \ll r_V$, the spherically symmetric solution for the cubic galileon is

$$\chi_{in} \sim \frac{r_s}{r}\left[\left(\frac{r}{r_v}\right)^{3/2} + C_{in}\left(\frac{r}{r_v}\right)^{3} + \dots\right] \tag{6.21}$$

while for large distances away from the source, $r \gg r_V$, it is

$$\chi_{out} \sim \frac{r_s}{r}\left[1 + C_{out}\left(\frac{r_V}{r}\right)^{3} + \dots\right] \tag{6.22}$$

where $C_{in/out}$ are constants of $O(1)$ which are not relevant for our explanation in this subsection, they are going to be determined explicitly further below. On large scales the solution of the galileon has the same profile as the newtonian potential, whilst in small scales it hides by being suppressed by factor of $\frac{r}{r_V}$. Note that with r_V now defined, the α parameter can be written as $\alpha \sim \frac{r_V^3}{r_s}$

A simple picture of how the Vainshtein mechanism operates is the following: the leading Newtonian profile of the galileon at large scales starts to deform as the observer moves down to the Vainstein radius, once she/he has passed across the r_v scale the non-linearities are turned on making the Newtonian profile to hide away by suppressing it more and more as she/he moves closer to the source. In the next subsection we formalise the treatment above and consider general theories with Vainshtein mechanism. In particular we shall see how the Vainshtein scale and the expansion parameter α emerge and what impact this can have on the PPNV expansion.

6.2.3 Paving the Way Towards PPNV: the Vainshtein Order

To develop a Parametrised Post-Newtonian Vainshteinian (PPNV) formalism, we must first understand some of the generic features of modified gravity theories with Vainshtein screening. The modification of gravity is normally associated with a light scalar degree of freedom which strongly affects the dynamics on cosmological scales when linearised perturbation theory is valid. However, in the presence of a heavy relativistic source, linearised perturbation theory breaks down at some macroscopic scale due to derivative self interactions of the new field χ.

Let us illustrate this with a generic example, schematically described by an action in the Einstein frame:

$$S \sim \int d^4x \left\{ M_p^2\sqrt{-g}R - (\partial\chi)^2 + O(\chi) + M_p h_{\mu\nu}\bar{O}^{\mu\nu}(\chi) + h_{\mu\nu}T^{\mu\nu} + \frac{\chi}{M_p}T \right\} \tag{6.23}$$

where $M_p^2 = \frac{1}{8\pi G}$ and where in general $G/G_N \sim O(1)$ (usually the measured Newtonian strength G_N is not equal to the bare gravitational strength G in the action but is typically related to it by an $O(1)$ quantity). This schematic form encompasses a number of modified gravity scenarios in the so-called decoupling limit, including dRGT massive gravity [89]. The canonical scalar field is coupled directly to matter with gravitational strength, but the Vainshtein mechanism is made possible by the derivative interactions between the scalar and the graviton and/or the self interactions. Assuming for the moment a unique strong coupling scale, Λ, we have that these operators contain terms like

$$O(\chi) \supset \frac{\partial^{2m}\chi^n}{\Lambda^{2m+n-4}}, \qquad \bar{O}^{\mu\nu}(\chi) \supset \frac{\partial^{2\bar{m}}\chi^{\bar{n}-1}}{\Lambda^{2\bar{m}+\bar{n}-4}} \tag{6.24}$$

where the integers $m, \bar{m} \geq 1,\ n, \bar{n} \geq 3$. The strong coupling scale marks the breakdown of perturbative unitarity, and in principle one may have to include a whole tower of higher dimensional operators to preserve unitarity at higher energies.

For a static and spherically symmetric profile, the classical potentials at large distances from a heavy source of mass M are simply Newtonian, $M_p h^c_{\mu\nu} \sim \chi^c_{lin} \sim \frac{M}{M_p}\frac{1}{r}$. Assuming this Newtonian behaviour, the interactions in (6.24) would become comparable with the leading order canonical terms when

$$\frac{1}{\Lambda^{2m+n-4}}\frac{1}{r^{2m}}\left(\frac{M}{M_p}\frac{1}{r}\right)^n \sim \frac{1}{r^2}\left(\frac{M}{M_p}\frac{1}{r}\right)^2 \implies r \sim \frac{1}{\Lambda}\left(\frac{M}{M_p}\right)^{\frac{n-2}{2m+n-4}}$$

with similar expressions for the barred integers. We see that in general different interactions yield different macroscopic scales. As a first pass in developing the post-Vainshteinian for- malism, let us only consider scenarios in which there is a unique macroscopic scale beyond the Schwarzschild radius, so that all nonlinear interactions become important at the same scale. This would be true for combinations of galileon interactions suppressed by the same strong coupling scale, for example. Generalisations that take care of multiple macroscopic scales, and multiple expansion parameters will be left for future study. Therefore, for the set of theories under consideration, there is a unique macroscopic scale of interest, which we identify with the Vainshtein radius,

$$r_V \sim \frac{1}{\Lambda}\left(\frac{M}{M_p}\right)^s, \qquad s = \max\left\{\frac{n-2}{2m+n-4}, \frac{\bar{n}-2}{2\bar{m}+\bar{n}-4}; n, m \in O(\chi), \bar{n}, \bar{m} \in \bar{O}^{\mu\nu}(\chi)\right\} \tag{6.25}$$

signaling the breakdown of classical perturbation theory. This is how the strong coupling manifests itself classically.

Let us recall that in the PPN formalism the leading order contribution is the Newtonian potential, satisfying $\nabla^2 U = -4\pi G_N \rho$ and is defined to be $O(2)$ in PPN. The orders of velocities and time derivatives are then inferred using the virial ($v^2 \sim U$) and Euler ($\partial_t \sim v \cdot \nabla$) relations. In the spherically symmetric scenario described above, we note that $U \sim \frac{r_s}{r}$, where $r_s \sim M/M_p^2$ is the Schwarzschild radius of the source, so there is a sense in which the PPN expansion is an expansion in $\sqrt{\frac{r_s}{r}}$. Similarly, we shall think of PPV as an expansion in $\left(\frac{r}{r_V}\right)^{\frac{3}{2}}$.

Although our analysis here is generic, the exponent 2 is ultimately motivated by the cubic galleon scenario. This is a sensible starting point since the cubic galleon is the lowest dimensional operator corresponding to a purely derivative self-interaction of a single scalar in a Lorentz invariant theory.

To gain further insight, consider what happens deep inside the Vainshtein radius. If the scalar dynamics is dominated by a pure interaction term, we would have

$$\frac{\partial^{2m}(\chi^c_{nonlin})^{n-1}}{\Lambda^{2m+n-4}} \sim \frac{T}{M_p}$$

for some m, n, and so for a static spherically symmetric configuration,

$$\frac{\chi^c_{nonlin}}{M_p} \sim \left(\frac{r}{r_V}\right)^{\frac{2m+n-4}{n-1}} \left(\frac{r_s}{r}\right).$$

This suggests that the scalar part of the physical metric that couples to matter is (2) in PPN and $\left(\frac{2}{3}\left[\frac{2m+n-4}{n-1}\right]\right)$in PPV. However, if the deep Vainshteinian behaviour is dominated by a mixed interaction then we would schematically have

$$M_p h_{\mu\nu} \frac{\partial^{2\bar{m}}(\chi^c_{nonlin})^{\bar{n}-2}}{\Lambda^{2\bar{m}+\bar{n}-4}} \sim \frac{T}{M_p}$$

for some $\bar{m}, \bar{n}$. For a static spherically symmetric configuration in which screening is effective, we expect $M_p h_{\mu\nu} \sim \frac{T}{M_p}$, and so

$$\frac{\chi^c_{nonlin}}{M_p} \sim \left(\frac{r}{r_V}\right)^{\frac{2\bar{m}+\bar{n}-4}{\bar{n}-2}} \left(\frac{r_s}{r}\right)$$

This now suggests that the scalar part of the physical metric that couples to matter is (2) in PPN and $\left(\frac{2}{3}\left[\frac{2\bar{m}+\bar{n}-4}{\bar{n}-2}\right]\right)$ in PPV.

The previous paragraph indicates two important things: (i) that even in the deep Vainshteinian region the leading order behavior of the physical metric is Newtonian, as it should be; and (ii) that what we really have here is a double expansion, owing to the

hierarchical difference between the the Vainshtein radius and the Schwarzschild radius. To this end we assign a combined order (N,V) to a quantity that is order N in PPN, and order V in PPV. In terms of Schwarzschild and Vainshtein radii, we may think of

$$(N,V) \sim \left(\frac{r_s}{r}\right)^{\frac{N}{2}} \left(\frac{r}{r_V}\right)^{\frac{3V}{2}}.$$

Thus, U and χ^c_{lin} are $(2,0)$, whilst χ^c_{nonlin} is

$$\left(2, \tfrac{2}{3}\left[\tfrac{2m+n-4}{n-1}\right]\right) \quad \text{or} \quad \left(2, \tfrac{2}{3}\left[\tfrac{2\bar{m}+\bar{n}-4}{\bar{n}-2}\right]\right),$$

depending on whether it is a pure scalar, or a mixed interaction that dominates the deep Vainshteinian region. PPN can be thought of as a expansion in the Schwarzschild radius, and is therefore equivalent to an expansion in the source. Similarly PPNV can be thought of as an expansion in Schwarzschild and Vainshtein radii, and for practical purposes this is best realised in terms of an expansion in the source, and an operator, α, that is independent of the source, but which carries PPV order. Given the Vainshtein radius (6.25), there is only one candidate for α (or powers thereof) , namely:

$$\alpha \sim M_p/\Lambda^{1/s}. \tag{6.26}$$

It is easy to see that α is $\left(-2,-\frac{2}{3s}\right)$. Operators containing powers of Λ should now be rewritten in terms of α. We will also assume that velocities are always determined by the virial relation with the Newtonian potential, since the scalar potential never dominates over the (Einstein frame) graviton if screening is active. The rules of the game are therefore as follows: the orders for velocities ($v \sim (1,0)$), time derivatives ($\partial_t \sim (1,0)$), space derivatives $\partial_i \sim (0,0)$, total energy density $\rho \sim (2,0)$, specific energy density ($\Pi \sim (2,0)$), and pressure $p \sim (4,0)$ are inherited from PPN [326], and do not care about the PPV expansion. The only operator to carry PPV order now is $\alpha \sim \left(-2,-\frac{2}{3s}\right)$.

For a given theory, we write the action explicitly in terms of α, and study the resulting field equations order by order in the double expansion. Schematically, for our generic example, we have

$$S \sim \int d^4x \left\{M_p^2\left[\sqrt{-g}R - (\partial\chi)^2 + P(\chi) + h_{\mu\nu}\bar{P}^{\mu\nu}(\chi)\right] + h_{\mu\nu}T^{\mu\nu} + \chi T\right\} \tag{6.27}$$

where we have rescaled $\chi \to M_p\chi$, and

$$\begin{aligned} P(\chi) &= \frac{O(M_p\chi)}{M_p^2} \supset \alpha^{n-2}(\alpha/M_p)^{(n-1)\varepsilon}\partial^{2m}\chi^n, \\ \bar{P}^{\mu\nu}(\chi) &= \frac{\bar{O}^{\mu\nu}(M_p\chi)}{M_p} \supset \alpha^{\bar{n}-2}(\alpha/M_p)^{(\bar{n}-2)\bar{\varepsilon}}\partial^{2\bar{m}}\chi^{\bar{n}-1} \end{aligned} \tag{6.28}$$

Recall that we have assumed each interaction has the unique value of $s = \frac{n-2}{2m+n-4}, \frac{\bar{n}-2}{2\bar{m}+\bar{n}-4}$ where $m,n \in (\chi)$ and $\bar{m},\bar{n} \in \bar{O}^{\mu\nu}(\chi)$. The PPNV analysis is straightforward beyond the Vainshtein radius where the leading order contributions are purely Newtonian i.e. zeroth order in PPV, and corrections carry *negative* PPV order as higher order terms in α begin to kick in. These corrections generate new classes of PPV potentials, and a complete formalism should include all possibilities, or at the very least, all possibilities that are relevant to models that appear in the literature.

In contrast, deep inside the Vainshtein radius, the leading behavior should again be Newtonian but with corrections carrying *positive* PPV order, requiring terms proportional to inverse powers of α. However, the action expressed in (6.27) is not well suited to an expansion in terms of these inverse powers. This is where the so-called *classical dual* [132, 233] comes in. For our schematic action (6.27), there exists a dual action describing the same classical physics [233]

$$\begin{aligned} S \sim \int M_p^2 \Bigg\{ \sqrt{-g}R - (\partial\chi)^2 + \sum_{r=0}^{r_{\max}} \left[\frac{\partial F}{\partial A_{\mu_1\ldots\nu_r}} + h_{\alpha\beta}\frac{\partial \bar{F}^{\alpha\beta}}{\partial A_{\mu_1\ldots\nu_r}} \right] \nabla_{i\mu_1}\ldots\nabla_{\mu_r}\chi \\ + \alpha^{-st}\left[F - \sum_r^{r_{\max}} \frac{\partial F}{\partial A_{\mu_1\ldots\mu_r}} A_{\mu_1\ldots\mu_r} \right] + \alpha^{-st} h_{\alpha\beta}\left[\bar{F}^{\alpha\beta} - \sum_r^{r_{\max}} \frac{\partial \bar{F}^{\alpha\beta}}{\partial A_{\mu_1\ldots\mu_r}} A_{\mu_1\ldots\mu_r} \right] \Bigg\} \\ + h_{\mu\nu}T^{\mu\nu} + \chi T \end{aligned} \tag{6.29}$$

where $r_{\max}$ is the largest value of $2m$, and

$$t = \max\left\{ \frac{2m+n-4}{n-1}, \frac{2\bar{m}+\bar{n}-4}{\bar{n}-2}; n,m \in O(\chi), \bar{n},\bar{m} \in \bar{O}^{\mu\nu}(\chi) \right\} \tag{6.30}$$

We also have combinations of polynomials in the auxiliary fields $A_{\mu_1\ldots\mu_r}$, i.e.

$$F \supset F_n(A, A_\mu, \ldots), \qquad \bar{F}^{\alpha\beta} \supset \bar{F}^{\alpha\beta}_{\bar{n}-1}(A, A_\mu, \ldots) \tag{6.31}$$

where F_n is order n in the auxiliary fields, while $\bar{F}^{\alpha\beta}_{\bar{n}-1}$ is order $(\bar{n}-1)$. These polynomials stem from the interactions given shown in (6.28). Introducing

$$\delta(m,n) = \frac{n-1}{2m+n-4}\left(t_{\text{-}}\frac{2m+n-4}{n-1}\right) \geq 0 \qquad \forall n,m \in O(\chi) \tag{6.32}$$

$$\bar{\delta}(\bar{m},\bar{n}) = \frac{\bar{n}-2}{2\bar{m}+\bar{n}-4}\left(t_{\text{-}}\frac{2\bar{m}+\bar{n}-4}{\bar{n}-2}\right) \geq 0 \qquad \forall \bar{n},\bar{m} \in \bar{O}^{\mu\nu}(\chi) \tag{6.33}$$

it can be shown that F_n scales as $\alpha^{-\delta(n-2)}$, while $\bar{F}^{\alpha\beta}_{\bar{n}-1}$ scales as $\alpha^{-\bar{\delta}(\bar{n}-2)}$. We now have an action made up of non-negative powers of $1/\alpha$, and as such it is well suited to an expansion that increases both the PPV order (as desired) and the PPN order. The PPV expansion deep inside the Vainshtein radius generates yet another class of PPV potentials, and due to the non-linear nature of the problem to leading order, we do not expect to be able to write these in closed form.

We shall now develop the PPNV scheme for the cubic galileon theory in order to illustrate the idea.

6.2.4 The PPNV Formalism

Having discussed the various issues related to PPN and to the Vainshtein mechanism, let us now summarize the steps that need to be followed in order to apply the PPNV expansion for the class of theories under consideration: i.e. those for which all interactions kick in at the same macroscopic scale.

- Determine the Vainshtein radius r_V for the theory. This is usually determined from the Einstein frame action using (6.25) and the discussion that precedes it.

- Form the expansion parameter α and determine its PPN order both inside and outside the Vainshtein radius.

- For the outside region, reduce the field equations of the theory *in the Jordan frame*, as is done in the case of PPN. Note that α usually carries a PPN order, so care must be taken to take this into consideration when performing the expansion.

- For each PPN order, solve the field equations to determine which potentials arise. Furthermore, for each PPN order, solve the scalar equation in PPV orders to determine the metric potentials to the required Vainshtein order.

- Dualize the theory in the Jordan frame and determine the field equations.

- For the inside region, reduce the field equations of the theory *in the Jordan frame*, as is done in the case of PPN.

- For each PPN order, solve the field equations to determine which potentials arise. Furthermore, for each PPN order, solve the scalar equation in PPV orders to determine the metric potentials to the required Vainshtein order.

6.2.4.a Example: Orders Notation of the Cubic Galileon Theory

To illustrate more clearly how to use our notation and conventions, let us to consider the cubic galileon theory for a spherically symmetric source studied above. In that case we can set the following rules to establish the PPNV hierarchy

- Lets consider a function of the spacetime coordinates $F^{(n)}(\vec{x},t)$, remember that the superindex in the parenthesis denotes: $O(V^n)$ where $V \sim \left(\frac{r_s}{r}\right)^{\frac{1}{2}}$ by the virial relation.

- The Vainshtein mechanism is manifested in that the solution of the galileon on scales smaller than r_V is an expansion in powers of $\frac{r}{r_V})^{\frac{3}{2}}$. Other quantities involved in the formalism depend on the solution of the galileon, then they can be expanded as well. Thus each order in this expansion of $F^{(n_1)}(\vec{x},t)$ is denoted as $F^{(n_1,n_2)}(\vec{x},t)$ where n_2 is the respective power of $\left(\frac{r}{r_V}\right)^{\frac{3}{2}}$.

- Notice that n_1 and n_2 can be either positive or negative depending on the position of the observer, e.g. in this notation the galileon solution inside r_V (6.21) is $O(2,1)$ and outside r_V (6.22) is $O(2,-2)$. Also given that $\alpha \sim \frac{r_V^3}{r_s}$, then α/r^2 is $O(-2,-2)$.

6.3 Case study: The Cubic Galileon Theory

In this section, we are going to apply the PPNV formalism to the simplest theory holding Vainshtein mechanism: the cubic galileon. Our main goal is to illustrate how the method is carried out and to draw up a simplified picture on how the physics works in this limit for this type of theory in both regions: outside r_V where the self-interactions are subdominant and lead to potential modifications of gravity on large scales, and inside r_V where the non-linearities are strong and give rise to the screening of the galileon.

6.3.1 A Short Introduction to the Cubic Galileon Theory

In order to demonstrate our formalism, we shall apply it to a particular case of a screening theory: the cubic Galileon theory. We begin by presenting the action and field equations in the standard form (we shall give an alternative, dual formulation further below). The action in the Einstein frame is

$$\begin{aligned} S[\tilde{g},\chi] &= \frac{1}{16\pi G}\int d^4x\sqrt{-\tilde{g}}\tilde{R}+\int d^4x\sqrt{-\tilde{g}}\{c_0-\frac{1}{2}\tilde{g}^{\mu\nu}\nabla_\mu\chi\nabla_\nu\chi \\ &- \frac{1}{\Lambda^3}\frac{1}{2}\tilde{g}^{\mu\nu}\nabla_\mu\chi\nabla_\nu\chi\tilde{\Box}\chi\})+S_M[g] \end{aligned} \tag{6.34}$$

where $G=\frac{1}{8\pi M_p^2}$ is the bare gravitational strength, $c_0>0$ is a constant, Λ is a mass scale (χ has dimensions of mass). Both G and M_p are not the measured value of Newton's constant and Planck mass but are rather parameters in the action; we shall return to this point further below.

Following the discussion above (6.25), we determine the Vainshtein scale. We have that for the Cubic Galileon the $\bar{O}^{\mu\nu}$ term is absent while the $O(\chi)$ term is $-\frac{1}{2\Lambda^3}\tilde{g}^{\mu\nu}\nabla_\mu\chi\nabla_\nu\chi\tilde{\Box}\chi$. Hence, $m=2$ and $n=3$ which gives the Vainshtein scale as

$$r_V=\frac{1}{\Lambda}\left(\frac{M}{M_p}\right)^{1/3} \tag{6.35}$$

as in (6.20). We also need the expansion parameter $\alpha=\frac{M_p}{\Lambda^3}$. The expansion orders for α are then found to be $\alpha\sim O(-2,-2)$, in other words, α lowers both the PPN and the Vainshtein order of any terms multiplying it by 2.

The Jordan frame is determined via a conformal transformation to a new metric $g_{\mu\nu} = e^{2\chi/M_p}\tilde{g}_{\mu\nu}$ which is minimally coupled to matter. Defining $\phi = e^{-2\chi/M_p}$ the action in the Jordan frame takes the form

$$S = \frac{1}{16\pi G}\left\{\int d^4x\sqrt{-g}\left[\phi R + \frac{2\omega}{\phi}Y\right] - \alpha\int d^4x\sqrt{-g}\frac{Y}{\phi^3}\Box\phi\right\} + S_m[g,\psi^A] \quad (6.36)$$

where $\omega = \frac{c_0-6}{4}$ and $Y \equiv -\frac{1}{2}g^{\mu\nu}\nabla_\mu\phi\nabla_\nu\phi$. The matter action S_m depends, in addition to a generic set of matter fields ψ^A, only on the metric $g_{\mu\nu}$ but not on the galileon field ϕ.

If $\alpha \to 0$ the theory tends to the Brans-Dicke theory of gravity with coupling parameter ω. As we shall show further below, the limit $\alpha \to \infty$ is General Relativity.

Varying the action with respect to $g_{\mu\nu}$ and ϕ and after some algebraic manipulations gives the generalized Einstein equations as

$$\begin{aligned} R_{\mu\nu} &= \frac{8\pi G}{\phi}(T_{\mu\nu} - g_{\mu\nu}\left(\frac{1+\omega}{3+2\omega}\right)T) + \frac{\omega}{\phi^2}\nabla_\mu\phi\nabla_\nu\phi + \frac{\nabla_\mu\partial_\nu\phi}{\phi} \\ &+ g_{\mu\nu}\left(\frac{1+\omega}{3+2\omega}\right)\frac{\alpha}{\phi}\{-\frac{2}{\phi^2}((\Box\phi)^2 - (\nabla\partial\phi)^2 - R^{\alpha\beta}\nabla_\alpha\phi\nabla_\beta\phi) \\ &- \frac{2}{\phi^3}\Box\phi Y - \frac{10}{\phi^3}\nabla_\alpha Y\nabla^\alpha\phi\} \\ &+ \frac{g_{\mu\nu}}{2}\frac{\alpha}{\phi^3}[-\frac{10}{\phi}\nabla_\lambda\phi\nabla^\lambda Y + 2\nabla_\lambda\phi\nabla^\lambda\Box\phi + \frac{2}{\phi}(\Box\phi)^2 - 2\Box Y] \\ &+ O(6,-2) \end{aligned} \quad (6.37)$$

and scalar equation as

$$\begin{aligned} (3+2\omega)\Box\phi + \frac{2\alpha}{\phi}\{(\Box\phi)^2 &- (\nabla\partial\phi)^2 - R^{\alpha\beta}\nabla_\alpha\phi\nabla_\beta\phi + \frac{1}{\phi}\Box\phi Y - \frac{18}{\phi^2}Y^2 \\ &+ \frac{5}{\phi}\nabla_\alpha Y\nabla^\alpha\phi\} = 8\pi GT \end{aligned} \quad (6.38)$$

We have chosen this form of the (generalized) Einstein equations as it is more convenient when applying the PPN (and by extension the PPNV) formalism.

6.3.2 The PPNV Expansion Outside the Vainshtein Radius

6.3.2.a The Leading Order: Brans-Dicke Theory

Outside the Vainshtein radius, the self-interactions of the galileon are subdominant and the matter terms lead the sources of the Field equations. It is straightforward to see that at leading order the field equation (6.38) basically reduces to that of a Brans-Dicke field. In contrast to what happens inside the Vainshtein region, for sufficiently large scales the galileon shows up as a linear field with small corrections due to the scalar self-interactions that may be responsible of modifications to the cosmological dynamics.

Thus, applying standard perturbation theory to the standard galileon theory is justified. Because the source is assumed to be non-relativistic it is reasonable to split the field in PPN orders

$$\phi = \phi_0^{(out)}(1+\varphi^{(2)}+\varphi^{(4)}+...) \tag{6.39}$$

where the superscript denotes the PPN order of each term and ϕ_0 is a constant cosmological background. After inserting the expansions of the metric and the scalar, the Newtonian equation for the galileon ($O(2)$)is given by

$$\vec{\nabla}^2\varphi^{(2)} - \frac{2\alpha}{(2+3\omega)\phi_0^{(out)}}\vec{\nabla}\cdot(\vec{\nabla}^2\varphi^{(2)}\vec{\nabla}\varphi^{(2)} - \frac{1}{2}(\vec{\nabla}\varphi^{(2)})^2)) = -\frac{8\pi G}{\phi_0^{(out)}(2+3\omega)}\rho \tag{6.40}$$

As $\varphi^{(2)}$ is sourced by terms depending on $\rho(\vec{x},t)$, the time-derivatives of the field are not expected to be relevant to this order, so we shall keep the assumption that time-derivatives of the galileon are $O(1)$ PPN.

Additionally to the equation of the scalar,we also have to solve the Einstein equations at order $O(2)$ to determine the metric at the same order. The relevant equations are

$$\begin{aligned} R_{00}^{(2)} &= \frac{8\pi G}{\phi_0^{(out)}}T_{00}^{(2)} + (1+\omega)\vec{\nabla}^2\varphi^{(2)} + \frac{\alpha}{2\phi_0^{(out)}}(\Box(\vec{\nabla}\varphi^{(2)})^2 - \frac{2}{\phi_0^{(out)}}(\vec{\nabla}^2\varphi^{(2)})^2 \\ &- 2\partial_i\vec{\nabla}^2\varphi^{(2)}\partial_i\varphi^{(2)}). \end{aligned} \tag{6.41}$$

$$\begin{aligned} R_{ij}^{(2)} &= \frac{8\pi G}{\phi_0^{(out)}}T_{ij}^{(2)} - \delta_{ij}(1+\omega)\vec{\nabla}^2\varphi^{(2)} + \partial_i\partial_j\varphi^{(2)} + \delta_{ij}\frac{\alpha}{\phi_0^{(out)}}[\frac{1}{\phi_0^{(out)}}(\vec{\nabla}^2\varphi^{(2)})^2 \\ &+ \partial_i\vec{\nabla}^2\varphi^{(2)}\partial_i\varphi^{(2)} - \frac{1}{2}\vec{\nabla}^2(\vec{\nabla}\varphi^{(2)})^2]. \end{aligned} \tag{6.42}$$

Having reduced our equations of motion to the first PPN order, according to (6.2.4) we proceed to solve them. Because the non-linear terms are small we can express $\varphi^{(2)}$, $h_{ij}^{(2)}$ and $h_{00}^{(2)}$ as PPV expansions as follows

$$\begin{aligned}
\varphi^{(2)} &= \varphi^{(2,0)} + \varphi^{(2,-2)} + \varphi^{(2,-4)} + \ldots = \sum_{n=0}^{\infty} \varphi^{(2,-2n)} \\
h_{ij}^{(2)} &= h_{ij}^{(2,0)} + h_{ij}^{(2,-2)} + h_{ij}^{(2,-4)} + \ldots = \sum_{n=0}^{\infty} h_{ij}^{(2,-2n)} \\
h_{00}^{(2)} &= h_{00}^{(2,0)} + h_{00}^{(2,-2)} + + h_{00}^{(2,-4)} + \ldots = \sum_{n=0}^{\infty} h_{00}^{(2,-2n)}
\end{aligned} \tag{6.43}$$

After inserting (6.43) into equation (6.40), at leading order it reduces to the equation of the Brans-Dicke scalar whose solution is

$$\varphi^{(2,0)} = \frac{2}{\phi_0^{(out)}(3+2\omega)} GU, \tag{6.44}$$

The leading order equations for the metric are solved by the Brans-Dicke PPN metric which holds a Newtonian profile. The explicit derivation of this can be found in [172] for $d = 3$. The time-time component is given by

$$h_{00}^{(2,0)} = \frac{4}{\phi_0^{(out)}} \frac{2+\omega}{3+2\omega} GU = 2G_N U. \tag{6.45}$$

By definition, the time-time component of the PPN metric corresponds to two times the *physical* Newtonian potential. Also, G_N is the physical Newton-constant given by $G_N = \frac{2G}{\phi_0^{out}} \frac{2+\omega}{2+3\omega}$ and corresponds to that measured in a Brans-Dicke theory. The relevant solution of $h_{ij}^{(2)}$ is given by

$$h_{ij}^{(2,0)} = 2\left(\frac{1+\omega}{2+\omega}\right) G_N U \delta_{ij} \tag{6.46}$$

$$h_{i0}^{(3,0)} = -\frac{1}{2}\left(\frac{7\omega+10}{\omega+2}\right) G_N V_i - -\frac{1}{2} G_N W_i \tag{6.47}$$

$$\begin{aligned}
h_{00}^{(4,0)} &= -2G_N^2 U^2 + 2\left(\frac{3+2\omega}{2+\omega}\right) G_N \Phi_1 + 2\left(\frac{1+2\omega}{2+\omega}\right) G_N^2 \Phi_2 \\
&+ 2G_N \Phi_3 + 6\left(\frac{1+\omega}{2+\omega}\right) G_N \Phi_4
\end{aligned} \tag{6.48}$$

The previous results are casted in the standard PPN gauge which is imposed by means of the following conditions

$$h^{\mu}_{i,\mu} - \frac{1}{2}h^{\mu}_{\mu,i} = \frac{\phi_{,i}}{\phi_0^{(out)}}. \tag{6.49}$$

$$h^{\mu}_{0,\mu} - \frac{1}{2}h^{\mu}_{\mu,0} = -\frac{1}{2}h_{00,0} + \frac{\phi_{,0}}{\phi_0^{(out)}} \tag{6.50}$$

As normally, we adopt the notation for partial derivatives as $\partial_\mu f = f_{,\mu}$. On one hand, in the standard PPN gauge, the general PPN metric defines the γ PPN parameter as a coefficient for the space-space components of the metric as follows

$$g_{ij} = (1 + 2\gamma G_N U)\delta_{ij}. \tag{6.51}$$

Then, as expected, the γ_{OG} parameter for galileons at leading order outside the Vainshtein region, is the same as for Brans-Dicke theory

$$\gamma_{OG}^{(2,0)} = \left(\frac{1+\omega}{2+\omega}\right) = \gamma_{BD}. \tag{6.52}$$

where the *OG* subindex means *Outside Galileon*. On the other hand, the β post-newtonian parameter in this highly-linear limit is

$$\beta_{OG}^{(2,0)} = 1 = \beta_{BD} = \beta_{GR} \tag{6.53}$$

In the standard physical interpretation of the PPN parameters, β is a quantitative measure of the nonlinearity in the superposition law of gravity of the theory in question. The fact that $\beta_{OG}^{(2,0)}$ is just like in GR is consistent with the linear feature of this theory a this regime. This in interesting because it tell us that the non-linearity of galileons only arises at post-Vainsteinian order which is relevant for scales nearby the Vainshtein boundary where the galileon needs starting to hide so the theory mimics GR. Nonetheless, we'll see later that still at the linear regime some remnants of non-linearities show up and they might be responsible for modifications of gravity at large linear scales.

6.3.2.b Post Newtonian Vainshtenian Solutions

We shall now consider the first correction to the fully linear Brans-Dicke solution arisen above. In order to compute the solution for the first correction to the linear equation, we need to take into account the subdominant non-linear terms terms appearing in the linear equations as is usually done in the standard perturbation theory. Let us go back to the post-Newtonian equation for the galileon (6.40). Assuming that our observer is placed closer to the source but still outside the Vainshtein region so that $kr_V \sim 1$ we need to solve this equation to next order in the post-Vainshteinian expansion (6.43). The corresponding equation for the correction is

$$\vec{\nabla}^2\varphi^{(2,-2)} = \frac{\alpha}{\phi_0^{(out)}(3+2\omega)}\vec{\nabla}\cdot\left\{2\vec{\nabla}\varphi^{(2,0)}\vec{\nabla}^2\varphi^{(2,0)} - \vec{\nabla}|\vec{\nabla}\varphi^{(2,0)}\cdot\vec{\nabla}\varphi^{(2,0)}|\right\}. \tag{6.54}$$

Noting the Laplacian acting on the 2nd term we define

$$\varphi^{(mix)} = \varphi^{(2,-2)} + \frac{\alpha}{(3+2\omega)\phi_0^{(out)}}|\vec{\nabla}\varphi^{(2,0)}|^2 \tag{6.55}$$

so that our equation after using (6.44) becomes

$$\vec{\nabla}^2\varphi^{(mix)} = -\frac{16\pi G\alpha}{(3+2\omega)^2(\phi_0^{(out)})^2}\vec{\nabla}\cdot\left[\rho\vec{\nabla}\varphi^{(2,0)}\right] \tag{6.56}$$

Then we can solve the above equation to get

$$\varphi^{(mix)}(t,\vec{x}) = \frac{4\alpha G}{(3+2\omega)^2(\phi_0^{(out)})^2}\int d^3x'\frac{1}{|\vec{x}-\vec{x}'|}\vec{\nabla}_{x'}\cdot\left[\rho(t,\vec{x}')\vec{\nabla}_{x'}\varphi^{(2,0)}(t,\vec{x}')\right] \tag{6.57}$$

After some integration by parts and using the identity

$$\vec{\nabla}\frac{1}{|\vec{x}'-\vec{x}|} = -\frac{1}{|\vec{x}'-\vec{x}|^3}(\vec{x}'-\vec{x}) \tag{6.58}$$

we find

$$\varphi^{(mix)}(t,\vec{x}) = \frac{2\alpha}{(3+2\omega)\phi_0^{(out)}}\left(\frac{G_N}{2+\omega}\right)^2 \int d^3x'\int d^3x''\frac{\rho(t,\vec{x}')}{|\vec{x}-\vec{x}'|^3}\frac{\rho(t,\vec{x}'')}{|\vec{x}'-\vec{x}''|^3}(\vec{x}-\vec{x}')\cdot(\vec{x}'-\vec{x}'') \tag{6.59}$$

To proceed we also need the term $|\vec{\nabla}\varphi^{(2,0)}|^2$ which is given by

$$\frac{\alpha}{(3+2\omega)\phi_0^{(out)}}|\vec{\nabla}\varphi^{(2,0)}|^2 = \frac{\alpha}{(3+2\omega)\phi_0^{(out)}}\left(\frac{G_N}{2+\omega}\right)^2 \int d^3x' \int d^3x''\rho(x')\rho(x'')\frac{(\vec{x}-\vec{x}')\cdot(\vec{x}-\vec{x}'')}{|x-x'|^3|x-x''|^3} \tag{6.60}$$

so that the full solution is

$$\varphi^{(2,-2)} = \frac{\alpha}{(3+2\omega)\phi_0^{(out)}}\left(\frac{G_N}{2+\omega}\right)^2 UG_1 \tag{6.61}$$

$$= \frac{1}{(\phi_0^{out})^3(3+2\omega)^3(8\pi M)^2} r_V^3 r_s UG_1 \tag{6.62}$$

where we define the first PPNV potential as

$$UG_1(t,\vec{x}) \equiv \int d^3x' \int d^3x''\rho(t,\vec{x}')\rho(t,\vec{x}'')\left\{\frac{(\vec{x}-\vec{x}')\cdot(\vec{x}-\vec{x}'')}{|\vec{x}-\vec{x}'|^3|\vec{x}-\vec{x}''|^3} - 2\frac{(\vec{x}-\vec{x}')\cdot(\vec{x}'-\vec{x}'')}{|\vec{x}-\vec{x}'|^3|\vec{x}'-\vec{x}''|^3}\right\} \tag{6.63}$$

Also, a differential definition of the first PPNV potential is going to be useful below, and it is given by

$$\vec{\nabla}^2(UG_1) \equiv \vec{\nabla}\cdot\left\{\vec{\nabla}U\vec{\nabla}^2U - \frac{1}{2}\vec{\nabla}(\vec{\nabla}U\cdot\vec{\nabla}U)\right\}. \tag{6.64}$$

Since $G = \frac{r_s}{8\pi M}$, we can define the following calligraphic potentials

$$\mathscr{U} \equiv \frac{r_s U}{8\pi M} \quad \rightarrow \quad O(2,0) \tag{6.65}$$

$$\mathscr{G}_1 \equiv \frac{r_V^3 G_1}{8\pi M} \quad \rightarrow \quad O(0,-2) \tag{6.66}$$

and then

$$\varphi^{(2,-2)} = \frac{1}{(\phi_0^{(out)})^3(3+2\omega)^3}\mathscr{U}\mathscr{G}_1. \tag{6.67}$$

The last notation makes the double expansion to be clearly manifested since the orders of the solution is established simply by means of the r_s and r_V^3 factors multiplying each potential: r_s multiplies the ratio of purely PPN potential to the total

mass providing only the PPN order, while r_V^3 multiplies the ratio of the first PPNV potential to the total mass providing only the PPV order. We shall be using both notations from now on.

Now we proceed to construct a solution for the PPNV at first order. First we shall obtain the expansion of the Einstein equation, by inserting 6.43 and pick the corresponding equations at the relevant orders. By doing that, we realise that the first correction in PPV of the time-time component at newtonian order obeys the following equation

$$\begin{aligned} -\frac{1}{2}\vec{\nabla}^2 h_{00}^{(2,-2)} &= (1+\omega)\vec{\nabla}^2\varphi^{(2,-2)} - \frac{\alpha}{\phi_0^{(out)}}[\frac{1}{\phi_0^{(out)}}(\vec{\nabla}^2\varphi^{(2,0)})^2 \\ &+ \partial_i\vec{\nabla}^2\varphi^{(2,0)}\partial_i\varphi^{(2,-2)} - \frac{1}{2}\vec{\nabla}^2(\vec{\nabla}\varphi^{(2,0)})^2], \end{aligned} \tag{6.68}$$

which is solved by

$$h_{00}^{(2,-2)} = \frac{\mathscr{U}}{\phi_0^{(out)}}\left[-\frac{2(1+\omega)}{(3+2\omega)^3}\mathscr{G}_1 + \frac{1}{\phi_0^{(out)}(3+2\omega)}\mathscr{I}\right]. \tag{6.69}$$

The solution for the metric is written in terms of a new PPNV potential $\mathscr{I}$ defined as

$$\vec{\nabla}^2(UI) \equiv \frac{1}{\phi_0^{(out)}}(U)^2 + \partial_i(\vec{\nabla}^2 U)\partial_i U - \frac{1}{2}\vec{\nabla}^2(\vec{\nabla}U)^2, \tag{6.70}$$

$$\mathscr{I} \equiv r_V^3\frac{I}{8\pi M}. \tag{6.71}$$

It is a natural feature of these sort of theories that the Newton coupling is dynamical. In order to determine G_N up to the first post-Vainshtenian order lets recall that $2G_N U \equiv h_{00}^{(2)}$ which can be obtained from adding up (6.69) and (6.45). Thus the classical measured Newton coupling in this case is given by

$$\begin{aligned} G_N &\equiv \left(1 - \frac{\mathscr{G}_1}{2(3+2\omega)(\phi_0^{(out)})^3}\left(\frac{1+\omega}{2+\omega}\right) + \frac{\mathscr{I}}{4(\phi_0^{(out)})^2(2+\omega)(3+2\omega)}\right)G_0 \\ &+ O(2,-3) \end{aligned} \tag{6.72}$$

where $G_0 \equiv \frac{G}{\phi_0^{(out)}}\left(\frac{4+2\omega}{3+2\omega}\right)$ is the Newton constant measured at larger scales when the theory is Brans-Dicke like. As expected the Newton strength is dynamic as

it depends on the space-time coordinates by means of the PPNV potentials. It is interesting to notice, on one hand, that the $\mathscr{G}_1$ accounts for effects of the galileon solution which starts to slightly show up upon the Brans-Dicke linear solution at linear scales close to the Vainshtein boundary. On the other hand $\mathscr{I}$ introduces effects due to modifications to the metric due to the direct coupling to the galileon in the Jordan frame.

Following a similar procedure with the spatial components of the Einstein equations, we can obtain the equation for $h_{ij}^{(2,-2)}$. Thus, first we apply the standard PPN gauge conditions obtaining the Riemann tensor at the relevant order

$$\begin{aligned} R_{ij}^{(2,-2)} &= -\delta_{ij}\frac{(1+\omega)}{\phi_0}\vec{\nabla}^2\varphi^{(2,-2)} + \frac{1}{\phi_0}\partial_i\partial_j\phi^{(2,-2)} - \delta_{ij}\frac{\alpha}{\phi^3}[\frac{1}{\phi_0}(\vec{\nabla}^2\phi^{(2,0)})^2 \\ &+ \partial_i\vec{\nabla}^2\phi^{(2,0)}\partial_i\phi^{(2,-2)} - \frac{1}{2}\vec{\nabla}^2(\vec{\nabla}\phi^{(2,0)})^2]. \end{aligned} \tag{6.73}$$

After fixing the gauge in a similar way as before, the equation governing $h_{ij}^{(2,-2)}$ is

$$\begin{aligned} -\frac{1}{2}\vec{\nabla}^2 h_{ij}^{(2,-2)} &= -\delta_{ij}[(1+\omega)\vec{\nabla}^2\varphi^{(2,-2)} - \frac{\alpha}{\phi_0^{(out)}}[\frac{1}{\phi_0^{(out)}}(\vec{\nabla}^2\varphi^{(2,0)})^2 \\ &+ \partial_i\vec{\nabla}^2\varphi^{(2,0)}\partial_i\varphi^{(2,-2)} - \frac{1}{2}\vec{\nabla}^2(\vec{\nabla}\varphi^{(2,0)})^2] \end{aligned} \tag{6.74}$$

which is solved by

$$h_{ij}^{(2,-2)} = -h_{00}^{(2,-2)} \tag{6.75}$$

In order to read off the γ parameter for this cubic galileon in the approach presented here, we need first to resum all the orders of the spatial component of the metric and second we need to renormalize the Newton coupling by changing the units to get the measured Newtonian potential Φ as an overall factor rather than simply GU. After doing so we get

$$\begin{aligned} h_{ij}^{(2)} &= \left(1 - \left(\frac{9+5\omega}{2+\omega}\right)\frac{\mathscr{G}_1}{2\phi_0^{(out)}(3+2\omega)^2} + \frac{\mathscr{I}}{4\phi_0^{(out)}(1+\omega)(2+\omega)}\right) \\ &\times \delta_{ij}\left(\frac{1+\omega}{2+\omega}\right)G_N U. \end{aligned} \tag{6.76}$$

Thus the γ parameter can be read off from the previous equation as

$$\gamma_{OG} = \gamma_{BD}\left(1 - \frac{\mathscr{G}_1}{2\phi_0^{(out)}(3+2\omega)^2}\left(\frac{9+5\omega}{2+\omega}\right) + \frac{\mathscr{I}}{4\phi_0^{(out)}(1+\omega)(2+\omega)}\right). \quad (6.77)$$

6.3.2.c Higher PPN Order Solutions

The geodesic equation for a test particle that we have already reviewed in (6.2.1), requires the time-time component of the perturbation above the Minkowski metric up to $O(4)$ in PPN. In order to derive the required $h_{00}^{(4,-2)}$ a long, cumbersome and straightforward computation should be carried out. For sake of clearness we shall make it here, however the way in which it is performed is similar as we did above with lower order metric fluctuations. We shall just describe briefly the computation and show the resulting expression along the way as follows: We first reduce the time-time component of the Einstein equations at order $O(4,-2)$. The differential Leibniz property has been used several times to simplify individual terms and the whole expression for $h_{00}^{(4,0)}$. It finally reduces to

$$\begin{aligned}
R_{00}^{(4,-2)} &= -(1+\omega)[-\frac{(\Box\phi)^{(4,-2)}}{\phi_0^{(out)}} + h_{00}^{2,0}\vec{\nabla}^2\varphi^{(2,-2)} + h_{00}^{2,1}\vec{\nabla}^2\varphi^{(2,0)} \\
&+ \varphi^{(2,-2)}\vec{\nabla}^2\varphi^{(2,0)} + \varphi^{(2,0)}\vec{\nabla}^2\varphi^{(2,-2)}] - 8\pi G\frac{\varphi^{(2,-2)}}{\phi_0^{(out)}}T_{00}^{(2)} \\
&+ \partial_0^2\varphi^{(2,-2)} + \alpha(h_{00}^{(2,0)} + 3\varphi^{(2,0)})[(\vec{\nabla}^2\varphi^{(2,0)})^2 + \partial_i\vec{\nabla}^2\varphi^{(2,0)}\partial_i\varphi^{(2,-2)} \\
&- \frac{1}{2}\vec{\nabla}^2(\vec{\nabla}\varphi^{(2,0)})^2] + \frac{\alpha}{3+2\omega}\{-\frac{5}{2\phi_0}[\vec{\nabla}^2(\varphi^{(2,0)}(\varphi_{,i}^{(2,0)})^2) - \varphi^{(2,0)}\vec{\nabla}^2(\varphi_{,i}^{(2,0)})^2) \\
&- (\varphi_{,i}^{(2,0)})^2)\vec{\nabla}^2\varphi^{(2,0)}] + \frac{1}{\phi_0^{(out)}}[\vec{\nabla}^2 h_{ij}^{(2,0)}\partial_i\varphi^{(2,0)}\partial_j\varphi^{(2,0)} - \vec{\nabla}^2(\partial_0\varphi^{(2,0)})^2 \\
&- \partial_0^2(\varphi_{,i}^{(2,0)})^2 + \frac{1}{2}(\partial_k h_{ii}^{(2,0)} - \partial_k h_{00}^{(2,0)})\partial_k(\varphi_{,i}^{(2,0)})^2 + 2\partial_0\vec{\nabla}^2\varphi^{(2,0)}\partial_0\varphi^{(2,0)} \\
&- 2h_{ij}^{(2,0)}\partial_i\vec{\nabla}^2\varphi^{(2,0)}\partial_j\varphi^{(2,0)} - \vec{\nabla}^2[\varphi^{(4,0)}\vec{\nabla}^2\varphi^{(2,0)} + (\Box\phi)^{(4,0)}\varphi^{(2,0)}] \\
&+ \vec{\nabla}^2\varphi^{(4,0)}\vec{\nabla}^2\varphi^{(2,0)} + \varphi^{(4,0)}\vec{\nabla}^2\vec{\nabla}^2\varphi^{(2,0)}] + \frac{1}{(\phi_0^{(out)})^2}[(\Box\phi)^{(4,0)}\vec{\nabla}^2\varphi^{(2,0)} \\
&+ \varphi^{(2,0)}\vec{\nabla}^2(\Box\phi)^{(4,0)} - \varphi^{(2,0)}(\partial_i\varphi^{(2,0)})^2 + 2\vec{\nabla}^2\varphi^{(2,0)}\frac{(\Box\phi)^{(4,0)}}{\phi_0^{(out)}}]\}
\end{aligned} \quad (6.78)$$

In order to work out the last equation we need $(\Box\phi)^{(4,-2)}$ and $\varphi^{(4,0)}$ which can be obtained from the post-post-newtonian scalar equation of motion at $O(4)$ given by

$$\begin{aligned}\vec{\nabla}^2\varphi^{(4)} &= \mathbf{S}^{(4)}(x,t) - \frac{4\alpha}{(3+2\omega)(\phi_0^{(out)})^2}[\vec{\nabla}^2(\vec{\nabla}\varphi^{(2)}\cdot\vec{\nabla}\varphi^{(4)}) \\ &\quad -\vec{\nabla}\cdot(\vec{\nabla}\varphi^{(2)}\vec{\nabla}^2\varphi^{(4)}) - \vec{\nabla}\cdot(\vec{\nabla}\varphi^{(4)}\vec{\nabla}^2\varphi^{(2)})] \end{aligned} \tag{6.79}$$

with

$$\begin{aligned}\mathbf{S}^{(4)}(x,t) &\equiv \frac{8\pi G}{3+2\omega}T^{(4)} + \partial_0^2\varphi^{(2)} - \partial_i h_{ik}^{(2)}\partial_k\varphi^{(2)} - h_{ik}^{(2)}\partial_i\partial_k\varphi^{(2)} + \frac{1}{2}(\partial_i h_{kk}^{(2)} \\ &- \partial_i h_{00}^{(2)})\partial_i\varphi^{(2)} + \frac{2\alpha}{(3+2\omega)(\phi_0^{(out)})^2}[2\vec{\nabla}^2\varphi^{(2)}(-\partial_0^2\varphi^{(2)} + \partial_i h_{ik}^{(2)}\partial_k\varphi^{(2)} \\ &+ h_{ik}^{(2)}\partial_i\partial_k\varphi^{(2)} - \frac{1}{2}(\partial_i h_{kk}^{(2)} - \partial_i h_{00}^{(2)})\partial_i\varphi^{(2)}) + 2(\partial_k\partial_0\varphi^{(2)})^2 \\ &+ (\partial_i h_{jk}^{(2)} - \frac{1}{2}\partial_k h_{ij}^{(2)})\partial_k\varphi^{(2)}\partial_i\partial_j\varphi^{(2)} - R_{ij}^{(2)}\partial_i\varphi^{(2)}\partial_j\varphi^{(2)}] \\ &- \frac{\alpha}{(3+2\omega)(\phi_0^{(out)})^3}[\vec{\nabla}^2\varphi^{(2)}(\vec{\nabla}\varphi^{(2)})^2 - 5\partial_i(\vec{\nabla}\varphi^{(2)})^2\partial_i\varphi^{(2)}] \end{aligned} \tag{6.80}$$

Notice that due to galilean symmetry the l.h.s. of (6.79) is a total derivative and so it can be integrated once, also this assures that superposition principle holds in all regions of space. Because (6.79) is a total derivative it we can expect that, even without making the Vainshtein expansion we are able to solve it , at least in theory. However, that is beyond the scope of this work.

However, in order to solve the metric up to the required order, the leading order equation for the galileon is required. By reducing (6.79) to leading order in PPV it gives

$$\vec{\nabla}^2\varphi^{(4,0)} = \frac{8\pi G}{2\omega+3}T^{(4)} + \varphi_{,00}^{(2,0)} - h_{jk,k}^{(2,0)}\varphi_{,i}^{(2,0)} - h_{jk}^{(2,0)}\varphi_{,ik}^{(2,0)} + \frac{1}{2}(h_{kk}^{(2,0)} - h_{00}^{(2,0)})_{,i}\varphi_i^{(2,0)}. \tag{6.81}$$

This can be integrated out straightaway by inserting the already known solutions at lower PPN order and using the standard PPN tools. Finally it is solved by

$$\varphi^{(4,0)} = \sum_{n=1}^{7} s_n\xi_n. \tag{6.82}$$

where ξ_n is a vector made with standard PPN potentials at $O(4,0)$. Both ξ_n and the coefficients s_n can be found in appendix (A).

To obtain the solution of $h_{00}^{(4,-2)}$ is the messiest part of this calculation. First, we need all the lower order solutions of the metric and the galileon along with $\phi^{(4,-2)}$. Because only $(\Box\phi)^{(4,-2)}$ is needed, things are much simpler. Secondly we work out the l.h.s. of (6.78), in order to do so we use the expression of the Riemann tensor up to second order and impose the standard PPN gauge. Finally, after such a process a very specific equation for $h_{00}^{(4,-2)}$ is obtained and is given by

$$
\begin{aligned}
-\vec{\nabla}^2 h_{00}^{(4,-2)} &= -\frac{2}{\phi_0^{(out)}}\varphi_{,00}^{(2,-2)} - h_{00,j}^{(2,0)}(h_{jk,k}^{(2,-2)} - \frac{1}{2}h_{kk,j}^{(2,-2)}) - h_{00,j}^{(2,-2)}(h_{jk,k}^{(2,0)} \\
- \;& \frac{1}{2}h_{kk,j}^{(2,0)}) + |\vec{\nabla}h_{00}^{(2,0)}\cdot\vec{\nabla}h_{00}^{(2,-2)}| - h_{jk}^{(2,0)}h_{00,jk}^{(2,-2)} - h_{jk}^{(2,-2)}h_{00,jk}^{(2,0)} - \frac{2(1+\omega)}{\phi_0^{(out)}} \\
\times \;& [-(\Box\phi)^{(4,-2)} + h_{00}^{2,0}\vec{\nabla}^2\varphi^{(2,-2)} + h_{00}^{2,1}\vec{\nabla}^2\varphi^{(2,0)} + \frac{\varphi^{(2,-2)}}{\phi_0^{(out)}}\vec{\nabla}^2\varphi^{(2,0)} \\
+ \;& \frac{\varphi^{(2,0)}}{\phi_0^{(out)}}\vec{\nabla}^2\varphi^{(2,-2)}] + \frac{2}{\phi_0^{(out)}}\partial_0^2\varphi^{(2,-2)} + \frac{2\alpha}{\phi_0^{(out)}}(h_{00}^{(2,0)} + 3\frac{\varphi^{(2,0)}}{\phi_0^{(out)}}) \\
\times \;& [\frac{1}{\phi_0^{(out)}}(\vec{\nabla}^2\phi^{(2,0)})^2\partial_i\vec{\nabla}^2\phi^{(2,0)}\partial_i\phi^{(2,-2)} - \frac{1}{2}\vec{\nabla}^2(\vec{\nabla}\phi^{(2,0)})^2] + \frac{\alpha}{(3+2\omega)(\phi_0^{(out)})^3} \\
\times \;& \{-\frac{5}{2\phi_0^{(out)}}[\vec{\nabla}^2(\varphi^{(2,0)}(\varphi_{,i}^{(2,0)})^2) - \varphi^{(2,0)}\vec{\nabla}^2(\varphi_{,i}^{(2,0)})^2) - (\varphi_{,i}^{(2,0)})^2)\vec{\nabla}^2\varphi^{(2,0)}] \\
- \;& \partial_0^2(\varphi_{,i}^{(2,0)})^2 + \Gamma_{\mu k}^{\mu(2,0)}\partial_k(\varphi_{,i}^{(2,0)})^2 + \vec{\nabla}^2[h_{ij}^{(2,0)}\partial_i\varphi^{(2,0)}\partial_j\varphi^{(2,0)} - (\partial_0\varphi^{(2,0)})^2] \\
- \;& \frac{2}{\phi_0^{(out)}}[-\frac{\varphi^{(2,0)}}{\phi_0^{(out)}}(\partial_i\varphi^{(2,0)})^2 + 2\vec{\nabla}^2\varphi^{(2,0)}(\Box\phi)^{(4,0)}] + 2\partial_0\vec{\nabla}^2\varphi^{(2,0)}\partial_0\varphi^{(2,0)} \\
- \;& 2h_{ij}^{(2,0)}\partial_i\vec{\nabla}^2\varphi^{(2,0)}\partial_j\varphi^{(2,0)} - \vec{\nabla}^2[\varphi^{(4,0)}\vec{\nabla}^2\varphi^{(2,0)} + (\Box\phi)^{(4,0)}\varphi^{(2,0)}] \\
+ \;& \vec{\nabla}^2\varphi^{(4,0)}\vec{\nabla}^2\varphi^{(2,0)} + \varphi^{(4,0)}\vec{\nabla}^2\vec{\nabla}^2\varphi^{(2,0)} + (\Box\phi)^{(4,0)}\vec{\nabla}^2\varphi^{(2,0)} \\
+ \;& \varphi^{(2,0)}\vec{\nabla}^2(\Box\phi)^{(4,0)}\} - 8\pi G\frac{2\varphi^{(2,-2)}}{(\phi_0^{(out)})^2}T_{00}^{(2)}.
\end{aligned}
\tag{6.83}
$$

Notice that this equation contains two sorts of terms: $O(4,-2)+\alpha O(6,0)$. This feature implies that we need further PPN potentials than the standard ones which usually are post-newtonian at most. The highest PPN order of such new potentials must be $O(6,-2)$ given the order of α which reduces by 2 the PPN order. It is interesting because possible effects appearing at $O(6)$ introduced by specific PPN potentials in GR or BDT are visible at $O(4)$ in this theory due to the presence of the galileon.

After working out a long and cumbersome calculation consisting in using the Leibniz property of the partial derivatives several times on various terms in (6.83), plugging the known lower order solutions found all along this section, rearranging and simplifying terms and integrating out the Laplacian, (6.83) is finally solved by

$$\begin{aligned} h_{00}^{(4,-2)} &= -2\kappa_1\Theta_1 - 2\kappa_2\Theta_2 + 2\sum_{I=1}^{8} p_I\Pi_I - \sum_{I=1}^{3}\varepsilon_I X_I \\ &- 2\sum_{k=1}^{3} z_k\Upsilon_k + 2\sum_{i=1}^{3}\sum_{k=1}^{5}[p_k^i\Pi_k^i - l_k^i\Lambda_k^i] \end{aligned} \tag{6.84}$$

Similarly as in the standard PPN formalism, the solution of $h_{00}^{(4,-1)}$ above is expressed in terms of new PPNV potentials whose definition is presented in appendix (B). The corresponding coefficients can be found there as well.

6.4 The Dual Cubic Galileon and The Strong Field Region

When the observer is placed close to the source, the field self-interactions become strong and the approach used in the outside region breaks down. Although, the non-linear equations governing this screening mechanism represent an obscure mathematical issue for these theories, their symmetries have led to create useful techniques which make possible to overcome these difficulties and still strike the problem by using a consistent perturbative approach. Recently and alternative dual recasting of these theories have been proposed in [132, 233]. The basic idea is to introduce auxiliary variables "dual" to the interaction terms in the standard action by Legendre transform. I turns out, that the equations of motion for these auxiliary variables can be treated perturbatively since the expansion parameter $1/\Lambda$ is flipped over to Λ thus in the region where the interactions are large $\Lambda \to 0$.

6.4.1 Dualizing the Cubic Galileon

The techniques to compute such a dual action was firstly launched by Gabadadze in [132], in their dual variables the resulting equations involve non-analytic functional forms which make the maths quite cumbersome. A neater and more direct approach was put forth in [233], where instead of using Legendre transforms as dual variables, the interaction terms are directly related to the auxiliary variables by using Legendre multipliers. In these variables simpler analytic equations arise keeping all the advantages of the Gabadadze approach. The dual action for the cubic galileon is given by

$$S_{\rm dual} = \frac{1}{16\pi G}\int d^4x\sqrt{-g}\left\{\phi R - \frac{\omega}{\phi}(\nabla\phi)^2 + \frac{1}{\phi^3}\left(A^2\Box\phi + 2ZA^\mu\nabla_\mu\phi\right) - \frac{2}{\sqrt{\alpha}}\frac{1}{\phi^3}ZA^2\right\} \tag{6.85}$$

where A_μ is the dual field corresponding to $\nabla_\mu\phi$ and Z is the dual field for $\Box\phi$. By extremizing the action with respect to the field and after some algebraic manipulation we find the two relations between the dual fields and gradients of ϕ

$$\nabla_\mu\phi = \alpha^{-\frac{1}{2}}A_\mu \tag{6.86}$$

$$\Box\phi = \alpha^{-\frac{1}{2}}Z \tag{6.87}$$

the generalized Einstein equations

$$\begin{aligned}\phi R_{\mu\nu} &= 8\pi G\left(T_{\mu\nu}-\frac{1}{2}Tg_{\mu\nu}\right)+\alpha^{-\frac{1}{2}}\left\{\nabla_\mu A_\nu+\frac{1}{2}Zg_{\mu\nu}+\frac{\omega}{\phi}\alpha^{-\frac{1}{2}}A_\mu A_\nu\right.\\ &\left.+\frac{1}{\phi^3}\left[-ZA_\mu A_\nu+A_{(\mu}\nabla_{\nu)}A^2+\frac{1}{2}ZA^2g_{\mu\nu}-3\alpha^{-\frac{1}{2}}\frac{A^2}{\phi}A_\mu A_\nu\right]\right\} \quad (6.88)\end{aligned}$$

and the field equation for the dual fields (which is equivalent to the scalar equation in the standard formulation)

$$\begin{aligned}-\Box A^2+2\nabla_\lambda(ZA^\lambda) &= -8\pi G\phi^2T+\alpha^{-\frac{1}{2}}[(2\omega+3)\phi^2Z-\frac{5}{\phi}A^\mu\nabla_\mu A^2+\frac{1}{\phi}ZA^2\\ &+\frac{9\alpha^{-\frac{1}{2}}}{\phi^2}A^4]. \quad (6.89)\end{aligned}$$

Once again, we have manipulated the field equations to put them into a form more useful for performing the PPN expansion. It can easily be checked that eliminating the dual fields from (6.88) and (6.89) using (6.86) and (6.87) recovers the fields equations in the standard formulation.

In the dual formulation the expansion parameter is $\alpha^{-1/2}$ which in this case will have order $O(1,1)$.

6.5 The PPNV Expansion Inside the Vainshtein Region

6.5.1 Leading Order Solutions: General Relativity

Inside the Vainshtein region the strong self-interactions play an important role since they lead the galileon to hide and allow the theory to pass the stringent probes at the solar system. The $O(2)$ dual equations for the cubic galileon are derived by using the definitions of the dual fields (6.86) and (6.87). We find that to PPN $O(2)$

Us

$$\phi_0^{(in)}\vec{\nabla}_i\varphi^{(2)} = \alpha^{-\frac{1}{2}}A_i^{(1)}=\alpha^{-\frac{1}{2}}\vec{\nabla}_iB^{(1)}, \quad (6.90)$$

$$\phi_0^{(in)}\vec{\nabla}^2\varphi^{(2)} = \alpha^{-\frac{1}{2}}Z^{(1)}=\alpha^{-\frac{1}{2}}\vec{\nabla}^2B^{(1)}, \quad (6.91)$$

where we have defined the scalar field B whose gradient gives the dual field A_μ. Thus, in general, the orders of φ will be one greater than the orders of the B field (either PPN or Vainshtein order). Notice that as the constant $\alpha^{-\frac{1}{2}}$ is of order $O(1,1)$,

it increases both the PPN order and the Vainshtein order of any terms multiplying it by one. This means that the lowest PPN order for the scalar perturbation φ is 2 while the lowest Vainshtein order for the scalar field perturbation φ is 1 (given that the lowest possible Vainshtein order for the B field is zero)

As for the outside region, we expand the scalar field as

$$\phi = \phi^{(in)} \left(1 + \varphi^{(2)} + \varphi^{(4)} + \dots\right) \tag{6.92}$$

where $\phi^{(in)}$ is a constant and φ a perturbation. Note that due to the non-perturbative nature of the theory at the Vainshtein surface, the constant $\phi^{(in)}$ will in general not be equal to $\phi^{(out)}$. However, they can in principle be related by appropriately matching the scalar ϕ across the two regions.

We now consider the generalized Einstein equations to second PPN order

$$R^{(2)}_{\mu\nu} = 8\pi G_N \left(T^{(2)}_{\mu\nu} - \frac{\eta_{\mu\nu}}{2} T^{(2)}\right) + \eta_{\mu\nu} \frac{\alpha^{-\frac{1}{2}}}{2\phi_0^{(in)}} \vec{\nabla}^2 B^{(1)} \tag{6.93}$$

First we take the time Einstein equation (6.93) and use (6.10) to the relevant order, so we get

$$\frac{1}{2}\vec{\nabla}^2 h^{(2)}_{00} = -4\pi G_N \rho + \frac{\alpha^{-\frac{1}{2}}}{2\phi_0^{(in)}} \vec{\nabla}^2 B^{(1)} \tag{6.94}$$

where

$$G_N = \frac{G}{\phi_0^{(in)}}. \tag{6.95}$$

We can determine $h^{(2)}_{00}$ completely in terms of the new potential $B^{(1)}$ as

$$h^{(2)}_{00} = 2G_N U + \frac{\alpha^{-\frac{1}{2}}}{\phi^{(in)}} B^{(1)} \tag{6.96}$$

Since the lowest Vainshtein order for $B^{(1)}$ is 0 taking the limit $\alpha^{-\frac{1}{2}} \to 0$ recovers General Relativity. Thus the Vainshtein mechanism is directly manifested in the dual formalism. In other words, to $O(2,0)$ the $B^{(1)}$ term does not contribute and we recover the usual Newtonian potential

$$h^{(2,0)}_{00} = 2G_N U \tag{6.97}$$

Remember that G_N has the meaning of the observable Newtonian gravitational constant inside the Vainshtein radius, i.e. the Newtonian constant measured by an experiment on Earth.

Now we turn to find the spatial components of the metric in terms of the dual fields as well. First we take the space-space components of (6.93),

$$\phi_0^{(in)} R_{ij}^{(2)} = \varphi_{,ij}^{(2)} + \delta_{ij} \frac{\alpha^{-\frac{1}{2}}}{2} \vec{\nabla}^2 B^{(1)} \tag{6.98}$$

which after using (6.12) at $O(2)$ and imposing the corresponding gauge condition becomes

$$\vec{\nabla}_k h_{ki} = \vec{\nabla}_i \left(\frac{1}{2} h_{ii}^{(2)} - \frac{1}{2} h_{00}^{(2)} + \alpha^{-\frac{1}{2}} B^{(1)} \right). \tag{6.99}$$

By making this, (6.98) turns into

$$-\frac{1}{2} \vec{\nabla}^2 h_{ij} = 4\pi G_N \rho \gamma_{ij} + \frac{1}{2\phi_0^{(in)}} \alpha^{-\frac{1}{2}} \vec{\nabla}^2 B^{(1)} \delta_{ij} \tag{6.100}$$

so that we obtain h_{ij} as

$$h_{ij} = \left(2G_N U - \frac{\alpha^{-\frac{1}{2}}}{\phi_0^{(in)}} B^{(1)} \right) \delta_{ij} \tag{6.101}$$

We notice that no new potential apart from $B^{(1)}$ arises. Once again as $\alpha^{-1/2} \to 0$ we recover GR, i.e.

$$h_{ij}^{(2,0)} = 2G_N U \delta_{ij} \tag{6.102}$$

An important point to make clear is that according to the general equations (6.86) and (6.87), the galileon inside the Vainshtein region is proportional to $\alpha^{-\frac{1}{2}}$. This implies straightaway that the galileon at any PPN order is completelly hidden away. Therefore, in the dual formalism the Vainshtein mechanism is fully manifested. This immediately lead us to realise that the solutions of the metric, at all PPN orders are basically those of GR. The relevant perturbations of the metric are given in terms of the standard PPN potentials as

$$\begin{aligned} h_{i0}^{(3,0)} &= -\frac{7}{2} \mathscr{V}_i - \frac{1}{2} \mathscr{W}_i \\ h_{00}^{(4,0)} &= -2\mathscr{U}^2 + 4\Phi_1 + 4\Phi_2 + 2\Phi_3 + 6\Phi_4 \end{aligned} \tag{6.103}$$

This results warrant that the galileon theory safely passes all the test at solar system scales which are well inside the Vainshtein region.

Now we aim to determine more explicitly the metric at first order in the PPNV expansion. As we realised above, if we would wish to get the metric at order 2 in PPN and all orders in PPV, it would suffice to find the solution of the galileon (at the same PPNV orders) and plug it into (6.101) and (6.96), as we did in [12] to determine G_N and γ.

6.5.2 Solving the Post-Newtonian Scalar Equation

Equation (6.89) and the relations (6.90) at $O(2)$ in PPN reduces to

$$\vec{\nabla}^2(\vec{\nabla}B^{(1)})^2 - 2\vec{\nabla}\cdot(\vec{\nabla}B^{(1)}(\vec{\nabla}^2B^{(1)})) = -8\pi GT^{(2)} + \alpha^{-\frac{1}{2}}(2\omega+3)(\phi_0^{(in)})^2\vec{\nabla}^2B^{(1)} \tag{6.104}$$

We proceed to solve it by expanding $B^{(1)}$ in PPV orders

$$B^{(1)} = B^{(1,0)} + B^{(1,1)} + \ldots = \sum_{n=0}^{\infty} B^{(1,n)} \tag{6.105}$$

(6.90) at leading order obeys

$$\vec{\nabla}^2(\vec{\nabla}B^{(1,0)})^2 - 2\vec{\nabla}\cdot(\vec{\nabla}B^{(1,0)}(\vec{\nabla}^2B^{(1,0)})) = (\phi_0^{(in)})^2 8\pi G\rho \tag{6.106}$$

However, at the same order, the terms involving $B^{(1)}$ disappear in the metric solutions (6.96) and (6.101). This happens because the solution for the metric to Vainshtein order 0 is simply General Relativity while the field $B^{(1)}$ decouples and obeys its own differential equation without coupling to the metric or matter evolution.

However, the field $B^{(1)}$ eventually, at next order, has a bearing on the metric. Unfortunately a general analytic solution to (6.106) is (to our knowledge) impossible to ger, except in idealized situations like spherical symmetry. Indeed, by simple shuffling of the terms involved, (6.106) can be re-written in the form

$$\vec{\nabla}^i\vec{\nabla}^jB^{(1,0)}\vec{\nabla}_i\vec{\nabla}_jB^{(1,0)} - \left(\vec{\nabla}^2B^{(1,0)}\right)^2 \;=\; -16\pi G\rho \tag{6.107}$$

We recognise the above equation as a Monge-Ampere equation whose general solution is unknown, and one has to resort to numerics. Thus, it is impossible to find this new Vainshteinian potential as a closed form integral as we have done in the case outside the Vainshtein radius.

Fortunately, the polynomial structure of (6.104) makes possible the use of perturbation theory. Once the lowest order solution is found, for instance $B^{(1,0)}$ then higher orders $B^{(1,n)}$ will obey a linearized equation coming from (6.104). More specifically, expanding order-by-order (6.104) may be re-written as

$$\begin{aligned}
\mathscr{L}(B^{(1,0)},B^{(1,0)}) &= 8\pi G(\phi_0^{(in)})^2\rho \\
\mathscr{L}(B^{(1,1)},B^{(1,0)})+\mathscr{L}(B^{(1,0)},B^{(1,1)}) &= \alpha^{-\frac{1}{2}}(3+2\omega)(\phi_0^{(in)})^2\vec{\nabla}^2B^{(1,0)} \qquad (6.108)\\
&\cdots
\end{aligned}$$

The operator $\mathscr{L}$ is the bi-linear operator $\mathscr{L}: C^\infty\times C^\infty\to C^\infty$ defined by

$$\mathscr{L}(u,v)=2\vec{\nabla}\cdot\left[(\vec{\nabla}^2v)\vec{\nabla}u\right]-\vec{\nabla}^2(\vec{\nabla}u\cdot\vec{\nabla}v) \qquad (6.109)$$

for two arbitrary functions $u,v\in C^\infty$. The operator $\mathscr{L}$ is a non-symmetric ($\mathscr{L}(u,v)\neq\mathscr{L}(v,u)$) bi-linear form, i.e. it obeys the properties $\mathscr{L}(u+v,w)=\mathscr{L}(u,w)+\mathscr{L}(v,w)$ and $\mathscr{L}(\lambda u,v)=\mathscr{L}(u,\lambda v)$. Then we can formally write the solutions to the hierarchy of linearizations (6.108) by considering the operator $\hat{\mathscr{L}}:C^\infty\to C^\infty$ defined by

$$\hat{\mathscr{L}}\mathscr{L}(u,v)=uv. \qquad (6.110)$$

The operator $\hat{\mathscr{L}}$ is distributive with respect to addition and to multiplication by a constant which ensures that $\mathscr{L}$ is invertible and a solution can be constructed [See appendix (C) for some probes]. The above hierarchy (6.108) can then in principle be solved order-by-order where the only input is the matter density ρ. Formally this is achieved via the operator $\hat{\mathscr{L}}$ which ensures that the solutions exist:

$$\begin{aligned}
(B^{(1,0)})^2 &= 8\pi G(\phi_0^{(in)})^2\hat{\mathscr{L}}(\rho(\vec{x},t)) \\
2B^{(1,1)}B^{(1,0)} &= \alpha^{-\frac{1}{2}}(3+2\omega)(\phi_0^{(in)})^2\hat{\mathscr{L}}(\vec{\nabla}^2B^{(1,0)}) \qquad (6.111)\\
&\cdots
\end{aligned}$$

6.5.2.a The Post Newtonian Vainshteinian Potentials

In the spirit of the PPN potentials and also the Vainshteinian potentials $\mathscr{G}_1$ and $\mathscr{I}$, the potentials $B^{(1,n)}$ can be rescaled to factor out any model-dependent parameters. We therefore define the series of Vainshteinian potentials for each Vainshtein order n as

$$V_n^{(in)} = \frac{1}{\sqrt{G}}\left[\frac{\sqrt{G\alpha}}{(2\omega+3)(\phi_0^{(in)})^2}\right]^n B^{(1,n)} \tag{6.112}$$

$$\begin{aligned} V_0^{(in)} &= \sqrt{4\hat{\pi}\mathscr{L}(\rho)} \\ V_1^{(in)} &= \frac{1}{2V_0^{(in)}}\hat{\mathscr{L}}(\vec{\nabla}^2 V_0^{(in)}) \\ &\dots \end{aligned} \tag{6.113}$$

6.5.2.b Recontruction of the Post-Newtonian Metric and Vainshteinian Parameters

Once we have determined the solution of the galileon in terms of the Vainshteinian potentials, the metric at $O(2)$ in PPN given by (6.96) and (6.101) can be reconstructed as

$$h_{00}^{(2)} = 2G_N U + 2\sum_n g_n^{(in)} G_N^{-n} V_n^{(in)} \tag{6.114}$$

$$h_{ij}^{(2)} = \left(2G_N\gamma U + 2\sum_n \gamma_n^{(in)} G_N^{-n} V_n^{(in)}\right)\delta_{ij} \tag{6.115}$$

where we have introduced the PPNV parameters $g_n^{(in)}$ and $\gamma_n^{(in)}$ along with the PPN parameter γ. For GR we have $\gamma = 1$ and $g_n^{(in)} = \gamma_n^{(in)} = 0$, for the Brans-Dicke theory $\gamma = \frac{1+\omega}{2+\omega}$ and $g_n^{(in)} = \gamma_n^{(in)} = 0$ while for the Cubic Galileon we have $\gamma = 1$ and

$$g_n^{(in)} = -\gamma_n^{(in)} = \frac{(2\omega+3)^n}{(4\pi)^{\frac{n+1}{2}}}\left[\frac{\Lambda\sqrt{\phi_0^{(in)}}}{M_p^{(nom)}}\right]^{\frac{3(n+1)}{2}} \tag{6.116}$$

where $M_p^{(nom)} = \frac{1}{\sqrt{8\pi G_N}}$ is the nomimal Planck mass (defined using the measured Newton's constant G_N rather than G.

6.5.3 PPNV At Higher PPN Orders

In the previous subsection we have determined all the ingredients to perform the Post-Newtonian Vainshteinian approximation. However, in this work we aim to go a little bit further and try to push the formalism forward up to Post Post-Newtonian order. To proceed with that task, all that is needed is to go one order beyond in the PPN expansion and to carry out the PPV perturbation treatment in the same way we did above. The relevance of deriving the whole PPNV solutions arises from the geodesic equation which requires such high order solutions. In order to make this subsection more readable we try just to present the important results and avoid describing the cumbersome steps involved in the calculation

Our main goal is to determine the metric components $h_{00}^{(4,1)}$ and $h_{i0}^{(3,1)}$ by following the same strategy as for the $O(2)$ in PPN. But first we are going to solve the equations for the dual fields. We reduce the general equations (6.86) and (6.87) to $O(3)$ and $O(4)$ in PPN which are given by

$$(\Box\varphi)^{(4)} = \alpha^{-\frac{1}{2}} Z^{(3)} = \alpha^{-\frac{1}{2}}(-\partial_0 A_0^{(2)} + \vec{\nabla}^2 B^{(3)} - \frac{1}{2}\partial_i (h_{kk} - h_{00}) A_i^{(1)}), \quad (6.117)$$

$$\vec{\nabla}_0 \varphi^{(2)} = \alpha^{-\frac{1}{2}} A_0^{(2)} = \alpha^{-\frac{1}{2}} \partial_0 B^{(1)}, \quad (6.118)$$

$$\vec{\nabla}_i \varphi^{(4)} = \alpha^{-\frac{1}{2}} A_i^{(3)} = \alpha^{-\frac{1}{2}} B_{,i}^{(3)}, \quad (6.119)$$

and the equation for the B field reduces to

$$\begin{aligned} \mathscr{L}(B^{(3)}, B^{(1)}) + \mathscr{L}(B^{(1)}, B^{(3)}) &- \alpha^{-\frac{1}{2}}(3+2\omega)(\phi_0^{(in)})^2 \vec{\nabla}^2 B^{(3)} \\ &= \\ \alpha^{-\frac{1}{2}}[2(\phi_0^{(in)})^2(3+2\omega)\varphi^{(2)}\vec{\nabla}^2 B^{(1)} &+ \frac{5}{\phi_0^{(in)}} \vec{\nabla} B^{(1)} \vec{\nabla}(\vec{\nabla} B^{(1)})^2 \\ -\frac{1}{\phi_0^{(in)}} \vec{\nabla}^2 B^{(1)} (\vec{\nabla} B^{(1)})^2] &- 8\pi G (\phi_0^{(in)})^2 (T^{(4)} + 2\varphi^{(2)} T^{(2)}). \end{aligned} \quad (6.120)$$

In the last equation $Z^{(3)}$ has been replaced according to the relation (6.117)

Because $\alpha^{-1/2}$ is order $O(1,1)$, in order to compute $\phi^{(4,1)}$ the B field is required at order $O(3,0)$. We expand the $B^{(3)}$ in PPV orders as

$$B^{(3)} = B^{(3,0)} + B^{(3,1)} + B^{(3,2)} + \ldots = \sum_{n=0}^{\infty} B^{(3,n)} \quad (6.121)$$

After having inserting this expansion into equation (6.120) and using the definitions (6.117,6.118,6.119), the leading PPV order equation corresponds to

$$\mathscr{L}(B^{(3,0)},B^{(1,0)})+\mathscr{L}(B^{(1,0)},B^{(3,0)})=\mathbf{S}^{(4,0)} \tag{6.122}$$

where

$$\begin{aligned}
\mathbf{S}^{(4,0)} &= \sum_{k=1}^{11}\left\{\sigma_k^0 S_k^{(4,0)}\right\} = -2\vec{\nabla}\cdot(\frac{1}{2}\vec{\nabla}B^{(1,0)}\partial_i(h_{kk}^{(2,0)}-h_{00}^{(2,0)})A_i^{(2,0)}) \\
- \;& 2\partial_0(\vec{\nabla}^2B^{(1,0)}A_0^{(2,0)})+\vec{\nabla}^2(A_0^{(2,0)})^2+\partial_0^2(\vec{\nabla}B^{(1,0)})^2-\frac{1}{2}\partial_i(h_{kk}^{(2,0)}-h_{00}^{(2,0)}) \\
\times \;& \partial_i(\vec{\nabla}B^{(1,0)})^2+2\partial_i(\vec{\nabla}^2B^{(1,0)}h^{ij(2,0)}A_j^{(1,0)})+\partial_i(h_{kk}^{(2,0)}-h_{00}^{(2,0)})\vec{\nabla}^2B^{(1,0)}A_i^{(1,0)} \\
- \;& 8\pi G(\phi_0^{(in)})^2T^{(4)}-\vec{\nabla}^2(A_k^{(1,0)}h^{kj(2,0)}A_j^{(1,0)})-2\vec{\nabla}\cdot(\vec{\nabla}B^{(1,0)}\partial_0A^{0(2,0)})
\end{aligned} \tag{6.123}$$

and the first PPV order equation into

$$\mathscr{L}(B^{(3,1)},B^{(1,0)})+\mathscr{L}(B^{(1,0)},B^{(3,1)})=\mathbf{S}^{(4,1)} \tag{6.124}$$

where

$$\begin{aligned}
\mathbf{S}^{(4,1)} &= \sum_{k=1}^{25}\left\{\sigma_k^1 S_k^{(4,1)}\right\} = -\{\mathscr{L}(B^{(3,0)},B^{(1,1)})+\mathscr{L}(B^{(1,1)},B^{(3,0)})\} \\
- \;& 16\pi G\phi_0^{(in)}\varphi^{(2,1)}T^{(2)}+\alpha^{-\frac{1}{2}}(3+2\omega)(\phi_0^{in})^2\vec{\nabla}^2B^{(3,0)}+2\partial_0^2(\vec{\nabla}B^{(1,0)}\cdot\vec{\nabla}B^{(1,1)}) \\
- \;& 2\vec{\nabla}\cdot[\vec{\nabla}B^{(1,0)}\partial_0A_0^{(2,1)}]-2\vec{\nabla}\cdot[\vec{\nabla}B^{(1,1)}\partial_0A_0^{(2,0)}]+2\vec{\nabla}^2(A_0^{(2,0)}A_0^{(2,1)}) \\
- \;& 2\partial_0(\vec{\nabla}^2B^{(1,1)}A_0^{(2,0)})-2\partial_0(\vec{\nabla}^2B^{(1,0)}A_0^{(2,1)})-\vec{\nabla}\cdot(\vec{\nabla}B^{(1,0)}\partial_k(h_{ii}^{(2,0)}-h_{00}^{(2,0)})A_k^{(1,1)}) \\
- \;& \vec{\nabla}\cdot(\vec{\nabla}B^{(1,0)}\partial_k(h_{ii}^{(2,1)}-h_{00}^{(2,1)})A_k^{(1,0)})-\vec{\nabla}\cdot(\vec{\nabla}B^{(1,1)}\partial_k(h_{ii}^{(2,0)}-h_{00}^{(2,0)})A_k^{(1,0)}) \\
- \;& \partial_k(h_{ii}^{(2,0)}-h_{00}^{(2,0)})\partial_k(\vec{\nabla}B^{(1,0)}\cdot\vec{\nabla}B^{(1,1)})-\frac{1}{2}\partial_k(h_{ii}^{(2,1)}-h_{00}^{(2,1)})\partial_k(\vec{\nabla}B^{(1,0)}\cdot\vec{\nabla}B^{(1,0)}) \\
- \;& \vec{\nabla}^2(A_k^{(1,0)}h_{km}^{(2,0)}A_m^{(1,1)})-\vec{\nabla}^2(A_k^{(1,0)}h_{km}^{(2,1)}A_m^{(1,0)})-\vec{\nabla}^2(A_k^{(1,1)}h_{km}^{(2,0)}A_m^{(1,1)}) \\
+ \;& 2\partial_k(\vec{\nabla}^2B^{(1,0)}h_{km}^{(2,0)}A_m^{(1,1)})+2\partial_k(\vec{\nabla}^2B^{(1,0)}h_{km}^{(2,1)}A_m^{(1,0)})+2\partial_k(\vec{\nabla}^2B^{(1,1)}h^{km(2,0)}A_m^{(1,0)}) \\
+ \;& \partial_k(h_{ii}^{(2,0)}-h_{00}^{(2,0)})\vec{\nabla}^2B^{(1,0)}A_k^{(1,1)}+\partial_k(h_{ii}^{(2,0)}-h_{00}^{(2,0)})\vec{\nabla}^2B^{(1,1)}A_k^{(1,0)} \\
+ \;& \partial_k(h_{ii}^{(2,1)}-h_{00}^{(2,1)})\vec{\nabla}^2B^{(1,0)}A_k^{(1,0)}+\frac{5\alpha^{-\frac{1}{2}}}{\phi_0^{(in)}}\vec{\nabla}B^{(1,0)}\cdot\vec{\nabla}(\vec{\nabla}B^{(1,0)}\cdot\vec{\nabla}B^{(1,0)}) \\
- \;& \frac{\alpha^{-\frac{1}{2}}}{\phi_0^{(in)}}\vec{\nabla}^2B^{(1,0)}\vec{\nabla}B^{(1,0)}\cdot\vec{\nabla}B^{(1,0)}.
\end{aligned} \tag{6.125}$$

Therefore the $B^{(3,0)}$ and ${}^{B}(3,1)$ fields required to solve the galileon up to post post-Newtonian Vainstenian order correspond to

$$B^{(3,0)} = \sum_{k=1}^{11} \sigma_k^0 \frac{\hat{\mathscr{L}}(S_k^{(4,0)})}{2B^{(1,0)}} \tag{6.126}$$

$$B^{(3,1)} = \sum_{k=1}^{25} \sigma_k^1 \frac{\hat{\mathscr{L}}(S_k^{(4,1)})}{2B^{(1,0)}} \tag{6.127}$$

All the Vainshtenian order equations are clearly linear and then it justifies they have an unique well defined solution for the homogeneous solution of equation (6.124). However, the fact that the post-Newtonian leading PV order solution $B^{(1,0)}$ is dual, i.e. it has two branches, makes the source $\mathbf{S}^{(4,1)}$ to have two branches as well. Thus the most general solution to (6.124) inherit such duality .

6.5.4 On the Need of Basis for Post-Post Newtonian Vainstenian Solutions

The explicit expression of (6.126) and (6.127) can be worked out explicitly in a similar fashion as we did for the post post-Newtonian Vainshteinian solutions of the metric outside the Vainshtein radius. That is, by means of the definitions of new PPNV potentials at the corresponding order. However we must say, it not a really important task. It is only important to point out that different potentials than the ones considered before are needed to do it. The specific definitions of them are of course conventional and hence not unique, however there's no way of express them in terms of the old ones. In order to understand this better, let us consider (6.122) and (6.124). The $S_k^{(4,n)}$ terms are nothing but specific combinations of products and linear operators of already know potentials $V_n^{in/out}$. A possible set new post-post Newtonian Vainshteinian potentials to write the solutions of (6.126) and (6.127) could be defined as

$$\begin{aligned} V_k^{in(3,0)} &\equiv \frac{\hat{\mathscr{L}}(S_k^{(4,0)})}{2V_0^{in}} \\ V_k^{in(3,1)} &\equiv \frac{\hat{\mathscr{L}}(S_k^{(4,1)})}{2V_0^{in}} \end{aligned}$$

so that

$$B^{(3,0)} = \sum_{k=1}^{11} \sigma_k^0 V_k^{in(3,0)}$$
$$B^{(3,1)} = \sum_{k=1}^{25} \sigma_k^1 V_k^{in(3,1)}$$

At this point, we don't know whether these $S_k^{(4,n)}$ are independent or not, or in other words if k_{max} is the minimum of possible number of terms in contrast to the number we found in the case outside the Vainshtein region. Althought the set can be reduced to an independent set. We must say that, in this work, we didn't get too far in the task of getting an independent set of potentials, or at least we don't know. But the important lesson we have learnt is that: together the standard post-post Newtonian potentials and those determined for the outside region, are not enough to describe the full PPN of a theory with Vainshtein mechanism as the cubic galileon. A price to pay for this lack is that we cannot have yet well defined PPNV parameters as we did in previous sections.

6.5.5 The Post Post Newtonian Vainshteinian Metric

Gathering all the solutions previously derived together, we can now determine the first PPV correction of the post post-Newtonian GR solution showed at (6.5.1).

The Einstein equations at higher PPN orders 3 and 4 and first PPV order are given by

$$R_{i0}^{(3,1)} = \varphi_{,i0}^{(2,1)}/\phi_0^{(in)}, \tag{6.128}$$

$$\begin{aligned} R_{00}^{(4,1)} &= -\frac{8\pi G}{\phi_0^{(in)}}\left(\frac{1}{2}g_{00}^{(2,1)}T^{(2)} + \varphi^{(2,1)}(T_{00} + \frac{1}{2}T^{(2)})\right) \\ &+ \frac{1}{(\phi_0^{(in)})^3}\vec{\nabla}^2\phi^{(2,1)}(\vec{\nabla}B^{(3,0)})^2 + \partial_0^2\varphi^{(2,1)} + \frac{1}{2}g_{00}^{2,0}\vec{\nabla}^2\varphi^{(2,1)} - (\Box\phi)^{(4,1)}) \end{aligned} \tag{6.129}$$

To proceed, we first used both R_{00} and R_{i0} given by (6.10) and (6.11) and we casted them into the standard PPN gauge defined by (6.49) and (6.50). Then we plugged the resulting expressions of R_{00} into (6.129). After doing so, we also introduced the known solutions at lower orders, we integrated out the differential equation and simplified

the resulting expression. Finally the first PPV correction of the post-post newtonian time-time component of the metric resulted to be

$$\begin{aligned} h_{00}^{(4,1)} &= \frac{\alpha^{-\frac{1}{2}}}{\phi_0^{(in)}}[-\frac{3}{4}P_1+\frac{5}{4}P_2-\frac{4}{(\phi_0^{(in)})^3}P_3-\frac{2}{\phi_0^3}P_4 \\ &- \sum_{k=1}^{11}\sigma_k^0 V_k^{in(3,0)}-\frac{11\sqrt{G}}{4}\mathscr{U}V_0^{in}+\frac{2G^{\frac{3}{2}}}{(\phi_0^{(in)})^3}V_0^{in}(\vec{\nabla}V_0^{in})^2] \end{aligned} \tag{6.130}$$

The P potentials are defined in appendix (B).

In the case of $h_{i0}^{(3,1)}$ the same procedure is much more straightforward, so after equating both sides, integrating out the Laplacian and simplifying we get

$$h_{i0}^{(3,1)} = \frac{1}{4}\vec{\nabla}^{-2}\varphi_{,i0}^{(2,1)}. = \frac{\alpha^{-\frac{1}{2}}\sqrt{G}}{4}\vec{\nabla}^{-2}V_{0,i0}^{in} \tag{6.131}$$

6.6 Back to Spherical Symmetry

In the first sections of this chapter we have presented and developed the full PPNV expansion for the cubic galileon theory to $O(2)$ in PPN both inside and outside the Vainshtein radius in terms of general potentials. The formalism for the standard theory, valid outside the Vainshtein radius, was also fully established to $O(4)$ in PPN. However, we didn't get that far with the dual theory, applicable in the strong field regime inside the Vainshtein region. Nevertheless, the way is largely walked in that direction. In order to illustrate the most relevant and well established results of this chapter, we now are going to present these results in the particular case of a spherically symmetric and static source.

We start from the expansion outside the Vainshtein radius. The second term inside the integral of the Vainshteinian potential (6.63) is antisymmetric in the exchange of $\vec{x}'$ and $\vec{x}''$ which means that it will vanish in any spherically symmetric situation. Using $\rho(t,\vec{x}) = M\delta^{(3)}(\vec{r}) = \frac{M}{4\pi}\frac{\delta(r)}{r^2}$ we evaluate the integral as $U_V = \frac{M^2}{r^4}$. Since the Newtonian potential is $U = \frac{M}{r}$, we determine the metric solution as

$$h_{00} = \frac{2G_0M}{r}\left[1-\beta_{(out)}\left(\frac{r_V}{r}\right)^3\right] \tag{6.132}$$

$$h_{ij} = \frac{2G_0M}{r}\left[\frac{1+\omega}{2+\omega}+\beta_{(out)}\left(\frac{r_V}{r}\right)^3\right]\delta_{ij} \tag{6.133}$$

where $\beta_{(out)} = \frac{1}{64\pi(3+2\omega)^2(2+\omega)(\phi_0^{(out)})^2}$.

We turn now to the region inside the Vainshtein radius. The operator $\mathscr{L}$ for spherical symmetry gives

$$\mathscr{L}(u,v) = u'v''' - u'''v' + \frac{2}{r}(v'u'' + 3u'v'') + \frac{4}{r^2}u'v'. \tag{6.134}$$

For the Vainshtein order 0 case, $u = v = V_0^{(in)}$ so that $\mathscr{L}(u,u) = \frac{4}{r^2}\frac{d}{dr}[r(u')^2] = \frac{M}{r^2}\delta(r)$ which gives the solution $V_0^{(in)} = \sqrt{Mr}$. This leads to the metric solution

$$h_{00}^{(2)} = 2G_N\frac{M}{r}\left[1 + 4\sqrt{2\pi}(\phi_0^{(in)})^{3/4}\left(\frac{r}{r_V^{(nom)}}\right)^{3/2}\right] \tag{6.135}$$

$$h_{ij}^{(2)} = 2G_N\frac{M}{r}\left[1 - 4\sqrt{2\pi}(\phi_0^{(in)})^{3/4}\left(\frac{r}{r_V^{(nom)}}\right)^{3/2}\right]\delta_{ij} \tag{6.136}$$

where we have defined the nomimal Vainshtein radius $r_V^{(nom)} = \frac{1}{\Lambda}\left(\frac{M}{M_p^{(nom)}}\right)^{1/3}$. Let us now turn to the values $\phi_0^{(in)}$ and $\phi_0^{(out)}$. In principle, one can rescale units, for instance, $\Lambda \to \Lambda\sqrt{\phi_0^{(out)}}$ and similarly for all other mass (and length) scales. Then one can set either of $\phi_0^{(in)}$ or $\phi_0^{(out)}$ (but not both) to unity by simple unit re-definition. It is a matter of choice which one, but for what follows we choose to set $\phi_0^{(in)} = 1$ as it is the most relevant to the solar system (in which case $G_N = G$ and $M_p^{(nom)} = M_p$).

The spherically symmetric solutions may also be interpreted with some caution in a different way. For the outer region case, defining an effective Newtonian constant $G_N^{(eff)} = G_0\left[1 - \beta_{(out)}\left(\frac{r_V}{r}\right)^3\right]$ which runs with scale, we can then define an effective γ parameter as

$$\gamma^{(eff,out)} = \frac{1+\omega}{2+\omega}\left[1 + 2\beta_{(out)}\frac{2+\omega}{1+\omega}\left(\frac{r_V}{r}\right)^3\right] \tag{6.137}$$

which also runs with scale. Likewise, for the inner scale, defining an effective Newtonian constant $G_N^{(eff)} = G\left[1 + 4\sqrt{2\pi}\left(\frac{r}{r_V}\right)^{3/2}\right]$ leads us to define the effective γ parameter as

$$\gamma^{(eff,in)} = 1 - 8\sqrt{2\pi}\left(\frac{r}{r_V}\right)^{3/2} \tag{6.138}$$

In principle one can take the above relations to derive constraints on the Vainshtein radius (and subsequently the scale Λ), however, caution should be taken. Unfortunately, we cannot take the existing constraints on γ at face value but the exact way the

constraints are derived must be taken into consideration (due to the variations of $G^{(eff)}$ and $\gamma^{(eff)}$ with scale. We leave this for a separate work.

For completeness, let us give a rough estimate of the deviations from GR in the solar system. In figure 1 we display the functions $h_{00}^{(2)}$ and h_{ij} versus r as well as the residuals from GR. We assume a spherically symmetric solar system with all matter concentrated in the sun. Then $M_{\odot}/M_p = 1.12 \times 10^{57}$ so that $r_V = 1.02 \times 10^{-5} \frac{1eV}{\Lambda}\, au$. For a choice of $\Lambda = 1/1000km \sim 2 \times 10^{-13} eV$ ($r_V \sim 5 \times 10^7 au$) (in order to get cosmic acceleration at the present epoch), this theory predicts deviations of the order $\sim 10^{-10}$ at the orbit of Jupiter and $\sim 10^{-9}$ at the orbit of Neptune. It would seem that these are too small to be detected.

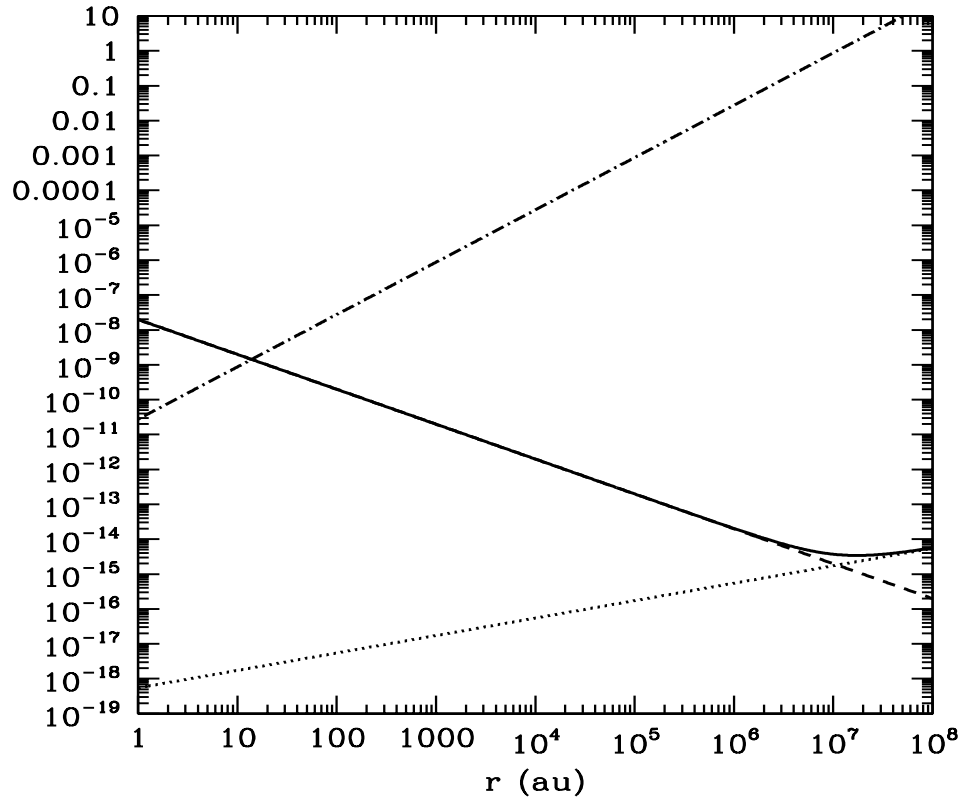

Fig. 6.1 Solutions for the potential $h_{00}^{(2)}$ for the Cubic Galileon inside the Vainstein radius. We display the Newtonian term (dash), the Vainshteinian correction (dotted), the total potential (solid) and $h_{00}^{(2,1)}/h_{00}^{(2,0)}$ (dash-dot).

However, other probes involve the β parameter which arises in the perturbation of the metric at $O(4)$ in PPN. By simply inserting the known solutions, perfom a cumbersome reduction of expressions and integrate the resulting spherically symmetric versions of equations (6.130) and (6.47) for the inner regime, we get the following solutions

$$h_{00}^{(4)} = -2\left\{1+\frac{1}{16\sqrt{\pi}}(35+\frac{3}{2\pi})\left(\frac{r}{r_v}\right)^{\frac{3}{2}}\right\}\left(\frac{r_s}{r}\right)^2, \tag{6.139}$$

In the same spirit as above, the effective running β parameter for the inside regime (which is the relevant one for the solar-system tests) is given by

$$\beta^{(eff,in)} = \left\{1+\frac{1}{16\sqrt{\pi}}(35+\frac{3}{2\pi})\left(\frac{r}{r_v}\right)^{\frac{3}{2}}\right\} \tag{6.140}$$

As any semiconservative theory with not preferred frame effects, the cubic galileon theory has $\alpha_i = \zeta_i = \hat{\xi} = 0$. In this case, linear combinations of β and γ (whose PPNV fluctuations are of the same order) are measured also in other solar system tests appart of the time-delay and deflection of light experiments, for instance $\eta_1 = 2\gamma + 2 - \beta$ is directly determined by measurements of the perihelion shifts while $\eta_2 = 4\beta - \gamma$ by tests of violations of the strong equivalence principle(SEP) like planetary laser ranging, the Nordtvedt effect experiments and geophysical tests of the Newton constant [326, 333]. In our solar-system $\beta - 1$ and γ for the cubic galileon theory roughly run from 10^{-12} to 10^{-6}. Althought current experiments are not able to detect η_1 and η_2 for this model, the rapid advance of technology has brought new instruments with unique performance that could lead to major improvements in the tests of relativistic gravity and already led to a host of recently proposed gravitational experiments that undoubtedly bring us great hope about constraining the PPNV parameters of the cubic galileon theory . For instance, the tracking of the the BepiColombo Laser Altimeter (BELA) at mercury [135, 306] would provide a measurement of η_i with an accuracy of $\sim 2\times 10^{-6}$. Other very promising experiments are those testing the SEP, for example it is expected that STEP will provide measurements up to order 10^{-18} [1].

6.7 Conclusion

We have fully established the PPNV formalism up to $O(2)$ for observers placed inside and outside the Vainshtein radius. For both thresholds we determined the full set of potentials needed to express the required PPN solutions of the metric and the galileon and therefore a new set of PPNV parameters were well defined. For the outside case we treated the standard configuration space of the cubic galileon perturbatively to carry out the PPNV approximation. In this case, it was possible to cast the relevant post-Newtonian potential, needed to express the galileon, as a closed integral. In turn, for the inside case we carried out the approximation in the dual configuration space. In contrast to the outside case, the solution of the post-Newtonian equation remains unknown so far, however some knowledge about it has been gained when we realised it holds the whole set of properties of bi-linear operators. The next order corrections were also investigated in both cases. The $O(4,0)$ and $O(4,-2)$ corrections of the field and metric corresponding to the outside case were determined in terms of an independent set of post-post Newtonian Vainshteinian potentials, however we didn't conclude the procedure to get formally the final PPNV parameters since we haven't solve yet the issue of the residual gauge freedom that in the standard PPN formalism translates into dropping away any dependence on the $\mathscr{B}$ potential of the metric at order $O(4)$ in PPN. Anyway some previous version of the actual formal values have been computed.

Assuming that our solar-system can be approximated as a spherically symmetric system whose mass is concentrated in the Sun, we derived some useful rough estimates of the range in which the effective running PPN parameters of the cubic galileon theory lay. According to this, we open the possibility of detecting signatures of the galileons at high precision gravitational experiments on solar-system scales in a near future such like those testing the SEP, for example STEP and the measurement of the perhelion shift o fmercury by the tracking of the the BepiColombo Laser Altimeter.

CHAPTER 7

DISCUSSION AND CONCLUSIONS

The objective of this Thesis is to test the viability of some theoretical frameworks suitable to describe gravitational phenomena at cosmological and astronomical scales. These frameworks were constructed to encompass possible modifications to the general relativistic gravitational theory and they also provide a tool to test it. Specifically, we generated some tools to test theories with Vainshtein screening mechanism on small astrophysical scales which tend to behave as the Brans-Dicke theory on very large cosmological scales. The Thesis is arranged in two main parts. Along the first part, made of chapters 3,4 and 5, we carry out a treatment of modified theories of gravity suitable to study cosmological phenomena. On the other hand, in the second part (chapter 6) we aim to study aspects of the phenomenology of gravitational astrophysical systems.

The first two chapters were fully introductory and they are needed to prepare the ground to address the subsequent chapters. In chapter 3 we explored the theoretical implications of BDT, the simplest alternative theory to GR, on the cosmological scale regime. We studied two types of models: rBDT and uBDT models . We discovered that the expansion history of BDT is close to ΛCDM however the very small discrepancies lead to important differences in recombination and henceforth on the CMB anisotropies. Signs of the new BDT modified expansion are manifested in the CMB anisotropies as a modified acoustic scale an extra damping effect appears changing the shape of the peaks specially on small angles with respect to the line of sight. The main features of BDT perturbations produce some changes in the late ISW. Additionally, matter perturbations were found not particular sensitive to the BDT parameters. In despite of these small effects, sufficiently precise measurements of $P(k)$ would be able to constrain importantly the BDT model. We also discovered that the Alcock-Paczynski distortion might be detectable at very high redshifts which the current surveys haven't reach. Weak CMB-lensing is directly coupled to the scalar perturbation and some

signatures of BDT may appear at small angular scales. These implications were key information to carry out the analysis with observational data.

In chapter 4 we explicitly compared the theoretical predictions of BDT against observational data by using different methods. One of the realisations we had in chapter 3 is that the anisotropies of the CMB are excellent measurements to be fitted by BDT was verified in chapter 4. By applying the MCMC technique we sample the parameters space of rBDT and uBDT in order to derive estimates of the BDT and cosmological parameters. We obtained very tight constraints of the BDT parameters according to the latest observations from Planck. Even before the first Planck data had been launched, we improved the existing constraints of $\omega > 120$ at 95% of C.L. using WMAP7 + SDSS-R4 derived by Acquaviva in [2] to $\omega > 269$ at the same C.L. using WMAP7+SPT within the uBDT. Constraints using this dataset for the rBDT are weaker and not fully reliable because of the peak in the 1D distribution of ω. The latter could be happening due to the tension between the measurements of θ_{rec} from SPT and WMAP so we feel more confident about the constraint arisen in uBDT. Such results also has the advantage that it can be thought as a large-scales limit of more general theories with self-interactions. We also set limits on the Newton constant today with the same data set which result to be $1.10^{+0.13}_{-0.14}$ at 95% of confidence level.

The inclusion of measurements of the temperature anisotropies of CMB from Planck, strongly improved our previous constraints on ω and ξ. Our best results with Planck+WMAP9(pol) is $\omega > 1834$ at 95% of C.L. and with Planck+PlanckLens $\omega > 2441$ at 95% of C.L. within the uBDT. Interestingly, contrary to our expectations, results within rBDT are weaker than within uBDT even when the parameters space of the former is smaller. What happens is that the ξ parameter helps to fit better the CMB, as a probe, the best fit model of uBDT with Planck+WMAP9(pol) has $-\log(\mathscr{L}) = 4905.94$ whilst the best-fit rBDT model with the same dataset is $-\log(\mathscr{L}) = 4991.32$ ($\mathscr{L}$ is the likelihood). As we see above, Planck+PlanckLens gives the best result for ω. But for ξ the best constraints are obtained for Planck+WMAP9(pol) as $\xi = 1.12^{+0.11}_{-0.11}$ at the 95% confidence level , significantly improving on previous work. In order to set stronger limits on ξ, we also fitted primordial BBN abundances of Helium-4 and Deuterium using the uBDT models. Our best constraint using Planck + WMAP9(pol) + ACT + SPT + BBN is given by 1.009 ± 0.014, notice that the error bar for ξ improves in one order of magnitude and the mean value of ξ is pushed from larger values to 1. Let us recall that the BDT is usually used as a consistent implementation of GR with a time-varying effective gravitational strength G_{eff}, in this context, limits on $\dot{G}_{eff}$ were imposed using different datasets. The worst value given by $2.45 \times 10^{-13}\ years^{-1}$ accordingly with WMAP alone and the best improved almost one order of magnitude $3.6 \times 10^{-14}\ years^{-1}$ according to PlanckTemp + PlanckLens + HL.

Now lets turn to the conclusions of constraints of BDT with other complementary dataset apart of the CMB. When one is aiming to constrain BDT using direct measurements of $P(k)$, care should be taken for handling the bias parameter and G_{eff}. In order to skip this possible issues we conclude that the rBDT are more convenient to fit $P(k)$ measurements. This choice is actually justified by the constraints on ξ above. The resulting constraint for ω within such models using $P(k)$ measurements at redshift $z = 0$ from SDSS-R4 is $\omega > 592.4$ at 95% of confidence level. Our result from WMAP7 has been importantly improved along with the constraints for the cosmological parameters. All these results together are consistent with ΛCDM up to 1σ. Furthermore, we updated constraints from [2] and other works before had been released. Normally, complementary data to test dark energy is included into the analysis. In the most popular code to carry out such analysis the standard implementation of this sort of tests account for measurements of H_0 from HST. However, we argue that such measurements are not model-independent. In order to reconstruct H_0 from the actual measured luminosity distances d_L, ΛCDM is granted as the correct fitting model. However, for consistency, if we aim to test the cosmic expansion arose in a cosmological model is important to use a model-independent approach. A possibility of this kind are tests of the expansion by means of the Alcock-Pazcynski effect. Unfortunately, these tests do not have the constraining power that the H_0 tests have at low redshifts. Nonetheless, we should keep this choice in mind along the near future since more precise measurements of the APT and at higher redshift are about coming.

In chapter 4 we also derived forecasts of constraints of ω for Euclid by using the Fisher matrix method to estimate maximum errors. We first set a baseline constraint for the BDT parameters which is further tightened by including the estimates of the covariance matrix of measurements of $\tilde{P}(k,\mu,z)$ by Euclid. The constraint for both datasets result to be very strong, even being close to the order of the limits from solar system, $\omega_{lower} = 1.7 \times 10^4$. By increasing the cut off and the number of redshift bins leads to a even tighter constraint $\omega \sim 10^5$. We found that ω has such a huge boost in order to fit the variation of the expansion rate well inside the error bars corresponding to the measurement of radial component which is sub-percentage level.However this last forecast is restricted to the requirement that the FoG effect is almost vanishing which is not necessarily true. In conclusion, measurements of RSD with the resolution of Euclid would be a powerful tool to constrain the BDT ω-parameter and we expect lower limits to lay between $10^4 - 10^5$ so the cosmological constraints for BDT reconcile with those derived from the solar-system experiments.

Finally, in despite of the simplicity of the BDT model, we argue that our constraints are useful to study the viability of more general theories including a extra scalar degree of freedom, encompassed into the general set of Horndeski theories. We constructed

the very specific subset of Horndeski theories that degenerate into Brans-Dicke theories at very large scales ℓ_*. The way we built up this class was simply by analytically expanding the general free functions defining a general Horndeski theory around their specific functional form for BDT. By using the explicit BDT solutions within the 95% limits of our best constraints, we set very conservative limits of the coefficients of the Horndeski's analytic expansion. We argue that the subset of Horndeski theories defined within such region of parameters actually approach to BDT at large cosmological scales within the corresponding confidence level. However this assertion stands to be verified in further research work in the future.

This last problem still needs further investigation and opens a number of questions which define new lines of research in the future. The first motivation we have to carry on investigating the Horndeski subclass is that it provides a framework to systematically classify and sort a host of modified theories of gravity. Furthermore, the fact that the subclass is perturbative expansion, allows us to establish a hierarchy of theories: at lower orders the theories tend to be simpler and more similar to BDT. Due to this feature we could also make the question: Is it possible that estimations of the parameters of simple theories associated with an order L in the hierarchy serve to set limits on the parameters of more complex theories at order H ($L < H$)? If affirmative, at which confidence level the resulting constraints of the H-theories would be?. Also we have another question in the context of cosmology: Is there any kind of attractor-mechanism present in this subclass such that given a theory at a level H in the hierarchy, as it evolves in time the solutions of its degrees of freedom tend to approach to those of theories at lower level in the hierarchy? This question is motivated by the attractor mechanism occurring in scalar-tensor theories: they hold a modification at early times whilst tend to mimic GR at late times. Since this matter is closely related with features of the equations of motion, we consider that a nice and useful way to address this problem would be using the dynamical systems approach which is suitable to analyse the features of configuration space of classical theories. Another point is, if we take any other theory of interest for example Galileons, we could in principle construct a similar subclass of Horndeski theories whose leading order action would be Galileons. So how this subclass would be linked with other subclasses?

It is important to stress that in this work, our goal is not to set constraints on the Horndeski's subclass. Our last conservative estimates to form the Horndeski subclass still need to be verified to be so, the only assertion we make is that the analytic expansion of the action we propose approximates the action of BDT if its coefficients lay inside such limits. The question on whether they stand as actual limits or not remains to be answered. We also must mention, that even though BDT arises as a cosmological limit of other more complex theories, we should not assume our

constraints are valid for all such theories. Our setup we do not propose any alternative mechanism able to describe the expansion history of our universe while other theories like Galileons or massive gravity actually do. Since this mechanism could have other effects beyond the history of expansion, it should be considered that our results do take them into account. Actually this motivates us to draw up another research problem for the future. It remains to investigate whether these effects potentially draw new detectable signatures on other observables like the CMB or LSS.

In chapter 5 we studied a very specific phenomenological setup for modified theories of gravity with a very concise objective: to derive constraints the gBDT parameters using observations of the CMB which would lead to an indirect determination of the rate of growth of LSS assumed to behave as a power law $\mu = \mu_0(1 + ra^s)$. The correspondence between this parametrization of the growth and the effective scalar-tensor theory is given by $\omega(a) = m\, a^n$ where $m = 1/2r\mu_0$ and $n = -s$. According to our baseline dataset was the CMB anisotropies from Planck and complementary BAO and HST tests, we derive a 1σ constraint for the exponent $n = -0.47^{+0.32}_{-0.47}$ and $m = 50.1 \pm 11.2$ or $m > 3.2 \times 10^3$. This result gives rise to two possible regimes where the possible modification has a better chance of being detected in current redshift surveys: 1) $\frac{\mu}{\mu_0} - 1 < 6.2 \times 10^{-3} a^{0.47^{-0.32}_{+0.47}}$ and 2) $\frac{\mu}{\mu_0} - 1 = 10^{-2} \pm 0.089 \times a^{0.47^{-0.32}_{+0.47}}$. These results are valid as far as the phenomenological setup considered here is valid.

In chapter 6, we have fully established the PPNV formalism up to $O(2)$ for observers placed inside and outside the Vainshtein radius. For both thresholds we determined the full set of potentials needed to express the required PPN solutions of the metric and the galileon and therefore a new set of PPNV parameters were well defined. For the outside case we treated the standard configuration space of the cubic galileon perturbatively to carry out the PPNV approximation. In this case, it was possible to cast the relevant post-Newtonian potential needed to express the galileon solution, as a closed integral. In turn, for the inside case we carried out the approximation in the dual configuration space. In contrast to the outside case, the solution of the post-Newtonian equation remains unknown so far, however some knowledge about it has been gained when we realised it holds the whole set of properties of bilinear operators. The next order corrections were also investigated in both cases. The $O(4,0)$ and $O(4,-2)$ corrections of the field and metric corresponding to the outside case were determined in terms of an independent set of post-post Newtonian Vainshteinian potentials, however, we did not conclude the procedure to get formally the final PPNV parameters since we have not solved yet the issue of the residual gauge freedom that in the standard PPN formalism translates into dropping away any dependence on the $\mathscr{B}$ potential of the metric at order $O(4)$ in PPN. Anyway some previous version of the actual formal values have been computed.

Assuming that our solar-system can be approximated as a spherically symmetric system whose mass is concentrated in the Sun, we derived some useful rough estimates of the range in which the effective running PPN parameters of the cubic galileon theory lay. According to this, we open the possibility of detecting signatures of the Galileons at high precision gravitational experiments on solar-system scales in a near future.

Now, we shall hold all the results of this Thesis together by stating our final conclusion. As we already mentioned, this thesis is made of two main parts. The first piece of this work (second in presentation) presents a proposal of a very general framework to study the phenomenology of metric modified theories of gravity bearing the Vainshtein mechanism. The basis of the formalism is motivated on the standard Parametrized Post Newtonian formalism and so its validity is restricted to regimes where the gravitational fields involved are sufficiently weak and the motion of matter is slow, typically this profile is fulfilled by non-relativistic bounded gravitational systems similar to our solar system. Since a host of gravitational system lay under these conditions, this work brings to the field a powerful tool to link this sort of modified theories with observations from coming precision experiments at the solar system and beyond. We explicitly developed the PPNV formalism for the simplest case: the cubic galileon theory. We computed all the necessary potentials required to fully determine the PPNV solutions of all the degrees of freedom involved. Assuming we live in an approximately spherically symmetric solar system, this paradigm allowed us to estimate the extent of detectability of the cubic galileon: some signatures would be detectable at experiments with accuracy of at least one part in 10^6. In this astrophysical part of the Thesis, we also realised that in the boundary, far beyond the Vainshtein radius, the cubic galileon , turns into the Brans-Dicke theory with great accuracy,. This fact bridges the two pieces of the Thesis. The second part of this Thesis encompasses the study of cosmological phenomena involved on the very large scales limit (even beyond the outside regime). In this cosmological part of the Thesis we basically found according to latest cosmological observations, that the scalar responsible for a potential modifications of ΛCDM is strongly suppressed. In despite of how bad such undetectability may sound, we believe it is not a curse indeed, lets recall that these models are promising mainly because they predict the expansion of the universe without assuming dark energy. Actually it is not a surprise that the modification is too tiny, not for nothing GR has settled down so firmly as the theoretical paradigm of gravitation, and the fact that these theories stick so tightly to GR in the well tested thresholds rather tell us about their reliability. So under this scope another objective of this work, has been to test GR being embedded in an ocean of alternative theories that incorporate other possible feasible signatures which cannot be simply dismissed

a-priori by us but rather selected or not by nature. Nonetheless, we also found that according to observations potentially some modifications may be detected.

REFERENCES

[1] The satellite test of the equivalence principle (step). http://einstein.stanford.edu/STEP/.

[2] Viviana Acquaviva, Carlo Baccigalupi, Samuel M. Leach, Andrew R. Liddle, and Francesca Perrotta. Structure formation constraints on the Jordan-Brans-Dicke theory. *Phys.Rev.*, D71:104025, 2005. doi: 10.1103/PhysRevD.71.104025.

[3] G. Riess Adam et al. A Redetermination of the Hubble Constant with the Hubble Space Telescope from a Differential Distance Ladder. *Astrophysical Journal*, 699:539, 2009.

[4] P. A. R. Ade et al. Planck 2013 results. XV. CMB power spectra and likelihood. *A& A*, 571:A15, 2013.

[5] P.A.R. Ade et al. Planck 2013 results. XX. Cosmology from Sunyaev-Zeldovich cluster counts. 2013.

[6] P.A.R. Ade et al. Planck 2013 results. XVI. Cosmological parameters. *Astron.Astrophys.*, 2014. doi: 10.1051/0004-6361/201321591.

[7] Aghanim. Sz counts from planck. http://euclidska.physics.ox.ac.uk/Euclid-SKA/170913/Aghanim.pdf.

[8] A. P.J. Steinhardt Albrecht. Cosmology for grand unified theories with radiatively. induced symmetry breaking. *Phys. Rev. Lett.*, 48:1220, 1982.

[9] Paczynski B. Alcock C. An evolution free test for non-zero cosmological constant. *Nature*, 281:358, 1979.

[10] Levon Pogosian Alessandra Silvestri Robert Crittenden Kazuya Koyama Alireza Hojjati, Gong-Bo Zhao. Cosmological tests of general relativity: a principal component analysis. *Phys. Rev. D*, 85:043508, 2012.

[11] Mustafa A. Amin, Robert V. Wagoner, and Roger D. Blandford. A sub-horizon framework for probing the relationship between the cosmological matter distribution and metric perturbations. *Mon. Not. Roy. Astron. Soc.*, 390:131, 2008.

[12] Paul M. Saffin Constantinos Skordis Ana Avilez-Lopez, Antonio Padilla. The parametrized post-newtonian-vainshteinian formalism. arXiv:1501.01985v1 [gr-qc].

[13] David H. Lyth Andrew R. Liddle. *Cosmological Inflation and Large-Scale Structure Paperback*. 2000.

[14] Melinda Andrews, Yi-Zen Chu, and Mark Trodden. Galileon forces in the solar system. *Phys. Rev. D*, 88:084028, Oct 2013. doi: 10.1103/PhysRevD.88.084028. URL http://link.aps.org/doi/10.1103/PhysRevD.88.084028.

[15] Anthony Challinor Antony Lewis. Weak gravitational lensing of the cmb. *Physics Reports*, 429:1–65, 2006.

[16] C. Armendariz-Picon, V. Mukhanov, and P. J. Steinhardt. Dynamical Solution to the Problem of a Small Cosmological Constant and Late-Time Cosmic Acceleration. *Physical Review Letters*, 85:4438, November 2000. doi: 10.1103/PhysRevLett.85.4438.

[17] C. Armendariz-Picon, V. Mukhanov, and Paul J. Steinhardt. Essentials of k-essence. *Phys. Rev. D*, 63:103510, Apr 2001. doi: 10.1103/PhysRevD.63.103510. URL http://link.aps.org/doi/10.1103/PhysRevD.63.103510.

[18] Doroshkevich A.G. Atrio-Barandela, F. Secondary ionization in a flat universe. *Astrophysical Journal*, 420:26, 1994.

[19] A. Avilez and C. Skordis. Cosmological constraints on brans-dicke theory. *Phys. Rev. Lett.*, 113:011101, Jul 2014. doi: 10.1103/PhysRevLett.113.011101. URL http://link.aps.org/doi/10.1103/PhysRevLett.113.011101.

[20] Eugeny Babichev and Cédric Deffayet. An introduction to the Vainshtein mechanism. *Class.Quant.Grav.*, 30:184001, 2013. doi: 10.1088/0264-9381/30/18/184001.

[21] J. S. Bagla, H. K. Jassal, and T. Padmanabhan. Cosmology with tachyon field as dark energy. *Phys. Rev. D*, 67:063504, Mar 2003. doi: 10.1103/PhysRevD.67.063504. URL http://link.aps.org/doi/10.1103/PhysRevD.67.063504.

[22] Tessa Baker, Pedro G. Ferreira, Constantinos Skordis, and Joe Zuntz. Towards a fully consistent parameterization of modified gravity. *Phys.Rev.*, D84:124018, 2011. doi: 10.1103/PhysRevD.84.124018.

[23] Tessa Baker, Pedro G. Ferreira, and Constantinos Skordis. The Parameterized Post-Friedmann Framework for Theories of Modified Gravity: Concepts, Formalism and Examples. *Phys.Rev.*, D87:024015, 2013. doi: 10.1103/PhysRevD.87.024015.

[24] Heavens A.F. Ballinger W.E., Peacock J.A. Measuring the cosmological constant with redshift surveys. *Mon. Not. Roy. Astron. Soc.*, 282:877, 1996.

[25] J. M. Bardeen. Gauge-invariant cosmological perturbations. *Phys. Rev.D*, 22:1882–1905, 1980.

[26] T. Barreiro, E. J. Copeland, and N. J. Nunes. Quintessence arising from exponential potentials. *Phys. Rev. D*, 61:127301, May 2000. doi: 10.1103/PhysRevD.61.127301. URL http://link.aps.org/doi/10.1103/PhysRevD.61.127301.

[27] John D. Barrow and Paul Parsons. The behaviour of cosmological models with varying-g. *Phys.Rev. D*, 55:1906–1936, 1997.

[28] Moss A. Battye, R.A. Evidence for massive neutrinos from cmb and lensing observations. *Phys. Rev. Lett.*, 112:051303, 2014.

[29] Richard A. Battye and Jonathan A. Pearson. Effective action approach to cosmological perturbations in dark energy and modified gravity. *JCAP*, 1207: 019, 2012. doi: 10.1088/1475-7516/2012/07/019.

[30] Richard A. Battye and Jonathan A. Pearson. Parametrizing dark sector perturbations via equations of state. *Phys.Rev.*, D88(6):061301, 2013. doi: 10.1103/PhysRevD.88.061301.

[31] David Beke. Scalar-Tensor theories from $\Lambda(\phi)$ Plebanski gravity. *J.Phys.Conf.Ser.*, 360:012043, 2012. doi: 10.1088/1742-6596/360/1/012043.

[32] C. L. Bennett et al. First year wilkinson microwave anisotropy probe (wmap) observations: Preliminary maps and basic results. *Astrophys.J.Suppl.*, 148:1, 2003.

[33] C.L. Bennett et al. Four-year cobe dmr cosmic microwave background observations: Maps and basic results. *Astrophysical Journal Letters*, 464::L1–L4., 1996.

[34] C.L. Bennett et al. Nine-Year Wilkinson Microwave Anisotropy Probe (WMAP) Observations: Final Maps and Results. *Astrophys.J.Suppl.*, 208:20, 2013. doi: 10.1088/0067-0049/208/2/20.

[35] P.G. Bergmann. Comments on the scalar-tensor theory. *Int. J. Theor. Phys.*, 1 (25), 1968.

[36] B. Bertotti, L. Iess, and P. Tortora. A test of general relativity using radio links with the Cassini spacecraft. *Nature*, 425:374, 2003. doi: 10.1038/nature01997.

[37] M. Betoule, R. Kessler, J. Guy, J. Mosher, D. Hardin, R. Biswas, P. Astier, P. El-Hage, M. Konig, S. Kuhlmann, J. Marriner, R. Pain, N. Regnault, C. Balland, B. A. Bassett, P. J. Brown, H. Campbell, R. G. Carlberg, F. Cellier-Holzem, D. Cinabro, A. Conley, C. B. D'Andrea, D. L. DePoy, M. Doi, R. S. Ellis, S. Fabbro, A. V. Filippenko, R. J. Foley, J. A. Frieman, D. Fouchez, L. Galbany, A. Goobar, R. R. Gupta, G. J. Hill, R. Hlozek, C. J. Hogan, I. M. Hook, D. A. Howell, S. W. Jha, L. Le Guillou, G. Leloudas, C. Lidman, J. L. Marshall, A. Möller, A. M. Mourão, J. Neveu, R. Nichol, M. D. Olmstead, N. Palanque-Delabrouille, S. Perlmutter, J. L. Prieto, C. J. Pritchet, M. Richmond, A. G. Riess, V. Ruhlmann-Kleider, M. Sako, K. Schahmaneche, D. P. Schneider, M. Smith, J. Sollerman, M. Sullivan, N. A. Walton, and C. J. Wheeler. Improved cosmological constraints from a joint analysis of the SDSS-II and SNLS supernova samples. , 568:A22, August 2014. doi: 10.1051/0004-6361/201423413.

[38] Chris Blake, Eyal Kazin, Florian Beutler, Tamara Davis, David Parkinson, et al. The WiggleZ Dark Energy Survey: mapping the distance-redshift relation with baryon acoustic oscillations. *Mon.Not.Roy.Astron.Soc.*, 418:1707–1724, 2011. doi: 10.1111/j.1365-2966.2011.19592.x.

[39] Jolyon K. Bloomfield, Éanna É. Flanagan, Minjoon Park, and Scott Watson. Dark energy or modified gravity? An effective field theory approach. *JCAP*, 1308:010, 2013. doi: 10.1088/1475-7516/2013/08/010.

[40] N.W. Boggess et al. The cobe mission: Its design and performance two years after the launch. *Astrophysical Journal*, 397:420, 1992.

[41] Efstathiou G. Bond, J.R. The statistics of cosmic background radiation fluctuations. *Mon. Not. Roy. Astron. Soc.*, 226:655, 1987.

[42] J. R. Bond and G. Efstathiou. Cosmic background radiation anisotropies in universes dominated by nonbaryonic dark matter. , 285:L45–L48, October 1984. doi: 10.1086/184362.

[43] J. R. Bond, B. J. Carr, and C. J. Hogan. Cosmic backgrounds from primeval dust. , 367:420–454, February 1991. doi: 10.1086/169640.

[44] H. Bondi and T. Gold. The Steady-State Theory of the Expanding Universe. , 108:252, 1948.

[45] Robert Brandenberger, Ronald Kahn, and William H. Press. Cosmological perturbations in the early universe. *Phys. Rev. D*, 28:1809–1821, Oct 1983. doi: 10.1103/PhysRevD.28.1809. URL http://link.aps.org/doi/10.1103/PhysRevD.28.1809.

[46] C. Brans and R. H. Dicke. Mach's principle and a relativistic theory of gravitation. *Phys. Rev.*, 124:925–935, 1961. doi: 10.1103/PhysRev.124.925.

[47] S. L. Bridle et al. Analytic marginalization over cmb calibration and beam uncertainty. *Mon.Not.Roy.Astron.Soc.*, 335:1193, 2002.

[48] Stephen Brooks and Andrew Gelman. Stephen brooks and andrew gelman. *Journal of Computational and Graphical Statistics*, 7:434–455, 1998.

[49] Emory F. Bunn. Detectability of microwave background polarization. *Phys. Rev. D*, 65:043003, Jan 2002. doi: 10.1103/PhysRevD.65.043003. URL http://link.aps.org/doi/10.1103/PhysRevD.65.043003.

[50] C. Burrage and D. Seery. Revisiting fifth forces in the galileon model. *JCAP*, 1008:011, 2010.

[51] T. Damour C. Armendariz-Picon and V. Mukhanov. k-inflation. *Phys. Lett. B*, 458:209–218, 1999.

[52] N. Kaloper C. Charmousis, R. Gregory and A. Padilla. Dgp specteroscopy. *JHEP*, 10:066, 2006.

[53] D. A. Steer C. Deffayet, X. Gao and G. Zahariade. From k-essence to generalised galileons. 280, 2011.

[54] G. Esposito-Farese C. Deffayet and A. Vikman. Covariant galileon. *Phys.Rev., D*, 79:084003, 2009.

[55] G. Gabadadze C. Deffayet and A. Iglesias. Perturbations of self-accelerated universe. *JCAP*, 0608:012, 2006.

[56] G. Gabadadze C. Deffayet, G. R. Dvali and A. I. Vainshtein. Nonperturbative continuity in graviton mass versus perturbative discontinuity. *Phys. Rev. D*, 65: 044026, 2002.

[57] C. Allende Prieto C. P. Ahn, R. Alexandroff et al. The tenth data release of the sloan digital sky survey: First spectroscopic data from the sdss-iii apache point observatory galactic evolution experiment. *Astrophysical Journal Supplement*, 211:17, 2014.

[58] C. Allende Prieto et al. C. P. Ahn, R. Alexandroff. The ninth data release of the sloan digital sky survey: First spectroscopic data from the sdss-iii baryon oscillation spectroscopic survey. *Astrophysical Journal Supplement*, 203:21, 2012.

[59] S. M. Carroll and E. A. Lim. Lorentz-violating vector fields slow the universe down. *Phys. Rev. D*, 70(12):123525, 2004.

[60] Sean M. Carroll. The cosmological constant. *LivingRev.Rel.*, 4:1, 2001.

[61] John Archibald Wheeler Charles W. Misner, Kip S. Thorne. *Gravitation (Physics Series)*. 1973.

[62] C.V.L. Charlier. *Arkiv. for Mat. Astron. Fys.*, 4:1, 1908.

[63] C.V.L. Charlier. *Arkiv. for Mat. Astron. Fys.*, 16:1, 1922.

[64] X. Chen and M. Kamionkowski. Cosmic microwave background temperature and polarization anisotropy in Brans-Dicke cosmology. *Phys.Rev.*, D60:104036, 1999. doi: 10.1103/PhysRevD.60.104036.

[65] T. Chiba. 1/r gravity and scalar-tensor gravity. *Phys. Lett. B*, 575:1, 2003.

[66] T. Chiba. Generalized gravity and ghost. *JCAP*, 0503:008, 2005.

[67] Takeshi Chiba, Takahiro Okabe, and Masahide Yamaguchi. Kinetically driven quintessence. *Phys. Rev. D*, 62:023511, Jun 2000. doi: 10.1103/PhysRevD.62.023511. URL http://link.aps.org/doi/10.1103/PhysRevD.62.023511.

[68] et al. Chris Blake. The wigglez dark energy survey: measuring the cosmic expansion history using the alcock-paczynski test and distant supernovae. *accepted for publication by Mon. Not. Roy. Astron. Soc.*, 1108.2637, 2011.

[69] et. al. Chris Blake. The wigglez dark energy survey: the growth rate of cosmic structure since redshift z=0.9. *arXiv:1104.2948 [astro-ph.CO]*, 2011.

[70] Nelson Christensen, Renate Meyer, Lloyd Knox, and Ben Luey. Ii: Bayesian methods for cosmological parameter estimation from cosmic microwave background measurements. *Class. Quant. Grav.*, 18:2677, 2001.

[71] Nelson Christensen, Renate Meyer, Lloyd Knox, and Ben Luey. II. Bayesian methods for cosmological parameter estimation from cosmic microwave background measurements. *Class.Quant.Grav.*, 18:2677, 2001. doi: 10.1088/0264-9381/18/14/306.

[72] Yi-Zen Chu and Mark Trodden. Retarded green's function of a vainshtein system and galileon waves. *Phys. Rev. D*, 87:024011, Jan 2013. doi: 10.1103/PhysRevD.87.024011. URL http://link.aps.org/doi/10.1103/PhysRevD.87.024011.

[73] Chia-Hsun Chuang. The clustering of galaxies in the sdss-iii baryon oscillation spectroscopic survey: single-probe measurements and the strong power of normalized growth rate on constraining dark energy. *arXiv:1303.4486 [astro-ph.CO]*, 2013.

[74] Edmund Bertschinger Chung-Pei Ma. Cosmological perturbation theory in the synchronous and conformal newtonian gauges. *Astrophys.J.*, 455:7–25, 1995.

[75] Timothy Clifton, Pedro G. Ferreira, Antonio Padilla, and Constantinos Skordis. Modified Gravity and Cosmology. *Phys.Rept.*, 513:1–189, 2012. doi: 10.1016/j.physrep.2012.01.001.

[76] A. Conley. Discovery of a multiply-lensed submillimeter galaxy in early hermes herschel/spire data. *Astrophysical Journal*, 732:L35, 2011.

[77] Edmund J. Copeland, Andrew R. Liddle, and David Wands. Exponential potentials and cosmological scaling solutions. *Phys. Rev. D*, 57:4686–4690, Apr 1998. doi: 10.1103/PhysRevD.57.4686. URL http://link.aps.org/doi/10.1103/PhysRevD.57.4686.

[78] Skordis C. Copeland, E. Modern cosmology notes. lecture notes.

[79] Neil Cornish, Laura Sampson, Nicolas Yunes, and Frans Pretorius. Gravitational Wave Tests of General Relativity with the Parameterized Post-Einsteinian Framework. *Phys.Rev.*, D84:062003, 2011. doi: 10.1103/PhysRevD.84.062003.

[80] Lovelock D. The four-dimensionality of space and the einstein tensor. *J. Math. Phys.*, 13:874–876, 1972.

[81] K. Koyama D. Gorbunov and S. Sibiryakov. More on ghosts in dgp model. *Phys. Rev., D*, 73:044016, 2006.

[82] et al. D. Kirkman. The cosmological baryon density from the deuterium-to-hydrogen ratio in qso absorption systems: D/h toward q1243+3047. *Astrophysical Journal Suppl.*, 149:1, 2003.

[83] C. M. Caves D. L. Lee, W. Ni and C. M. Will. Theoretical frameworks for testing relativistic gravity. v - post-newtonian limit of rosen's theory. *Astrophysical Journal*, 206:555–558, 1976.

[84] Thibault Damour. Gravitation, experiment and cosmology. based on lectures given at les houches 1992, susy-95 and corfu 1995, to appear in the proceedings of the 5th hellenic school of elementary particle physics. *IHES*, 95:104, 1996.

[85] Thibault Damour and Joseph H. Taylor. Strong field tests of relativistic gravity and binary pulsars. *Phys.Rev.*, D45:1840–1868, 1992. doi: 10.1103/PhysRevD.45.1840.

[86] Kyle S. Dawson et al. The baryon oscillation spectroscopic survey of sdss-iii. *The Astronomical Journal*, 145:10, 2013.

[87] P.; et al. de Bernardis. A flat universe from high-resolution maps of the cosmic microwave background radiation. *Nature*, 404:955–959, 2000.

[88] A. de Felice and S. Tsujikawa. f(r) theories. *Living Reviews in Relativity*, 13:3, 2010.

[89] Claudia de Rham, Gregory Gabadadze, and Andrew J. Tolley. Resummation of massive gravity. *Phys. Rev. Lett.*, 106:231101, Jun 2011. doi: 10.1103/PhysRevLett.106.231101. URL http://link.aps.org/doi/10.1103/PhysRevLett.106.231101.

[90] W. de Sitter. Contributions to a british association discussion on the evolution of the universe. *Nature*, 128:706, 1931.

[91] C. Deffayet. Cosmology on a brane in minkowski bulk. *Phys.Lett. B*, 502: 199–208, 2001.

[92] C. Deffayet and J.-W. Rombouts. Ghosts, strong coupling and accidental symmetries in massive gravity. *Phys. Rev. D*, 72:044003, 2005.

[93] C. Deffayet, Xian Gao, D. A. Steer, and G. Zahariade. From k-essence to generalised Galileons. *Phys.Rev.*, D84:064039, 2011. doi: 10.1103/PhysRevD.84.064039.

[94] P. A. M. Dirac. A new basis for cosmology. *Proceedings of the Royal Society of London A*, 165:199, 1938.

[95] Eisenstein D.J. Dark energy and cosmic sound. *New Astronomy Reviews*, 49: 360–365, 2005.

[96] Jubas J.M. Dodelson, S. Reionization and its imprint on the cosmic microwave background. *Phys. Rev. Lett.*, 70:2224, 1993.

[97] Scott Dodelson. *Modern Cosmology*. Academic Press, Elsevier, 2003.

[98] Y. B.; Syunyaev R. A. Doroshkevich, A. G.; Zel'Dovich. Fluctuations of the microwave background radiation in the adiabatic and entropic theories of galaxy formation. *Soviet Astronomy*, 22:523, 1978.

[99] I. T. Drummond. Bimetric gravity and "dark matter". *Phys. Rev. D*, 63(4): 043503, 2001.

[100] J. Dunkley, E. Calabrese, J. Sievers, G.E. Addison, N. Battaglia, et al. The Atacama Cosmology Telescope: likelihood for small-scale CMB data. 2013.

[101] Joanna Dunkley, Martin Bucher, Pedro G. Ferreira, Kavilan Moodley, and Constantinos Skordis. Fast and reliable MCMC for cosmological parameter estimation. *Mon. Not. Roy. Astron. Soc.*, 356:925–936, 2005. doi: 10.1111/j.1365-2966.2004.08464.x.

[102] Ruth Durrer. *The Cosmic Microwave Background*. 2008.

[103] G. Dvali. Predictive power of strong coupling in theories with large distance modified gravity. *New J. Phys.*, 8:326, 2006.

[104] G. R. Dvali, Gregory Gabadadze, and Massimo Porrati. 4D gravity on a brane in 5D Minkowski space. *Phys. Lett.*, B485:208–214, 2000. doi: 10.1016/S0370-2693(00)00669-9.

[105] A. S. Eddington. On the instability of Einstein's spherical world. , 90:668–678, May 1930.

[106] A.S. Eddington. The end of the world: from the standpoint of mathematical physics. *Nature*, 127:447, 1931.

[107] Phillip Zukin Edmund Bertschinger. Distinguishing modified gravity from dark energy. *Phys.Rev.D*, 78:024015, 2008.

[108] Shinji Tsujikawa Edmund J. Copeland, M. Sami. Dynamics of dark energy. *Int.J.Mod.Phys.D*, 15:1753–1936, 2006.

[109] G. Efstathiou, W.J. Sutherland, and S.J. Maddox. The cosmological constant and cold dark matter. *Nature*, 348:705–707, 1990. doi: 10.1038/348705a0.

[110] George Efstathiou. H0 revisted. arXiv:1311.3461 [astro-ph.CO].

[111] Moody SJ. Efstathiou G. Maximum likelihood estimates of the two- and three-dimensional power spectra of the apm galaxy survey. *Mon. Not. Roy. Astron. Soc.*, 325:1603–1615, 2001.

[112] A. Einstein. Die feldgleichungen der gravitation. *Sitzungsberichte der Koniglich Preußischen Akademie der Wissenschaften (Berlin) Seite*, page 844–847, 1915.

[113] A. Einstein. Erklarung der perihelbewegung des merkur aus der allgemeinen relativitatstheorie. *Sitzungsberichte der Koniglich Preußischen Akademie der Wissenschaften (Berlin)*, page 831–839, 1915.

[114] A. Einstein. Die grundlage der allgemeinen relativitatstheorie. *Annalender Physik*, 354:769–822, 1916.

[115] A. Einstein. *Ann. Phys.*, 69:436, 1922.

[116] A. Einstein. *Structure Cosmologique de l'Espace.* 1933.

[117] D. J. Eisenstein et al. Detection of the Baryon Acoustic Peak in the Large-Scale Correlation Function of SDSS Luminous Red Galaxies. submitted to the Astrophysical J., astro-ph/0501171.

[118] Glenn Elert. The Physics Hypertextbook. http://physics.info/nucleosynthesis.

[119] Pekar V. Eotvos, R.V. and E. Fekete. Beitrage zum gesetze der proportionalitat von tragheit und gravitat. *Ann. Phys. (Leipzig)*, 68:11–66, 1922.

[120] Lattimer J.M. Schramm D.N. Epstein, R.I. The origin of deuterium. *Nature*, 263:198, 1976.

[121] Mangano G. Miele G. Pisanti O. Esposito, S. *JHEP 0009*, 2000.

[122] Mangano G. Miele G. Pisanti O. Esposito, S. A degenerate big bang nucleosynthesis from cmb observations? *Nucl.Phys. B*, 568:421, 2000.

[123] A. G. Riess et al. Bvri light curves for 22 type ia supernovae. *Astron. J.*, 117: 707, 1999.

[124] Amanullah et al. The hubble space telescope cluster supernova survey: Ii. the type ia supernova rate in high-redshift galaxy clusters. *arXiv:1010.5786 [astro-ph.CO]*, 2010.

[125] Becker et. al. Evidence for reionization at z 6: Detection of a gunn-peterson trough in a z = 6.28 quasar. *Astronomical Journal*, 122:2850, 2001.

[126] N.Suzuki et. al. The hubble space telescope cluster supernova survey: V. improving the dark energy constraints above z>1 and building an early-type-hosted supernova sample. *Astrophysical Journal*, 746:85, 2012.

[127] K.A. Olive et al. (Particle Data Group). The review of particle physics. *Chin. Phys. C*, 38:090001, 2014.

[128] Valerio Faraoni. Scalar field mass in generalized gravity. *Class.Quant.Grav.*, 26:145014, 2009.

[129] D.J. Fixsen. The Temperature of the Cosmic Microwave Background. *Astrophys.J.*, 707:916–920, 2009. doi: 10.1088/0004-637X/707/2/916.

[130] A. Friedmann. *Z.Phys.*, 10:377, 1922.

[131] Starobinsky A. A. Frolov A. V., Kofman L. Prospects and problems of tachyon matter cosmology. *Phys. Lett. B*.

[132] Gregory Gabadadze, Kurt Hinterbichler, and David Pirtskhalava. Classical Duals of Derivatively Self-Coupled Theories. *Phys.Rev.*, D85:125007, 2012. doi: 10.1103/PhysRevD.85.125007.

[133] G. Gamow. Expanding universe and the origins of elements. *Phys. Rev.*, 70: 572–573, 1946.

[134] W. R. Gilks, S. Richardson, and D. J. Speigelhalter. *Markov Chain Monte Carlo in Practice*. Chapman and Hall, London, 1995.

[135] J. Gouman et al. Bepicolombo laser altimeter performance tests. *European Planetary Science Congress Abstracts*, 9:64, 2014.

[136] K. S. Stelle. Classical gravity with higher derivatives. *General Relativity and Gravitation*, 9:353–371, 1978.

[137] David Pirtskhalava Gregory Gabadadze, Kurt Hinterbichler. Classical duals of derivatively self-coupled theories. *Phys.Rev. D*, 85:125007, 2012.

[138] Giulia Gubitosi, Federico Piazza, and Filippo Vernizzi. The Effective Field Theory of Dark Energy. *JCAP*, 1302:032, 2013. doi: 10.1088/1475-7516/2013/02/032.

[139] A. Guth and S-Y. Pi. Fluctuations in the new inflationary universe. *Physical Review Letters*, 49:1110, 1982.

[140] A. Guth and S-Y. Pi. Quantum mechanics of the scalar field in the new inflationary universe. *Physical Review D*, 32:1899, 1985.

[141] A.H. Guth. Inflationary universe: A possible solution to the horizon and flatness problems. *Physical Review D*, 23:347, 1981.

[142] J. S. Bagla H. K. Jassal and T. Padmanabhan. Understanding the origin of cmb constraints on dark energy. *Mon. Not. R. Astron. Soc.*, 000:1–12, 2010.

[143] E. R. Harrison. Fluctuations at the threshold of classical cosmology. *Physical Review D 1*, 10:2726–2730, 1970.

[144] E. R. Harrison. Fluctuations at the threshold of classical cosmology. *Phys. Rev. D*, 1:2726–2730, May 1970. doi: 10.1103/PhysRevD.1.2726. URL http://link.aps.org/doi/10.1103/PhysRevD.1.2726.

[145] W.K. Hastings. Monte carlo samping methods using markov chains and their applications. *Biometrika*, 57:97–109, 1970. doi: 10.1093/biomet/57.1.97.

[146] S. Hawking. The development of irregularities in a single bubble inflationary universe. *Physics Letters B*, 115:295, 1982.

[147] Alan Heavens. Bayesian statistics in cosmology. *Lectures and workshops at SCMA V*, 2011.

[148] G. Horndeski. Second-order scalar-tensor field equations in a four-dimensional space. *International Journal of Theoretical Physics*, 10(6):363–384, 1974.

[149] Gregory Walter Horndeski. Second-order scalar-tensor field equations in a four-dimensional space. *Int.J.Theor.Phys.*, 10:363–384, 1974. doi: 10.1007/BF01807638.

[150] F. Hoyle. A New Model for the Expanding Universe. , 108:372, 1948.

[151] Sugiyama N. Hu, W. Small scale integrated sachs-wolfe effect. *Phys. Rev. D*, 50:627, 1994.

[152] W. Hu and I. Sawicki. Models of f(r) cosmic acceleration that evade solar-system tests. *Phys. Rev. D*, 76:064004, 2007.

[153] Wayne Hu. Parametrized Post-Friedmann Signatures of Acceleration in the CMB. *Phys. Rev.*, D77:103524, 2008. doi: 10.1103/PhysRevD.77.103524.

[154] Wayne Hu and Ignacy Sawicki. A Parameterized Post-Friedmann Framework for Modified Gravity. *Phys. Rev.*, D76:104043, 2007. doi: 10.1103/PhysRevD.76.104043.

[155] White M. Hu W. Power spectra estimation for weak lensing. *Astrophysical Journal*, 554:67–73, 2001.

[156] E. P. Hubble. A spiral nebula as a stellar system: Messier 33. , 63:236–274, May 1926. doi: 10.1086/142976.

[157] E. P. Hubble. Extragalactic nebulae. , 64:321–369, December 1926. doi: 10.1086/143018.

[158] Seljak U Rutledge RE Magnier E et al. Hui L, Burles S. On estimating the qso transmission power spectrum. *Astrophysical Journal*, 552:15–35, 2001.

[159] Nichol RC. Huterer D, Knox L. The angular power spectrum of edinburgh/durham southern galaxy catalogue galaxies. *Astrophysical Journal*, 555: 547–557, 2001.

[160] Fabio Iocco, Gianpiero Mangano, Gennaro Miele, Ofelia Pisanti, and Pasquale D. Serpico. Primordial Nucleosynthesis: from precision cosmology to fundamental physics. *Phys.Rept.*, 472:1–76, 2009. doi: 10.1016/j.physrep.2009.02.002.

[161] F. Bourliot P. G. Ferreira J. Zuntz, T. G. Zlosnik and G. D. Starkman. Vector field models of modified gravity and the dark sector. *Phys. Rev. D*, 81(10): 104015, 2010.

[162] T. Jacobson. Einstein-aether gravity: a status report. *PoS, QG-PH*, 20, 2007.

[163] Gustavo Niz Javier Chagoya, Kazuya Koyama and Gianmassimo Tasinato. Galileons and strong gravity. *Journal of Cosmology and Astroparticle Physics*, 10:055, 2014.

[164] Pascual Jordan. *Schwerkraft und Weltall*. 1955.

[165] Jr. K. Nordtvedt. Post newtonian metric for a general class of scalar tensor gravitational theories and observational consequences. *Astrophysical Journal*, 161:1059–1067, 1970.

[166] C. Kahn and F. Kahn. Letters from einstein to de sitter on the nature of the universe. *Nature*, 257:451, 1975.

[167] Manoj Kaplinghat, Lloyd Knox, and Constantinos Skordis. Rapid Calculation of Theoretical CMB Angular Power Spectra. *Astrophysical Journal*, 578:665, 2002. doi: 10.1086/342656.

[168] Lawrence Kawano. Let's go: Early universe ii, primordial nucleosynthesis the computer way. *Fermilab-pub,92*, 4:A, 1992.

[169] P. Kerszberg. *Einstein and the History of General Relativity*. 1990.

[170] Khoury and A. Weltman. Chameleon cosmology. *Phys. Rev. D*, 69:044026, 2004.

[171] Khoury and A. Weltman. Chameleon fields: Awaiting surprises for tests of gravity in space. *Phys. Rev. Lett.*, 93:171104, 2004.

[172] Matthew D Klimek. Parameterized post-newtonian coefficients for brans–dicke gravity with d + 1 dimensions. *Classical and Quantum Gravity*, 26(6), 2009.

[173] L. Knox, N. Christensen, and C. Skordis. The age of the universe and the cosmological constant determined from cosmic microwave background anisotropy measurements. *Astrophys.J.*, 563:L95–L98, 2001. doi: 10.1086/338655.

[174] H. Kodama and M. Sasaki. Cosmological perturbation theory. *Prog. Theoret. Phys. Suppl.*, 78:1–166, 1984.

[175] E. Komatsu et al. Seven-Year Wilkinson Microwave Anisotropy Probe (WMAP) Observations: Cosmological Interpretation. *Astrophys.J.Suppl.*, 192:18, 2011. doi: 10.1088/0067-0049/192/2/18.

[176] A. Kosowsky. *Annals Phys.*, 246:49–85, 1996.

[177] Eleftherios L. Papantonopoulos, editor. *The Invisible Universe: Dark Matter and Dark Energy*, volume 720 of *Lecture Notes in Physics*. 2007.

[178] K. Koyama L. Pogosian, A. Silvestri and G. B. Zhao. How to optimally parametrize deviations from general relativity in the evolution of cosmological perturbations. *Phys. Rev. D*, 81:104023, 2010.

[179] G. Lamaitre. Note on de sitter's universe. *J.Math.Phys.*, 4:188, 1925.

[180] G. Lamaitre. Expansion of the universe, a homogeneous universe of constant mass and increasing radius accounting for the radial velocity of extra-galactic nebulae. *MNRAS*, 91:483, 1931.

[181] G. Lemaitre. L'univers en expansion. *Ann.Soc.Sci.Bruxelles*, 47A:49, 1927.

[182] G. Lemaître. Expansion of the universe, A homogeneous universe of constant mass and increasing radius accounting for the radial velocity of extra-galactic nebulae. , 91:483–490, March 1931.

[183] G. Lemaître. Expansion of the universe, The expanding universe. , 91:490–501, March 1931.

[184] Antony Lewis. Efficient sampling of fast and slow cosmological parameters. *Phys. Rev.*, D87:103529, 2013. doi: 10.1103/PhysRevD.87,103529.

[185] Antony Lewis and Sarah Bridle. Cosmological parameters from cmb and other data: A monte carlo approach. *Phys. Rev. D*, 66:103511, Nov 2002. doi: 10.1103/PhysRevD.66.103511.

[186] Antony Lewis, Anthony Challinor, and Anthony Lasenby. Efficient computation of CMB anisotropies in closed FRW models. *Astrophysical Journal*, 538:473–476, 2000.

[187] Antony Lewis, Anthony Challinor, and Neil Turok. Analysis of cmb polarization on an incomplete sky. *Phys. Rev. D*, 65:023505, Dec 2001. doi: 10.1103/PhysRevD.65.023505. URL http://link.aps.org/doi/10.1103/PhysRevD.65.023505.

[188] Yi-Chao Li, Feng-Quan Wu, and Xuelei Chen. Constraints on the brans-dicke gravity theory with the planck data. *Phys. Rev. D*, 88:084053, Oct 2013. doi: 10.1103/PhysRevD.88.084053. URL http://link.aps.org/doi/10.1103/PhysRevD.88.084053.

[189] E. A. Lim. Can we see lorentz-violating vector fields in the cmb? *Phys. Rev. D*, 71(6):063504, 2005.

[190] A.D. Linde. A new inflationary universe scenario: A possible solution of the horizon, flatness, homogeneity, isotropy and primordial monopole problems. *Phys. Lett.B*, 108:389, 1982.

[191] Jim Moran Lincoln Greenhill Alice Argon Liz Humphreys, Mark Reid. Toward a new geometric distance to the active galaxy ngc 4258. iii. final results and the hubble constant. arXiv:1307.6031 [astro-ph.CO].

[192] Nicholas Loutrel, Nicolas Yunes, and Frans Pretorius. A Parametrized post-Einsteinian Framework for Gravitational Wave Bursts. 2014.

[193] D. Lovelock. The einstein tensor and its generalizations. *Journal of Mathematical Physics*, 12:498–501, 1971.

[194] Lifshitz E. M. On the gravitational stability of the expanding universe. *J. Phys. USSR*, 10:116, 1946.

[195] M. Porrati M. A. Luty and R. Rattazzi. Strong interactions and stability in the dgp model. *JHEP*, 0309:029, 2003.

[196] D. C. Rodrigues M. Banados, A. Gomberoff and C. Skordis. A note on bigravity and dark matter. *Phys. Rev. D*, 79:063515, 2009.

[197] P. G. Ferreira M. Banados and C. Skordis. Eddington-born-infeld gravity and the large scale structure of the universe. *Phys. Rev. D*, 79(6):063511, 2009.

[198] B. P. Carlin M. K. Cowles. Markov chain monte carlo convergence diagnostics: a comparative review. *J. Am. Stat. Assoc.*, 91:883, 1996.

[199] L. Knox M. Kaplinghat and C. Skordis. Rapid calculation of theoretical cmb angular power spectra. *Astrophysical Journal*, 578:665, 2002.

[200] E Bunn M Tegmark. A method for extracting maximum resolution power spectra from microwave sky maps. *Astrophysical Journal*, 455:1–6, 1995.

[201] A. de la Macorra and G. Piccinelli. Cosmological evolution of general scalar fields and quintessence. *Phys. Rev. D*, 61:123503, May 2000. doi: 10.1103/PhysRevD.61.123503. URL http://link.aps.org/doi/10.1103/PhysRevD.61.123503.

[202] Douglas Scott Martin White and Joseph Silk. Anisotropies in the cosmic microwave background. *Annu. Rev. Astron. Astrophys.*, 32:319, 1994.

[203] Suto Y. Matsubara T. Cosmological redshift distortion of correlation functions as a probe of the density parameter and the cosmological constant. *Astrophysical Journal*, 470:L1, 1996.

[204] et al. Matthew Colless. The 2df galaxy redshift survey: spectra and redshifts. *Mon. Not. R. Astron. Soc.*, 328:1039–1063, 2001.

[205] Allan R. Matthews, Thomas A.; Sandage. Optical identification of 3c 48, 3c 196, and 3c 286 with stellar objects. *Astrophysical Journal*, 138:30–56, 1963.

[206] Michael Strauss Michael Vogeley Alexander Szalay Max Tegmark, Andrew Hamilton. Measuring the galaxy power spectrum with future redshift surveys. *Astrophysical Journal*, 499:555–576, 1998.

[207] Nicholas Metropolis, Arianna W. Rosenbluth, Marshall N. Rosenbluth, Augusta H. Teller, and Edward Teller. Equation of state calculations by fast computing machines. *Journal of Chemical Physics*, 21:1087–1092, 1953.

[208] Jeffrey A. Willick Michael A. Strauss. The density and peculiar velocity fields of nearby galaxies. *Phys.Rept.*, 261:271–431, 1995.

[209] Daniel V. Schroeder Michael E. Peskin. *An Introduction to Quantum Field Theory (Frontiers in Physics)*. 1995.

[210] Andrew H. Jaffe Imperial College of Science Technology Michael P. Hobson, University of Cambridge and Andrew R. Liddle University of Sussex Pia Mukherjee University of Sussex David Parkinson University of Sussex Medicine, London, editors. *Bayesian Methods in Cosmology*. 2014.

[211] A. A. Michelson and E. W. Morley. Relative motion of earth and luminiferous ether. *Am. J. Science*, 34:333, 1887.

[212] C. W. Misner. The Isotropy of the Universe. , 151:431, February 1968. doi: 10.1086/149448.

[213] V. F. Mukhanov. Physical foundations of cosmology. 2005.

[214] V. F. Mukhanov, H. A. Feldman, and R. H. Brandenberger. Theory of cosmological perturbations. , 215:203–333, June 1992.

[215] V.F. Mukhanov. Nucleosynthesis without a computer. *Int. J. Theor. Phys.*, 43: 669, 2004.

[216] Ryo Nagata, Takeshi Chiba, and Naoshi Sugiyama. WMAP constraints on scalar- tensor cosmology and the variation of the gravitational constant. *Phys.Rev.*, D69:083512, 2004. doi: 10.1103/PhysRevD.69.083512.

[217] J.V. Narlikar and T. Padmanabhan. Inflation for astronomers. *Annual Reviews of Astronomy and Astrophysics*, 29:325, 1991.

[218] P. Naselsky and I. Novikov. Microwave background anisotropy on scales 10 arcmin - 2 deg as an indicator of the cosmological model. *Astrophysical Journal*, 413:14–17, 1993.

[219] R. M. Neal. Probabilistic inference using markov chain monte carlo methods. Technical report, Dept. of Computer Science, University of Toronto, 1993. CRG-TR-93-1 (available online).

[220] Radford M. Neal. The short'cut metropolis method. *Technical Report*, (0506), August 2005.

[221] A. Nicolis and R. Rattazzi. Classical and quantum consistency of the dgp model. *JHEP*, 0406:059, 2004.

[222] Alberto Nicolis, Riccardo Rattazzi, and Enrico Trincherini. The Galileon as a local modification of gravity. *Phys.Rev.*, D79:064036, 2009. doi: 10.1103/PhysRevD.79.064036.

[223] Alberto Nicolis, Riccardo Rattazzi, and Enrico Trincherini. The Galileon as a local modification of gravity. *Phys.Rev.*, D79:064036, 2009. doi: 10.1103/PhysRevD.79.064036.

[224] Odintsov S. D. Nojiri, S. Quantum desitter cosmology and phantom matter. *Phys. Lett. B*, 562:147, 2003.

[225] S. Nojiri and S. D. Odintsov. Introduction to modified gravity and gravitational alternative for dark energy. *Int. J. Geom. Meth. Mod. Phys.*, 4:115, 2007.

[226] Jr. Nordtvedt, K. Equivalence principle for massive bodies i. phenomenology. *Phys. Rev.*, 169:1014, .

[227] Jr. Nordtvedt, K. Equivalence principle for massive bodies ii. theory. *Phys. Rev.*, 169:1017, .

[228] Jr. Nordtvedt, K. Testing relativity with laser ranging to the moon. *Phys. Rev.*, 170:1186, .

[229] Kenneth Nordtvedt. Equivalence Principle for Massive Bodies. 2. Theory. *Phys.Rev.*, 169:1017–1025, 1968. doi: 10.1103/PhysRev.169.1017.

[230] Steigman G. Olive, K. A. and T. P. Walker. Primordial nucleosynthesis: theory and observations. *Phys. Rep.*, 333:389, 2000.

[231] V. K . Onemli and R. P. Woodard. Superacceleration from massless, minimally coupled phi**4. *Class. Quant. Grav.*, 19:4607, 2002.

[232] Bharat Ratra P. J. E. Peebles. The cosmological constant and dark energy. *Rev.Mod.Phys.*, 75:559–606, 2003.

[233] Antonio Padilla and Paul M. Saffin. Classical Duals, Legendre Transforms and the Vainshtein Mechanism. *JHEP*, 1207:122, 2012. doi: 10.1007/JHEP07(2012)122.

[234] White M. Padmanabhan N. Constraining anisotropic baryon oscillations. *Phys. Rev. D.*, 77:3540, 2008.

[235] A. B. Palei. Integrating Photometers. , 12:164, August 1968.

[236] David Parkinson, Signe Riemer-Sorensen, Chris Blake, Gregory B. Poole, Tamara M. Davis, et al. The WiggleZ Dark Energy Survey: Final data release and cosmological results. *Phys.Rev.*, D86:103518, 2012. doi: 10.1103/PhysRevD.86.103518.

[237] P. J. Peebles. Primeval Helium Abundance and the Primeval Fireball. *Physical Review Letters*, 16:410–413, March 1966. doi: 10.1103/PhysRevLett.16.410.

[238] P. J. E. Peebles.

[239] P. J. E. Peebles. Primordial Helium Abundance and the Primordial Fireball. II. , 146:542, November 1966. doi: 10.1086/148918.

[240] P. J. E. Peebles. Recombination of the Primeval Plasma. , 153:1, July 1968. doi: 10.1086/149628.

[241] P. J. E. Peebles and J. T. Yu. Primeval Adiabatic Perturbation in an Expanding Universe. , 162:815, December 1970. doi: 10.1086/150713.

[242] Phillip James Edwin Peebles. *Large-Scale Structure of the Universe Paperback*. 1980.

[243] Schramm D.N. Turner E.L. Kron R.G. Peebles, P.J.E. The case for the relativistic hot big bang cosmology. *Nature*, 352:769, 1991.

[244] A. A. Penzias and R. W. Wilson. A Measurement of Excess Antenna Temperature at 4080 Mc/s. , 142:419–421, July 1965. doi: 10.1086/148307.

[245] Will J. Percival. Baryon acoustic oscillations in the sloan digital sky survey data release 7 galaxy sample. *Mon.Not.Roy.Astron.Soc.*, 401:2148–2168, 2010.

[246] White M. Percival W.J. *Mon. Not. Roy. Astron. Soc.*, 393:297, 2009.

[247] S. Perlmutter et al. Measurements of Omega and Lambda from 42 High-Redshift Supernovae. *Astrophysical Journal*, 517:565–586, 1999. doi: 10.1086/307221.

[248] Federico Piazza and Filippo Vernizzi. Effective Field Theory of Cosmological Perturbations. *Class.Quant.Grav.*, 30:214007, 2013. doi: 10.1088/0264-9381/30/21/214007.

[249] R. V.; Rebka Jr. G. A. Pound. Gravitational red-shift in nuclear resonance. *Physical Review Letters*, 3:439–441, 1959.

[250] Cambridge University Press, editor. *Numerical Recipes: The Art of Scientific Computing*. third edition, 2007.

[251] H. Bethe R. Alpher and G. Gamow. The origin of chemical elements. *Phys. Rev.*, 73:803, 1948.

[252] R. C. Myers R. Gregory, N. Kaloper and A. Padilla. A new perspective on dgp gravity. *JHEP*, 10:069, 2007.

[253] A.E. Raftery and S.M. Lewis. How many iterations in the gibbs sampler? in bayesian statistics. 1992.

[254] Bharat Ratra and P. J. E. Peebles. Cosmological consequences of a rolling homogeneous scalar field. *Phys. Rev. D*, 37:3406–3427, Jun 1988. doi: 10.1103/PhysRevD.37.3406. URL http://link.aps.org/doi/10.1103/PhysRevD.37.3406.

[255] A. C. S. Readhead, C. R. Lawrence, S. T. Myers, W. L. W. Sargent, H. E. Hardebeck, and A. T. Moffet. A limit of the anisotropy of the microwave background radiation on arc minute scales. , 346:566–587, November 1989. doi: 10.1086/168039.

[256] Fowler W.A. Reeves, H. and F. Hoyle. Galactic cosmic ray origin of li, be and b in stars. *Nature*, 226:727, 1970.

[257] Adam G. Riess et al. Observational evidence from supernovae for an accelerating universe and a cosmological constant. *Astron.J.*, 116:1009–1038, 1998. doi: 10.1086/300499.

[258] et al. Riess, A. A redetermination of the hubble constant with the hubble space telescope from a differential distance ladder. *Astrophys.J.*, 699:539–563.

[259] H. Robertson. On relativistic cosmology. *Phil. Mag.*, 5:835, 1928.

[260] H. P. Robertson. The apparent luminosity of a receding nebula. Mit 3 Abbildungen. , 15:69, 1938.

[261] N. Rosen. General relativity and flat space. ii. *Physical Review*, 57:150–153, 1940.

[262] N. Rosen. A bi-metric theory of gravitation. *General Relativity and Gravitation*, 4:435–447, 1973.

[263] M. S. Turner S. Burles, K. M. Nollett. What is the big-bang-nucleosynthesis prediction for the baryon density and how reliable is it? *Physical Review D*, 63(6):063512, 2001.

[264] Wolfe A.M. Sachs, R.K. Perturbations of a cosmological model and angular variations of the microwave background. *Astrophysical Journal*, 147:73, 1967.

[265] V. Sahni. Dark matter and dark energy. *Lect.NotesPhys.*, 653:141–180, 2004.

[266] V. Sahni and A.A. Starobinsky. The case for a positive cosmological λ-term. *International Journal of Modern Physics D*, 9:373, 2000.

[267] Varun Sahni and Yuri Shtanov. Did the universe loiter at high redshifts? *Phys. Rev. D*, 71:084018, Apr 2005. doi: 10.1103/PhysRevD.71.084018. URL http://link.aps.org/doi/10.1103/PhysRevD.71.084018.

[268] Riello M. Cassisi S. Piotto G. Salaris, M. The initial helium abundance of the galactic globular cluster system. *Astron. Astroph.*, 420:911, 2004.

[269] K.K. Schaffer, T.M. Crawford, K.A. Aird, B.A. Benson, L.E. Bleem, et al. The First Public Release of South Pole Telescope Data: Maps of a 95-square-degree Field from 2008 Observations. *Astrophys.J.*, 743:90, 2011.

[270] H. Schmidt. Fourth order gravity: Equations, history, and applications to cosmology. *International Journal of Geometric Methods in Modern Physics*, 4: 209, 2007.

[271] Román Scoccimarro. Redshift-space distortions, pairwise velocities, and nonlinearities. *Phys. Rev. D*, 70:083007, Oct 2004. doi: 10.1103/PhysRevD.70.083007. URL http://link.aps.org/doi/10.1103/PhysRevD.70.083007.

[272] L. Searle and Sargent W.L.W. Inferences from the cosmposition of two dwarf blue galaxies. *Astrophysical Journal*, 173:25, 1972.

[273] L. Searle and Sargent W.L.W. The structure of seyfert nuclei. *Comments Ap. and Space Phys.*, 4:1, 1972.

[274] Uros Seljak and Matias Zaldarriaga. A Line of sight integration approach to cosmic microwave background anisotropies. *Astrophys.J.*, 469:437–444, 1996. doi: 10.1086/177793.

[275] H-J. Seo and D.J. Eisenstein. Probing dark energy with baryonic acoustic oscillations from future large galaxy redshift surveys. *Astrophysical Journal*, 598:720, 2003.

[276] I.I. Shapiro. *A radar test of the constancy of the gravitational interaction. In On the measurement of cosmological variations of the gravitational constant*. 1978.

[277] J. Silk. Cosmic black-body radiation and galaxy formation. *Astrophysical Journal*, 151:459, 1968.

[278] Joseph Silk. Introduction to the cmb. http://www.astro.ubc.ca/people/scott/cmb_intro.html.

[279] Alessandra Silvestri, Levon Pogosian, and Roman V. Buniy. Practical approach to cosmological perturbations in modified gravity. *Phys.Rev.*, D87(10):104015, 2013. doi: 10.1103/PhysRevD.87.104015.

[280] Constantinos Skordis. Consistent cosmological modifications to the Einstein equations. *Phys. Rev.*, D79:123527, 2009. doi: 10.1103/PhysRevD.79.123527.

[281] Constantinos Skordis. Consistent cosmological modifications to the einstein equations. *Phys.Rev.D*, 79:123527, 2009.

[282] V.M. Slipher. The radial velocity of the andromeda nebula. *Lowell Observatory Bulletin*, 58:56, .

[283] V.M. Slipher. The detection of nebulae rotation. *Lowell Observatory Bulletin*, 62, .

[284] V.M. Slipher. Spectrographic observations of nebulae. *Popular Astronomy*, 23: 21, .

[285] V.M. Slipher. *Proc. Amer. Phil.Soc.*, 56:403, .

[286] Bennett C.L. Kogut A. Wright E.L. Aymon J. et al. Smoot, G.F. Structure in the cobe differential microwave radiometer first-year maps. *Astrophysical Journal Lett.*, 396:L1, 1992.

[287] G. F.; et al. Smoot. Structure in the cobe differential microwave radiometer first-year maps. *Astrophysical Journal Letters*, 396, 1992.

[288] Yong-Seon Song et al. Theoretical priors on modified growth parametrisations. *JCAP*, 1004:018, 2010.

[289] L. Spitzer. *Physical Processes in the Interstellar Medium*. 1978.

[290] A. A. Starobinsky. A new type of isotropic cosmological models without singularity. *Physics Letters B*, 91(1):99–102, 1980.

[291] A. A. Starobinsky. Dynamics of phase transition in the new inflationary universe scenario and generation of perturbations. *Phys. Lett. B*, 117:175, 1982.

[292] G. Steigman. Primordial nucleosynthesis in the precision cosmology era. *Ann. Rev. Nucl. Part. Sci.*, 57:463, 2007.

[293] K. S. Stelle. Renormalization of higher-derivative quantum gravity. *Phys. Rev. D*, 16(4):953–969, 1977.

[294] I. I. Kogan T. Damour and A. Papazoglou. Nonlinear bigravity and cosmic acceleration. *Phys. Rev. D*, 66(10):104025, 2002.

[295] P. G. Ferreira T. G. Zlosnik and G. D. Starkman. Growth of structure in theories with a dynamical preferred frame. *Phys. Rev. D*, 77(8):084010, 2008.

[296] J. Yokoyama T. Kobayashi, M. Yamaguchi. Generalized g-inflation: Inflation with the most general second-order field equations. *Prog. Theor. Phys.*, 126: 511–529, 2011.

[297] V. Faraoni T. P. Sotiriou. f(r) theories of gravity. *Reviews of Modern Physics*, 82:451–497, 2010.

[298] Atsushi Taruya, Takahiro Nishimichi, and Shun Saito. Baryon acoustic oscillations in 2d: Modeling redshift-space power spectrum from perturbation theory. *Phys. Rev. D*, 82:063522, Sep 2010. doi: 10.1103/PhysRevD.82.063522. URL http://link.aps.org/doi/10.1103/PhysRevD.82.063522.

[299] Nishimichi T. Taruya A., Saito S. Forecasting the cosmological constraints with anisotropic baryon acoustic oscillations from multipole expansion. *Phys. Rev. D*, 83:3527, 2011.

[300] Fowler L.A. Taylor, J.H. and J.M. Weisberg. Measurements of general relativistic effects in the binary pulsar psr1913+16. *Nature*, 277:437, 1979.

[301] J. M. Taylor, J. H.; Weisberg. A new test of general relativity - gravitational radiation and the binary pulsar psr 1913+16. *Astrophysical Journal*, 253:908–92, 1982.

[302] ESA team. Anisotropies of the cosmic microwave background. http://www.esa.int/spaceinimages/Images/2013/03/Planck_CMB.

[303] Max Tegmark and Angelica de Oliveira-Costa. How to measure cmb polarization power spectra without losing information. *Phys. Rev. D*, 64:063001, Aug 2001. doi: 10.1103/PhysRevD.64.063001. URL http://link.aps.org/doi/10.1103/PhysRevD.64.063001.

[304] Max Tegmark et al. Cosmological Constraints from the SDSS Luminous Red Galaxies. *Phys.Rev.*, D74:123507, 2006. doi: 10.1103/PhysRevD.74.123507.

[305] Kenneth Nordtvedt Thibault Damour. General relativity as a cosmological attractor of tensor-scalar theories. *Physical Review Letters*, 70:15, 1993.

[306] N. Thomas et al. The bepicolombo laser altimeter (bela): Concept and baseline design. *Science Direct, Planetary and Space Science*, 55:1398–1413, 2007.

[307] K. I. Umezu, K. Ichiki, and M. Yahiro. Cosmological constraints on Newton's constant. *Phys.Rev.*, D72:044010, 2005. doi: 10.1103/PhysRevD.72.044010.

[308] L. Arturo Ureña López and Tonatiuh Matos. New cosmological tracker solution for quintessence. *Phys. Rev. D*, 62:081302, Sep 2000. doi: 10.1103/PhysRevD.62.081302. URL http://link.aps.org/doi/10.1103/PhysRevD.62.081302.

[309] Matias Zaldarriaga Uros Seljak. A line of sight approach to cosmic microwave background anisotropies. *Astrophys.J.*, 469:437–444, 1996.

[310] R. Utiyama and B. S. Dewitt. Renormalization of a classical gravitational field interacting with quantized matter fields. *Journal of Mathematical Physics*, 3: 608–618, 1962.

[311] Peiris H. V. and Spergel D. N. Cross-correlating the sloan digital sky survey with the microwave sky. *Astrophysical Journal*, 540:605, 2000.

[312] H. Feldman V. Sahni and A. Stebbins. Loitering universes. *Astrophysical Journal*, 385:1, 1992.

[313] A. I. Vainshtein. To the problem of nonvanishing gravitation mass. *Phys. Lett.*, B39:393, 1972. doi: 10.1016/0370-2693(72)90147-5.

[314] N. Vittorio and J. Silk. Fine-scale anisotropy of the cosmic microwave background in a universe dominated by cold dark matter. , 285:L39–L43, October 1984. doi: 10.1086/184361.

[315] R. V. Wagoner. Big bang nucleosynthesis revisted. *Astrophysical Journal*, 179: 343–360, 1973.

[316] R. V. Wagoner, W. A. Fowler, and F. Hoyle. On the Synthesis of Elements at Very High Temperatures. , 148:3, April 1967. doi: 10.1086/149126.

[317] Robert V. Wagoner. Scalar-tensor theory and gravitational waves. *Phys. Rev. D*, 1:3209–3216, Jun 1970. doi: 10.1103/PhysRevD.1.3209. URL http://link.aps.org/doi/10.1103/PhysRevD.1.3209.

[318] R. M. Wald. *General Relativity*. 1984.

[319] Naoshi Sugiyama Wayne Hu. Anisotropies in the cosmic microwave background: An analytic approach. *Astrophys.J.*, 444:489–506, 1995.

[320] Hans J. Weber and George B. Arfken. *Essential Mathematical Methods for Physicists*. 2003.

[321] Steven Weinberg. *Gravitation and Cosmology. Principles and Applications of the General Theory of Relativity*. 1972.

[322] Steven Weinberg. The Cosmological constant problems. pages 18–26, 2000.

[323] C. Wetterich. Cosmology and the fate of dilatation symmetry. *Nucl. Phys. B*, 302:668, 1998.

[324] H. Weyl. Gravitation und elektrizit. *Sitzungsber. Preuss. Akad. d. Wiss. Teil*, 1: 465, 1918.

[325] H. Weyl. Zur allgemeinen relativitatstheorie. *Phys. Z.*, 24:230, 1923.

[326] C. Will. *Theory and experiment in gravitational physics*. Cambridge University Press, Cambridge, 1981.

[327] C. Will. The Confrontation between General Relativity and Experiment. *Living Rev. Rel.*, 9:3, 2006.

[328] C. M. Will and Jr. K. Nordtvedt. Conservation laws and preferred frames in relativistic gravity. ii. experimental evidence to rule out preferred-frame theories of gravity. *Astrophysical Journal*, 177:775, 1972.

[329] Clifford M. Will. Theoretical Frameworks for Testing Relativistic Gravity. 2. Parametrized Post-Newtonian Hydrodynamics, and the Nordtvedt Effect. *Astrophys.J.*, 163:611–627, 1971. doi: 10.1086/150804.

[330] Clifford M. Will. Was einstein right? a centenary assessment. 2014.

[331] Clifford M. Will. The confrontation between general relativity and experiment. *Living Rev. Rel.*, 17:4, 2014.

[332] Clifford M. Will and Jr. Nordtvedt, Kenneth. Conservation Laws and Preferred Frames in Relativistic Gravity. I. Preferred-Frame Theories and an Extended PPN Formalism. *Astrophys.J.*, 177:757, 1972. doi: 10.1086/151754.

[333] J.G. Williams et al. New test of the equivalence principle from lunar laser ranging. *Phys. Rev. Lett.*, 36:551–554, 1976.

[334] M. L. Wilson and J. Silk. On the anisotropy of the cosmological background matter and radiation distribution. I - The radiation anisotropy in a spatially flat universe. , 243:14–25, January 1981. doi: 10.1086/158561.

[335] R. Woodard. Avoiding dark energy with 1/r modifications of gravity. *Lect.Notes Phys.*, 720:403–433, 2007.

[336] Alison Wright. Nobel prize 2011: Perlmutter, schmidt & riess. *Nature Physics*, 7:833, 2011.

[337] Fengquan Q. Wu and Xuelei Chen. Cosmic microwave background with Brans-Dicke gravity II: constraints with the WMAP and SDSS data. *Phys.Rev.*, D82: 083003, 2010. doi: 10.1103/PhysRevD.82.083003.

[338] et. al. Y. Izatov. Helium abundance in the most metal-deficient blue compact galaxies: I zw 18 and sbs 0335–052. *Astrophysical Journal*, 527:757, 1999.

[339] I.V. Tanatarov Yu.L. Bolotin. A thousand problems in cosmology: Horizons. arXiv:1310.6329 [physics.ed-ph], 2013.

[340] Nicolas Yunes and Frans Pretorius. Fundamental Theoretical Bias in Gravitational Wave Astrophysics and the Parameterized Post-Einsteinian Framework. *Phys.Rev.*, D80:122003, 2009. doi: 10.1103/PhysRevD.80.122003.

[341] Oliver Zahn and Matias Zaldarriaga. Probing the Friedmann equation during recombination with future CMB experiments. *Phys.Rev.*, D67:063002, 2003. doi: 10.1103/PhysRevD.67.063002.

[342] Y. B. Zeldovich. A hypothesis, unifying the structure and the entropy of the universe. *Mon. Not. Roy. Astron. Soc.*, 160:7–8, 1972.

[343] Y. B. Zel'dovich. A hypothesis, unifying the structure and the entropy of the universe. *Mon. Not. Roy. Astron. Soc.*, 160:1P–3P, 1972.

[344] Ya.B. Zel'dovich. The cosmological constant and the theory of elementary particles. *Sov. Phys. – Uspekhi*, 11:381, 1968.

[345] Pengjie Zhang, Michele Liguori, Rachel Bean, and Scott Dodelson. Probing Gravity at Cosmological Scales by Measurements which Test the Relationship between Gravitational Lensing and Matter Overdensity. *Phys. Rev. Lett.*, 99: 141302, 2007. doi: 10.1103/PhysRevLett.99.141302.

APPENDIX A

THE STANDARD POST-NEWTONIAN TOOLS

A.1 Post-Newtonian Potentials

The possible terms that may appear in the post-Newtonian metric, are

1) g_{ij} must behave as a three-dimensional tensor under rotations, thus the only terms that can appear in it are $U\delta_{ij}$ and U_{ij} where

$$U = \int d^3x' \frac{\rho(x',t)}{|x-x'|}, \tag{A.1}$$

$$\nabla^2 U = -4\pi\rho, \tag{A.2}$$

Note that $\mathscr{U} = G_N U$ is the Newtonian potential in GR rather than U. U has units of energy since $\mathscr{U}$ is addimensional and both are $O(2)$.

$$U_{ij} = \int d^3x' \frac{\rho(x',t)(x-x')_i(x-x')_j}{|x-x'|^3} \tag{A.3}$$

This potentials can be written in terms of the superpotential

$$\chi(x,t) \equiv \int d^3x' \rho(x',t)|x-x'| \tag{A.4}$$

$$\chi_{,ij} = -\delta_{ij}U + U_{ij}$$

$$\nabla^2\chi = -2U \tag{A.5}$$

2) g_{ij} must behave as a three-dimensional vector under rotations, thus the only terms that can appear in it must be combinations of V_i and W_i, where

$$V_i = \int d^3x' \frac{\rho(x',t)v_i}{|x-x'|} \tag{A.6}$$

$$W_i = \int d^3x' \frac{\rho(x',t)(x-x')_i v\cdot(x-x')}{|x-x'|^3}. \tag{A.7}$$

The vector potentials can be related to derivatives of the superpotential. First lets use the continuity equation

$$\frac{\partial\rho}{\partial t} + \nabla\cdot(\rho\vec{v}) = 0 \tag{A.8}$$

which leads to $\frac{\partial}{\partial t} \sim -\vec{v}\cdot\vec{\nabla}$ and thus

$$\chi_{,i0} = V_i - W_i \tag{A.9}$$

3) g_{00} to $O(4)$ should be scalar under rotations. The only terms that may be considered are $U^2, \phi_W, \phi_1, \phi_2, \phi_3, \phi_4, A, B$ where

$$\Phi_W \equiv \int d^3x' d^3x'' \rho'\rho'' \frac{x-x'}{|x-x'|^3}\cdot\left(\frac{x'-x''}{|x-x''|} - \frac{x-x''}{|x'-x''|}\right) \tag{A.10}$$

$$\Phi_1 \equiv \int d^3x' \frac{\rho' v'^2}{|x-x'|} \tag{A.11}$$

$$\Phi_2 \equiv \int d^3x' \frac{\rho' U'}{|x-x'|} \tag{A.12}$$

$$\Phi_3 \equiv \int d^3x' \frac{\rho'\Pi'}{|x-x'|} \tag{A.13}$$

$$\Phi_4 \equiv \int d^3x' \frac{P'}{|x-x'|} \tag{A.14}$$

$$A \equiv \int d^3x' \frac{\rho'[v\cdot(x-x')]^2}{|x-x'|^3} \tag{A.15}$$

$$B \equiv \int d^3x' \frac{\rho'}{|x-x'|}(x-x')\cdot\frac{dv'}{dt} \tag{A.16}$$

The some of the above definitions in a differential version and other useful relations are given by

$$\nabla^2\Phi_1 = -4\pi\rho v^2 \tag{A.17}$$
$$\nabla^2\Phi_2 = -4\pi\rho U = U\nabla^2 U \tag{A.18}$$
$$\nabla^2\Phi_3 = -4\pi\rho\Pi \tag{A.19}$$
$$\nabla^2\Phi_4 = -4\pi p \tag{A.20}$$
$$\nabla^2 V_i = -4\pi v_i \tag{A.21}$$
$$(\nabla U)^2 = \nabla^2(\frac{1}{2}U^2 - \Phi_2) \tag{A.22}$$
$$U_{,0} = -V_{i,i} \tag{A.23}$$
$$U_{,00} = -\frac{1}{2}\nabla^2\chi_{,00} = -\frac{1}{2}\nabla^2(A+B-\Phi_1) \tag{A.24}$$

A.2 Renomalized Post-Newtonian Potentials

$$\tilde{\mathscr{V}_i} \equiv G_0 V_i \tag{A.25}$$
$$\tilde{\mathscr{W}_i} \equiv G_0 W_i \tag{A.26}$$
$$\mathscr{U} \equiv GU = \frac{r_s U}{8\pi M} \to O(2,0) \tag{A.27}$$
$$\phi_k = G\Phi_k, \quad k = 1,3,4 \tag{A.28}$$
$$\phi_2 = G^2\Phi_2 \tag{A.29}$$
$$\phi_5 = G^2\Phi_5 \tag{A.30}$$
$$\mathscr{A} = GA \tag{A.31}$$
$$\mathscr{B} = GB \tag{A.32}$$

A.2.1 Definitions For $\varphi^{(4,0)}$ Solution

$$\xi_1 \equiv -\frac{1}{2}(\mathscr{A}+\mathscr{B}-\phi_1) \tag{A.33}$$
$$\xi_{k=2,..,4} \equiv \phi_{k=2,..,4} \tag{A.34}$$
$$\xi_5 \equiv \mathscr{U}^2 \tag{A.35}$$

A.3 The Standard Post-Newtonian Gauge

Lets first consider a generic gauge transform generated by a ξ function

$$x^\mu \rightarrow x^\mu + \xi^\mu \tag{A.36}$$
$$g_{\mu\nu} \rightarrow g_{\mu\nu} - \xi_{\mu;\nu} - \xi_{\nu;\mu} \tag{A.37}$$

In order to retain the post-newtonian character of $g_{\mu\nu}$ and the quasi-Cartesian character of the coordinate system, and to remain in the universe rest frame ξ function must satisfy

1) $\xi_{\mu;\nu} + \xi_{\nu;\mu}$ is post-newtonian $(O(2))$.

2) $\xi_{\mu;\nu} + \xi_{\nu;\mu} \rightarrow 0$ and $\frac{|\xi_\mu|}{|x_\mu|} \rightarrow 0$ far away from the system.

Lets first consider a generic gauge transform generated by a ξ function

$$x^\mu \rightarrow x^\mu + \xi^\mu \tag{A.38}$$
$$g_{\mu\nu} \rightarrow g_{\mu\nu} - \xi_{\mu;\nu} - \xi_{\nu;\mu} \tag{A.39}$$

In order to retain the post-newtonian character of $g_{\mu\nu}$ and the quasi-Cartesian character of the coordinate system, and to remain in the universe rest frame ξ function must satisfy

1) $\xi_{\mu;\nu} + \xi_{\nu;\mu}$ is post-newtonian $(O(2))$.

2) $\xi_{\mu;\nu} + \xi_{\nu;\mu} \rightarrow 0$ and $\frac{|\xi_\mu|}{|x_\mu|} \rightarrow 0$ far away from the system.

In the standard formulation , the gradient of the superpotential χ is the only one that satisfies this. So

$$\xi_0 = \lambda_1^0 \chi_{,0} \tag{A.40}$$
$$\xi_j = \lambda_2^0 \chi_{,j} \tag{A.41}$$

λ_1^0 and λ_2^0 are fixed such that g_{ij} is diagonal and isotropic and g_{00} doesn't contain the $\mathscr{B}$ potential. In this way the standard post-newtonian gauge is defined and it doesn't have any physcial interpretation.[1]

In order to apply this gauge choice our PPNV prescription, the condition 1) above may be extended as

[1] In my opinion this choice is completelly arbitrary and conventional. I think that the point of $\mathscr{B}$ appearing in g_{00} or not is just matter of personal taste.

1) $\xi_{\mu;\nu} + \xi_{\nu;\mu}$ is post-newtonian, however it may involve post-post newtonian potentials P such that $r_v^3/r_s P$ is post-newtonian.

In our case potentials whose gradient satisfies 1) should be in terms of the superpotential in order to satisfy 2) as well. Those are: $\rho\nabla^2\chi$, $U\nabla^2\nabla^2\chi$ and $\chi\nabla^2\rho$.

For a gauge choice defined by (A.41) plus a linear combination of the gradients of these potentials , terms in $g_{00}^{(4,1)}$ containing $\mathscr{B}$ can be eliminated by a choice of the corresponding new λ coefficients in front of them.

In this way we keep the conventional PPN gauge: g_{ij} is isotropic and diagonal and $\mathscr{B}$ doesn't appear in g_{00}.

APPENDIX B

THE POST-NEWTONIAN VAINSHTEINIAN TOOLS

B.1 PPNV Potentials:Outside the Vainshtein Radius

The following potentials needed to express the solution for $h_{00}^{(4,-2)}$ given by (6.84).

$$\Pi_1 = \mathscr{U}^2\mathscr{G}_1 \tag{B.1}$$
$$\Pi_2 = \mathscr{U}\nabla^2\Phi_2 \tag{B.2}$$
$$\Pi_3 = \mathscr{U}\nabla^2\mathscr{U}^2 \tag{B.3}$$
$$\Pi_4 = 4\pi\mathscr{U}\nabla^{-2}\rho^2 \tag{B.4}$$
$$\Pi_5 = 4\pi\mathscr{U}\nabla^{-2}(\mathscr{U}\nabla^2\rho) \tag{B.5}$$
$$\Pi_6 = \frac{1}{2}(\mathscr{U}^2)_{,00} - \Phi_{2,00} \tag{B.6}$$
$$\Pi_7 = (\mathscr{U}_{,0})^2 = \vec{V}\cdot\vec{V} \tag{B.7}$$
$$\Pi_8 = \mathscr{U}\hat{T}^{(4)} \tag{B.8}$$
$$\Pi_k^1 = \xi_k\nabla^2\mathscr{U} \tag{B.9}$$
$$\Pi_k^2 = \nabla^2(\xi_k\mathscr{U}) \tag{B.10}$$
$$\Pi_k^3 = \mathscr{U}\nabla^2\xi_k \tag{B.11}$$

$$\Lambda_k^1 = \nabla^{-2}[\xi_k \nabla^2 \nabla^2 \mathscr{U}] \tag{B.12}$$
$$\Lambda_k^2 = \nabla^{-2}[\nabla^2 \xi_k \nabla^2 \mathscr{U}] \tag{B.13}$$
$$\Lambda_k^3 = \nabla^{-2}[\mathscr{U} \nabla^2 \nabla^2 \xi_k] \tag{B.14}$$
$$\Theta_1 = \nabla^{-2}[\mathscr{U} \mathscr{G}_1 \nabla^2 \mathscr{U}] \tag{B.15}$$
$$\Theta_2 = \nabla^{-2}[\mathscr{U} \nabla^2 (\mathscr{U} \mathscr{G}_1)] \tag{B.16}$$
$$\Upsilon_1 = \nabla^{-2}[\mathscr{U}_{,0} \nabla^2 \mathscr{U}_{,0}] \tag{B.17}$$
$$\Upsilon_2 = \nabla^{-2}[\hat{\rho} \nabla^2 \hat{\rho}^2] \tag{B.18}$$
$$\Upsilon_3 = \nabla^{-2}[\hat{\rho} \nabla^2 (\mathscr{U} \nabla^2 \hat{\rho})] \tag{B.19}$$
$$X_1 = \nabla^{-2}[\mathscr{U} (\nabla^2 \mathscr{U})^2] \tag{B.20}$$
$$X_2 = \nabla^{-2}[\hat{T}^{(4)} \nabla^2 \mathscr{U}] \tag{B.21}$$
$$X_3 = \nabla^{-2}[\mathscr{U} \nabla^2 \hat{T}^{(4)}] \tag{B.22}$$

B.2 PPNV Potentials:Outside the Vainshtein Radius

The following are some of the potentials required to express the solution of $h_{00}^{(4,1)}$ given by (6.130)

$$\nabla^2 P_1 = -4\pi G \rho B^{(0,1)} \tag{B.23}$$
$$\nabla^2 P_2 = \mathscr{U} \nabla^2 B^{(1,0)} \tag{B.24}$$
$$\nabla^2 P_3 = \nabla B^{(1,0)} \cdot \nabla (\nabla B^{(1,0)})^2 \tag{B.25}$$
$$\nabla^2 P_4 = B^{(1,0)} \nabla^2 (\nabla B^{(1,0)})^2 \tag{B.26}$$

B.2.1 Higher order PPNV Parameters

Coefficients of the Post-Post Newtonian Vainshteinian Potentials needed to write $h_{00}^{(4,-2)}$. For potentials (6.84) normalized with bare Newton constant, when the normalization changes adimensional constant factors must to be added to these expresions

$$
\begin{aligned}
\{p_k^3\} &= \{-\frac{\alpha(\omega+1)}{(\omega+2)^2(2\omega+3)\phi_0^{(out)}}, \frac{\alpha\left(-40\omega^2-72\omega+20(2\omega+3)\phi_0^{(out)}-27\right)}{4(\omega+2)^3(2\omega+3)\phi_0^{(out)}}, \\
&\quad \frac{2\alpha(\omega+1)}{(\omega+2)^2\phi_0^{(out)}}, -\frac{6\alpha(\omega+1)}{(\omega+2)^2\phi_0^{(out)}}, \frac{\alpha\left(-24\omega^2-56\omega+20(2\omega+3)\phi_0^{(out)}-27\right)}{8(\omega+2)^3(2\omega+3)\phi_0^{(out)}}\} \\
\{p_k^1\} &= \{-\frac{\alpha(2\omega+1)}{4(\omega+2)^2(2\omega+3)\phi_0^{(out)}}, -\frac{\alpha(2\omega+1)^2}{2(\omega+2)^3(2\omega+3)\phi_0^{(out)}}, \frac{\alpha(2\omega+1)}{2(\omega+2)^2\phi_0^{(out)}}, \\
&- \frac{3\alpha(2\omega+1)}{2(\omega+2)^2\phi_0^{(out)}}, -\frac{\alpha(2\omega+1)}{4(\omega+2)^3(2\omega+3)\phi_0^{(out)}}\} \\
\{p_k^2\} &= \{\frac{\alpha(\omega+1)}{2(\omega+2)^2(2\omega+3)\phi_0^{(out)}}, \frac{\alpha(\omega+1)(2\omega+1)}{(\omega+2)^3(2\omega+3)\phi_0^{(out)}}, -\frac{\alpha(\omega+1)}{(\omega+2)^2\phi_0^{(out)}}, \\
&\quad \frac{3\alpha(\omega+1)}{(\omega+2)^2\phi_0^{(out)}}, \frac{\alpha(\omega+1)}{2(\omega+2)^3(2\omega+3)\phi_0^{(out)}}\} \\
\{P_i\} &= \{-\frac{\alpha(\omega+1)}{(\omega+2)^3\phi_0^{(out)}}, \frac{(\phi_0^{(out)})^2}{2(\omega+2)^2}, -\frac{(\phi_0^{(out)})^2}{4(\omega+2)^2}, -\frac{(\phi_0^{(out)}-2)\phi_0^{(out)}}{2(\omega+2)^2}, -\frac{(\phi_0^{(out)})^2}{2(\omega+2)^2}, \\
&\quad -\frac{\alpha}{2(\omega+2)^2\phi_0^{(out)}}, \frac{\alpha(2\omega+1)}{2(\omega+2)^2(2\omega+3)\phi_0^{(out)}}, -\frac{2\pi\alpha(2\omega+3)}{(\omega+2)^2\phi_0^{(out)}}\} \\
\{l_k^1\} &= \{-\frac{\alpha(4\omega+5)}{4(\omega+2)^2(2\omega+3)\phi_0^{(out)}}, -\frac{\alpha(2\omega+1)(4\omega+5)}{2(\omega+2)^3(2\omega+3)\phi_0^{(out)}}, \frac{\alpha(4\omega+5)}{2(\omega+2)^2\phi_0^{(out)}}, \\
&\quad -\frac{3\alpha(4\omega+5)}{2(\omega+2)^2\phi_0^{(out)}}, -\frac{\alpha\left(5\omega^2+13\omega+\left(2\omega^2+7\omega+6\right)\phi_0^{(out)}+8\right)}{(\omega+2)^3(2\omega+3)\phi_0^{(out)}}\} \\
\{l_k^2\} &= \{\frac{\alpha(10\omega+9)}{4(\omega+2)^2(2\omega+3)\phi_0^{(out)}}, -\frac{\alpha\left(24\omega^2+34\omega+\left(52\omega^2+98\omega+46\right)\phi_0^{(out)}+5\right)}{4(\omega+2)^3(2\omega+3)\phi_0^{(out)}}, \\
&\quad \frac{\alpha(6\omega+7)}{2(\omega+2)^2\phi_0^{(out)}}, -\frac{3\alpha(6\omega+7)}{2(\omega+2)^2\phi_0^{(out)}}\}, \\
&\quad \frac{\alpha\left(-18\omega+\left(52\omega^2+98\omega+46\right)\phi_0^{(out)}-23\right)-16\pi\left(2\omega^2+7\omega+6\right)(\phi_0^{(out)})^3}{8(\omega+2)^3(2\omega+3)\phi_0^{(out)}}\} \\
\{l_k^3\} &= \{-\frac{\alpha(\omega+1)}{2(\omega+2)^2(2\omega+3)\phi_0^{(out)}}, -\frac{\alpha\left(16\omega^2+30\omega+4\left(2\omega^2+7\omega+6\right)\phi_0^{(out)}+11\right)}{2(\omega+2)^3(2\omega+3)\phi_0^{(out)}}, \\
&\quad \frac{\alpha(\omega+1)}{(\omega+2)^2\phi_0^{(out)}}, -\frac{3\alpha(\omega+1)}{(\omega+2)^2\phi_0^{(out)}}, \frac{\alpha\left(28\omega^2+56\omega+4\left(2\omega^2+7\omega+6\right)\phi_0^{(out)}+23\right)}{8(\omega+2)^3(2\omega+3)\phi_0^{(out)}}
\end{aligned}
$$

$$
\begin{aligned}
\{\varepsilon_k\} &= \{-\frac{\alpha\left(\left(24\omega^2+56\omega+8(\omega+1)^2\right)(\phi_0^{(out)})^5-2\left(2\omega^2+9\omega+9\right)(\phi_0^{(out)})^2\right)}{2(\omega+2)^3(2\omega+3)(\phi_0^{(out)})^3} \\
&\quad +\frac{\alpha\left(\left(4\omega^2+32\omega+39\right)\phi_0^{(out)}+30\right)}{2(\omega+2)^3(2\omega+3)(\phi_0^{(out)})^3},-\frac{2\pi\alpha(2\omega+3)(\phi_0^{(out)}-4)}{(\omega+2)^2(\phi_0^{(out)})^2}, \\
&\quad -\frac{2\pi\alpha(2\omega+3)}{(\omega+2)^2\phi_0^{(out)}}\} \\
\{z_k\} &= \left\{\frac{\alpha(6\omega+7)}{(\omega+2)^2(2\omega+3)\phi_0^{(out)}},\frac{4\pi^2\alpha(2\omega-1)}{(\omega+2)^3\phi_0^{(out)}},\frac{16\pi^3\alpha(2\omega-1)(\phi_0^{(out)}-2)}{(\omega+2)^3(\phi_0^{(out)})^2}\right\} \\
\{\kappa_k\} &= \left\{-\frac{2\omega^2+3\omega+3}{(\omega+2)^3(2\omega+3)\phi_0^{(out)}},-\frac{(\omega+1)(2\omega-1)}{(\omega+2)^3(2\omega+3)\phi_0^{(out)}}\right\} \\
\{s_k\} &= \left\{-\frac{\phi_0^{(out)}}{2(\omega+2)},-\frac{(2\omega+1)\phi_0^{(out)}}{(\omega+2)^2},\frac{(2\omega+3)\phi_0^{(out)}}{\omega+2},-\frac{3(2\omega+3)\phi_0^{(out)}}{\omega+2},-\frac{\phi_0^{(out)}}{2(\omega+2)^2}\right\}
\end{aligned}
$$

APPENDIX C

BI-LINEAR OPERATORS

Def 1 - Consider $u, v \in C^\infty$. Lets define the following non-lineal mapping $\mathscr{L} : C^\infty \times C^\infty \to C^\infty$ as

$$\mathscr{L}(u,v) = \nabla^2(\nabla u \cdot \nabla v) - 2\nabla \cdot (\nabla u(\nabla^2 v)) \tag{C.1}$$

Having defined the operator $\mathscr{L}$, it is straightforward to show that $\mathscr{L}$ is a non-symmetric bi-linear form since

$$\begin{aligned} \mathscr{L}(u+v,w) &= \mathscr{L}(u,w) + \mathscr{L}(v,w) && \text{(C.2)} \\ \mathscr{L}(\lambda u, v) &= \mathscr{L}(u, \lambda v) && \text{(C.3)} \\ \mathscr{L}(u,v) &\neq \mathscr{L}(v,u) && \text{(C.4)} \end{aligned}$$

and

Def 2- $\hat{\mathscr{L}} : C^\infty \to C^\infty$

$$\hat{\mathscr{L}}\mathscr{L}(u,v) = uv. \tag{C.5}$$

Notice that $\hat{\mathscr{L}}$ distributes over sums of $\mathscr{L}$
Since

$$\mathscr{L}(u+v,u+v) = \mathscr{L}(u,u) + \mathscr{L}(v,v) + \mathscr{L}(u,v) + \mathscr{L}(v,u)$$

then

$$\begin{aligned} \hat{\mathscr{L}}\mathscr{L}(u+v,u+v) = u^2 + v^2 + 2uv &= \hat{\mathscr{L}}\mathscr{L}(u,u) + \hat{\mathscr{L}}\mathscr{L}(v,v) + \hat{\mathscr{L}}\mathscr{L}(u,v) + \hat{\mathscr{L}}\mathscr{L}(v,u) \\ &= \hat{\mathscr{L}}(\mathscr{L}(u,u) + \mathscr{L}(v,v) + \mathscr{L}(u,v) + \mathscr{L}(v,u)). \end{aligned}$$

$\hat{\mathscr{L}}$ also distributes over product by a constant

$$\hat{\mathscr{L}}\mathscr{L}(cu,v) = cuv = c\hat{\mathscr{L}}\mathscr{L}(u,v)$$

$\mathscr{B}$ has the same property.

When spherical symmetry is imposed $\mathscr{L}$ reduces to

$$\mathscr{L}(u,v) = -\frac{2}{r}(3u'v'' + v'u'') - \frac{4}{r^2}v'u' + u^{(3)}v' - u'v^{(3)} \tag{C.6}$$

and

$$\mathscr{L}(u,u) = -\frac{4}{r^2}\frac{d}{dr}[r(u')^2] \tag{C.7}$$

Both are clearly invertible in the sense we can find the function $|u|$ if $\mathscr{L}(u,u)$ (or $\mathscr{L}(u,u)$) is known.

In the general case it's straight forward to show that $\hat{\mathscr{L}}$ also exists. The probe goes as follows The operators $\mathscr{L}_R \equiv \mathscr{L}(u,\cdot)$ and $\mathscr{L}_L \equiv \mathscr{L}(\cdot,u)$ are linear for a fixed function $u \neq 0 \in C^\infty$. Because u is infinitely differentiable and its derivatives are continue then $\mathscr{L}_R[v] = 0$ and $\mathscr{L}_L[v] = 0$ define linear homogeneous partial differential equations with unique solution each. The proof that $\hat{\mathscr{L}}$ exists is straightforward

By definition

$$\hat{\mathscr{L}}\mathscr{L}(u,\cdot)[v] = uv = \hat{\mathscr{L}}\mathscr{L}(\cdot,u)[v] \tag{C.8}$$

on the other hand, $\mathscr{L}/\mathscr{R}$ is invertible if and only if there exists an unique $\mathscr{L}_{L/R}^{-1}$ such that

$$\mathscr{L}_L^{-1}\mathscr{L}_L[v] = v = \mathscr{L}_R^{-1}\mathscr{L}_R[v] \tag{C.9}$$

then the following must be true

$$\hat{\mathscr{L}} = u\mathscr{L}_L^{-1} = u\mathscr{L}_R^{-1}. \tag{C.10}$$